



UNIVERSIDAD DE CHILE
FACULTAD DE CIENCIAS FÍSICAS Y MATEMÁTICAS
DEPARTAMENTO DE GEOLOGÍA

**COSEISMIC LANDSLIDES DURING STRONG SHALLOW
CRUSTAL AND MEGATHRUST EARTHQUAKES:
CONTROLLING FACTORS AND CONCEPTUAL HAZARD
GEOMODELS**

**TESIS PARA OPTAR AL GRADO DE DOCTORA EN
CIENCIAS MENCION GEOLOGÍA**

ALEJANDRA JEANNETTE SEREY AMADOR

**PROFESOR GUÍA:
SERGIO SEPÚLVEDA VALENZUELA**

**MIEMBROS DE LA COMISION:
STELLA MOREIRAS
GREGORY DE PASCALE**

**SANTIAGO DE CHILE
2020**

RESUMEN DE LA TESIS PARA OPTAR AL GRADO DE:

Doctora en Ciencias, mención Geología

POR: Alejandra Serey Amador

FECHA: 07/10/2020

PROFESOR GUÍA: Sergio A. Sepúlveda Valenzuela

REMOCIONES EN MASA COSÍSMICAS DURANTE FUERTES TERREMOTOS CORTICALES SUPERFICIALES Y TERREMOTOS DE SUBDUCCION: FACTORES CONTROLADORES Y GEOMODELOS CONCEPTUALES DEL PELIGRO

Fuertes terremotos en Chile a menudo se asocian con una cadena de peligros en cascada que incluyen movimiento vibratorio del suelo, licuefacción, tsunamis y remociones en masa cosísmicas. En áreas montañosas tectónicamente activas, las remociones en masa representan el peligro geológico más frecuente y pueden ser responsables de las mayores pérdidas económicas durante y después de fuertes sismos debido a las destrucciones masivas que podrían producirse. Además, en todo el mundo, los deslizamientos cosísmicos matan a miles de personas con una creciente tendencia impulsada por intervenciones antrópicas, el aumento de la población mundial y procesos naturales.

Un enfoque clave para la investigación sobre remociones en masa generadas sísmicamente en áreas montañosas ha sido la preparación de inventarios completos y confiables de deslizamientos cosísmicos. Nuestro país es uno de los países con mayor actividad sísmica en el mundo. Por lo tanto, existen recientes y diferentes tipos de terremotos generadores de deslizamientos en Chile. El objetivo de esta investigación es identificar las características principales en la ocurrencia de deslizamientos durante grandes terremotos en Chile. Se busca mejorar la comprensión de su mecánica, distribución espacial y factores controladores geológicos, así como obtener información cualitativa para el desarrollo de modelos conceptuales para el reconocimiento del peligro de deslizamientos cosísmicos provocado por terremotos corticales superficiales y terremotos de subducción en diferentes ambientes montañosos de los Andes chilenos. Para ello, se estudiaron en detalle los eventos del Maule de 2010 y de Aysén de 2007.

En primer lugar, fue necesaria la preparación de inventarios completos de los deslizamientos cosísmicos del terremoto M_w 8,8 del Maule, de tipo subducción de 2010 (32.5°S - 38.5°S), y el terremoto M_w 6,2 de Aysén, tipo cortical superficial de 2007 (45.3°S). Estos inventarios representan las características desencadenantes de remociones en masa de los dos principales tipos de eventos sísmicos chilenos. En total, se mapearon 1.226 deslizamientos (área total afectada 120.500 km² aprox.) y 781 deslizamientos (área total afectada 1.350 km² aprox.), respectivamente. El volumen total removido es de 10,6 Mm³ aprox. por el terremoto del Maule y 122,3 Mm³ aprox. por el terremoto de Aysén. En ambos, los eventos se distribuyen de manera desigual en las áreas de estudio, predominando las remociones en masa disgregadas. El análisis estadístico de la base de datos del terremoto del Maule sugiere que el relieve y la litología son los principales factores geológicos que controlan los deslizamientos cosísmicos, mientras que el factor sísmico con mayor correlación con la ocurrencia de deslizamientos es la relación entre las aceleraciones máximas horizontales y verticales del suelo. Los resultados y la comparación con otros eventos sísmicos sugieren que el número de deslizamientos generados por terremotos de subducción es menor que los eventos provocados por terremotos corticales superficiales en al menos uno o dos órdenes de magnitud. Por otro lado, la base de datos de terremotos de Aysén sugiere que la distancia al plano de ruptura de las fallas es un factor de primer orden en la distribución de los deslizamientos junto con los efectos de sitio de amplificación topográfica.

Finalmente, a partir de la comparación de estos dos inventarios de deslizamientos inducidos por terremotos en Chile con otros del extranjero, se han determinado factores de controles topográficos, geomorfológicos, geológicos y sísmicos en la ocurrencia de remociones en masa cosísmicas provocadas por sismicidad cortical superficial y terremotos de subducción. Con estos resultados, se han construido cuatro duplas de modelos representativos de ambientes geomorfológicos de deslizamientos cosísmicos en los Andes del centro de Chile: Cordillerano Glacial, Cordillerano Fluvial, Cordillerano Plutónico y Frente de Montaña colindante a área urbana. Se indica el comportamiento esperado de las laderas durante los terremotos corticales superficiales y de subducción. Cada uno expresa características representativas sobre el peligro de remociones en masa cosísmicas (tipos, distribución espacial y tamaños), sus posibles consecuencias y sugerencias de posibles acciones de mitigación o intervenciones de ingeniería. Estos modelos son una herramienta poderosa para la evaluación del peligro de deslizamientos inducidos por terremotos.

Esta tesis ha proporcionado una visión más acabada de los deslizamientos cosísmicos chilenos, proporcionando una primera línea de base sobre los deslizamientos provocados por terremotos en Chile. El presente estudio describe las diferencias entre los factores condicionantes y las características de las remociones en masa provocadas por terremotos de subducción y terremotos corticales superficiales. Sobre esta base, estudios futuros podrán desarrollar metodologías para la evaluación del peligro de deslizamientos cosísmicos a escala regional adaptada a las condiciones tectónicas chilenas.

ABSTRACT OF THESIS FOR THE DEGREE OF:

Doctor of Science in Geology

BY: Alejandra Serey Amador

DATE: 07/10/2020

ADVISOR: Sergio A. Sepúlveda Valenzuela

**COSEISMIC LANDSLIDES DURING STRONG SHALLOW CRUSTAL AND
MEGATHRUST EARTHQUAKES: CONTROLLING FACTORS AND CONCEPTUAL
HAZARD GEOMODELS**

Chile is one of the most seismically active countries on Earth. Strong earthquakes in Chile are often associated with a chain of cascading hazards, such as ground shaking, liquefaction, tsunamis and coseismic landslides. In tectonically-active mountain areas, landslides represent the most frequent geological hazards and can cause major economic losses during and after strong earthquakes. Additionally, around the world, coseismic landslides kill thousands of people with an increasing trend driven by human interventions, increasing global population, and natural processes.

A key focus for research on seismically triggered landslides in high-mountain areas is the development of fully comprehensive, reliable inventories of coseismic landslides. There are different types of earthquake-induced landslides in Chile. Therefore, these need to be taken into consideration due to differences between crustal sources versus the megathrust plate boundary. The aim of this research is to identify the main characteristics of landslide occurrence during strong earthquakes in Chile. It seeks to improve the understanding of their mechanics, spatial distribution and geological controlling factors as well as to obtain qualitative inputs for the development of conceptual models for the recognition of coseismic landslides hazard in different mountain environments in the Chilean Andes. For these purpose, the earthquakes of Maule 2010 and Aysén 2007 were studied in detail.

First, two comprehensive coseismic landslides inventories were prepared: the M_w 8.8 megathrust Maule earthquake in 2010 (32.5°S - 38.5°S), and the M_w 6.2, shallow crustal Aysén earthquake in 2007 (45.3° S). These inventories are representative of the landslide triggering characteristics of the two main Chilean groups of seismic events. In total, 1,226 landslides (total affected area c.120,500 km²) and 781 landslides (total affected area c. 1,350 km²) were mapped, respectively. The total landslide volume triggered is c. 10.6 Mm³ by the Maule earthquake and c. 122.3 Mm³ by the Aysén earthquake. Both of them, the events are unevenly distributed in the study areas, dominantly disrupted slides. Statistical analysis of the Maule earthquake database suggests that relief and lithology are the main geological factors controlling coseismic landslides, while the seismic factor with higher correlation with landslide occurrence is the ratio between peak horizontal and peak vertical ground accelerations. The results and comparison with other seismic events elsewhere suggest that the number of landslides generated by megathrust earthquakes is lower than events triggered by shallow crustal earthquakes by at least one or two orders of magnitude. On the other hand, the Aysén earthquake database suggests that distance to the rupture plane of faults is a first-order factor in the distribution of landslides together with topographic amplification site effects.

Finally, from the comparison of these two local earthquake-induced landslide inventories in Chile with others from abroad it was possible to determine main controlling factors in the occurrence of coseismic landslides triggered by megathrust earthquakes and shallow crustal seismicity. With these results, four pairs of representative geomodels of coseismic landslide geomorphological environments in the Andes of central Chile were built: Glacial cordilleran, Fluvial cordilleran, Plutonic cordilleran and Mountain front bordering urban area. These geomodels provide expected slope performance during megathrust earthquakes and shallow crustal earthquakes. Each one exhibits representative characteristics of coseismic landslide hazards (main types, spatial distribution and sizes), their potential consequences and suggestions of possible mitigation actions or engineering interventions. These geomodels are a powerful tool for earthquake-induced landslide hazard assessment.

This pioneer thesis has supplied a deeper insight into Chilean coseismic landslides, providing a first baseline on landslides triggered by Chilean earthquakes. The present study describes the differences between conditioning factors and characteristics of landslides triggered by megathrust and strong shallow crustal earthquakes. Further studies could develop methodologies for seismically-induced landslide hazard assessment at a regional scale adapted for the Chilean tectonic conditions.

Es una cría
Creación y creador
♥

AGRADECIMIENTOS

A Sergio Sepúlveda, por ser un excelente guía en este camino del PhD, por ser un maravilloso referente en la investigación de las remociones en masa en Chile, y por sobre todo agradezco su inmensurable paciencia. Especialmente en épocas realmente complejas de la vida, tanto al inicio (gestación, nacimiento y puerperio) como al término de este viaje que es el PhD (pandemia). Más que guía, todos estos años, su rol ha sido de un jardinero.

El carpintero diseña un objeto que no existe y actúa de una forma tal que conduce a la producción del objeto deseado. Por ejemplo construye una mesa. Al hacerlo, el indudablemente toma materiales que están a su disposición pero no son mesa. Enseguida se apoya en su diseño para generar acciones que culminan con la producción de un objeto nuevo que, sin su intervención, no hubiera existido. El jardinero, por el contrario, hace algo diferente. Su intervención consiste simplemente en facilitar que se expresen en su mayor plenitud fuerzas ya existentes, de orientar la dinámica de agentes, que existen antes que el aparezca en escena y que tienen capacidad autónoma de crecimiento y desarrollo. Su obra es de otra naturaleza. Él no es responsable del crecimiento de sus plantas. Su labor se ve limitarlas a sembrarlas en un lugar y no en otro, a podarlas cuando correspondía, a regarlas a ponerlas a la luz y las temperaturas adecuadas, a abonar el terreno, etc. Sin embargo, las flores que ese jardín ahora ofrece son el resultado tanto de las “labores” de las propias plantas como del cuidado que a estas le ha prestado el jardinero. Lo que hace lo hace con el cuidado de no violentar, de no imponer, de tan solo facilitar el crecimiento de un ser autónomo, para que este alcance lo que él(ella) y solo él(ella) puede lograr.

Al Programa de Cooperación Internacional RCUK-Conicyt Newton Fund, proyecto NE/N000315/1 “Seismically-induced landslides in Chile: New tools for hazard assessment and disaster prevention” y al Fondecyt 1140317. A CONICYT PFCHA/ DOCTORADO NACIONAL /2015 – 21150559. A Dave Petley, Bill Murphy, Melanie Froude, Matt Brain por su amplio apoyo, basta sabiduría y paciencia. A los chilenos Sebastián Moya, Eleonora Muñoz, Marisol Lara, Jasson Tondreau y Camila Apablaza por su continuo soporte y experticia. A los integrantes de la comisión: Stella Moreiras y Gregory de Pascale, por su idoneidad, cooperación, infinita paciencia, ayuda y excelente disposición.

A Catalina Sandoval del equipo de Armadillo por tanto apañe con el inglés, excelente disposición y compromiso.

A mi manada de lobas, Artemisas, Sororitas, Útera y BDR. A mis ancestras. A mis amigas. A las científicas madres. Somos las nietas de las brujas que no pudieron quemar.

A la familia elegida, mis amadas amigas de la vida y sus crías: Mary, Paty, Ely, Natita de leche, Carito, Fran, Anto, Magda y Ais.

A toda mi amada familia biodanzante. A la comunidad en el mágico río Calcurrupe (camino de brujas y brujos), donde se está gestando la Universidad Biocéntrica del Sur. Porque no hay acto más político que el abrazo. Y como dijo Rolando Toro “Lucharemos

hasta el último de día por el cambio, un cambio afectivo” porque no es fácil para los humanos comprender que los frutos de la inteligencia procedan del amor.

Agradezco a la comunidad geológica beauchefiana amorosa. A mis compañeras y compañeros de postgrado: Estefa, Franki, Karli, Karen, Giss, Fran, Sam, Amanda, Seba, Atax, Tommy, David, Pablo, Bascu, Italo. A Verónica, Maritza, Blanca, Mariela, Rosa, Rosita, Yaki, Roberto, Julio, Omar, Mario y William.

A mi familia, mi madre, mi padre y mi hermano, porque sin su infinito e incondicional amor y apoyo en todos los momentos significativo de mi vida, simplemente no sería la persona quien soy.

Al Nico, por transitar, fluir, gozar, vivir el cotidiano durante la pandemia, enfrentarnos a los desafíos, surfear la ola de la vida, ir, volver, intentarlo otra vez, amarnos, compartirnos y habitamarnos.

Finalmente, quiero agradecerme a mí, por mi aguante, resiliencia ♥ y estar en constante transmutación junto a la cría.

CONTENTS

1. INTRODUCTION

1.1	GENERAL BACKGROUND.....	1
1.2	RESEARCH RATIONALE AND OBJECTIVES.....	6
1.2.1	RESEARCH HYPOTHESES.....	6
1.2.2	GENERAL OBJECTIVES.....	6
1.2.3	SPECIFIC OBJECTIVES.....	6
1.3	THESIS OUTLINE.....	7

2. STUDY AREAS

2.1	THE ANDES OF CENTRAL CHILE.....	9
2.2	THE PATAGONIAN ANDES.....	11

3. METHODOLOGY

3.1	COMPREHENSIVE COSEISMIC LANDSLIDE INVENTORY CRITERIA	14
3.1.1	METHODS.....	14
3.1.2	SELECTING REMOTE SENSING IMAGENS.....	15
3.1.3	COSEISMIC LANDSLIDES CLASIFICATIONS.....	16
3.1.4	COSEISMIC LANDSLIDES MAPPING CRITERIA.....	20
3.1.5	COSEISMIC LANDSLIDES DATABASES.....	22
3.1.6	STATISTICAL ANALYSIS OF COSEISMIC LANDSLIDES.....	23
3.2	EVALUATION OF CONTROLLING FACTORS OF COSEISMIC LANDSLIDES.....	24
3.3	CONCEPTUAL MODELS FOR THE RECOGNITION OF COSEISMIC HAZARD.....	25

4. COSEISMIC LANDSLIDES

4.1	INTRODUCTION.....	26
4.2	SHALLOW CRUSTAL SEISMICITY VS MEGATHRUST EARTHQUAKES.....	27
4.3	A NOTE ON TERMINOLOGY.....	28
4.4	REFERENCES OF EARTHQUAKES TRIGGERED LANDSLIDES.....	41
4.5	COSEISMIC LANDSLIDES DISTRIBUTION.....	31
4.6	FACTOR THAT INFLUENCE THE DYNAMIC RESPONSE OF HILLSLOPES UNDERGOING SEISMIC SHAKING.....	35
4.6.1	HILLSLOPE RELIEF.....	35
4.6.2	BEDROCK LITHOLOGY.....	36
4.6.3	SEISMIC FAULT EFFECTS.....	36

4.6.4	GROUND MOTION PARAMETERS.....	38
4.6.5	TOPOGRAPHIC AMPLIFICATION.....	39
4.6.6	ANTHROPIC FACTORS.....	40
4.7	THE LONG-TERM EVOLUTION OF COSEISMIC LANDSLIDES.....	41
5.	LANDSLIDES INDUCED BY THE 2010 CHILE MEGATHRUST EARTHQUAKE: A COMPREHENSIVE INVENTORY AND CORRELATIONS WITH GEOLOGICAL AND SEISMIC FACTORS	
5.1	INTRODUCTION.....	44
5.2	THE 2010 M _w 8.8 MAULE EARTHQUAKE.....	45
5.3	GEOLOGICAL AND GEOMORPHOLOGICAL SETTING OF THE COSEISMIC LANDSLIDES.....	47
5.4	THE 2010 M _w 8.8 MAULE EARTHQUAKE GROUND MOTION DISTRIBUTION.....	48
5.5	LANDSLIDES INDUCED BY THE 2010 MAULE MEGATHRUST EARTHQUAKE.....	52
5.5.1	LANDSLIDE INVENTORY AND CORRELATIONS WITH RELIEF AND GEOLOGY.....	52
5.5.2	SPATIAL ANALYSIS OF COSEISMIC LANDSLIDE DISTRIBUTION AND GROUND MOTION.....	57
5.6	DISCUSSION.....	61
5.7	CONCLUSION.....	66
6.	CASE STUDY: UPDATE COMPREHENSIVE INVENTORY OF LANDSLIDES INDUCED BY THE 2007 AYSÉN EARTHQUAKE	
6.1	INTRODUCTION.....	67
6.2	UPDATE COMPREHENSIVE INVENTORY.....	67
6.3	ANALYSIS OF COSEISMIC LANDSLIDES.....	72
6.4	DISCUSSION.....	75
6.5	CONCLUSIONS.....	76
7.	DEVELOPING CONCEPTUAL MODELS FOR THE RECOGNITION OF COSEISMIC LANDSLIDES HAZARD FOR SHALLOW CRUSTAL AND MEGATHRUST EARTHQUAKES IN DIFFERENT MOUNTAIN ENVIRONMENTS– AN EXAMPLE FROM THE CHILEAN ANDES	
7.1	INTRODUCTION.....	78
7.2	COSEISMIC LANDSLIDES IN THE MOUNTAIN ENVIRONMENT OF CHILE.....	79
7.2.1	THE SEISMOTECTONIC SETTING AND SEISMICITY OF CHILE.....	80
7.3	GEOMODEL CONSTRUCTION.....	83
7.3.1	DATA USED IN CONSTRUCTION OF THE GEOMODELS.....	83

7.3.2	DISTRIBUTION AND CHARACTERISTIC OF COSEIMIC LANDSLIDES FOR GEOMODELS IN THE CHILEAN ANDES...	84
7.3.3	FACTORS THAT INFLUENCE THE DYNAMIC RESPONSE OF HILLSLOPES UNDERGOING SEISMIC SHAKING.....	87
7.4	CONCEPTUAL HAZARD MODELS.....	90
7.4.1	GLACIAL CORDILLERAN ENVIRONMENT.....	90
7.4.2	FLUVIAL CORDILLERAN ENVIRONMENT.....	94
7.4.3	PLUTONIC CORDILLERAN ENVIRONMENT.....	98
7.4.4	MOUNTAIN FRONT ENVIRONMENT.....	102
7.5	DISCUSSION.....	106
7.6	CONCLUSION.....	109
8. FINAL DISCUSSION AND CONCLUSIONS		
8.1	FINAL DISCUSSION.....	111
8.2	THESIS CONCLUSION.....	116
8.3	FUTURE PERSPECTIVE.....	117
BIBLIOGRAPHY.....		119
ANNEX		

LIST OF FIGURES

2.1	Morphostructural and seismotectonic setting of central Chilean Andes.....	10
2.2	Morphostructural and seismotectonic setting of Patagonian Andes (45.5°S).....	13
3.1	Mentiroso Island Landslide complex.....	21
3.2	Mentiroso Island Landslide complex.....	21
4.1	Upper boundaries of area and epicentral distances for earthquake-induced landslides proposed by <i>Keefer (1984)</i>	32
4.2	Predicted total landslide volume plotted against estimated total landslide volume for 40 earthquakes (<i>Marc et al., 2015</i>).....	33
4.3	Frequency density function of landslides area (km ²), based on a theoretical law proposed by <i>Malamud et al. (2004)</i>	34
4.4	The long-term evolution of the surface area of landslides associated with the 2005 Kashmir earthquake, extracted from <i>Shafique (2020)</i>	42
5.1	Rupture zone, slip distribution (extracted from <i>Lorito et al., 2013</i>) and the isoseismal map (grey lines) inside the damage area of 2010 Maule earthquake (based upon data from <i>Astroza et al., 2012</i>).....	58
5.2	Simplified geologic map (modified from <i>SERNAGEOMIN, 2003</i>) and the distribution of slope angle in the area of 2010 coseismic landslide inventory.....	48
5.3	Interpolated maps of the peak ground accelerations of PGAH, PGAV and PGAH/PGAV ratio.....	51
5.4	Interpolated maps of the peak ground accelerations of PGVH, PGVV and PGVH/PGVV ratio.....	51
5.5	The comprehensive landslide inventory for the 2010 Maule earthquake.....	54
5.6	Histograms of landslide counts normalized by geologic unit based on landslide classification, simplified geologic units, landslides types and disaggregated slope intervals of 20°.....	56
5.7	Landslide concentrations (LC) normalized to the maximum concentration value.....	58
5.8	Scatter plots of landslide concentration (LC) vs PGAH/PGAV values obtained from map.....	59
5.9	N° landslides vs distance to rupture plane. LC vs Distance to rupture plane.....	61
5.10	Dependence of Total number of landslide N _{LT} and earthquake moment magnitude M _w to shallow crustal and megathrust earthquakes.....	62
5.11	Landslide relative position on the slopes.....	65
6.1	Update comprehensive inventory of landslides triggered by the 2007 Aysén earthquake.....	70
6.2	Frequency density function of landslides area (km ²).....	73
6.3	Landslide relative position on the slopes.....	74

6.4	Landslides counts normalized vs Distance to the faults.....	75
7.1	Morphostructural and seismotectonic setting of central Chilean Andes.....	81
7.2	Examples of landslides triggered by earthquakes in Chile.....	86
7.3	Glacial cordilleran environment. Conceptual geomodels of coseismic landslides induced by shallow crustal earthquake.....	93
7.4	Glacial cordilleran environment. Conceptual geomodels of coseismic landslides induced by megathrust earthquake.....	94
7.5	Fluvial cordilleran environment. Conceptual geomodels of coseismic landslides induced by shallow crustal earthquake.....	97
7.6	Fluvial cordilleran environment. Conceptual geomodels of coseismic landslides induced by megathrust earthquake.....	98
7.7	Plutonic cordilleran environment. Conceptual geomodels of coseismic landslides induced by shallow crustal earthquake.....	101
7.8	Plutonic cordilleran environment. Conceptual geomodels of coseismic landslides induced by megathrust earthquake.....	101
7.9	Mountain front bordering urban area environment. Conceptual geomodels of coseismic landslide induced by shallow crustal earthquake.....	104
7.10	Mountain front bordering urban area environment. Conceptual geomodels of coseismic landslides induced by meagathrust earthquake.....	105

LIST OF TABLES

3.1	Coseismic landslides classifications based on <i>Hungr et al. (2014)</i> and <i>Keefner (1984)</i> and examples from coseismic landslide in study areas.....	18
4.1	Glossary and abbreviations (Murphy, 2015).....	29
4.2	List of earthquakes triggered landslides reviewed in this thesis.....	30
3.2	Comparative table of comprehensive coseismic landslides inventories of Chile...53	
5.1	Data obtained from the Accelerograph Chilean Network, Universidad de Chile..49	
5.2	Comparative table of comprehensive coseismic landslides inventories of Chile...63	
6.1	Summary of most common correlations of coseismic landslides in the Chilean Andes contrasting the megathrust plate boundary earthquakes with crustal earthquakes.....	72
7.2	Terrain characteristics and coseismic landslide hazards for the Glacial Cordilleran environment.....	92
7.3	Terrain characteristics and coseismic landslide hazards for the Fluvial Cordilleran environment.....	96
7.4	Terrain characteristics and coseismic landslide hazards for the Plutonic Cordilleran environment.....	100
7.5	Terrain characteristics and coseismic landslide hazards for the Mountain front environment.....	103

7.6	Potential risks and suggested mitigation measures for coseismic landslides to be generated in the mountain environment of Chile.....	106
-----	--	-----

1. INTRODUCTION

1.1 GENERAL BACKGROUND

The term “landslide” is considered a North American word equivalent to the English word “landslip” in the Oxford English Dictionary (*Onions, 1993*). The term “landslip” was first introduced by *Lyell (1833)* in his masterpiece *Principles of Geology*, where it was defined as “a portion of land that has slid down in consequence of disturbance by an earthquake or from being undermined by water washing away the lower beds which supported it.” The first use of “landslide” appeared in the *Jeffersonian Magazine* published in Albany on the 10th of March 1838 under the heading “...the City of Natchez was thrown into consternation by a landslide” (*Cruden, 2003*). A variation of this term, “land slide,” was first observed in *Niles' National Register* on the 6th of October 1838 under the heading “Land slide in Vicksburg” (*Cruden, 1991*). *Sharpe (1938)* defined “landslide” as the perceptible downward slide or fall of a relatively dry mass of earth, rock, or mixture of the two. This term and its definition were adopted and updated by *Varnes (1958)* in his landslide classification system.

Landslides are a complex natural phenomenon that constitutes a serious natural hazard in many countries (*Brabb and Harrod, 1989*). Landslides are an important landscape forming process, providing the main mechanism for sediment release from slopes to permit transportation through the fluvial system (*Petley, 2010*). Thus, in advecting mountain chains, landslides play a key role in allowing the development of a long-term dynamic equilibrium between uplift and erosion, and in reducing slopes to their threshold angle (*Parker et al., 2011*). In so doing, landslides can directly impact humans (*Alexander, 2004*). Because the ability of the unprotected human body to withstand burial and/or impact by debris is limited, fatalities frequently result (*Sanchez et al., 2009; Petley, 2010a*), compounded by the roles that humans play in increasing landslide occurrence (*Petley, 2012*). Unfortunately, the concentration of loss causing landslides occurs in areas with high degrees of marginalization, which indicates that the most marginalized populations are the most prone to experience the effect of any sort of landslide (*Diaz et al., 2019*)

Massive rock avalanches are major geohazards in high-relief mountains and form some of the largest landslide deposits on Earth. For example, Komansu rock avalanche, a landslide with exceptional runout. The deposit is located in the central Alai Valley in southern Kyrgyzstan, originally covered an area $\sim 100\text{-}150\text{ km}^2$, contained a volume of about 8 km^3 and had a total runout length of $\sim 28\text{ km}$. It is thus one of the longest runout subaerial non-volcanic rock avalanches thus far identified on Earth. The landslide deposit is ancient – the slide has been dated at 5,000 to 11,000 years BP, which is the period after the retreat of the glaciers in this region (*Robinson et al., 2014*). These giant rock avalanches with long runout distances are clearly extremely destructive. As people increasingly populate the high mountains the likelihood of a mass fatality event, especially during a great magnitude earthquake, increases. Indeed, in tectonically-active mountain areas, landslides are also a major cause of fatalities and economic losses during and after great magnitude earthquakes (e.g. *Sepúlveda et al., 2005; Jibson et al., 2006; Qi et al., 2010; Dai et al., 2011*).

In nature, landslides trigger agents can be identified as rainfall, earthquakes, volcanic eruptions, or the undercutting of slopes by fluvial, coastal or weathering processes (*Grade & Crozier, 2005*).

Landslides triggered by earthquakes are common phenomena in the Andes of Central and southern Chile. This is attributed to main two factors: firstly, the tectonic evolution of Chile and secondly, the glaciation of the Andes resulting in variable geological conditions. The geological evolution of Andes has resulted from the effects of east-directed subduction of Pacific (and proto-Pacific) ocean floor beneath the South American continent. This subduction is the force that generated the Andes, which primary uplift dates back to a Miocene event, but whose emergence continues today, as exemplified by major earthquake activity (*Pankhurst and Hervé, 2007*). Consequently, Chile is known to be one of the most seismically active countries in the world, with regularly occurring earthquakes of moment magnitudes (M_w) exceeding 7 (*Lomnitz, 2004*). Megathrust seismicity ($M_w \geq 8$ interplate earthquakes in the subduction zone plate contact) has taken place approximately every dozen years and 10 megathrust earthquakes have occurred along the Chilean coast in the past century (*Barrientos, 2018*).

The second factor is that the Andes of Central and southern Chile is a glaciated mountain terrain, and as such, it features steep topography, strong erosional features and rock masses that have been weakened by the effects of ice action and last glacial cycles. *Clapperton (1994)* highlights that the pattern of glaciation/deglaciation of the Andes is complex and that changes in moisture in the atmosphere combined with lowering temperatures led to a complex change in snowline during the Pleistocene (e.g. slope instability related to permafrost degradation and debulking effect).

Several seismogenic zones are recognized in Chile based on the analyses of large earthquakes, the hypocentral locations of earthquakes large enough to be recorded at teleseismic distances, and studies of smaller earthquakes carried out with recent permanent and temporary local networks (*Barrientos, 2018*). In general terms, the Chilean earthquakes-induced landslides can be separated into two broad types of seismicity: megathrust earthquake and shallow crustal events.

Megathrust earthquakes could have a great capacity to induce large numbers of landslides and mobilise large volumes of sediment because of their comparatively high frequency of occurrence. For example, during the M_w 9.5 Valdivia earthquake extensive landsliding occurred (*Duke, 1960; Wright & Mella, 1963*). Three large landslides (2-30 Mm^3 of volume) on poorly consolidated sediments at the San Pedro River attracted particular attention due to the formation of landslide dams and the threat to the city of Valdivia c. 80 km from the slides (*Davis & Karzulovic, 1963*). *Serey et al. (2019)* provide an inventory of landslides induced by the 2010 M_w 8.8 Maule earthquake, one of the few world comprehensive, reliable inventory of coseismic landslides available for megathrust earthquakes. In total, 1,226 landslides were mapped over a total area of c. 120,500 km^2 , dominantly small disrupted slides. However, the estimated total landslide volume is only c. 10.6 $M m^3$. The events are unevenly distributed in the study area, the majority of landslides located in the Principal Andean Cordillera and a very constrained region near the coast on the Arauco Peninsula, forming landslide clusters (*Serey et al., 2019*). Additionally, *Candia et al. (2017)* showed that there were more coseismic landslides that impacted critical infrastructure in areas with the largest fault slip at the plate boundary during the 2015 M_w 8.3 Illapel earthquake (31.6°S).

Strong crustal earthquakes ($M_w \geq 6$) are important in seismic and coseismic hazard assessments because the strong motions that reach the surface due to limited distance for the seismic waves to attenuate and could be characterized through parameters such as PGA. For example, in Southern Chile, the Aysén Fjord earthquake (21 April 2007, M_w 6.2) triggered over 500 landslides of different types (*Sepúlveda et al., 2010*) of which the largest was the Punta Cola rock avalanche with a volume of c. 22 Mm^3 (*Oppikofer et al., 2012*). The triggering of landslides around and into the fjord resulted in a powerful displacement wave that killed eleven people (*Sepúlveda & Serey, 2009; Naranjo et al., 2009*).

A key focus for research on seismically triggered landslides in high-mountain areas has been the development of approaches to create reliable estimates of the likely pattern of landslides in future earthquakes. This has been usually undertaken through the development of statistical relations between specific earthquake events of different magnitudes and the number, area or volume of landslides triggered by each event (e.g. *Keefer 1984; Rodriguez et al., 1999; Malamud et al., 2004a; Malamud et al., 2004b; Marc et al., 2016; Havenith et al., 2016*). Recently *Marc et al. (2016)* compiled and analysed extensive databases of over 40 earthquakes ranging between M_w 5.1 and M_w 8.6, with a primary focus on shallow crustal earthquakes, allowing the presentation of a seismologically consistent expression for the total area and volume of populations of earthquake-triggered landslides. However, in comparison with shallow crustal earthquakes the number of complete landslide inventories for megathrust earthquakes is small, meaning that there is huge uncertainty in such estimates. Prior to this study, only one fully comprehensive, reliable inventory of coseismic landslides, based on field inventories and visual analysis of aerial or satellite images, has been available for megathrust earthquakes. This is the inventory for the 2011 M_w 9.0 Tohoku earthquake (*Wartman et al., 2013*). Therefore, there is a need to improve these datasets. The 2010 Maule earthquake provides a key opportunity to understand better the distribution and controls for the generation of landslides triggered by megathrust earthquakes. Hence, it is primal to complete and analyse landslide inventories for recent and different types of earthquakes in Chile, like the 2007 and 2010 events. With both datasets is possible to identify the main characteristics of landslide occurrence during strong earthquakes in Chile. This analysis seeks to improve the understanding of their mechanics, spatial distribution and geological controlling factors as well as to obtain qualitative inputs for

the development of models for coseismic landslides induced by shallow crustal and megathrust earthquakes in different mountain Cordilleran environment.

In the seismically active mountainous terrain, the coseismic landslides are contributing significant losses to the communities, infrastructure and modifying the landscape of the affected area (*Huang & Fan, 2013; Tang et al., 2016*). For example, the 2016 M_w 7.8 Kaikōura earthquake in New Zealand triggered more than 10,000 landslides over an area of about 10,000 km². Fortunately, the area affected by landslides is comparatively remote and there were no recorded landslide-related fatalities (*Stevenson, 2017*). However, the landslides dammed rivers, blocked roads and railways, and disrupted agricultural land throughout this region. In fact, the largest landslide triggered by the earthquake had an approximate volume of 20 (± 2) Mm³, with a runout distance of about 2.7 km, forming a dam on the Hapuku River (*Massey et al., 2018*).

Finally, it is estimated that around the world, coseismic landslides kill many thousands of people with an increasing trend driven by natural processes, increasing global population and human interventions (*Petley et al., 2006; Fan et al., 2019a; 2019b*). Furthermore, on a worldwide scale, coseismic landslides have attracted extensive attention among the scientists because the massive destructions that might produce. Unfortunately, spite our country is one of the most seismically active countries in the world, the term of earthquake-induced landslide is relatively new, and few coseismic landslide research and publication are found (*Sepúlveda et al., 2008; Sepúlveda & Serey 2009; Sepúlveda et al., 2010; Redfield et al., 2011; Oppikofer et al., 2012; Yugsi-Molina et al., 2012; Araya et al., 2013; Lastra et al., 2013; Hermanns et al., 2014; Sepúlveda et al., 2016*). Hence, this study provides a key opportunity to identify the main characteristics of landslide occurrence during high magnitude earthquakes in Chile and provide complete line base research about induced-earthquake landslides hazard in our country.

1.2 RESEARCH RATIONALE AND OBJECTIVES

1.2.1 RESEARCH HYPOTHESES

The hypotheses for this research are the following:

- Potentially damaging landslides can be induced by both shallow crustal and megathrust earthquakes in mountain environment of Chile and abroad.
- The landslides spatial distribution, volume and other characteristics depend on the earthquake type. Therefore, different seismic scenarios must be considered for hazard assessment and prevention measures.
- Detailed analyses of earthquake-triggered landslide inventories in Chile and abroad would allow the development of conceptual models for the recognition of coseismic landslides hazard for shallow crustal and megathrust earthquakes in different mountain environments in the Chilean Andes.

1.2.2 GENERAL OBJECTIVES

The purpose of this research is to identify the main characteristics of landslide occurrence during strong earthquakes in the Andes of central and southern Chile. It seeks to improve the understanding of their mechanics, spatial distribution and geological controlling factors as well as to obtain qualitative inputs for the development of conceptual models for the recognition of coseismic landslides hazard for shallow crustal and megathrust earthquakes in different mountain environments in the Chilean Andes.

1.2.3 SPECIFIC OBJECTIVES

Specific objectives of the research are the following:

1. To identify the main characteristics of coseismic landslides triggered by megathrust and shallow crustal earthquakes in the central and southern Chile.
2. To compare and differentiate topographic, geomorphological, geological and seismic controlling factors in the occurrence of earthquake-triggered

landslides originated by megathrust and shallow crustal earthquakes in central and Southern Chile.

3. To develop a series of conceptual models for the recognition of coseismic landslides hazard for shallow crustal and megathrust earthquakes in different environments in the Andes of central Chile.

THESIS OUTLINE

The main aims and the hypothesis that light this research area pointed out in the first chapter. Then, study areas and their main characteristic are present in the second section. The third chapter is concerned with the methodology used for this study.

The state of the art of coseismic landslides in Chile and abroad are summarized in Chapter four introducing the main focus of this thesis concerning on distinguishing coseismic landslides triggered by shallow earthquakes and megathrust earthquakes. Focusing on spatial analyses distribution and correlation with factors that influence the dynamic response of hillslopes undergoing seismic shaking.

Chapter five presents a comprehensive inventory of landslides induced by the M_w 8.8 2010 Maule earthquake between 32.5° S and 38.5° S, and to analyze their correlations with geological (lithology) slope and seismic factors (rupture distance, PGA, PGV), thereby providing new insight into the factors controlling coseismic landslides in megathrust earthquakes. This chapter was developed as manuscript that was published in *Landslides* (Serey et al., 2019). (Serey, A., Piñero-Feliciangeli, L., Sepúlveda, S.A. et al. *Landslides* (2019) 16: 1153. <https://doi.org/10.1007/s10346-019-01150-6>).

Chapter six provides an update comprehensive inventory of landslides induced by the 2007 M_w 6.2 Aysén earthquake and to analyze main seismic controlling factors in the occurrence of coseismic landslides.

Chapter seven gives an example of developing conceptual models for the recognition and management of landslides triggered by earthquakes in the Andean cordilleran environment. These have been split into slope performance during megathrust earthquakes and shallow crustal earthquakes. In addition to the identified hazards,

potential mitigation measures are outlined based on the rock slope engineering. This segment of the study correspond a published paper in the Quarterly Journal of Engineering Geology and Hydrogeology (Serey A; Sepúlveda, SA, Murphy, W; Petley DN; De Pascale, G (2020) *Developing conceptual models for the recognition of coseismic landslides hazard for shallow crustal and megathrust earthquakes in different mountain environments – an example from the Chilean Andes. Quarterly Journal of Engineering Geology and Hydrogeology*, <https://doi.org/10.1144/qjegh2020-023>).

Lastly, the final discussion and the most important conclusions of this research are summarized in Chapter eight.

2. THE STUDY AREAS

2.1 THE ANDES OF CENTRAL CHILE

The Andes represent the geodynamic archetype of a convergent, non-collisional mountain range, generated by subduction of the oceanic lithosphere of the Nazca (Farallon) Plate beneath the continental lithosphere of the South American Plate (*Pardo-Casas & Molnar, 1987*). Consequently, the present-day architecture of the Andes Mountains is largely the result of convergence between the Pacific–Nazca and South American plates. These mountains are a consequence of crustal shortening, principally accommodated by eastward thrusting, which leads to crustal thickening and surface uplift (*Isacks 1988; Sheffels 1990; Allmendinger et al., 1997*). Subduction is also evidenced by an almost continuous line of both active and dormant volcanoes, mostly andesitic stratovolcanoes, which run almost the entire length of the country.

The Andes of central Chile (32.5° S to 41.5° S) are composed of a number of morphostructural units from west to east: the Coastal Cordillera, the Central Valley, the Principal Cordillera (spanning Chile and Argentina), the Frontal Cordillera, the Argentine Precordillera and the Pampean Ranges (*Jordan et al., 1983*) (Figure 2.1). The Chilean Coastal Cordillera consists of low and topographically-smooth mountains composed predominantly of Late Paleozoic and Mesozoic igneous rocks, with paired belts of Paleozoic metamorphic rocks cropping out south of Pichilemu (34° S). The Central Valley is a depression with a Mesozoic to Quaternary sedimentary infill (*Pankhurst and Hervé 2007; Charrier et al., 2015*); from Santiago to the south, this is the main agricultural zone and contains several major cities, including the capital. The Principal Cordillera is a chain of high mountains with a strong relief and steep slopes that in its western part in Chilean territory mostly comprises Oligocene–Miocene continental volcanoclastic rocks, intruded by Miocene–Pliocene granitoids (*Pankhurst and Hervé 2007; Charrier et al., 2015*).

Longitudinally, the climate transits from Mediterranean to Temperate, with the annual rainfall increasing southward from ~250 to >2000 mm. In the Mediterranean segment, the annual precipitation is concentrated during the Austral Winter (June–Aug). Nonetheless, during the Austral Summer (Dec–Feb), the Principal Cordillera is affected by convective rainfall (*Tolorza et al., 2019*).

The Cordilleran environment is characterised by being an active, folded orogen with a high topographic relief and steep slopes. Cycles of high activity (driven by periods of relatively rapid uplift) that initiate periods of intense erosion as rivers cut down to lower base levels and produce steep-sided valleys. Many of these valleys have limited stability, with the immature weathered surfaces continually being eroded. Hillslopes are typically mantled with colluvium and/or taluvium that is unstable when undercut (*Tolorza et al., 2019*).

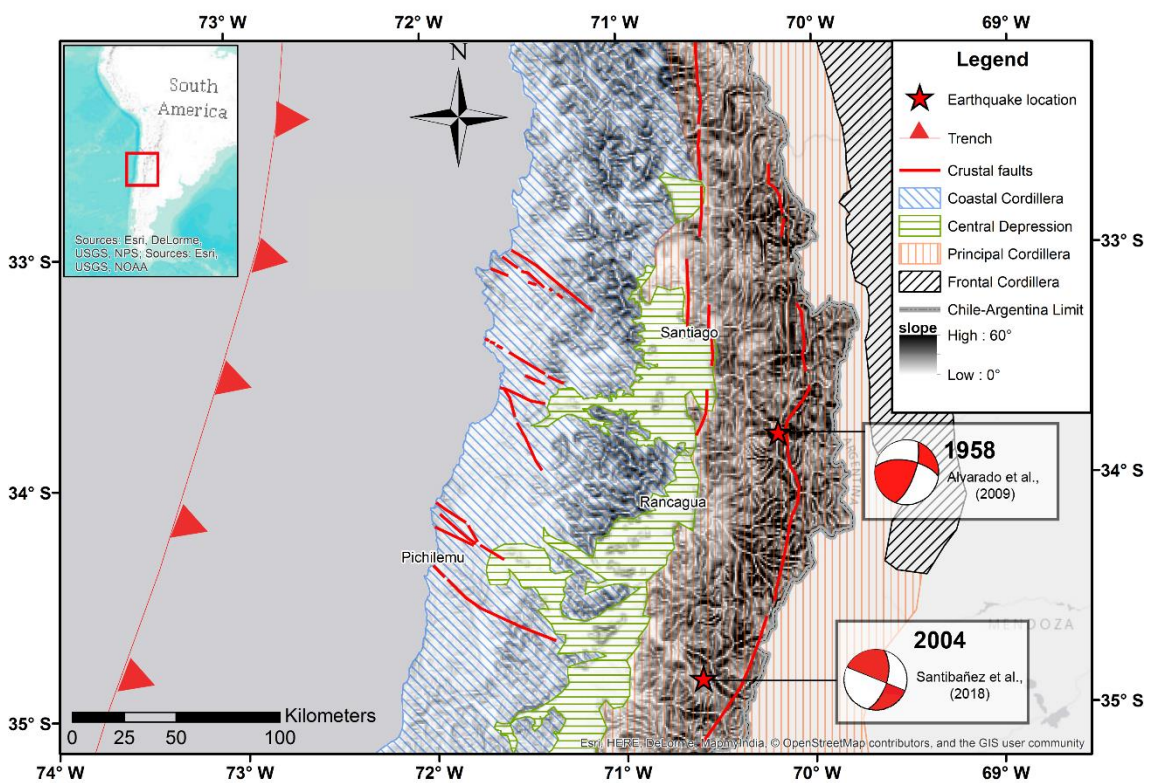


Figure 2.1. Morphostructural and seismotectonic setting of central Chilean Andes. Major crustal fault in the Chilean Andes extracted from *Armijo et al. (2010)* and *Santibañez et al. (2018)*.

2.2 THE PATAGONIAN ANDES

The southern part of Chile is characterized by the presence of a large number of fjords, termed the Patagonian fjordland. One of these is the Aysén Fjord an east-west oriented fjord located at 45°20'S and 73°10'W stretching in Chilean Patagonia with 65 km long. Bordering on the west by the Elephant Fjord, and on the east by the cities of Puerto Aysén and Puerto Chacabuco. On the north, side area the Macá and Cay volcanoes, as well as the Yulton and Meullín lakes. On the south side area the monogenetic volcanoes of the Pescado River and the Cóndor and Riesco lakes. It hosts many salmon farms, the most important economic activity of the region.

The study area (Figure 2.2) is located near the southern termination of the subduction margin between the Nazca and South American plates with a convergence rate estimated at ~6.6 cm/yr (*Angermann et al., 1999*). The fjord is crossed by the most relevant tectonic structure of the region, the Liquiñe-Ofqui Fault System (LOFS), a major NNE right-lateral strike-slip structure that accommodates the parallel component of the oblique subduction (*Cembrano & Hervé, 1993; Lavenu & Cembrano, 1994; Cembrano et al., 2002; Cembrano et al., 2007*). The LOFS is an active transpressive fault system that extends for ~1,200 km between 38° and 47°S (*Forsythe & Prior, 1992; Hervé, 1994; Cembrano et al., 1996; Lavenu & Cembrano, 1999; Cembrano et al., 2002; Legrand et al., 2011*). A large scale, the system is formed by two NNE parallel regional lineaments connected by at least four NE en échelon lineaments that define a duplex structure (*Hervé, 1994*).

The fjord cuts the North Patagonian Batholith (NPB), which is composed of three NNE trending belts of dioritic to granitic composition, the two lateral belts are Mesozoic and the central belt is Miocene (*Cembrano et al., 2002*). In the Aysén Fjord region, the plutonic complex mainly consists of foliated gabbros, diorites, quartz diorites, granodiorites, and tonalites, with some dyke swarms and gneissic bands (*Bartholomew, 1984*). At present, till and shallow volcanogenic soils cover the slopes in many places, which are mostly forested (*Sepúlveda et al., 2010*).

The high (> 1000 m) relief and geomorphology of this region is characterized by a primary tectonic control superimposed by glacial modeling. This combination results in

an abrupt relief of U-shaped valleys, the orientations of which follow the LOFS tectonic trend. At present, till and shallow volcanogenic soils cover the slopes in many places, which are mostly forested (*Sepúlveda et al., 2010*). In addition, long steep slopes mixed with high monthly precipitation rate (> 200 mm/month on average) leads to high erosion rates and landslide activity in the area (*Sepúlveda et al., 2010*). Glacial dynamic reconstructions by *McCulloch et al. (2000)* indicate that the study area became ice free ~15 ka ago.

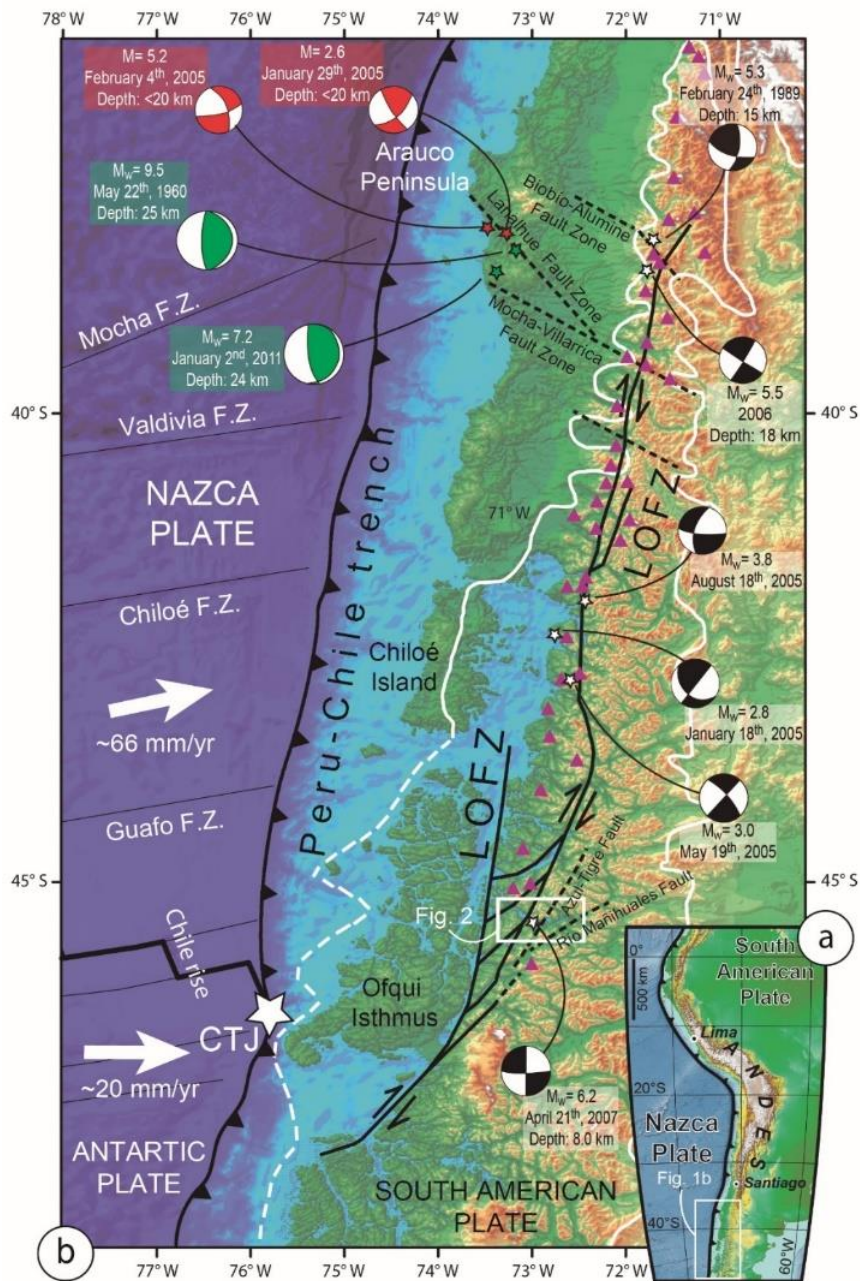


Figure 2.2. Morphostructural and seismotectonic setting of Patagonian Andes (45.5°S). (a) Geotectonic framework of South America showing regional tectonics (b) Regional tectonic context at the triple junction of the Nazca, Antarctic and South American plates. Regional map showing the location and extent of LOFS (continuous black lines), transverse fault systems (TFS; segmented black lines) and main volcanoes (purple triangles) [after *Hervé, 1994; Moreno & Naranjo, 2003; Rosenau et al., 2006; Cembrano & Lara, 2009*]. Published focal mechanisms of crustal earthquakes are shown for the LOFS (black), TFS (red) and megathrust earthquakes (green) [*Cifuentes, 1989; Barrientos & Acevedo-Aránguiz, 1992; Haberland et al., 2006; Lange et al., 2008; Legrand et al., 2011*]. Convergence velocity vectors after *Angermann et al. [1999]*. White lines show the approximate maximum extension of the Pleistocene ice sheet during the Last Glacial Maximum [modified from *Thomson et al., 2010*]. Figure extracted from *Villalobos et al. (2020)*.

3. METHODOLOGY

3.1 COMPREHENSIVE COSEISMIC LANDSLIDE INVENTORY CRITERIA

3.1.1 METHODS

An earthquake-triggered landslide inventory map can be prepared by several methods, including field investigations, visual interpretation of aerial photographs, digitizing paper-based landslide inventories, computer screen-based visual interpretation of high-resolution remote sensing images, and automatic extraction from remote sensing images (Xu, 2015; Hungr, 2018).

Field investigations were widely used before the remote sensing technology emerged. Nowadays it is almost impracticable to only rely on field investigations to prepare comprehensive and detailed inventories of earthquake-triggered landslides, but it is often a powerful tool for visual interpretation and verification of aerial photographs because some coseismic landslides recognized from aerial photographs or remote sensing images should be corroborated by inspection in the field to prove their objectivity (Hungr, 2018).

With the advent of the remote sensing technology, **visual interpretation of remote sensing images**, saving a large amount of fieldwork, has become the main method for preparation of landslide inventories. Computer screen-based visual interpretation of high-resolution remote sensing images (especially high-resolution satellite images) is currently the most popular method for preparing earthquake-triggered landslide inventory maps. In this method, at first, remote sensing images are precisely geographically registered; then landslides can be mapped based on the registered satellite images on a GIS platform. In addition, landslide inventory maps can be prepared based on threedimensional perspective of the digital elevation model (DEM) for more precise and objective visual interpretation. Recently, this method has become the most popular tool for earthquake-triggered landslide inventory mapping (Xu *et al.*, 2009a; b; 2013a; Dai *et al.*, 2011; Gorum *et al.*, 2011).

Due to the high cost and time associated with manual mapping of thousands or tens of thousands of landslides over large areas, automated mapping techniques are increasingly used (e.g. *Martha et al., 2010; Mondini et al., 2011; Parker et al., 2011*). **Automatic extraction from remote sensing images** is based on advanced remote sensing image processing technologies. Coseismic landslides can be separated by data processing and mathematical analysis. There are several advantages of this method such as high efficiency and quite high accuracy (*Martha et al., 2012; Moosavi et al., 2014*). However, pre-earthquake landslides, bare rocks, roads, and resident districts are easily extracted and mixed into coseismic landslides. Thus, obvious errors appear in inventories maps by just using earthquake-triggered landslides automatic extraction (*Parker et al., 2011; Xu et al., 2013a*).

Therefore, inventories of coseismic landslides should be constructed by the visual interpretation method rather than the automatic extraction of satellite images. Although the visual interpretation method is dominant in the preparation of earthquake-triggered landslide inventory maps, it should be supplemented with inspection in the field.

Both comprehensive coseismic landslides inventories discussed here, from the 2007 M_w 6.2 shallow crustal Aysén earthquake and the 2010 M_w 8.8 megathrust Maule earthquake, were based on field inventories and visual analysis of aerial or satellite images.

3.1.2 SELECTING REMOTE SENSING IMAGES

Making a truly comprehensive landslide inventory map requires remotely sensed imagery that meets several criteria; the more of these criteria that can be met, the more useful the resulting inventory map will be in subsequent analyses. Ideally, the imagery should meet the following criteria (*Harp et al., 2011; Xu, 2015*):

1. The imagery must be continuous and span the entire landslide distribution.
2. The imagery must have a resolution that allows identification of individual landslides as small as a few metres across.
3. Remote sensing images taken before an earthquake should be collected as much as possible.

4. Remote sensing images of pre-earthquake and post-earthquake should be obtained close to the time of earthquake occurrence for obtaining initial state of the terrain and infrastructure affected by the earthquake.
5. The imagery (as cloud-free as possible) must be acquired as soon as possible after the earthquake to capture the initial aspects of the landslides and the terrain or infrastructure that they affect.

Coseismic landslide triggered by the 2010 Maule earthquake were mapped by interpreting Landsat satellite images (Landsat 5-7-8; provider, NASA; resolution, 30 m) before and after the earthquake using Google Earth. A visual inspection of these strips was done at an eye height of ~ 1–2 km, decreasing the height when an alteration was detected in the vegetation, or when bare spots or typical mass movement morphologies were present (Soeters & Van Western, 1996). I visually inspected the earliest available images after the earthquake, mapping at 1:2000 and 1:10,000. Once a landslide was identified, the location was compared with the latest available preseismic image without cloud or snow cover and the landslide was mapped as polygon. Validation fieldwork was undertaken in the coastal regions, where the higher densities of landslides are located. The minimum size considered for the mapping was 30 m², although field inspections showed that an indefinite number of small mass movements were not recognised on the satellite images.

Coseismic landslide triggered by the 2007 Aysén earthquake were re-classified and re-mapped from the original inventory by Sepúlveda *et al.* (2010) during a field trip in February 2016, supplemented by interpretation of air photographs at different scales (1,20:000 to 1:70,000) and Landsat satellite images (Landsat 5-7-8; provider, NASA; resolution, 30 m), before and after the earthquake using Google Earth.



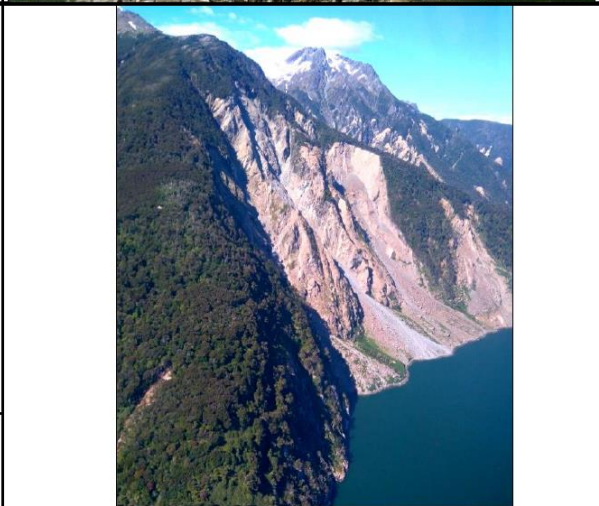
3.1.3 COSEISMIC LANDSLIDES CLASSIFICATIONS

A large number of landslide classification systems have emerged since the mid-19th century (Baltzer, 1875; Howe, 1909; Sharpe, 1938; Varnes, 1958; Hutchinson, 1968; Cruden and Varnes, 1996; Hungr *et al.*, 2014). One such classification system, the Varnes system (Varnes, 1958, 1978), has gained worldwide acceptance (IAEG, 1990; EPOCH, 1993; WP/WLI, 1993a, 1993b; Cruden and Varnes, 1996; USGS, 2008).





Varnes (1978) divided geomaterials into bedrock, debris, and earth, where “bedrock” referred to hard or firm rock that is intact and in its natural place before the initiation of mass movement, “debris” was material in which 20 to 80% of the fragments are larger than 2 mm in size, and “earth” was material in which approximately 20% or fewer of the fragments are larger than 2 mm, including a range of materials from non-plastic sand to highly plastic clay. *Hungr et al. (2001)* expressed doubt on the validity of the criterion that the 20% limit of coarse clasts (grain diameter larger than 2 mm) may not have a significant impact on the mechanical behaviour of the geomaterials. *Hungr et al. (2014)* proposed a list of geomaterials types simplifying existing soil and rock description systems of rock, clay, mud, silt, sand, gravel, boulders, debris, peat, and ice. However, they suggest that ambiguities in geomaterials type will always remain due to a lack of well-defined boundaries between different types of geomaterials (*Hungr et al., 2014*).

Keefner (1984) studied 40 historic earthquakes before 1980 to establish statistical relationships between the occurrence of earthquake-triggered landslides and some earthquake parameters. In addition, *Keefner (1984)* proposed a classification scheme of coseismic landslides which is based on the principles and terminology of the landslide classification of *Varnes (1978)*. It categorizes landslides primarily by material type prior to landslide initiation and character of movement, and secondarily by such other attributes as degree of internal disruption and water content. Material types are rock or soil in their engineering sense. An engineering soil is a loose, unconsolidated or poorly cemented aggregate of solid particles, derived from breakdown of rock material by weathering and/or erosion (*Bell, 2000*). Rock and soil slumps and block slides are grouped as ‘coherent slides’, while rock and soil falls and avalanches, rock slides and disrupted soil slides are grouped as ‘disrupted slides’ (see Table 3.1 for illustration).

Table 3.1 Coseismic landslides classifications based on *Hungr et al. (2014)* and *Keefer (1984)* and examples from coseismic landslide in study areas.

Landslides Types (<i>Hungr, 2014</i>)	Keefer's (1984) grouping of landslides	Examples
<p>Rock avalanches. Extremely rapid, massive, flow-like motion of fragmented rock from a large rock slide or rock fall.</p>	<p>Disrupted slides and falls</p>	
<p>Example: Punta Cola rock avalanche (triggered by the 2007 Aysén earthquake)</p>		
<p>Rock planar slide. Rock wedge slide. Rock rotational slide ("rock slump")</p>	<p>Coherent slides. Slumps that fragment can fall into the "disrupted slides and falls" category</p>	
<p>Example: Rock block slides and falls on the Aysen fjord (triggered by the 2007 Aysén earthquake)</p>		
<p>Rock irregular slides ("rock collapse"). Sliding of a rock mass on an irregular rupture surface consisting of a number of randomly oriented joints, separated by segments of intact rock ("rock bridges"). Occurs in strong rocks with non-systematic structure. Failure mechanism is complex and often difficult to describe Often very sudden and extremely rapid.</p>	<p>Disrupted slides and falls</p>	
<p>Example: Rock slides in Mentirosa Island Landslides complex (triggered by the 2007 Aysén earthquake)</p>		

* Photographers: Alejandra Serey, Sergio Sepúlveda and Gregory De Pascale.

Landslides Types (<i>Hungr, 2014</i>)	Keefe's (1984) grouping of landslides	Examples
<p>Debris avalanches. Defined as very rapid to extremely rapid shallow flow of partially or fully saturated debris on a steep slope, without confinement in an established channel. Occurs at all scales.</p>	<p>Disrupted slides and falls</p>	
<p>Example: Debris avalanches in Acantilada Bay (triggered by the 2007 Aysén earthquake)</p>		
<p>Debris slides. Sliding of a mass of granular material on a shallow, planar surface parallel with the ground. Usually, the sliding mass is a veneer of colluvium, weathered soil, or pyroclastic deposits sliding over a stronger substrate. Many debris slides become flow-like after moving a short distance and transform into extremely rapid debris avalanches.</p>	<p>Disrupted slides and falls</p>	
<p>Example: Debris slide in Arauco Peninsula (triggered by the 2010 Maule earthquake)</p>		
<p>Debris flow. Very rapid to extremely rapid surging flow of saturated debris in a steep channel. Strong entrainment of material and water from the flow path.</p>	<p>Lateral spreads and flow slides.</p>	
<p>Example: Debris flow in Estero Frio (triggered by the 2007 Aysén earthquake)</p>		
<p>Liquefaction spread. Extremely rapid lateral spreading of a series of soil blocks, floating on a layer of saturated (loose) granular soil, liquefied by earthquake shaking or spontaneous liquefaction.</p>	<p>Lateral spreads and flow slides</p>	
<p>Example: Lateral spread (triggered by the 2010 Maule earthquake, image extract from <i>Duhart et al. 2010</i>)</p>		

* Photographers: Alejandra Serey, Sergio Sepúlveda and Gabriel Orozco.

3.1.4 COSEISMIC LANDSLIDES MAPPING CRITERIA

The landslide inventory should be constructed as polygons to ensure that it can be used to perform future statistical analysis of the landslides. The principles include the following criteria: all landslides should be mapped as long as they can be recognized from images; both the boundary and source area position of landslides should be mapped; spatial distribution pattern of earthquake-triggered landslides should be continuous; the bundling of several adjacent landslides into a single map polygon, known as amalgamation effect, should be divided into distinct events.

Amalgamation typically occurs when the spatial density of landslides is high and the resolution of images from which they are mapped relatively low, making it difficult to differentiate multiple landslides in a perturbed area. Coalescence of multiple small slope failures into a larger landslide area may locally prevent the correct identification of the smallest failures (*Malamud et al., 2004a*). If uncorrected, amalgamation can lead to severely erroneous results and interpretations in many domains (*Marc & Hovius, 2015*). Landslide depth is often assumed to scale with area, giving rise to strongly non-linear area– volume relations, which assign disproportionate importance to landslides with the largest surface areas. Accurate landslide area mapping, differentiating precisely between individual events is therefore of most importance (*Li et al., 2014*). This also applies to studies considering the area–frequency distribution of landslides, whether to assess landslide hazard and risk associated with extreme events (*Malamud et al., 2004b*). Finally, any attempt to understand the physics of landslide triggering from mapped landslide patterns could suffer from the effects of incorrectly mapped landslide outlines and the artificial prominence of large disturbed areas (*Montgomery & Dietrich, 1994; Meunier et al., 2008*).

A good example is the **Mentirosa Island Landslide complex**, Chilean Patagonia (Figures 3.1 and 3.2). Triggered by the M_w 6.2 Aysén earthquake on 21 April 2007 on the Liquiñe-Ofqui Fault zone (LOFZ), this was one of the largest of a total 538 mapped earthquake-triggered landslides (*Sepúlveda & Serey 2009; Sepúlveda et al., 2010*), with an estimated total volume of 8 million m^3 (*Sepúlveda & Serey, 2009*). It is located less than 5 km from the earthquake epicentre.

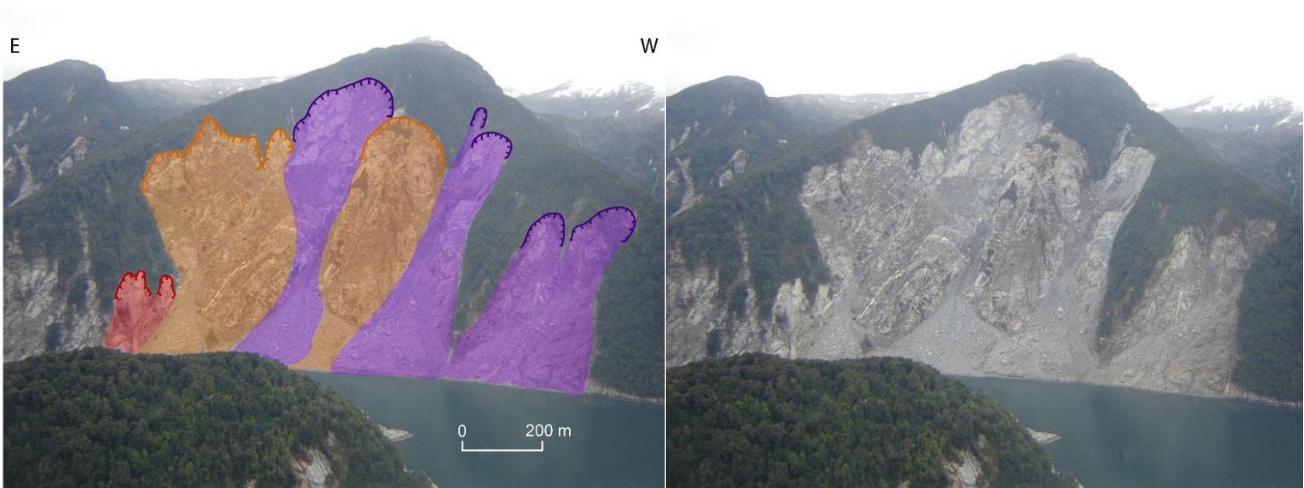


Figure 3.1. Mentirosa Island Landslide complex. In purple rockslides, in orange debris avalanches, in red rockfalls. The scar for each is shown.

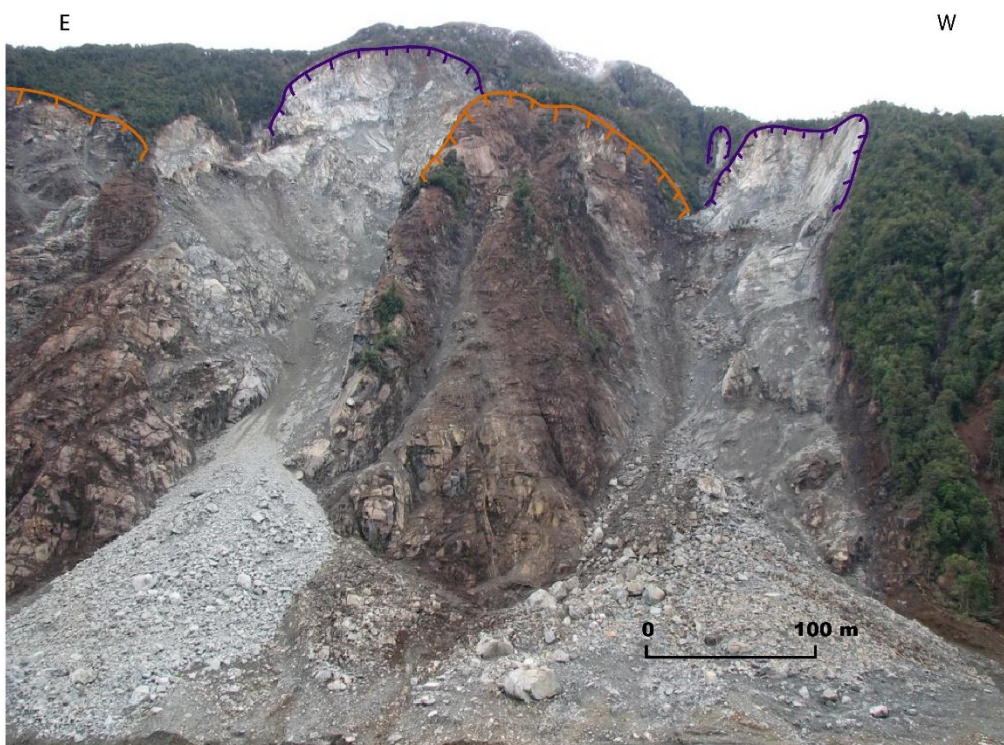


Figure 3.2. Mentirosa Island Landslide complex. In purple rockslides scars, in orange debris avalanches scars.

3.1.5 COSEISMIC LANDSLIDE DATABASES

Coseismic landslide inventory maps and accompanying geo-referenced databases may contain a wide variety of data. The essential information and mapping criteria includes the following:

- All coseismic landslides should be mapped as long as they can be recognized from images. *Harp et al. (2011a)* suggested an ideal landslide inventory should contain all of the landslides that are possible to detect down to sizes of 1-5 m in length. For example, if moderate resolution remote sensing images are used, such as ASTER (15 m resolution of multispectral images), only landslides of length at least larger than 15 m can be detected. In some actual inventories, landslides of small scales, for example less than 10 m in length, often occupy a relatively small proportion (*Xu, 2015*).
- Coseismic landslide type, using a classification system that is capable of reflecting the mechanism of motion and its likely character. It can be the *Keefe (1984)* classification for earthquake-induced landslides or the recent update research based on a renewed Varnes classification of landslide types, developed by *Hungr et al. (2014)*. Validation fieldwork has to be undertaken.
- The entire area perturbed by a coseismic landslide, including scar, runout and deposit, should be delineated as a single polygon. In addition, to achieve better identification, the landslides source areas should be extracted and expressed as points or polygons. At present, delineating landslide source areas from remote sensing images is often subjective because the lower boundary of a source area of a landslide is difficult to recognize.
- Coseismic landslides recognition should avoid the effects of amalgamation in landslides mapping. Coalescing landslides should be divided into individual ones. Several landslides often occur on a natural slope because high density and large number of earthquake-triggered landslides. An individual landslide shows source area integrity consistency on the remote sensing image, and topography of the landslide shows performance of the same natural slope. If source areas of two

landslides or more are separated, we should separate these landslides based on expert knowledge, remote sensing image and topographic characteristics, and selected field investigation even their accumulated materials are connected together. In short, the baseline of differentiation of individual landslides is to consider consistency of landslide material and integrity of landslides. Several individual landslides in low-resolution images may be misjudged into a single larger landslide because the distances of them are less than the resolution of the image. Therefore, the higher resolution of the images used, the easier individual landslides are separated and the more objective landslide inventory maps prepared (Xu, 2015).

- Spatial distribution of coseismic landslides should be continuous. This includes two meanings: one is that there should be no image covered blank areas, which is accepted by the majority of researchers. The other is that a few abnormal landslides scattered far away from the earthquake source should be excluded from the landslide inventory, because these landslides often occur on slopes, which are highly prone to slide, but with little relevance to the earthquake (Xu, 2015).

3.1.6 ANALYSIS OF COSEISMIC LANDSLIDES

The spatial analysis of coseismic landslide distribution consisting of the following measures.

- Total area affected (Km²)
- Maximum distance to the epicentre (km)
- Frequency density function of landslides area, based on Inverse-Gamma distribution function, a theoretical law proposed by *Malamud et al. (2004a)*
- Total landslide volume estimated using published area–volume relationships proposed by *Larsen et al. (2010)* (Mm³)

Furthermore, the compiled datasets have to be compared with the curves by *Keefner (1984)* and *Rodriguez et al. (1999)* regarding the maximum landslide area and the epicentral distance.

Volume

Larsen et al. (2010) published area–volume relationships that can be used to estimate the volume of a landslide,

$$V' = \lambda A'^{\gamma}$$

Where the predicted volume V' of a given landslide area A' depends on a scaling exponent γ and intercept λ .

From mapped disturbed areas A' ($\lambda=0.146$ and $\gamma=1.33$ for mixed bedrock and soil failures, while $\lambda=0.234$ and $\gamma=1.41$ for bedrock landslides). It can be assumed that landslides with $A' > 10^5$ m² involved bedrock, and that smaller landslides were mixed bedrock and soil failures (*Marc et al., 2016*). Coseismic landslide inventories maps typically do not distinguish between scar and deposit, lumping the two into one area measure. According to *Larsen et al. (2010)*, scars and deposits have area–volume relations with the same power-law exponent, implying constant size ratios between scar and deposit areas of 1.1 and 1.9 for mixed and bedrock landslides, respectively. Hence, it is possible to estimate the scar area (A') by dividing the mapped landslide area by 2.1 and 2.9 for mixed and bedrock landslides, respectively, assuming that runout was equal to the scar length.

3.2 EVALUATION OF CONTROLLING FACTORS OF COSEISMIC LANDSLIDES

The 2010 M_w 8.8 Maule earthquake

First of all, it was necessary the construction of a simplified geologic map and the distribution of slope angle in the area of the 2010 Maule earthquake coseismic landslide inventory (elevation data for the slope angle map is coming from ASTER GDEM, product of METI and NASA, resolution 30 m). Then, correlations of coseismic landslide types with relief and bedrock lithology were tested through histograms of landslide counts normalized by simplified geologic unit area vs landslide classification and slope.

The spatial pattern of landslides was analysed calculating a map of landslide density or landslide concentration (LC) prepared with the GMT (Generic Mapping Tools) and

Python. The calculation was done across a moving grid of size $0.5^\circ \times 0.5^\circ$ through the 120,500 km² landslide-affected area. LC was defined as:

$$LC = (\text{Sum area of all landslides within the grid}) / (\text{total area of the grid}).$$

Python and GMT (Generic Mapping Tool) scripting were used for the implementation of the calculation.

Scatter plots of LC against PGVH, PGVV, PGVH/PGVV, PGAH, PGAV and PGAH/PGAV are part of the spatial analysis of coseismic landslides distribution and ground motion. I also evaluated the potential correlation between LC parameter with distance to rupture plane calculating the landslide smallest distance (linear distance). The rupture plane grid points were obtained by joint inversion from *Lorito et al. (2011)*, and the smallest distance was calculated using a Matlab script developed by *Escobar (2013)*.

The 2007 M_w 6.2 Aysén earthquake

Whereas for the inventory of the 2007 Aysén earthquake, I used a histogram to determine the correlation of coseismic landslides with distance to the seismic faults. Finally, for both Chilean comprehensive inventories, I evaluated if topographic site effects influenced the triggering of landslides during earthquakes through a graphic method proposed by *Meunier et al. (2008)* that represent the position of coseismic landslides on the slopes, combining the normalised distance of the landslide top to the ridge crest and the normalised distance of the landslide toe to the nearest stream.

3.3 CONCEPTUAL MODELS FOR THE RECOGNITION OF COSEISMIC HAZARD

From the database contained on the two Chilean comprehensive coseismic landslides inventories (*Sepúlveda & Serey 2009; Sepúlveda et al. 2010; Serey et al. 2017; Serey et al. 2019; and this work*), in addition to data from landslide inventories from the geologic record proposed as likely induced by seismic activity (*Antinao & Gosse, 2009; Moreiras & Sepúlveda, 2015*), I have determined topographic, geomorphological, geological and seismic controlling factors in the occurrence of earthquake-triggered landslides. With

these results, I have built four representative geomodels of coseismic landslide geomorphological environments in the Andes of central Chile. For the graphic construction of geomodels, Adobe Illustrator cs6 was used.

4. COSEISMIC LANDSLIDES

4.1 INTRODUCTION

Seismically triggered landslides are a major hazard and cause of secondary losses associated with earthquakes, with effects sometimes exceeding those of direct shaking (*Bird & Bommer, 2004*). Moreover, they have been found to be important actors in mountain building and landscape evolution (*Hovius et al., 2011; Li et al., 2014*).

The documentation and synthesis of data on landslide occurrence during earthquakes has led to greatly increased understanding of the hazards associated with earthquake-induced landslides and to the development of models and methods for hazard mapping and evaluation. However, the number of earthquakes with relatively complete data on landslide occurrence is still small, and one of the most pressing research needs is for complete landslide inventories for many more events in a wider variety of environments. Whereas many additional inventories in all regions are needed, data from seismically active regions of continental Asia and the Middle East, the Andean region of South America, the tropical western Pacific, and intraplate regions worldwide would be especially desirable. Such additional data, coupled with the increasing use of GIS and other current analytical tools should lead to substantial additional refinements in models relating seismic shaking and geologic conditions to slope failure, and thus to our ability to minimize damage and loss of life from seismically generated landslides (*Keefer et al. 2002*).

This chapter reviews the characteristics of earthquake-induced landslides and principal factors that influence the dynamic response of hillslopes undergoing seismic shaking.

4.2 SHALLOW CRUSTAL SEISMICITY VS MEGATHRUST EARTHQUAKES

In the tectonic setting of Chile, seismicity is related to different mechanisms. Several seismogenic zones are recognized in Chile: large interplate earthquakes (depths 45–55 km); large intermediate-depth earthquakes (60–200 km); shallow crustal seismicity (depths 0–20 km); and outer-rise earthquakes along the subduction margin between the Nazca and South American Plates (*Barrientos, 2018*). The main Chilean earthquake-induced landslides are megathrust earthquake and shallow crustal events.

Megathrust seismicity corresponds to high magnitude (above 8) interplate earthquakes in the subduction zone plate contact. Because of their comparatively high frequency of occurrence, these earthquakes are responsible for most of the historic damage. They are located along the coast from Arica (18° S) to the triple junction at Taitao Peninsula (46° S). These events take place as a result of the convergence of the Nazca beneath the South American plate at a rate of about 7.4 cm/yr (*Argus et al., 2010*). Further south, the Antarctic plate subducts beneath the South American plate at a rate of ~8.1 cm/yr (*Lara et al., 2018*). $M \geq 8$ earthquakes are usually accompanied by notable coastal elevation changes and, depending on the amount of seafloor vertical displacement, by catastrophic tsunamis. Their rupture zones extend down to 45–53 km depth (*Tichelaar & Ruff, 1991*) and their lengths can reach well over 1000 km. Return periods for $M \sim 8$ (and above) events are of the order of 80–130 years for any given region in Chile, and about a dozen years when the country is considered as a whole (*Barrientos, 2018*). The latest examples of this type of earthquakes were the 2010 M_w 8.8 Maule, the 2014 M_w 8.2 Iquique, and the 2015 M_w 8.3 Illapel earthquakes (*Barrientos et al., 2004; Candia et al., 2017; Barrientos, 2018*). Megathrust earthquakes seem to have much longer return periods, of the order of a few centuries for any given region (*Cifuentes, 1989; Barrientos and Ward, 1990*). Recent off-fault strong ground motion indicator paleoseismological studies carried out in southern Chile indicate recurrence intervals of ~300 years for these very large earthquakes (*Cisternas et al., 2005; Moernaut et al., 2014*).

Shallow crustal seismicity is important in seismic and coseismic hazard assessments because the strong ground motions (measured in % of gravity as peak ground accelerations, or PGA) that reach the surface due to limited distance for the seismic waves to attenuate. Shallow crustal seismicity (0–20 km) that occurs throughout Chile such as

the Cordilleran region of south–central Chile (e.g. Liquiñe-Ofqui fault zone) is a consequence of the oblique convergence of the Nazca Plate. Magnitudes up to 7.1 have been reported for earthquakes in this region (44,5°S y 73°W, 21 November 1927) (*Greve, 1964*). The Andean Principal Cordillera in the central part of Chile is also an important area with important crustal seismicity because of the risk to high population density and critical infrastructure. *Godoy et al. (1999) and Barrientos et al. (2004)* carried out structural and seismicity studies to understand this region, in which the largest recorded earthquake (less than 10 km depth) took place on 4 September 1958 (M 6.3, *Alvarado et al., 2009*), causing extensive rockfalls and a few large landslides (*Sepúlveda et al., 2008*). Shallow crustal seismicity with a relative large magnitude (> 5.5) was recently observed beneath the Andes main Cordillera at latitudes 19.6° S (Aroma; July 2001), 35.8° S (Melado River; August 2004), 38° S (Barco Lagoon; December 2006), and 45° S (Aysén Fjord; April 2007). All these events show significant strike-slip component of displacement (*Barrientos, 2018*).

4.3 A NOTE IN TERMINOLOGY

The study of coseismic landslides crosses geology, geotechnical engineering, and seismology. Therefore, terms in common usage in one field may not be readily known to other readers. Table 2.1 provides a glossary of terms that includes the abbreviation, full name, and a brief description (along with a citation as appropriate). For example, peak ground acceleration (PGA) will always be given as a fraction of the acceleration due to gravity (i.e., a PGA of 0.5 g is $\sim 4.9 \text{ m/s}^2$).

Table 4.1. Glossary and abbreviations. Extracted from *Murphy (2015)*.

Abbreviation	Term	Brief Description
α	Slip surface angle	The angle of the sliding surface in a planar stability model, or an angle of thrust.
A_{crit}	Critical acceleration	The threshold acceleration for a slope to accumulate displacement. Sometimes given the notation K_c .
D_N	Newmark displacement	The calculated displacement, measured in centimetres, of a sliding block subjected to a forced vibration.
D	Duration	The time over which shaking occurs. This is often expressed as a "bracketed" duration that is the duration between the first and last occurrences of a given acceleration (normally 0.01 or 0.05 g).
d	Epicentral distance	The distance between the earthquake epicenter and the landslide (or any given site of interest). Given in kilometers. " d_{hyp} " is used to describe "hipocentral" distance, that is, the distance in kilometers between the hypocenter and the site of interest.
	Epicenter	The geographic location of an earthquakes. Normally given in latitude and longitude
F	Factor of safety	The ratio of shear strength to shear stress in slope-stability calculations for the ambient (nonsesimic) state of stress
f	Frequency	The number of cycles of loading per second of an earthquake ground motion. Frequency is expressed in Hertz (Hz). The same data are often presented as "period" ($1/f$), which is measured in seconds.
	Focal depth	The depth from the ground surface to the point of nucleation of an earthquake
g	Acceleration due to gravity	Ground accelerations are given as a decimal fraction of g, for example, 0.5 g is a ground motion of 4.9 m/s^2
	Hypocenter	The location of an earthquake in three dimensions-normally described in terms of latitude, longitude, and focal depth. This is normally the point of rupture initiation.
I_a	Arias intensity	A description of earthquake ground motions, which is a function of the middle 90 percent of the energy recorded arriving at a site. Expressed as metres per second.
k, k_h, k_v	Seismic coefficient	Additional stress component applied to a pseudostatic slope-stability analysis to represent additional loading from earthquake shaking. k_h refers to the seismic coefficient in a horizontal direction and k_v refers the loads applied in the vertical direction.
M	Earthquake magnitude	This is a description of the amount of energy released by an earthquake. Numerous different magnitude scales are used. The most common are

		M_w , M_s , and M_L . They are moment magnitude, surface wave magnitude, and local magnitude.
<i>PGA</i>	Peak ground acceleration	The maximum ground motion recorded on an acceleration-time (accelerogram) history.
<i>PGD</i>	Peak ground displacement	The maximum ground motion recorded on a displacement-time (seismogram) history.
<i>PGV</i>	Peak ground velocity	The maximum ground motion recorded on a velocity-time history.
V_s	Shear wave velocity	The speed at which shear waves propagate through the ground. It is often used as an indicator of ground conditions on site. A shear wave velocity of 760 m/s is the boundary between engineering soils and engineering rocks.

4.4 REFERENCES OF EARTHQUAKES TRIGGERED LANDSLIDES

Table 4.2. List of main earthquakes triggered landslides reviewed in this thesis.

Earthquake	Year	M_w	Earthquake type	References
Daily City, CA, USA	1957	5.3*	shallow crustal	<i>Keefer (2002)</i>
Guatemala	1976	7.6	shallow crustal	<i>Keefer (2002)</i>
Coalinga, CA, USA	1983	6.5	shallow crustal	<i>Keefer (2002)</i>
Loma Prieta, CA, USA	1989	7.0	shallow crustal	<i>Keefer (2002)</i>
Finisterre, Papua Guinea	1993	6.9	shallow crustal	<i>Meunier et al., (2007)</i>
Northridge, CA, USA	1994	6.7	shallow crustal	<i>Jibson (1995)</i>
Hyogoken-Nanbu, Japan	1995	6.9	shallow crustal	<i>Keefer (2002)</i>
Umbria-Marche, Italy	1997	6.0	shallow crustal	<i>Keefer (2002)</i>
Chi-chi, Taiwan	1999	7.6	shallow crustal	<i>Huang et al., (2001); Khazai and Sitar, (2004); Sepúlveda et al., (2005); Lin et al., (2006)</i>
Kashmir, Pakistan	2005	7.6	shallow crustal	<i>Owen et al., (2008); Kamp et al., (2010); Khattak et al., (2010); Saba et al., (2010); Mahmood et al., (2015); Shafique, (2020)</i>
Aysén, Chile	2007	6.2	shallow crustal	<i>Sepúlveda et al., (2010)</i>

Wenchuan, China	2008	8.3	shallow crustal	<i>Fan et al., (2009); Huang and Li, (2009); Tang et al., (2009); Xu et al., (2009a); Xu et al., (2009b); Qi et al., (2010); Xu and Li, (2010); Dai et al., (2011); Gorumn et al., (2011); Parker et al. (2011); Xu et al., (2012); Xu and Xu, (2012); Wang et al., (2012); Tang et la., (2016); Zhang and Zhang, (2017); Fan et al., (2019a)</i>
Canterbury, New Zealand	2010	7.1	shallow crustal	<i>Gledhill et al., (2011); Bradley, (2012)</i>
Christchurch, New Zealand	2011	6.2	shallow crustal	<i>Kaiser et al., (2012); Stirling et al., (2012)</i>
Lushan, China	2013	6.6	shallow crustal	<i>Tang et al., (2015); Wang (2015)</i>
Kaikōura, New Zealand	2016	7.8	shallow crustal	<i>Stevenson, (2017); Massey et al., (2018)</i>
Nyingchi, China	2017	6.4	shallow crustal	<i>Zhao et al., (2019)</i>
Valdivia, Chile	1960	9.5	megathrust	<i>Davis & Karzulovic, (1963)</i>
Pisco, Perú	2007	8.0	megathrust	<i>Lacroix et al. (2013)</i>
Tohoku, Japan	2011	9.0	megathrust	<i>Wartman et al. (2013)</i>
Illapel, Chile	2015	8.3	megathrust	<i>Candia et al., (2017)</i>

*Earthquake magnitudes are all moment or equivalent moment magnitudes except for Daily City (local magnitude)

4.5 COSEISMIC LANDSLIDE DISTRIBUTION

Statistical relationships between earthquake events of different magnitudes and the number, area or volume of triggered landslides have been developed from different case studies. The simplest approach was introduced by *Keefe (1984)*, who compiled a dataset of over 40 landslide inventories from large earthquakes. The resulting relationship between number of landslides, area affected by landslides or epicentral distance of those landslides and earthquake magnitude provides a first order estimate of the likely impacts. Subsequent studies (e.g. *Rodriguez et al. 1999*) have validated the initial findings of *Keefe (1984)*. Note however that there is scatter over at least two orders of magnitude in the number and area of landslides associated with any given size (and this scatter is likely to be larger than indicated as earthquakes that triggered very few landslides were

not included in the dataset). In reality, this type of analysis allows the maximum area or distance from the epicentre affected by landslides for a particular seismic event to be estimated (the upper boundary shown in Figure 4.1), but little else at present.

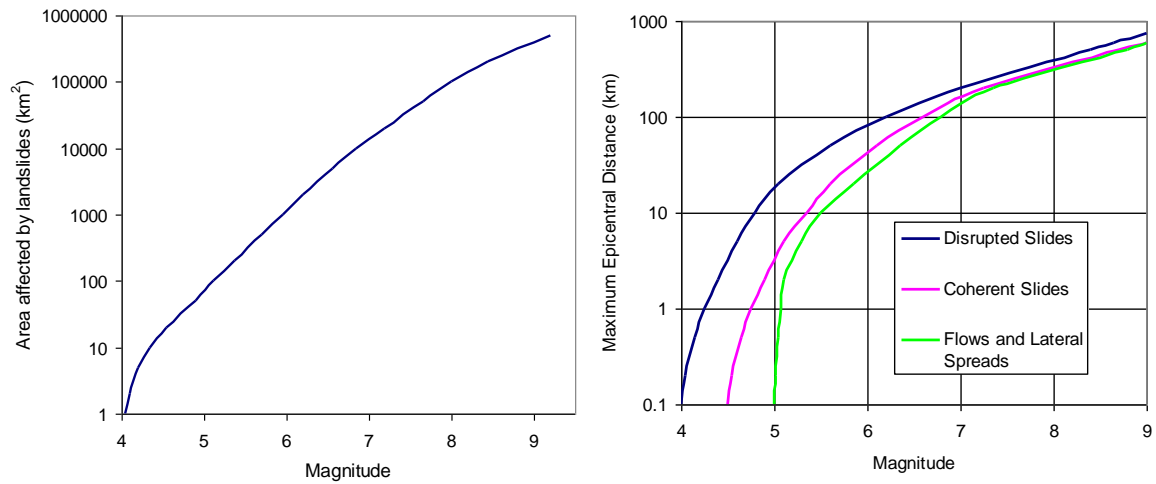


Figure 4.1. Upper boundaries of area and epicentral distances for earthquake-induced landslides proposed by *Keefe (1984)* extracted from *Sepúlveda (2004)*.

Landslide volumes are of particular interest because they can be related to erosion rates (e.g. *Malamud et al., 2004b; Larsen et al., 2010; Marc et al., 2016*). Mean volumes are sensitive to the largest landslides, whereas the mean areas are less sensitive (*Hungr, 2018*).

Marc et al. (2016) present a new, seismologically consistent expression for the total area and volume of populations of earthquake-triggered landslides. This model considers explicitly the effects of seismic moment, source depth, and rupture mechanism on triggered landsliding. It also incorporates the modulating influence of landscape steepness, here defined as the modal slope of the affected topography, on the amount of landsliding, and constrained using an extensive database of 40 shallow crustal earthquakes ranging between M_w 5.1 and M_w 8.6.

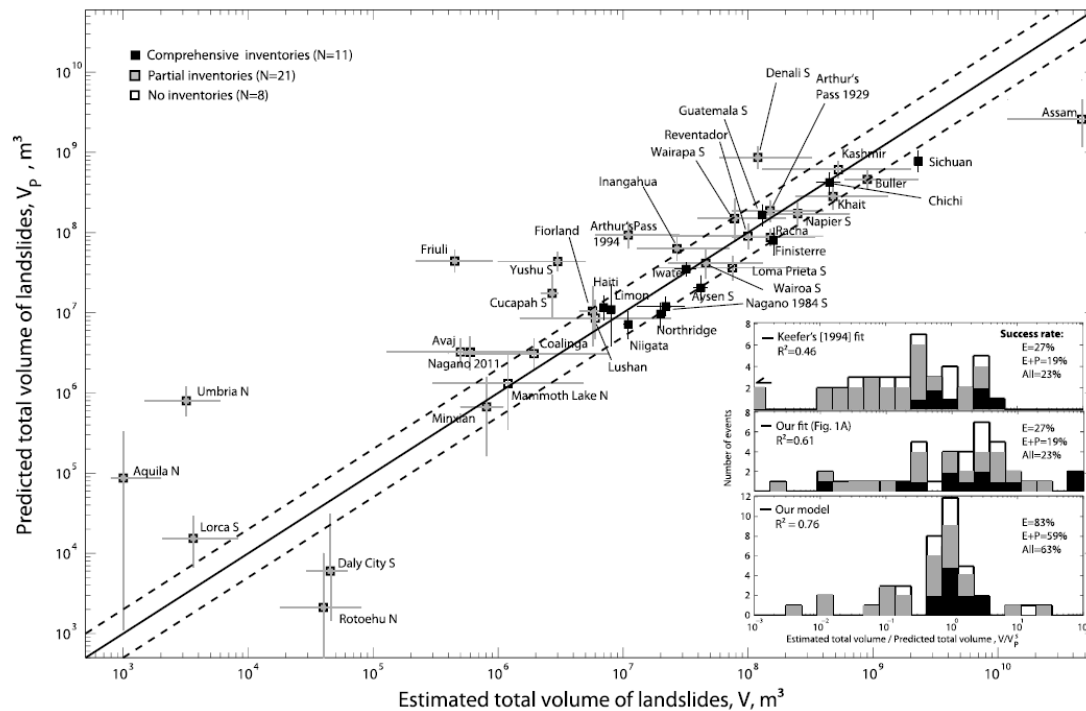


Figure 4.2. Predicted total landslide volume plotted against estimated total landslide volume for 40 earthquakes (Marc *et al.*, 2015).

Another typical analysis focuses on the frequency–magnitude relationships of landslides areas (or volume) in any single event. The frequency–area distribution of a landslide event proposed by *Malamud et al. (2004a)* quantifies the number of landslides that occurs with different sizes. They examine the following three well-documented landslide events:

- Coseismic landslides triggered by the 1994 M_w 6.7 Northridge (California, USA). The inventory, covering about 10,000 km², was elaborated by *Harp and Jibson (1995, 1996)*, contains 11,111 landslides, for a total landslide area of 23.8 km².
- Landslides triggered by a snowmelt event following a sudden change in temperature on 1997 in the Umbria, Italy. *Cardinali et al. (2000)* compiled the inventory, covering an area of about 2,000 km², contains 4,233 landslides, for a total landslide area of 12.7 km²
- Landslides triggered by heavy rainfall from Hurricane Mitch in 1998, Guatemala. *Bucknam et al. (2001)* mapped the landslides from 1:40,000 scale aerial photographs, covering an area of about 10,000 km². The inventory contains 9594 landslides.

Malamud et al. (2004a) find that the landslide areas for all three are well approximated by the same three-parameter inverse-gamma distribution, with parameter values $p=1.40$, $a=1.28 \times 10^{-3} \text{ km}^2$, $s=1.32 \times 10^{-4} \text{ km}^2$ (see Figure 2.3). For small landslide areas this distribution has an exponential ‘roll-over’ and for medium and large landslide areas it decays as a power-law with exponent -2.40 . One implication of this landslide distribution is that the mean area of landslides in the distribution is independent of the size of the event.

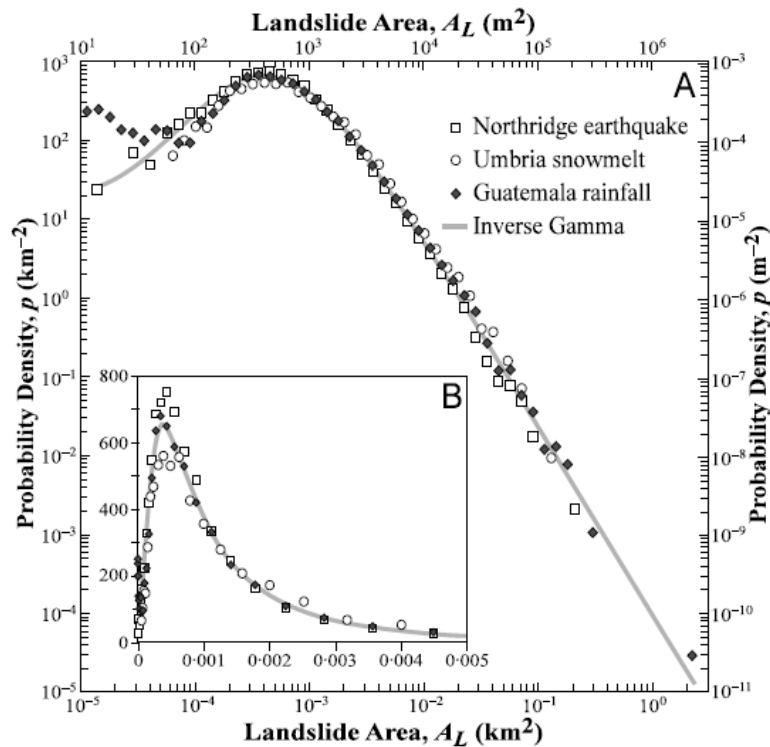


Figure 4.3. Frequency density function of landslides area (km^2), based on Inverse-Gamma distribution function, a theoretical law proposed by *Malamud et al. (2004)* for three landslides inventories: (1) landslides triggered by the 1994 Northridge earthquake, USA (open squares) (*Harp & Jibson, 1995, 1996*); (2) landslides triggered by a snowmelt event in the Umbria region of Italy in 1997 (open circles) (*Cardinali et al., 2000*); (3) landslides triggered by heavy rainfall from Hurricane Mitch in Guatemala in 1998 (Closed diamonds) (*Bucknam et al., 2001*).

Malamud et al. (2004a) show that inverse-gamma landslide distribution is applicable for those substantially complete inventories dominated by flows and slides. They exclude from these inventories very long low-density debris flows – hyperconcentrated streamflows – as they believe the applicable physics more closely represents floods compared to flows and slides. Additionally, they consider rockfall-dominated inventories separately. Flows and slides are controlled primarily by slope stability processes, whereas

rockfalls are controlled by the fragmentation of intact rock along joint sets (*Malamud et al., 2004a*).

4.6 FACTORS THAT INFLUENCE THE DYNAMIC RESPONSE OF HILLSLOPES UNDERGOING SEISMIC SHAKING

It is important to be able to reliably estimate the likely pattern of landslides in a future earthquake at regional scale. Distributions of coseismic landslides are dependent on factors that influence the dynamic response of hillslopes undergoing seismic shaking (e.g. *Newmark, 1965; Jibson, 2011*). These factors can be broadly grouped into those that influence the intensity of event-specific seismic ground motions, and the strength of hillslope materials and the static shear stresses acting on them, which may remain more consistent from one event to the next. Empirical studies have revealed a number of proxy variables that can be used to represent these factors at the regional scale. The most common correlations of coseismic landslides are with hillslope relief factors, bedrock lithology, proximity of the fault, seismic wave attributes, site effects and anthropic factors.

4.6.1 HILLSLOPE RELIEF

It is well-established that relief exerts a strongly dominant control on landsliding both in terms of preconditioning (higher, steeper slopes) and topographic amplification of shaking. Furthermore, it is a key factor for both shallow crustal earthquakes and megathrust zone events. For example, according to *Zhao et al. (2019)*, the landslides in slope gradients of 35°-55° account for 70%(whole area), 70% (hanging wall area) and 71% (footwall area) of the landslides triggered by the 2017 Mw 6.4 Nyingchi earthquake. Similar results reported by *Jibson (2000); Wasowski et al., (2002); Xu et al., (2014); Tang et al., (2015); and Fan et al., (2018)* for coseismic landslides in different parts of the world. Another similar instance occurred in the Ms 8.0 Wenchuan earthquake in 2008, where the number of landslides increased with increasing slope elevation until the maximum was reached at 1,200-2,000 m asl, above this altitude the number of landslides decreased (*Qi et al. 2010*). According to *Wang (2015)* the correlation between the number of landslides and elevation is closely related to the effect of seismic amplification or the peak ground acceleration (PGA).

4.6.2 BEDROCK LITHOLOGY

Depending on the size of ground motions, no geological unit is not prone to coseismic landslides (*Murphy, 2015*). However, the type of material and mass (rock masses are a combination of rock material and the fracture systems) will constrain the type of landslide that can occur (*Murphy, 2015*). In some earthquakes, bedrock lithology is the first-order factor in the generation of landslides. For example, the majority of landslides triggered by the M_w 9.0 megathrust Tohoku earthquake in 2011 occurred in the youngest (Neogene) geologic units of the region. Furthermore, coseismic landslide erosion (i.e., debris mobilization) was controlled by lateral spreading within Quaternary sediments (*Wartman et al., 2013*). Another similar case occurred in the case of the M_w 8.8 Maule earthquake in 2010, a megathrust event, higher landslide densities are associated with low strength Neogene sedimentary rocks, suggesting an important lithologic control as a major factor in the generation of landslides (*Moya et al., 2015*).

However, in many strong shallow crustal events, bedrock lithology is not a primary factor to consider in the generation of landslides, like the 1999 M_w 7.6 Chi-Chi earthquake, Taiwan (*Sepúlveda et al., 2005*); the 2008 M_w 8.3 Wenchuan earthquake, China (*Gorum et al., 2011*); and the 2005 Kashmir earthquake, Pakistan (*Kamp et al., 2010*). According to *Wang (2015)*, there is no obvious correlation between landslide concentration and rock age (younger or older lithological units) for the 2013 M_w 6.6 Lushan and the M_w 8.3 Wenchuan earthquakes (China). Indeed, differences in the distributions of landslides across different lithologies arise because young or old strata are coincidentally clustered around the rupture zone of the seismogenic fault, and these rock masses are extremely fractured and underwent strong shaking.

4.6.3 SEISMIC FAULT EFFECTS

It has been widely observed that the landslides triggered by shallow crustal earthquake are tending to be distributed in clusters along the causative fault (*Keefer, 2000; 2002; Khazai & Sitar, 2004; Huang & Li, 2009*). Most common reasons are the hanging wall and directivity effects. Directivity effects are associated with the rupture direction of the fault, tending to generate larger ground motions toward this orientation (*Somerville et al., 1997; Somerville 2003*). The hanging-wall effect relates with larger ground motions on

the block above an inclined fault (the hanging-wall block) and is common on shallow crustal earthquakes in thrust faults (e.g., *Abrahamson & Somerville 1996*). For thrust faults, it has been observed (e.g: the 1999 M_w 7.6 Chi-Chi earthquake, Taiwan; 1994 M_w 6.7 Northridge earthquake, United State; and the 1993 M_w 6.9 Finisterre earthquake, Papua New Guinea) that landslide density peaked in the hanging wall of the seismogenic fault (*Meunier et al., 2007*). In other well-known example, the 2008 M_w 8.3 Wenchuan earthquake, China, most of the landslides in Minjiang River occurred on the hanging wall block of the Wenchuan– Maowen fault (*Gorum et al., 2011*). Following *Qi et al. (2010)* landslides are distributed primarily along the causative faults of Yingxiu–Beichuan Fault and Guanxian–Anxian Fault. Landslides are not only clustered around the causative faults with surface ruptures, but also the active faults adjacent to the causative faults. The distributed landslides triggered by the M_w 8.3 Wenchuan earthquake are mainly depended on the distance to the causative faults and slope gradient (*Qi et al., 2010*). Another example is the M_w 7.6 Kashmir earthquake, in Pakistan in 2005, in which most of the landslides were located on the hanging wall block of the fault and landslides distribution was asymmetric (*Sato et al., 2007; Mahmood et al., 2015*). Extensive slope cracking developed as a result of the Kashmir earthquake. According to *Khattak et al. (2010)*, a high array of density cracks were developed on hill slopes both on hanging wall and footwall side of the fault and these cracks have the potential to fail.

As *Zhao et al. (2019)* point out, the landslides triggered by the 2017 M_w 6.4 Nyingchi earthquake (China) were not distributed uniformly, and the landslides in the hanging wall area were much larger and denser than those in the footwall area. According to statistics, 1319 coseismic landslides were concentrated in the hanging wall area, and 501 coseismic landslides were located in the footwall area, accounting for 72.5% and 27.5% of the landslides, respectively. These results indicate that an obvious hanging wall effect occurred in the Nyingchi event. A similar phenomenon was also observed in the 2013 Lushan earthquake and the 2017 Jiuzhaigou earthquake, which were both located on the eastern Tibetan Plateau (*Tang et al., 2015*). The coseismic landslides triggered by the 2017 M_w 6.4 Nyingchi earthquake were obviously distributed along the riverbank and seismic fault, especially in the hanging wall area. In addition, the coseismic landslides were mainly concentrated on steep slopes. The landslide-prone slope angles were mainly 40-50° (*Zhao et al., 2019*). The number of landslides decreased with distance from the seismic fault, with the highest landslide concentration occurring at a distance of 3 km,

accounting for approximately 39% of the landslides. In addition, 676 landslides were concentrated within 6-10 km, accounting for 37% of the landslides. In the hanging wall area, the landslide concentration decreased with increasing distance, more than 50% of the landslides were concentrated at a distance of 4 km; a similar trend was not found in the footwall area, and approximately 50% of the landslides were concentrated within 6-10 km. The statistical data analysis also indicated that nearly all of the landslides were located within 15 km of a seismic fault (*Zhao et al., 2019*).

4.6.4 GROUND MOTION PARAMETERS

The spatial density of coseismic landslides is, all else being equal, set by the intensity of ground shaking (*Meunier et al., 2007*). Therefore, seismic wave attenuation and site effects determine the spatial distribution of landslides in detail (*Meunier et al., 2008; 2013*).

Models permitting the prediction or rapid estimation of the total area or total volume of landsliding due to earthquakes can therefore aid in seismic hazard assessment and disaster management as well as research of landscape evolution in tectonically active settings. Not surprisingly, seismic moment has been shown to be a first-order control on the area affected by landsliding (*Keefe, 1984; Rodriguez et al., 1999*) and the total volume of triggered landslides (*Keefe, 1994*)

In many researches about shallow crustal earthquake-induced landslides, ground motion, (e.g. PGA, PGV, PGH, Arias intensity and MMI) had been found the most significant factor in triggering removal mass. For example, in the 1999 M_w 7.6 Chi-Chi earthquake, overall 74% of all slope failures occurred in regions with vertical ground motions greater than 0.2 g and 81% of all slope failures occurred in the region with mean horizontal peak ground accelerations (PGA) greater than 0.15 g (*Khazai & Sitar 2004*). Another important case is the 2010 Darfield (Canterbury, New Zealand) M_w 7.1 earthquake. Peak ground accelerations on the Canterbury Plains reached a maximum of ~1.3 times that of gravity (g) near the Greendale Fault (*Gledhill et al., 2011; Bradley, 2012*). Finite-element modelling of un-instrumented ridge-tops in the Port Hills (east of the Greendale Fault) where boulders were displaced in the 2010 Canterbury earthquake indicates frequency-dependent amplification of PGAs of up to 80% greater than at the base of the hills

(*Khajavi et al., 2012*). *Stahl et al. (2014)* reported that the nearest strong motion seismometer recorded a peak vertical acceleration of 0.79 g and peak horizontal accelerations of 0.45 to 0.51 g.

Nevertheless, no clear correlations have been found for landslides distributions with intensity and ground motion in research about megathrust events analyses. Exceptionally for the 2015 Mw 8.3 Illapel megathrust earthquake, *Candia et al., (2017)* found that the zones that experienced the greatest coseismic slip, appeared to have the largest volumes of rockfall that impacted roads. On the other hand, *Wartman et al., (2013)* compared the landslide database with ground-motion recordings of the Mw 9.0 Tohoku earthquake in 2011 but no correlation between landslide intensity and ground shaking within the area affected was detected.

4.6.5 TOPOGRAPHIC AMPLIFICATION

Densmore & Hovius (2000) recognized that earthquake-triggered landslides in rock slopes have a relatively uniform distribution on steep slopes, but in presence of topographic amplification the triggering of landslides at or near the crests is increased as a result of higher levels of acceleration at the top of slopes. Topographic amplification is a site effect caused by the interaction of the incoming seismic waves with certain geomorphological features, such as steep slopes in areas of strong topographic relief, which results in larger amplitudes of the ground motion toward the ridge crests and therefore landslide triggering (e.g., *Sepúlveda et al., 2005; Brennan & Madabhush 2009; Sepúlveda et al., 2010*). Recent studies indicate that the seismic shaking at the mountain top is approximately three to six times that at its foot (*Wang et al., 2012; Wang et al., 2018*). This causes larger susceptibility to landsliding in the upper parts of the slopes. The crowns of the landslides are generally in the uppermost part of the slope, which has been proposed as an indication of landslide triggering related to topographic amplification of the seismic waves (e.g., *Densmore & Hovius 2000; Sepúlveda et al., 2005; Meunier et al., 2008*). In the Mw 6.2 Aysén earthquake, a shallow crustal event, about two thirds of the landslides start in the upper quarter of the slope, while over 90% start in the upper half, which suggests that larger ground motions due to topographic site effects influenced the triggering of landslides during the earthquake (*Sepúlveda et al., 2010*). Similar situation *Sepúlveda et al., (2005)* observed in the spatial distribution of the rock slope

failures triggered by the 1999 M_w 7.6 Chi-Chi earthquake in the Tachia Valley. The landslides crowns located close to the top of the slopes, where the ground shaking would be anticipated to be stronger under topographic amplification conditions (*Sepúlveda et al., 2005*). Another instance occurred in the 2017 M_w 6.4 Nyingchi earthquake, in these shallow crustal seismic event, the coseismic landslides in the hanging wall area are mainly concentrated in the middle part and upper part of the mountain (*Xu & Li 2010; Zhao et al., 2019*).

4.6.6 ANTHROPIC FACTORS

An additional key factor is the degree of human disturbance of the landscape. Human-Induced Landslides (HIL) refer to landslide events that are directly triggered or partially aggravated by anthropic activities. Most of them are the results of anthropogenic factors such as modification of the topography, change of the water circulations, land use changes, ageing of infrastructure, etc. (*Jaboyedoff et al., 2018*). *Petley et al., (2006)*; *Sudmeier-Rieux et al., (2007)*; and *Owen et al., (2008)* have all argued that humans are a key factor in a substantial proportion of earthquake-induced landslides, primarily as a result of: slope modification, often along transportation lines or to allow building constructions; land-use change; and changes in the soil water conditions. For instance, in the case of the 2005 M_w 7.6 Kashmir earthquake, landslides were concentrated in specific areas that were associated with geomorphology, lithology and human factors. More than half of landslides were in some way associated with road construction and human activity (*Mahmood et al., 2015*). According to *Keefner (1984)* and *Barnard et al. (2001)*, the modification of landscape by humans is the most essential factor for generating landslides in tectonic areas. This increased occurrence of landslides in settled areas then has key implications in the aftermath of the earthquake (*Marui & Nadim, 2009*).

4.7 THE LONG-TERM EVOLUTION OF COSEISMIC LANDSLIDES

Large shallow crustal earthquakes are a highly efficient way to generate landslides in mountainous areas. Landslides also prolong the impacts of the earthquake, often for years. Typically landslides occur extensively in heavy rainfall events in the years after the shallow crustal earthquake, causing high levels of damage and loss of life (e.g. *Dadson et al., 2004; Wang et al., 2015; Marc et al., 2015*).

Analyzing multiple post-earthquake temporal landslide inventories reveals that succeeding to the shallow crustal earthquake, the rate of erosion and landslides shows a surge in the following few years and subsequently normalize gradually (*Lin et al., 2006; Saba et al., 2010; Hovius et al., 2011; Zhang & Zhang, 2017; Fan et al., 2019a, 2019b*). After the large shallow crustal earthquakes, risk of coseismic landslides persists for years and therefore evaluating the evolution of post-earthquake coseismic landslides and the associated impacts are important to get an insight of the triggering mechanism, hazard assessment, and disaster risk reduction. Temporal images allow to monitor the landslide features over time to compare with the potential triggering and causative factors that can be used for landslide hazard and risk assessment; and ultimately assist for effective mitigation measures (*Hervás et al., 2003; Casagli et al., 2016*).

For example, *Shafique (2020)* study the evolution of the 2005 M_w 7.6 Kashmir earthquake-induced landslides in Pakistan and India. The earthquake has killed about 90,000 people, leaving millions homeless, and causing an economic loss of N5 billion US\$ (ADB and WB, 2005). *Shafique (2020)* has used archive SPOT satellite imagery to map the landslides in the earthquake affected area of Pakistan, in the vicinity of the towns of Balakot and Muzaffarabad, before and after the earthquake. Analysis of the temporal landslide inventories based on the visual image interpretation for the years 2005, 2010, 2014, 2016 and 2018, demonstrates that the coseismic landslides area is decreasing with time (Figure 4.4). The decline in the landslide area was slower between 2005 and 2010, however, it is accelerated from 2010 to 2018. Mainly responsible for the extremely active landslides are the monsoon rainfall, river incisions, and anthropogenic factors. Comparison of the temporal landslides inventories with the rainfall record shows that despite the wet spells of monsoon seasons, the landslide area is continuously decreasing.

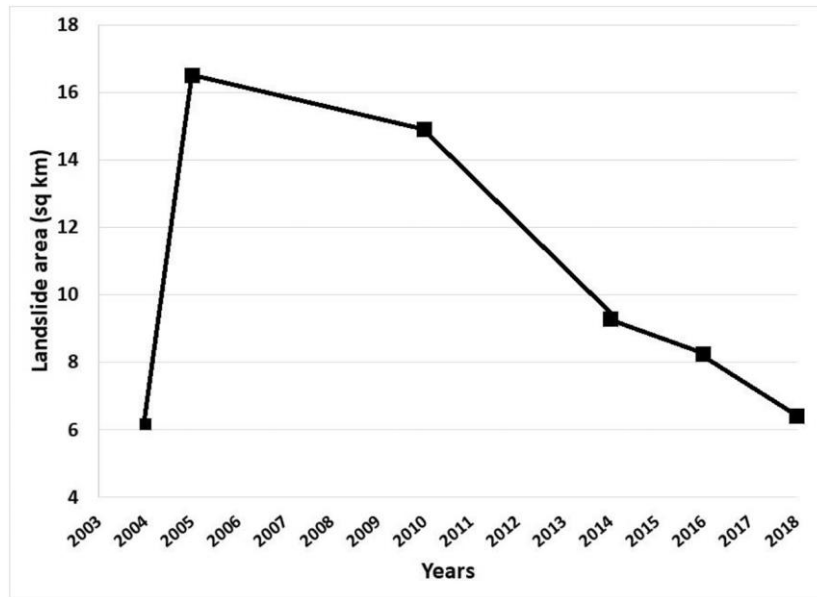


Figure 4.4. The long-term evolution of the surface area of landslides associated with the 2005 Kashmir earthquake, extracted from *Shafique (2020)*.

5 LANDSLIDES INDUCED BY THE 2010 CHILE MEGATHRUST EARTHQUAKE: A COMPREHENSIVE INVENTORY AND CORRELATIONS WITH GEOLOGICAL AND SEISMIC FACTORS

Published as:

Serey A, Piñero-Feliciangeli L, Sepúlveda SA, Poblete F, Petley DN, Murphy W (2019) Landslides induced by the 2010 Chile megathrust earthquake: a comprehensive inventory and correlations with geological and seismic factors. *Landslides*, 16(6), 1153-1165. <https://doi.org/10.1007/s10346-019-01150-6>.

ABSTRACT

The 2010 M_w 8.8 Maule earthquake, which occurred in the subduction contact between the Nazca and the South American tectonic plates off the coast of Chile, represents an important opportunity to improve understanding of the distribution and controls for the generation of landslides triggered by large megathrust earthquakes in subduction zones. In total 1226 landslides were mapped over a total area of c.120,500 km², dominantly disrupted slides. The total landslide volume is c. 10.6 Mm³. The events are unevenly distributed in the study area, the majority of landslides located in the Principal Andean Cordillera and a very constrained region near the coast on the Arauco Peninsula, forming landslide clusters. Statistical analysis of our database suggests that relief and lithology are the main geological factors controlling coseismic landslides, while the seismic factor with higher correlation with landslide occurrence is the ratio between peak horizontal and peak vertical ground accelerations. The results and comparison with other seismic events elsewhere suggest that the number of landslides generated by megathrust earthquakes is lower than events triggered by shallow crustal earthquakes by at least one or two orders of magnitude, which is very important to consider in future seismic landslide hazard analysis.

Keywords: coseismic landslides, megathrust earthquake, Chile.

5.1 INTRODUCTION

Landslides represent perhaps the most frequent geological hazard present in mountainous environments, due to the geological, geomorphological and geotechnical characteristics of steep upland landscapes. Most notably, in tectonically-active mountain areas, landslides are a major cause of fatalities and economic losses during and after strong earthquakes (e.g. *Sepúlveda et al. 2005; Jibson et al. 2006; Sato et al. 2007; Qi et al. 2010; Dai et al. 2011*).

A key focus for research on seismically-triggered landslides in high mountain areas had been the development of approaches to create reliable estimates of the likely pattern of landslides in future earthquakes. This has usually undertaken through the development of statistical relations between specific earthquake events of different magnitudes and the number, area or volume of landslides triggered by each event (e.g. *Keefer, 1984; Rodriguez et al., 1999; Malamud et al., 2004a; Malamud et al., 2004b; Marc et al., 2016; Havenith et al., 2016*). Recently *Marc et al. (2016)* compiled and analysed extensive databases of over 40 earthquakes ranging between M_w 5.1 and M_w 8.6, with a primary focus on shallow crustal earthquakes, allowing the presentation of a seismologically consistent expression for the total area and volume of populations of earthquake-triggered landslides. Similarly, *Malamud et al. (2004a)*, provided quantitative estimates of the total number of landslides (N_{LT}) expected for an earthquake of a given magnitude; for example this estimates that around 500,000 landslides would be generated for an event on the scale of the 2010 M_w 8.8 Maule earthquake, which occurred in the subduction zone between the Nazca and the South American tectonic plates of the coast of Chile. However, in comparison with shallow crustal earthquakes the number of complete landslide inventories for megathrust earthquakes is small, meaning that there is huge uncertainty in such estimates. Prior to the study reported here, only one fully comprehensive, reliable inventory of coseismic landslides, based on field inventories and visual analysis of aerial or satellite images, has been available for megathrust earthquakes. This is the inventory for the 2011 M_w 9.0 Tohoku earthquake (*Wartman et al., 2013*). Therefore, there is a need to improve these datasets. The 2010 Maule earthquake, reported here, provides a key opportunity to understand better the distribution and controls for the generation of landslides triggered by megathrust earthquakes.

This paper builds on the pilot study of *Serey et al. (2017)* to provide a comprehensive inventory of landslides induced by the Maule earthquake, and to analyse their correlations with geological (slope, lithology) and seismic factors (rupture distance, PGA, PGV), thereby providing new insight into the factors controlling coseismic landslides in megathrust earthquakes.

5.2 THE 2010 M_w 8.8 MAULE EARTHQUAKE

The 2010 M_w 8.8 Maule earthquake, which occurred on 27 February 2010, is the sixth largest event in the United States Geological Survey (USGS) global catalogue and the second largest to have been recorded in Chile, just behind the 1960 Valdivia earthquake. It is the largest earthquake to have been recorded instrumentally in Chile. The rupture zone matches a seismic gap dating to 1835. Prior to the earthquake, several authors (*Campos et al., 2002; Moreno et al., 2008; Ruegg et al., 2009*), suggested that the area had a high probability of generating an earthquake in the near future, based on GPS data that showed an eastward terrain shift up to 4 cm a^{-1} (*Cisternas, 2011*).

The earthquake rupture was located along the tectonic zone in which the Nazca plate is subducted beneath the South American plate, for which the convergence rate is $c.6.6 \text{ cm a}^{-1}$ (*Angermann et al., 1999*). The hypocenter was located at the geographic coordinates 36.290° S , 73.239° W with a depth of 37 km according to the National Seismological Service of University of Chile (SSN). The rupture zone extended 450 km along the Chilean coast and 150 km from east to west. The speed and time of propagation is of the order of 2.5 to 3.5 km / s and 110 s respectively (*Barrientos, 2010*).

Thirty-two accelerometers recorded the strong motion, with reliable peak values of 0.93 g (horizontal component) at Angol station and 0.70 g (vertical component) at Llolleo station (*Boroschek et al., 2012; Figure 4.1*).

The rupture process of the Maule earthquake was characterized by the behaviour of asperities (*Lay et al., 2010; Delouis et al., 2010; Tong et al., 2010; Lorito et al., 2011*) (Figure 5.1). An asperity with high levels of slip (the main asperity) was located in the northern part of the seismic gap, approximately in the same rupture area as the 1928 M_w 7.6 Talca earthquake (*Ruiz et al., 2012*).

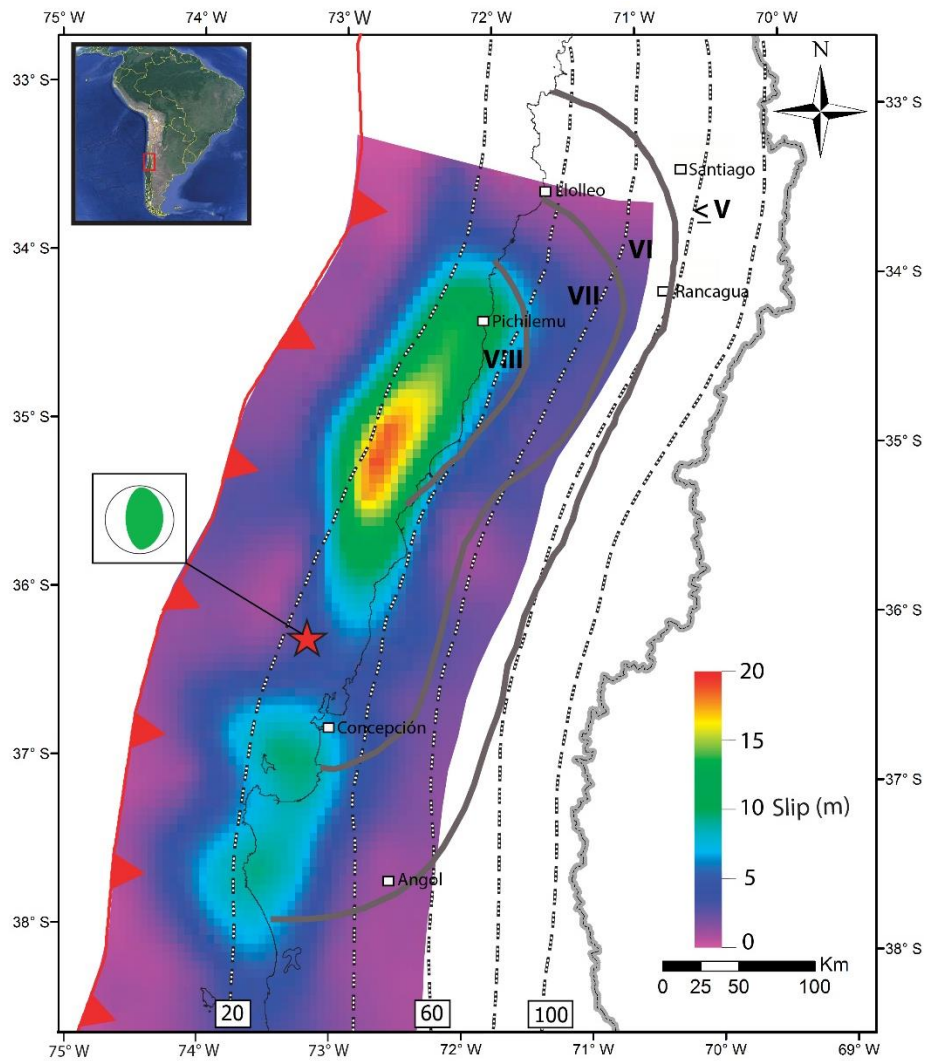


Figure 5.1. Rupture zone, slip distribution (extracted from *Lorito et al., 2013*) and the isoseismal map (grey lines) inside the damage area of 2010 Maule earthquake (based upon data from *Astroza et al. 2012*). The red line with triangles is the trench between the Nazca and South America Plates (*Bird, 2003*), Slab1.0 plate interface contours from the USGS (grey dotted lines). The green and white focal mechanism is taken from the United States Geological Survey centroid moment tensor.

5.3 GEOLOGICAL AND GEOMORPHOLOGICAL SETTING OF THE COSEISMIC LANDSLIDES

The Andes represent the geodynamic archetype of a convergent, non-collisional mountain range, generated by subduction of the oceanic lithosphere of the Nazca (Farallon) Plate beneath the continental lithosphere of the South American Plate (*Pardo-Casas & Molnar, 1987*). Consequently, the present-day architecture of the Andes Mountains is largely the result of convergence between the Pacific–Nazca and South American plates. These mountains are a consequence of crustal shortening, principally accommodated by eastward thrusting, which leads to crustal thickening and surface uplift (*Isacks 1988; Sheffels 1990; Allmendinger et al., 1997*). Subduction is also evidenced by an almost continuous line of both active and dormant volcanoes, mostly andesitic stratovolcanoes, which run almost the entire length of the country. The Andes of central Chile (32.5° S to 41.5° S) are composed of a number of morphostructural units from west to east: the Coastal Cordillera, the Valley, the Principal Cordillera (spanning Chile and Argentina), the Frontal Cordillera, the Argentine Precordillera and the Pampean Ranges (*Jordan et al., 1983*). For reference, Figure 5.2 shows a simplified geologic map and the distribution of slope angle in the area of the Maule earthquake coseismic landslide inventory (elevation data for the slope angle map is coming from ASTER GDEM, product of METI and NASA, resolution 30 m). The Chilean Coastal Cordillera consists of low and topographically-smooth mountains composed predominantly of Late Paleozoic and Mesozoic igneous rocks, with paired belts of Paleozoic metamorphic rocks cropping out south of Pichilemu (34° S). The Central Valley is a depression with a Mesozoic to Quaternary sedimentary infill (*Pankhurst and Hervé 2007; Charrier et al., 2015*); from Santiago to the south, this is the main agricultural zone and contains several major cities, including the capital. The Principal Cordillera is a chain of high mountains with a strong relief and steep slopes that in its western part in Chilean territory mostly comprises Oligocene–Miocene continental volcanoclastic rocks, intruded by Miocene–Pliocene granitoids (*Pankhurst and Hervé 2007; Charrier et al., 2015*). The Frontal Cordillera is composed of units formed during the Gondwana orogeny in the Late Paleozoic to Early Mesozoic. Older Paleozoic rocks appear in the Pampean range.

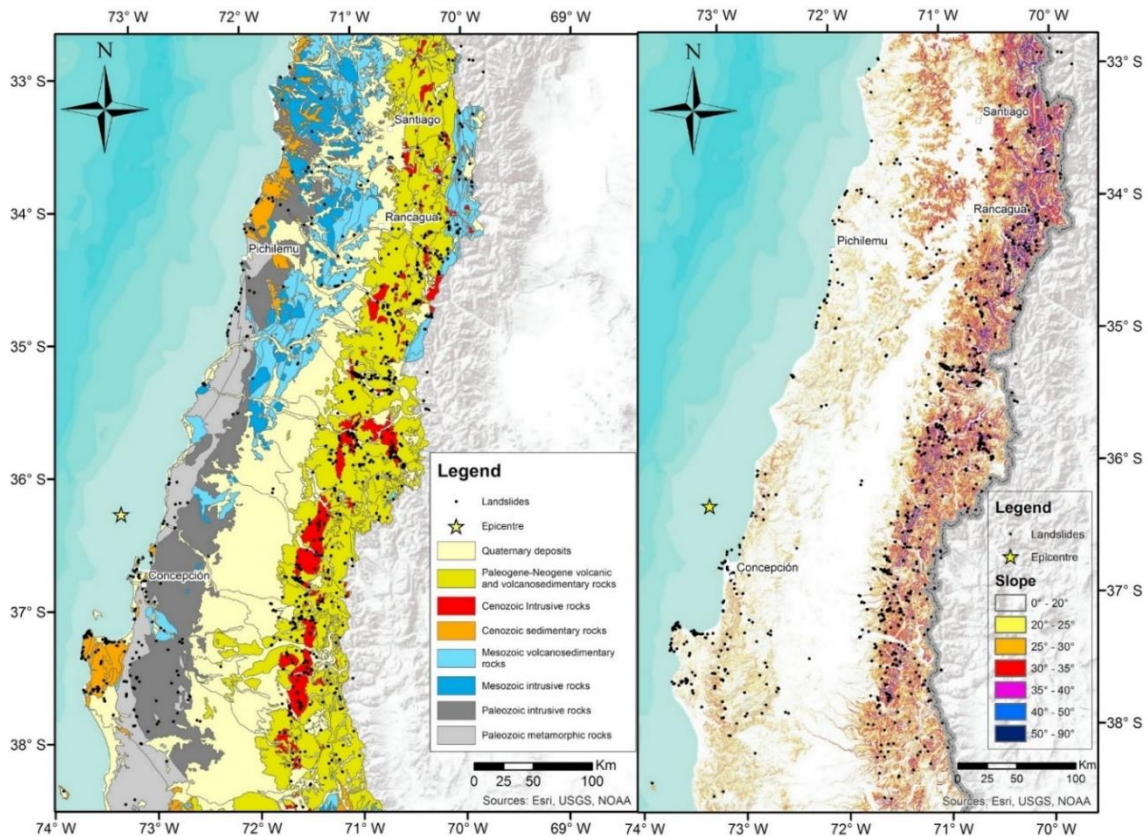


Figure 5.2. Simplified geologic map (modified from *SERNAGEOMIN*, 2003) and the distribution of slope angle in the area of 2010 coseismic landslide inventory.

5.4 THE 2010 M_w 8.8 MAULE EARTHQUAKE GROUND MOTION DISTRIBUTION

Interpolated maps of the peak horizontal and vertical acceleration components (PGA_H), (PGA_V) and normalized PGA_H/PGA_V values have been generated (Figure 5.3), based on information available from 32 stations from the strong motion network of the National Seismological Centre, Universidad de Chile (Table 5.1). Similarly, interpolated maps of the peak horizontal and vertical velocity components (PGV_H), (PGV_V) and normalized PGV_H/PGV_V values shown in Figure 5.4. The interpolation methodology used for all maps was based on an adjustable tension continuous curvature surface gridding algorithm, with the tension parameter set to 0.25. The implementation was done using Generic Mapping Tools (GMT).

Table 5.1. Data obtained from the Accelerograph Chilean Network, Universidad de Chile. Peak horizontal ground acceleration (PGAH), peak vertical ground acceleration (PGAV), peak horizontal ground velocity (PGVH), peak vertical ground velocity (PGVV).

Seismological station	PGAH	PGAV	PGVH	PGVV	Latitude	Longitude
Copiapó	0.029	0.008	0.0300	0.010	-27.3737	-70.3216
Vallenar	0.019	0.010	0.0275	0.015	-28.5766	-70.7552
Papudo	0.421	0.155	0.1670	0.248	-32.5200	-71.4500
Viña del mar centro	0.034	0.186	0.3260	0.124	-33.0249	-71.5529
Viña del mar el sato cerro	0.353	0.260	0.3760	0.422	-33.0472	-71.5099
Valparaiso UTSFM	0.304	0.079	0.0780	0.082	-33.0300	-71.6200
Valparaiso almendral	0.265	0.145	0.2910	0.223	-33.0300	-71.6200
Llolleo	0.564	0.702	0.2350	0.304	-33.6200	-71.6000
Santiago centro	0.310	0.182	0.1680	0.186	-33.4670	-70.6520
Santiago Maipu	0.562	0.240	0.4400	0.220	-33.5087	-70.7714
Santiago La Florida	0.236	0.130	0.1500	0.105	-33.5139	-70.6052
Santiago Peñalolén	0.295	0.280	0.2930	0.127	-33.5014	-70.5792
Santiago Puente Alto	0.265	0.130	0.3145	0.162	-33.5780	-70.5810
Matanzas	0.461	0.234	0.3700	0.277	-33.9600	-71.8700
Hualañe	0.461	0.390	0.3880	0.350	-34.9763	-71.8059
Talca	0.477	0.243	0.1950	0.274	-35.4300	-71.6300
Constitución	0.640	0.352	0.4100	0.620	-35.3400	-72.4000
Concepción	0.402	0.397	0.5800	0.492	-36.8283	-73.0482
Angol	0.928	0.281	0.3600	0.087	-37.7900	-72.7100
Valdivia	0.138	0.051	0.1840	0.066	-39.8314	-73.2391
Curicó	0.471	0.198	0.2770	0.294	-34.9905	-71.2367
Concepción San Pedro	0.650	0.550	No data	No data	-36.8442	-73.1086
Santiago Antumapu	0.340	0.210	No data	No data	-33.5692	-70.6335
El Roble	0.190	0.110	No data	No data	-32.9763	-71.0149
Pichilemu	0.160	0.130	No data	No data	-34.3904	-72.0034
Santiago San Jose de Maipo	0.470	0.240	No data	No data	-33.8475	-70.2035
Santiago FCFM	0.170	0.140	No data	No data	-33.4563	-70.6624
Casablanca	0.330	0.230	No data	No data	-33.2590	-71.1376
Los Molles	0.160	0.070	No data	No data	-32.2320	-71.5070
Santiago Las Americas	0.310	0.160	No data	No data	-33.4520	-70.5310
Olmué	0.360	0.150	No data	No data	-32.9940	-71.1730
Viña del mar Marga Marga	0.340	0.260	No data	No data	-33.0470	-71.5100
Los Vilos	0.030	0.020	No data	No data	-31.9200	-71.5000
Zapallar	0.180	0.110	No data	No data	-32.5700	-71.4700
Santiago Santa Lucia	0.320	0.260	No data	No data	-33.4400	-70.6400
Cabildo	0.320	0.130	No data	No data	-32.4270	-71.0690
Melipilla	0.770	0.380	No data	No data	-33.6800	-71.2200

In previous studies coseismic landslide initiation has in general been related to the peak horizontal ground acceleration parameter (PGA_H) (following *Terzaghi, 1950*). For the Maule earthquake the maximum horizontal acceleration recorded was 1.25 g at Cauquenes station, although the accelerometer saturated because the different components over-crossed (*Saragoni & Ruiz, 2012*). Thus, the PGA_H value for Cauquenes has not been included in our analysis (Figure 5.3a) because it is not considered to be a reliable measurement.

The distribution of PGA_H values of the 2010 M_w 8.8 Maule Earthquake show a minimum measured ground shaking value of 0.02 g at Vallenar station (latitude -28.576) north of the study area, and a maximum reliable value at Angol station of 0.97 g. However, Angol may have been severely affected by site effects (*Felipe Leyton, personal communication*), which directly affects the interpolation result, indicating a zone of intense shaking centered at Angol. In general, the Tohoku 2011 Earthquake generated higher values of PGA_H (max. = 2.02 g) (*Wartman et al., 2013*) than the Maule Earthquake.

In common with *Saragoni & Ruiz (2012)*, our PGA_H map shows attenuation towards the east, with peak PGA_H values reducing from c.1.0 g to c.0.2 g for distances of 100 km from the rupture plane that defines the main asperity.

The PGAV distribution is shown in Figure 5.3b. The recorded values for this parameter range between 0.008 and 0.700 g. Notably, the spatial distribution of PGAV does not resemble the PGA_H map. From Figure 4.3b, a peak value of 0.7 g at Llolleo in the north of the rupture area, and a more extended area of high values (up to 0.55 g) recorded near the coast at Concepcion close to the southernmost asperity, dominate the pattern. PGAV values are typically c.0.3 g at a distance of 100 - 120 km from the asperities.

In Figure 5.3c we show the ratio between PGA_H and PGAV. An interesting pattern is observed for this parameter, giving smaller values near the coast, nearer to the asperity, and greater values are observed in further regions, up to 120 - 140 km from the asperities at the Principal Cordillera.

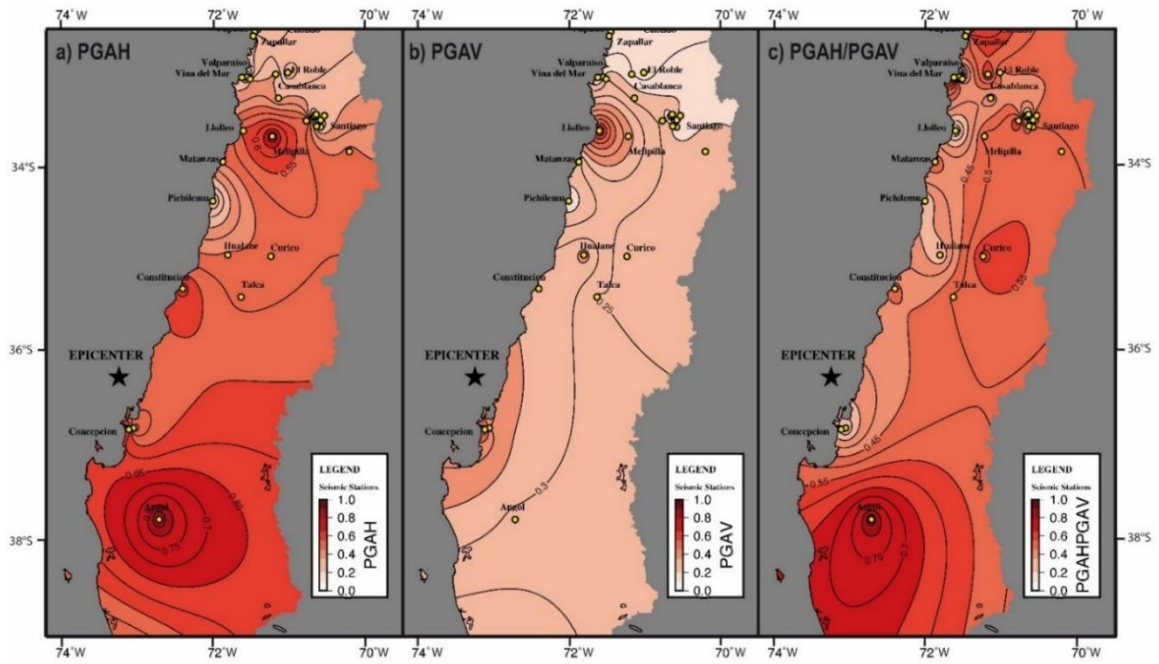


Figure 5.3. Interpolated maps of the peak ground accelerations of a) PGAH, b) PGAV and c) PGAH/PGAV ratio obtained from 32 stations from the Accelerograph Chilean Network from Universidad de Chile.

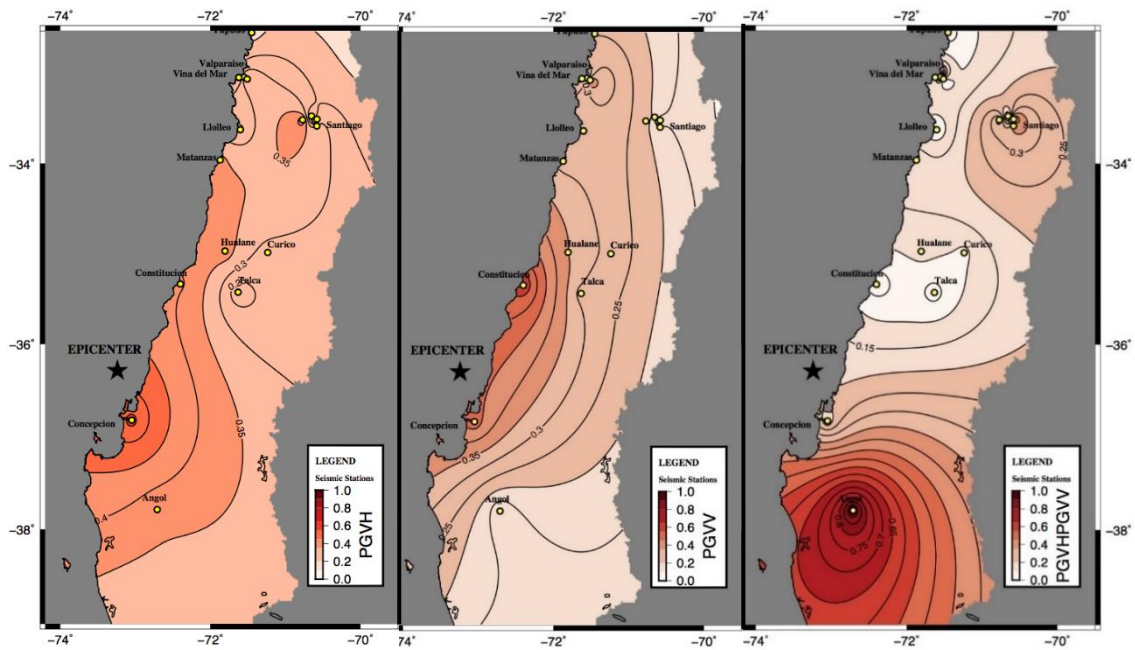


Figure 5.4. Interpolated maps of the peak ground accelerations of a) PGVH, b) PGVV and c) PGVH/PGVV ratio obtained from 32 stations from the Accelerograph Chilean Network from Universidad de Chile.

5.5 LANDSLIDES INDUCED BY THE 2010 MAULE MEGATHRUST EARTHQUAKE

5.5.1 LANDSLIDE INVENTORY AND CORRELATIONS WITH RELIEF AND GEOLOGY

Serey et al. (2017) presented a pilot inventory of landslides generated by the Maule earthquake from the analysis of satellite images and bibliographic information for a part of the area affected by the earthquake, between 32.5° S and 38.5° S°, with the Chile-Argentina border providing the eastern boundary of the mapped area. This paper expands the dataset to the Principal Cordillera (Argentine side) and the Frontal Cordillera, providing for the first time a complete landslide inventory for the Maule earthquake. This represents only the second full inventory of coseismic landslides for a subduction zone earthquake based on field inventories and visual analysis of aerial or satellite images.

For the bibliographic compilation, *Serey et al. (2017)* collected information about recorded landslides events triggered by the Maule earthquake. They reviewed 107 technical reports of the National Geological and Mining Survey of Chile (SERNAGEOMIN) related to the earthquake, from which the relevant information pertaining to landslides and lateral spreads was extracted. They also reviewed the georeferenced reports of road network interruption problems caused by the earthquake, undertaken by the Ministry of Public Works and incorporated an inventory of lateral spreads provided by *Verdugo et al. (2012)*, and the inventory of landslides in the coastal fringe of the Biobio administrative region provided by *Mardones & Rojas (2012)*.

The landslides were mapped by interpreting Landsat satellite images (Landsat 5-7-8, Provider:NASA, resolution: 30 m, mostly temporal span: 2008-2013) before and after the earthquake using Google Earth. A visual inspection of these strips was done at an eye height of ~1-2 km, decreasing the height when an alteration was detected in the vegetation, or when bare spots or typical mass movement morphologies were present (*Soeters & Van Western 1996*). We visually inspected the earliest available images after the earthquake, mapping at 1:2000 and 1:10,000. Once a landslide was identified, the

location was compared with the latest available pre-seismic image without cloud or snow cover and the landslide was mapped as polygon. Validation fieldwork was undertaken in the coastal regions, where the higher densities of landslides are located, in order to identify and classify landslides by failure mode. Field inspections allowed the addition of a number of small mass movements that were not identified in the satellite images. The minimum size considered for the mapping was 30 m², although field inspections showed that an indefinite number of small mass movements were not recognized on the satellite images. Thus in keeping with all such studies, our inventory is censored for very small landslides (i.e. those with a surface area of less than 30 m²).

In total 1226 landslides were mapped (Figure 5.5) over a total area of c.120,500 km². The maximum distance to the epicentre is 487 km. The total landslide volume is c. 10.6 Mm³, estimated using published area-volume relationships proposed by *Larsen et al. (2010)*. The inventory includes 1059 disrupted slides, 110 flows, 49 lateral spreads and eight coherent slides, following the *Keefe (1984)* classification for earthquake-induced landslides. Most of the landslides (over 850, mainly disrupted shallow slides and falls) are located in the farther Andes Principal Cordillera, which has a stronger relief and steeper slopes than the Coastal Cordillera, despite the lower earthquake intensities. A large number of landslides (387) are in the size range of 1000 m² to 5000 m², while just a few (29) have more than 50,000 m². Landslides located in the Valley are limited and are mainly lateral spreads caused by liquefaction.

The compiled dataset has been compared with the curves by *Keefe (1984)* and *Rodriguez et al. (1999)* regarding the maximum landslide area and the epicentral distance (*Serey et al., 2017*). It was observed that the geographical distribution is in agreement with the predictions defined for an earthquake of magnitude M_w 8.8. However, the events are not evenly distributed in the study area, and *Serey et al. (2017)* highlighted the presence of landslide clusters. The most important cluster (127 failures) is located in the Arauco Peninsula, Biobio region, mainly triggered in low strength Neogene, marine sedimentary rocks. These rocks has been tested by *Moya (2016)*, showing differential stress-strain behaviour depending on the testing conditions and an increase in the shear strength under cyclic testing.

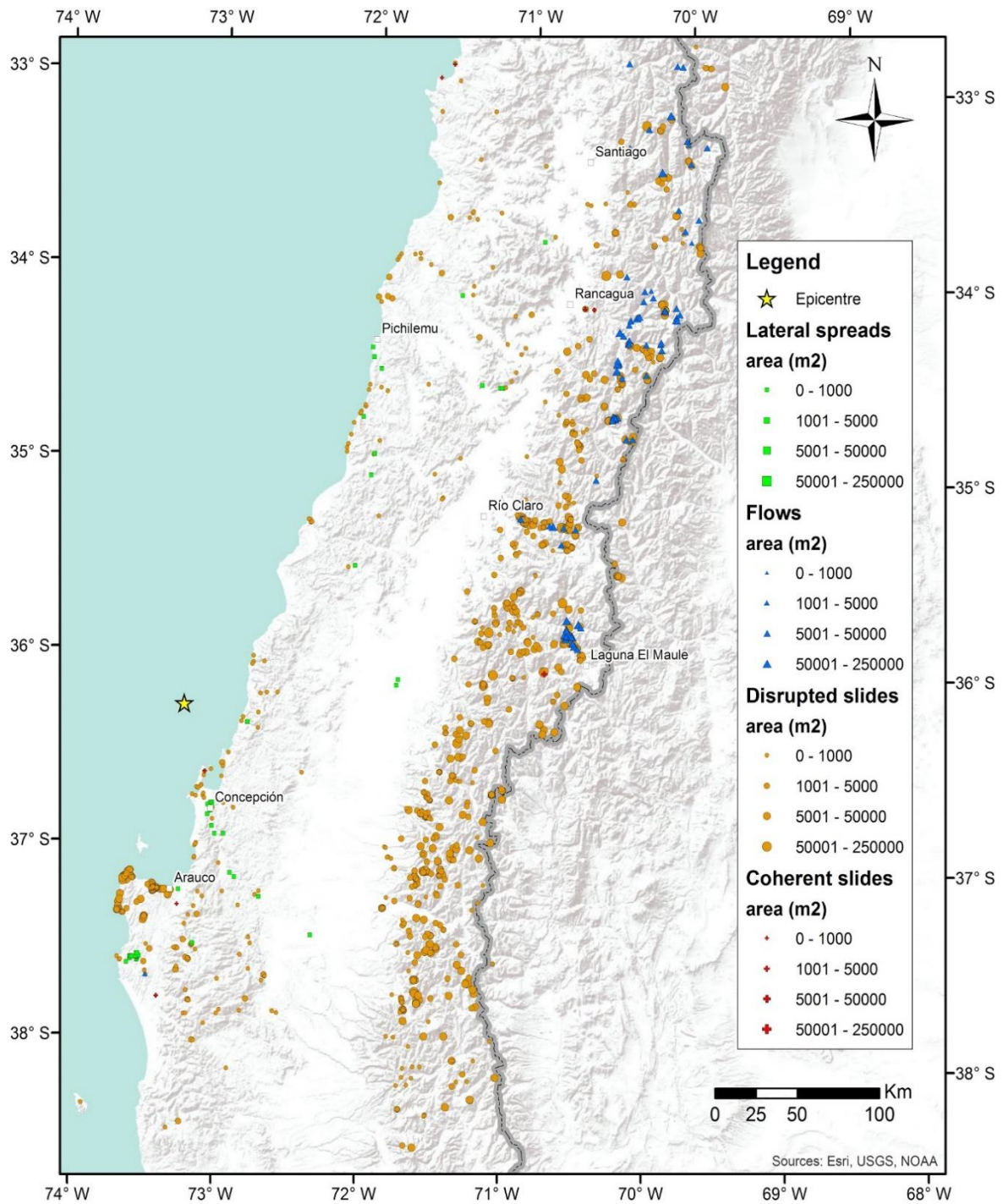


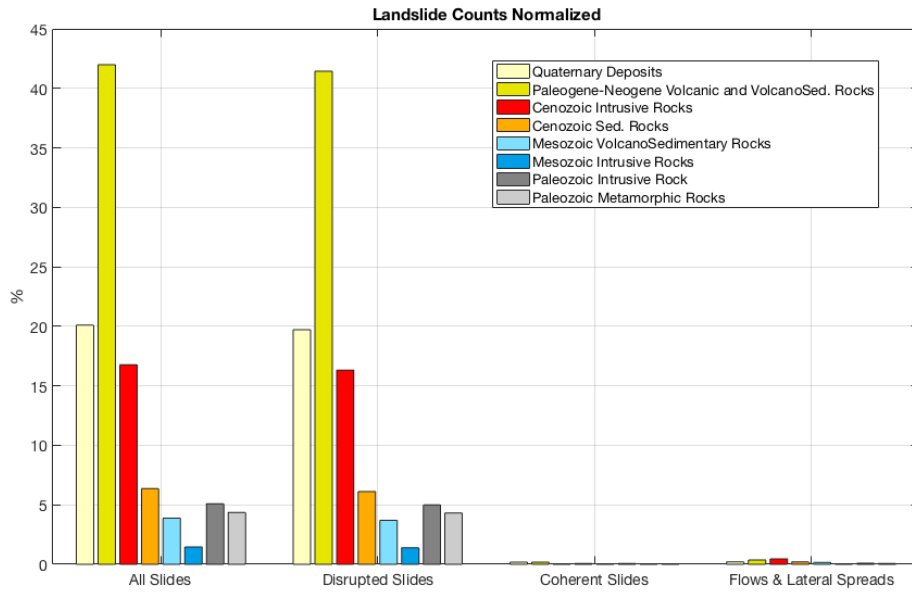
Figure 5.5. The comprehensive landslide inventory for the 2010 Maule earthquake.

Figure 5.6a shows a histogram of landslide counts normalized by geologic unit area based on the landslide classification, simplified geologic units and landslides types. Landslide occurrence is more frequent in Paleogene-Neogene volcanic and volcano sedimentary rocks, with a total of 42% of landslides. The Quaternary deposits and

Cenozoic intrusive rocks represent 20% and 16 %, respectively. In total, these three geologic units cover 79 % of the whole inventory. Disrupted landslides were the dominant type of landslides triggered by the 2010 Maule earthquake. Other types of landslides, coherent slides and flows and lateral spreads were minor, representing less than 2% of the total. The percentage of disrupted landslides generated in Paleogene-Neogene volcanic and volcano sedimentary rocks, which was the most dominant from the classified geologic units, covered c.41%. The other two most important geological units that exhibit landslide occurrence were Quaternary deposits and Cenozoic intrusive rocks, adding up 36 % of the total. In other words, the majority of the landslides triggered by the Maule earthquake occurred in the youngest geological units in the area. Furthermore, in one of the landslide clusters of the Maule inventory, in the Arauco Peninsula, landslides were mainly triggered in low strength Neogene, marine sedimentary rocks, suggesting an important lithologic control as a major factor in the generation of landslides (*Moya et al., 2015; Moya, 2016*). These results coincide well with those obtained for coseismic landslides triggered by the 2011 Tohoku earthquake (M_w 9.0, subduction earthquake), where majority of landslides occurred in the youngest (Neogene) geologic units of the region (*Wartman et. al 2013*). Thus, for both comprehensive megathrust coseismic landslide inventories lithology proves to be an extremely important factor.

In total, 55% of landslides occurred on slope angles between 20° and 40° (Figure 5.6b), whilst 39% of landslides occurred between on slopes of less than 20°. In contrast, less than 6.3 % of slope failures occurred for angles greater than 40°. This predominance of coseismic landslides on slopes between 20° and 40° has been observed elsewhere, including the 2005 M_w 7.6 Kashmir earthquake (*Sato et al., 2007; Kamp et al., 2008; Owen et al., 2008*) and the 2008 M_w 8.3 Wenchuan earthquake (*Gorum et al., 2011*).

a)



b)

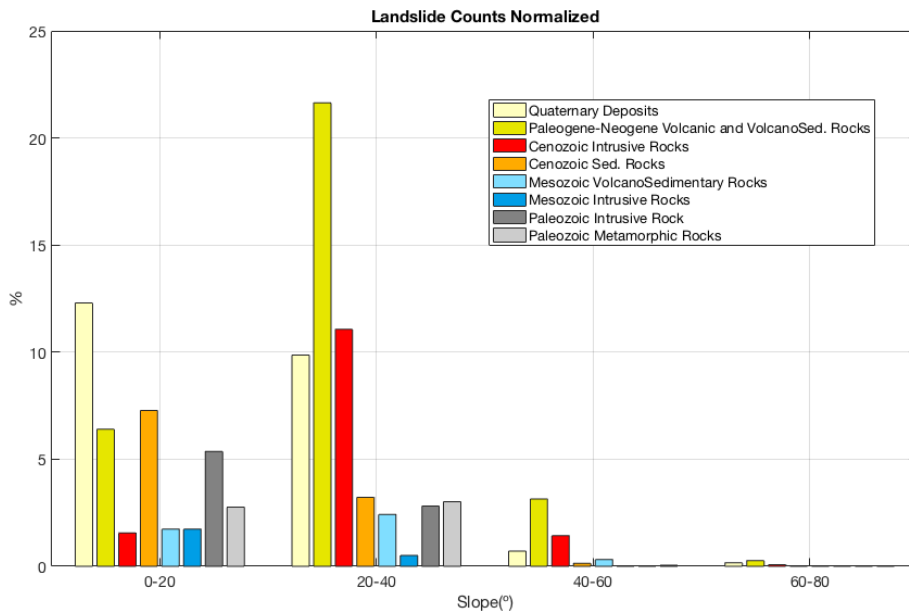


Figure 5.6. a) Histogram of landslide counts normalized by geologic unit based on landslide classification, simplified geologic units and landslide types. b) Histogram shows, landslides counts normalized by geologic units and disaggregated slope intervals of 20°.

5.5.2 SPATIAL ANALYSIS OF COSEISMIC LANDSLIDE DISTRIBUTION AND GROUND MOTION

The spatial pattern of landslides was analysed calculating a map of landslide density or landslide concentration (LC). The calculation was done across a moving grid of size $0.5^\circ \times 0.5^\circ$ through the $120,500 \text{ km}^2$ landslide-affected area. LC was defined as:

$$\text{LC} = (\text{Sum area of all landslides within the grid}) / (\text{total area of the grid}).$$

Python and GMT (Generic Mapping Tool) scripting were used for the implementation of the calculation.

In Figure 5.7 the LC results from calculation is shown for: a) all landslides, b) coherent slides, c) disrupted slides and d) flows and lateral spreads triggered by the 2010 M_w 8.8 Maule earthquake. The LC map for all landslides (Figure 4.7a) shows that the events are very unevenly distributed in the study area, with the majority of landslides are located in the Principal Andean Cordillera (especially in the vicinity of Río Claro, Laguna El Maule, Rancagua) and a limited zone near the coast on the Arauco Peninsula, as noted previously.

Coherent slides provide less than 0.5% of the whole database and are well constrained in the Laguna El Maule cluster (Figure 5.7b). The geologic units with maximum coherent landslide occurrence are the Quaternary deposits and Paleogene-Neogene volcanic and volcano-sedimentary rocks.

Disrupted landslides were concentrated in two main areas, corresponding to the Rio Claro and Arauco clusters noted above (Figure 5.7c). The Rio Claro cluster, with an approximate area of $2,500 \text{ km}^2$, lies in an area in which Paleogene-Neogene volcanic and volcanic sedimentary rocks, in which Cenozoic intrusive rocks crop out. The second disrupted slides cluster lies near the coast in the Arauco zone, with an area of $c.500 \text{ km}^2$, where Cenozoic sedimentary rocks are the main geologic unit cropping out in the area. The areas of high concentration for flows and lateral spreads, which represent less than 2% of the total, correspond to the Laguna El Maule and Rancagua clusters (Figure 5.7d).

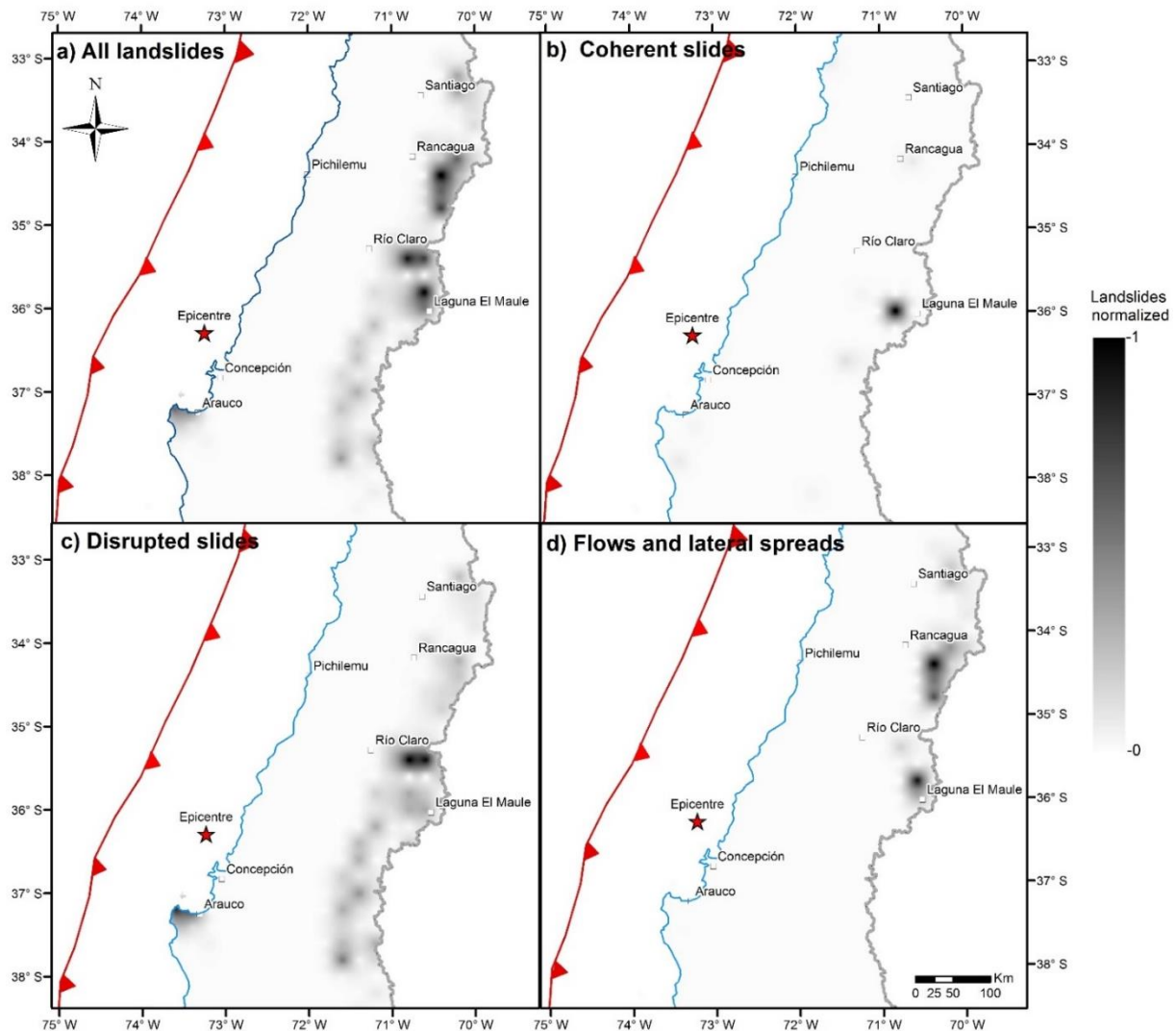


Figure 5.7. Landslide concentrations (LC) normalized to the maximum concentration value. Areas in dark colours shows landslides clusters described in the text. In blue coastline. The red line with triangles is the trench between the Nazca and South America Plates (*Bird, 2003*). a) LC of all landslides. b) LC of coherent slides. c) LC of disrupted slides. d) LC of flows and lateral spreads.

The spatial distribution of PGAH has two zones of higher shaking, with the largest being located at Angol in the south of our study area and the other in the area of Melipilla in the north, near Santiago. There is no evident correlation between the horizontal peak ground acceleration and the LC distributions for different landslides types (disrupted slide, coherent, flows and lateral spreads). It is noted that the PGAV the values attenuate from west to east from Concepcion (maximum value of 0.55 g) to smaller values in the east of the country. This means that for the locations of high landslide concentration the values for the vertical acceleration parameter are low, typically less than 0.3 g. In conclusion, our analysis suggest no evident correlation between the LC distribution and

the regional PGA distribution (for PGAH as for PGAV), which mirrors the conclusion of *Wartman et al. (2013)* for the 2011 M_w 9.0 Tohoku earthquake. However, the correction with the ratio of PGAH to PGAV appears to be stronger. Scatter plots of LC against PGAH/PGAV suggest that most of landslides are triggered for values that are bounded between PGAH/PGAV values of 0.45 and 0.60 (Figure 5.8a). This area coincides exactly with the Principal Cordillera, corresponding to high mountains with a strong relief and steep slopes. The distribution is controlled by disrupted landslides (Figure 5.8c). For the coherent slides, the PGAH/PGAV band is very narrow, approximately 0.5 and 0.52 (Figure 5.8b). A secondary peak is observed in the range of 0.6 and 0.7. A much broader band for flows and lateral spreads is observed between 0.45 and 0.58 (Figure 5.8d).

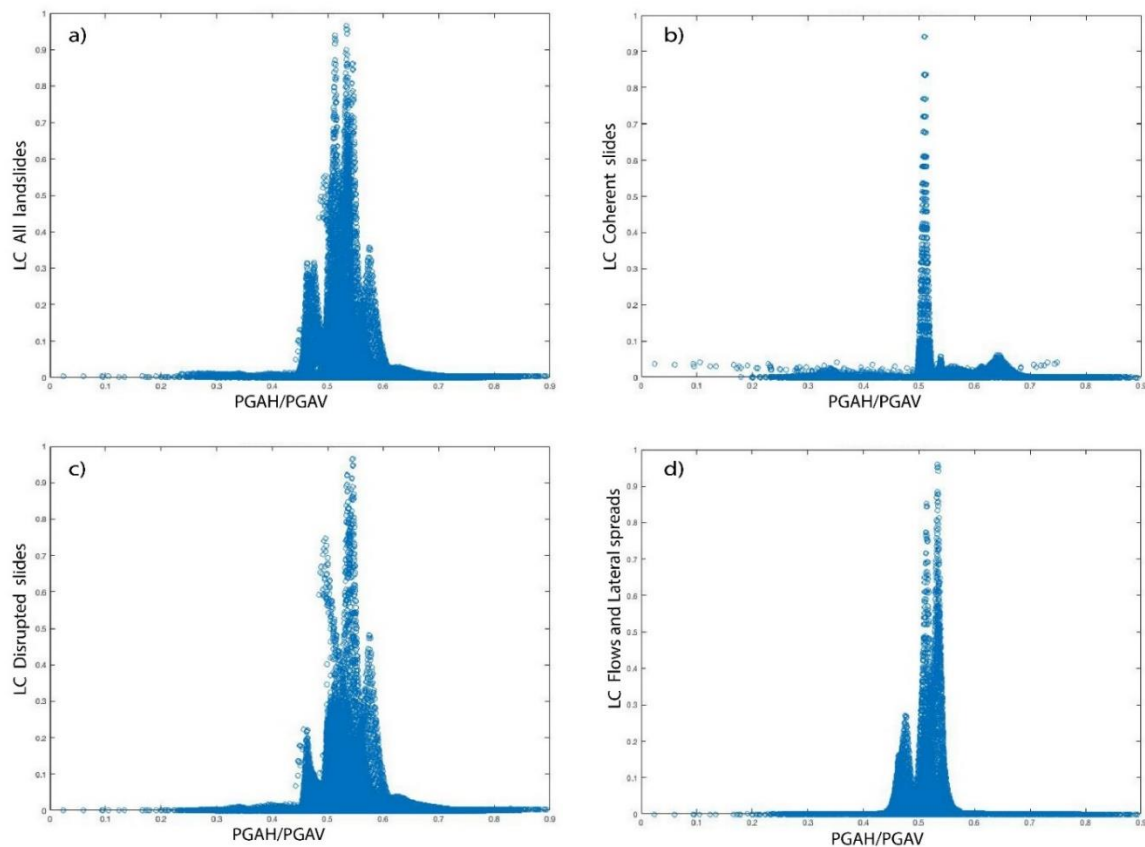
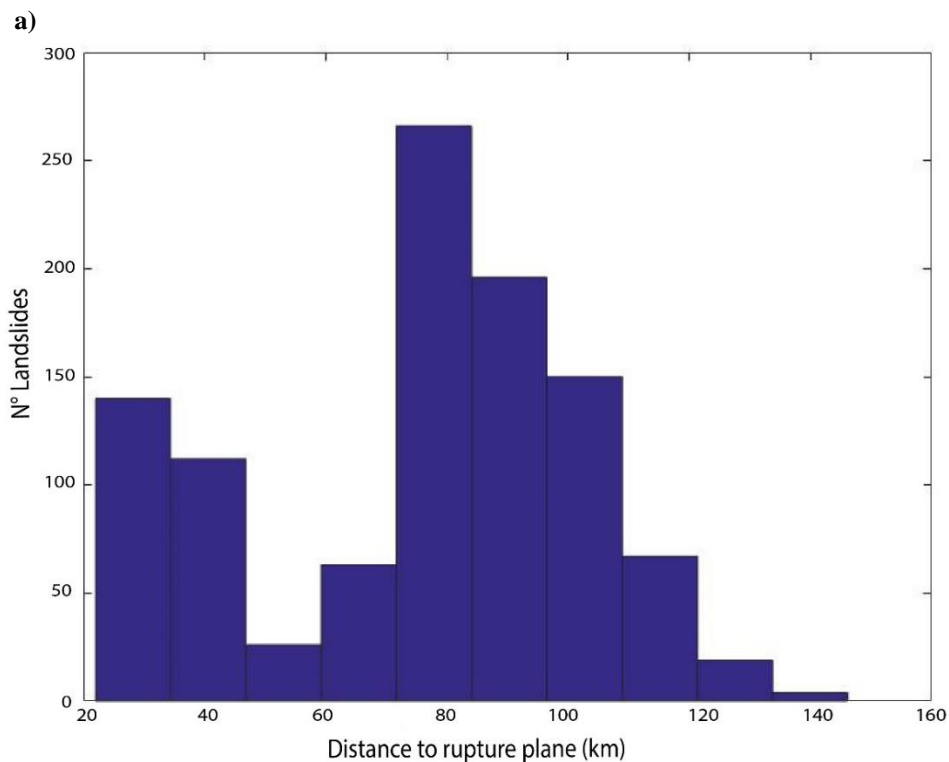


Figure 5.8. Scatter plots of landslide concentration (LC), obtained from Figure 5.7, vs PGAH/PGAV values obtained from map (Figure 5.3). a) Corresponds to all Landslide; b) disrupted landslide; c) coherent landslides; and d) flows and lateral spreads.

We also evaluated the potential correlation between LC parameter with distance by calculating the landslide smallest distance (linear distance) to the rupture plane, analogous to the analysis of *Keefe (2000)* for the 1989 Loma Prieta, California event

(plotted in bins on numbers of landslides in Figure 5.9 and as a scattergraph of LC in Figure 5.9b). The rupture plane grid points were obtained by joint inversion from *Lorito et al. (2011)*, and the smallest distance was calculated using a Matlab script developed by Escobar (2013).

Overall, a substantial number of landslides occur near the source, at distances from 20 to 40 km. This pattern reduces at 40 to 70 km. At 80 km from the source, landslide occurrence drastically increases and then starts to reduce systematically. A likely interpretation to the result could be related to the fact that rupture plane (zone) is parallel to the mountain ranges. Basins with low relative relief (i.e. low landslide potential) located between the cordilleras typically lie at 40 to 60 km from the rupture plane. Therefore, landslide occurrence is not to be correlated directly to the distance to the rupture plane, but is mainly controlled by the surface relief.



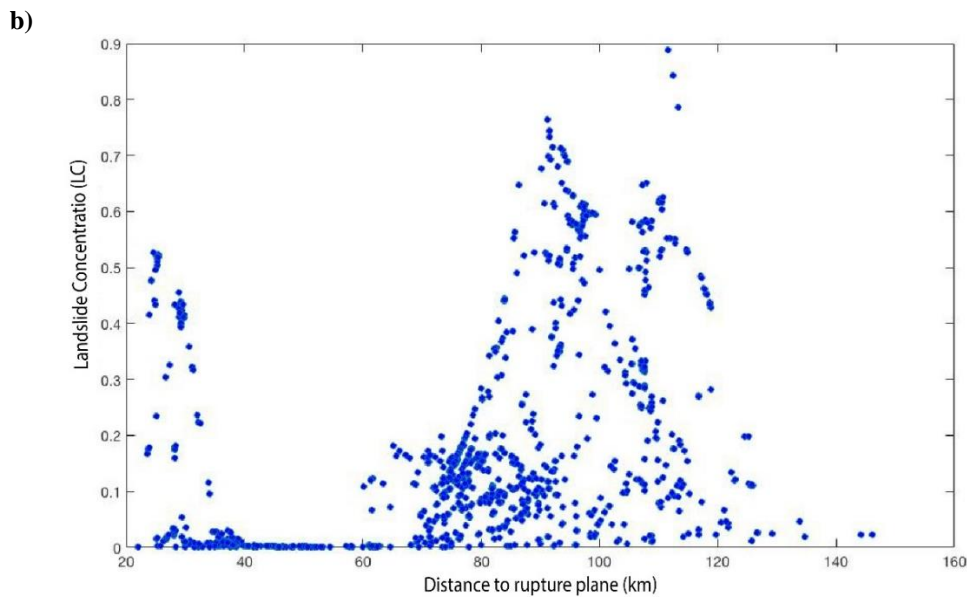


Figure 5.9. a) N° landslides vs distance to rupture plane. b) LC vs Distance to rupture plane.

5.6 DISCUSSION

In general, there is a strong coincidence between the results of this study and those from a study of the 2010 M 9.0 Tohoku earthquake (*Wartman et al., 2013*), as follows:

- Given the width of the rupture zone generating this large magnitude earthquake, a substantial majority of landslides occurred in a zone underlain by the causative thrust.
- The spatial distribution of landslides is extremely heterogeneous, with clusters of landslides being observed.
- Disrupted landslides were the dominant type of landslides triggered by the Maule earthquake and associated aftershocks.
- A majority of landslides occurred in the youngest geologic units. The young rock materials are poorly cemented weak rocks and the degree of cementation of these poor quality rock masses is likely to be a controlling factor rather than the age.
- There is no clear correlation between ground motion (PGA) and landslide intensity. It should be recognized that PGA does not represent other potentially important characteristics such as frequency content, duration, or the multiple phases of shaking recorded at some locations, whose influence on landslides should be studied in more depth.

Figure 5.10 shows the relationship between the total number of landslide (N_{LT}) and earthquake moment magnitude (M_w) for shallow crustal and megathrust earthquakes (Table 5.2). It is notable that the total number of landslides triggered for the megathrust earthquakes is substantially lower, typically by one to two orders of magnitude, than it would be expected for shallow crustal earthquakes. We suggest that there may be a fundamentally different landslide response to megathrust earthquakes in subduction plate contacts compared with shallow crustal events. The former tend to trigger a much smaller number of landslides compared to those generated by shallow crustal earthquakes.

Attenuation models predict PGA values, but not the specific waves that cause them (P, S or Surface waves). Earthquakes that generate fault rupture at the surface, are likely to produce greater amounts of surface waves, which typically is what causes damage. We can speculate that a megathrust earthquake suffers much higher surface waves attenuation than shallow crustal earthquakes, triggering a smaller amount of landslides.

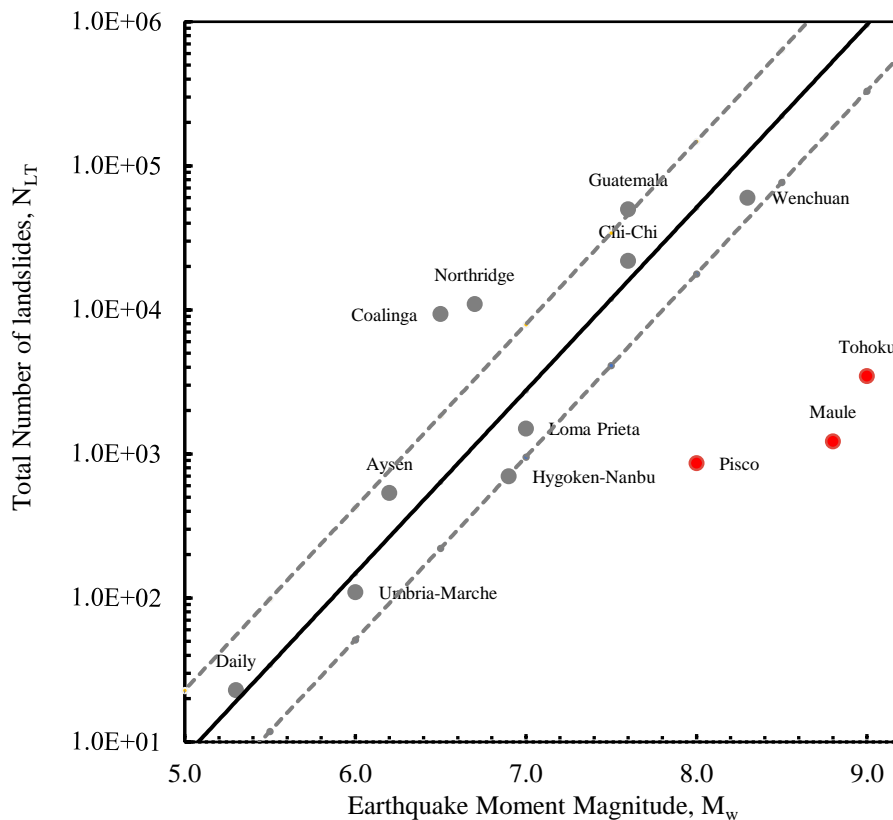


Figure 5.10. Dependence of Total number of landslide N_{LT} and earthquake moment magnitude M_w to shallow crustal (grey) and megathrust (red) earthquakes. Solid line is the correlation from the relationship proposed by *Malamud et al. (2004b)* with the grey dashed lines providing the corresponding error bounds.

Table 5.2. Comparative table of different landslide-generating earthquakes

Earthquake	M_w	Earthquake type	N_{LT}	m_L
Daily City, CA, USA	5.3**	shallow crustal	23 ^(a)	1.4
Umbria-Marche, Italy	6.0	shallow crustal	110 ^(a)	2.0
Aysén, Chile	6.2	shallow crustal	538 ^(b)	2.7
Coalinga, CA, USA	6.5	shallow crustal	9,389 ^(a)	4.0
Northridge, CA, USA	6.7	shallow crustal	11,000 ^(c)	4-0
Hygoken-Nanbu, Japan	6.9	shallow crustal	700 ^(a)	2.8
Loma Prieta, CA, USA	7.0	shallow crustal	1,500 ^(a)	3.2
Chi-chi, Taiwan	7.6	shallow crustal	22,000 ^(d)	4.3
Guatemala	7.6	shallow crustal	50,000 ^(a)	4.7
Wenchuan, China	8.3	shallow crustal	60,000 ^(e)	4.8
Pisco, Perú	8.0	megathrust	866 ^(f)	2.9
Maule, Chile	8.8	megathrust	1,226 ^(g)	3.1
Tohoku, Japan	9.0	megathrust	3,477 ^(h)	3.5

* N_{LT} is the total number of landslides associated with the triggered event; * m_L is the landslide-event magnitude ($m_L = \log N_{LT}$; Malamud *et al.* 2004b); **Earthquake magnitudes are all moment or equivalent moment magnitudes except for Daily City (local magnitude); ^(a) Keefer (2002); ^(b) Sepúlveda *et al.* (2010); ^(c) Jibson (1995); ^(d) Huang *et al.*, (2001); ^(e) Gorum *et al.*, 2011; ^(f) Lacroix *et al.* (2013) ; ^(g) This study; ^(h) Wartman *et al.* (2013)

It is difficult to draw definitive conclusions about this observation, given the limited number of megathrust events. However, we can speculate as to possible reasons for this effect. These might include:

- 6 In the case of the megathrust earthquakes, the distance from the fault plane to the topography is much larger than is the case for many shallow crustal earthquakes. This may affect the key seismic parameters that control slope stability. Whilst it is conventionally considered that this parameter may be PGAH, this study and others fail to find a strong relationship between landslide occurrence and the regional distribution of PGAH. It is not known if this is because modelled values of PGAH are incorrect, or that this parameter is not the key control.
- 7 The type of faulting mechanism may affect the characteristics of the seismic waves, such as for example the frequency range. Whether faulting produces surface rupture may also change the characteristics of shaking.
- 8 The availability of topography susceptible to failure varies between the two settings, with shallow crustal earthquakes often being associated with areas of steep terrain and high relative relief close to the fault plane. Whilst megathrust earthquake may

also be associated with areas of steep terrain, these are typically at a much larger distance from the fault plane.

- 9 The susceptibility of the rocks may vary across the two tectonic settings. Thus, for example, the lithologies close to the fault plane for shallow crustal earthquakes may be weaker, with higher densities of persistent discontinuities, allowing more landslides to be generated

In the case of the 2011 M_w 9.0 Tohoku earthquake, the majority of the disrupted landslides appear to have originated at or near the crest of steep slope, suggesting that the topographic modification of ground motion played a role in their initiation (*Warman et al., 2013*). Topographic amplification is a site effect caused by the interaction of the incoming seismic waves with certain geomorphological features, such as steep slopes in areas of strong topographic relief, which results in larger amplitudes of the ground motion toward the ridge crests (e.g., *Densmore & Hovius 2000; Sepúlveda et al., 2005; Meunier et al., 2008*). *Meunier et al. (2008)* proposed a graphic method to represent the position of landslides on the slopes, combining the normalized distance of the landslide top to the ridge crest and the normalized distance of the landslide toe to the nearest stream. This method is applied in Figure 5.11. A concentration of circles close to the y-axis represents that coseismic landslides are strongly clustered near ridge crests, such as for shallow crustal earthquakes of Northridge (*Meunier et al., 2008*) and Aysén in southern Chile (*Sepúlveda et al., 2010*). In the last one, about two thirds of the landslides start in the upper quarter of the slope, while over 90% start in the upper half, which suggests that larger ground motions due to topographic site effects influenced the triggering of landslides during the earthquake (*Sepúlveda et al., 2010*). Figure 5.11 shows that landslides induced by the Maule earthquake are not clustered close to the ridge tops, so we could disregard a predominant topographic site effect in their generation, although it may have played a role locally.

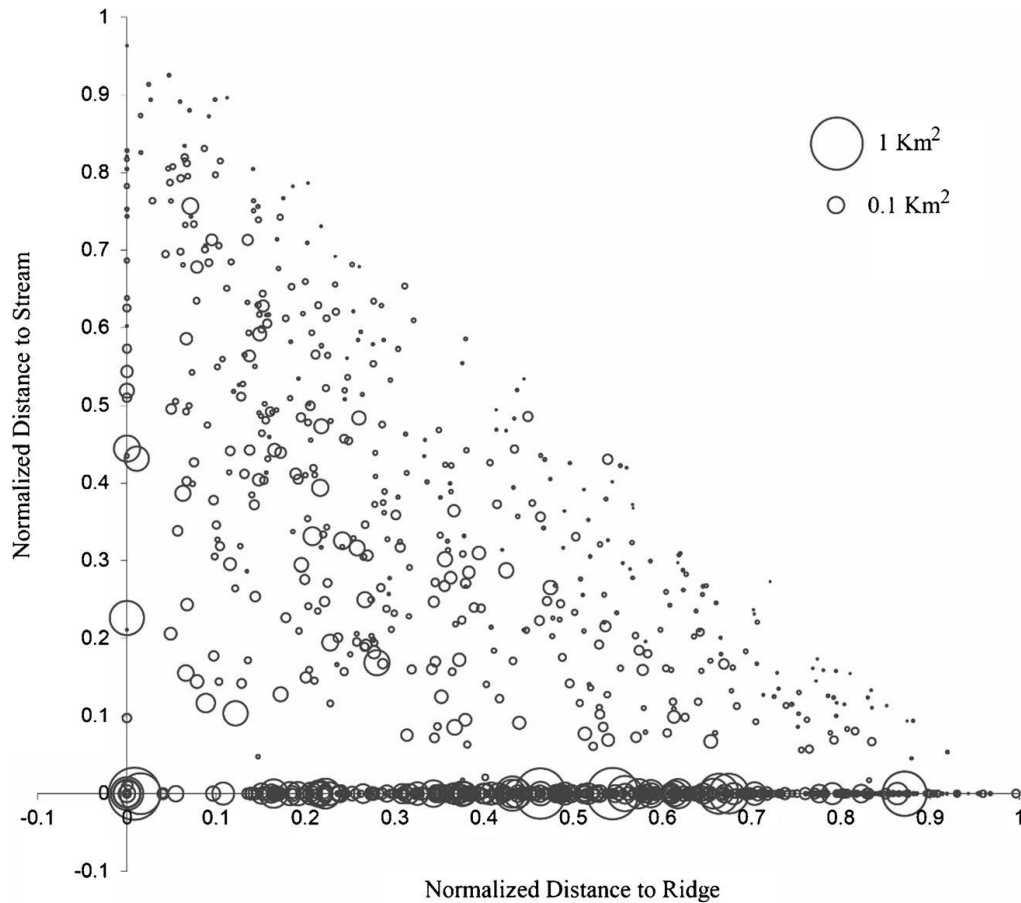


Figure 5.11. Landslide relative position on the slopes. Normalized distance of the landslide crowns to ridge tops against normalized distance of landslide toes to nearest streams. The size (surface area) of the landslide is indicated with a circle of variable diameter.

It is difficult to establish a direct correlation between observed PGA values and does PGA’s obtained from ground motion prediction equations. In this context, GMPE for Chilean subduction zone (*Idini et al., 2017*), estimate a decrease from c. 0.2g to 0.15g (in a normalized logarithmic scale) up to a rupture distance c. 200 km. These results correlate well with our PGAV map (Figure 5.5b) but not with PGAH values (Figure 5.5a) that could be caused by other effects (e.g. site effect, Angol station).

We observe that the key seismic parameter that appears to explain the distribution of landslides best is the ration between PGAH and PGAV. It is not clear as to why this might be the case, but *Brain et al. (2014)* suggested that wave phasing, and the associated coincidence of horizontal and vertical accelerations, may play a key role in determining slope response. The role of slip surface normal accelerations in the initiation of landslides is seen as significant by *Huang et al. (2001)* and the complexity

generated by rapidly fluctuating normal and shearing stresses during shaking deserves much further investigation.

5.7 CONCLUSIONS

We have compiled and analysed an inventory of landslides triggered by the 2010 M 8.8 Maule earthquake in the Chilean subduction zone. We find that the number and density of landslides triggered by the earthquake is lower than might have been expected for a seismic event of this scale (by one to two orders of magnitude) than for a shallow crustal earthquake of a similar or even lower magnitude, in common with observations for the 2011 M_w 9.0 Tohoku earthquake in Japan. Landslides occurred primary on low to moderate angled slopes towards the western side of the main Andean range, accompanied by clusters of landslides in the lower Coastal Range. For the 2010 Maule earthquake, we suggest that relief exerted a strongly dominant control on coseismic landsliding, with lithology the second most relevant conditioning factor, with more landslides in younger rocks. We find a poor correlation between PGA and landslide occurrence, and with distance from the fault plane, but note a much stronger correlation between landslide concentration and the ratio between horizontal and vertical peak accelerations.

These results suggest that the number and distribution of coseismic landslides may differ significantly between megathrust and shallow crustal earthquakes, although further research through the collation of high quality inventories is required as further megathrust earthquakes occur. At present the paucity of inventories for megathrust earthquakes defies the proposal of a definitive explanation for this observation. However, it may prove to be important in terms of the relative distribution of hazards associated with earthquakes in areas affected by megathrust earthquakes. Chile has a high concentration of large magnitude rock avalanches in the Andes; these results may suggest that they may be associated with proximal, lower magnitude shallow crustal earthquakes rather than larger but distal megathrust events.

6. CASE STUDY: UPDATE COMPREHENSIVE INVENTORY OF LANDSLIDES INDUCED BY THE 2007 AYSÉN EARTHQUAKE

6.1 INTRODUCTION

On April 21, 2007 an M_w 6.2, strike-slip mechanism earthquake struck the region of Aysén, Chilean Patagonian Andes. It was the peak of unusual seismic activity of over 7000 earthquakes that started four months before in the Aysén fjord area (45.3°S, 73.0°W, *Legrand et al., 2011*). The seismic activity source is the Liquiñe-Ofqui Fault System (LOFS), a major active transpressional intra-arc fault system of NNE trend and that accommodates the parallel component of the oblique subduction of Nazca plate beneath the South American plate (*Cembrano et al., 1996; Cembrano et al., 2007; Legrand et al., 2011,; Vargas et al., 2013*). The most remarkable are the dextral-normal NE-SW-striking Quitralco fault (QF) and the N-S striking strike-slip Río Cuervo (RCF) and Punta Cola faults (PCF) (*Villalobos et al., 2020*). By combining tectonic observations with local seismicity data, *Villalobos et al. (2020)* propose a seismotectonic model for the evolution of the 2007 seismic sequence where three structures were progressively activated from the depth towards the upper continental crust, causing surface rupture along the PCF and with earthquakes (i.e. partial ruptures along other faults).

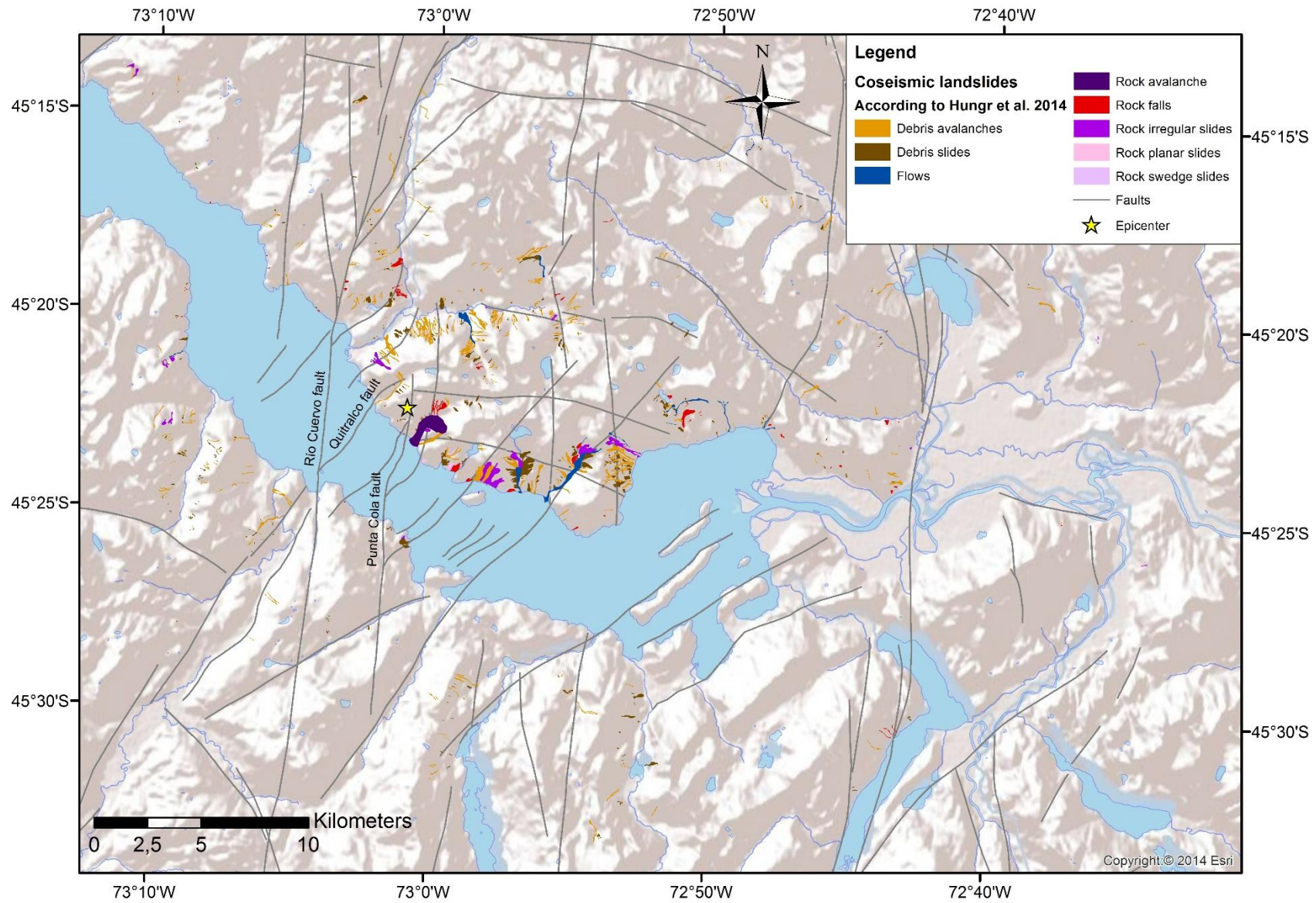
The main shock (M_w 6.2, M_s 6.3; Global CMT Catalog, 2008; NEIC, 2008) occurred at 13:50 local time on April 21. The reported intensity was VII in nearby towns (over 20 km away) of Puerto Aysén and Puerto Chacabuco, causing moderate damage. No proper local instrumental information on the mainshock and aftershocks was retrieved from the purpose-installed local network, as most instruments of were damaged or destroyed by the local tsunami, thus precise localization of the main shock could not been obtained (*Sepúlveda et al., 2010*).

6.2 UPDATE COMPREHENSIVE INVENTORY

A first version of the 2007 earthquake-triggered landslide inventory for the Aysén earthquake was published by *Sepúlveda et al. (2010)*. A total of 538 landslides were mapped from field observations and remote sensing analysis, and classified following the indications by *Keefner (1984)* with some adaptations to the area of study. The earthquake-

induced landslides were classified as rock slides and avalanches, rock falls, shallow soil and soil-rock slides, and debris flows.

Following the principles of coseismic landslides identification from remote sensing images, selecting remote sensing images, and building coseismic landslides attribute database (Third chapter), I provide an update comprehensive inventory of landslides triggered by the 2007 Aysén earthquake based on research of *Sepúlveda et al. (2010)* (Figure 6.1). Landslides were re-classified based on a renewed Varnes classification of landslide types, developed by *Hungr et al. (2014)*. Coseismic landslides were re-mapped during a field trip in February 2016, supplemented by interpretation of air photographs at different scales (1:20,000 to 1:70,000) and Landsat satellite images (Landsat 5-7-8; provider, NASA; resolution, 30 m), before and after the earthquake using Google Earth.



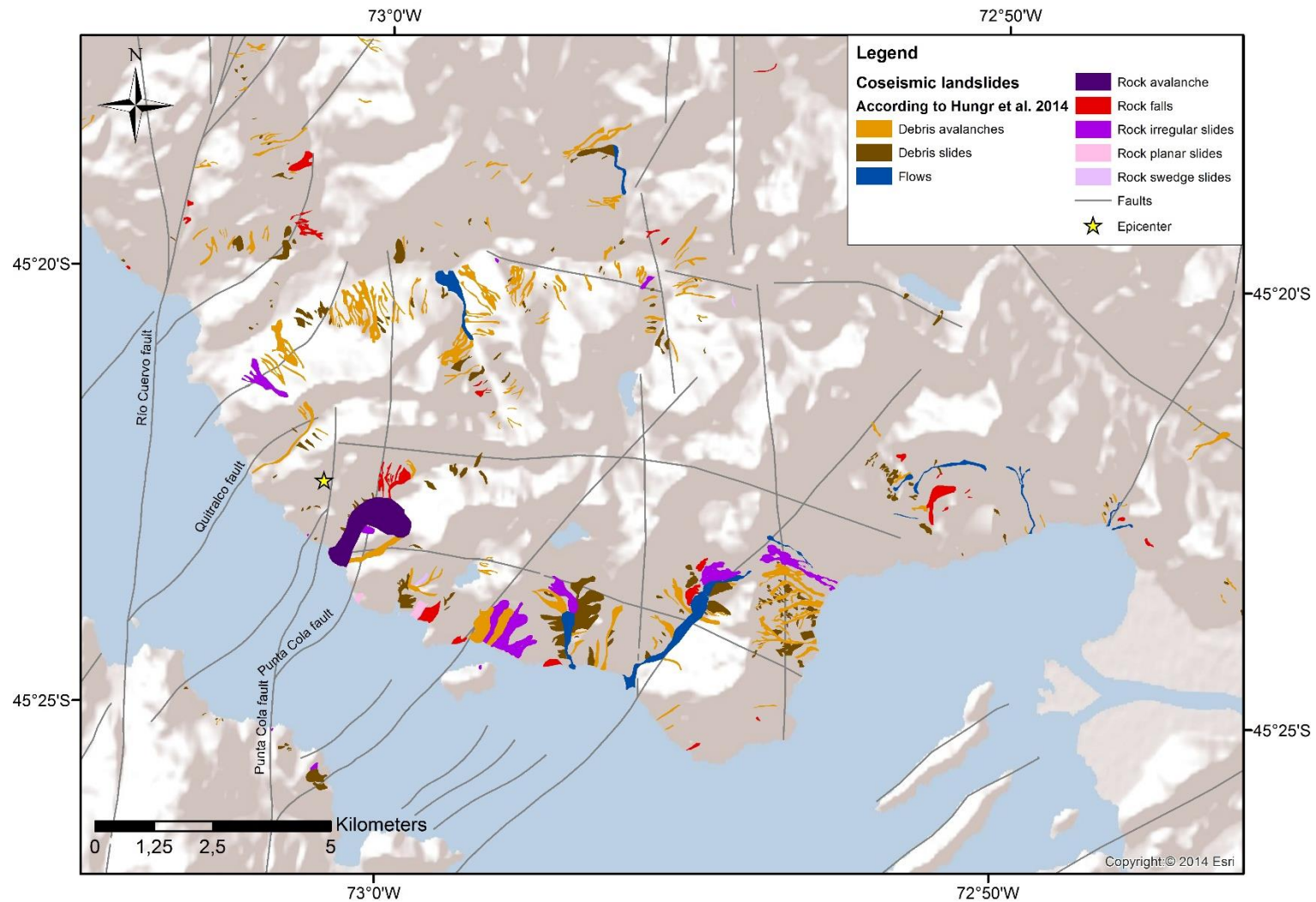


Figure 6.1. Update comprehensive inventory of landslides triggered by the 2007 Aysén earthquake based on research of *Sepúlveda et al. (2010)*.
 Up, Scale 1:200.000. Down, zoom in the area with a major concentration of coseismic landslides, scale 1:100.000.

The slides were mostly triggered in steep slopes in the fjord and adjacent glacial valleys formed by strong intrusive igneous rocks of the North Patagonian Batholith, usually covered by shallow volcanic soils formed by pyroclasts from the nearby volcanoes. Fewer slides were induced in the slopes of small monogenetic volcanoes that distribute along the LOFZ trace.

The largest landslide was a rock avalanche in the lateral creek of Punta Cola, in the epicentral area. This landslide has been studied in detail by *Redfield et al. (2011)* and *Oppikoffer et al. (2012)*, who described the rock slide area structure and the rock avalanche geomorphology, respectively. The volume was estimated as 22 Mm³ by *Oppikoffer et al. (2012)*, from which around 55-65% reached the fjord, about 1 km away from the source (*Oppikoffer et al., 2012; Vollmer, 2017*). *Sepúlveda et al. (2010)* suggested the importance of topographic amplification effects in triggering the largest rock slope failures. This was tested by preliminary slope stability analyses by *Serey (2011)* and by numerical modelling for Punta Cola by *Escudero (2017)* and *Aravena (2017)*, confirming the presence of topographic site effects as well the importance of local faults in the slope destabilization. Meanwhile, numerical modelling of the rock avalanche suggests velocities of up to 20-30 m/s (*Vollmer, 2017*).

The largest landslides such as the Punta Cola rock avalanche and the Mentirosa Island Landslide complex (Figures 3.1 and 3.2), along with several smaller coastal rock slope failures and some debris flows, caused displacement waves in the fjord, which killed ten people and caused major damage in salmon farm infrastructure along the fjord shores (*Naranjo et al., 2009; Sepúlveda & Serey, 2009*). The major landslides caused significant changes in the fjord sea bottom, forming spectacular ring shaped structures by the sediment being pushed by the incoming debris, as studied by oceanographic campaigns in the fjord (*Van Daele et al., 2013; Hermanns et al., 2014; Lastras et al., 2016*).

In total 781 landslides were re-mapped. Debris avalanches (322) and debris slides (338) are the most common of landslides induced by the earthquake. They are shallow translational failures (generally less than 2–3 m deep) and small (up to few hundred thousands of square metres in surface area) that involved the whole volcanic soil cover and possibly the uppermost weathered layer of bedrock. Rock falls (65) occurred on steep rock slopes or more commonly by the detachment of rock blocks from subvertical cliffs.

Debris flow deposits (17) generated by the debris of the formerly described landslides can be observed. The combination of debris with running water in the creeks, temporal damming of streams, and some fluidization of the sliding masses during movement would have allowed the formation of the flows

6.3 ANALYSIS OF COSEISMIC LANDSLIDES

Calculated volume of landslides and total volume slide for both Chilean inventories (Table 6.1), c. 90% corresponds to rock landslides (rockslides and rock avalanche).

Table 6.1. Comparative table of comprehensive coseismic landslides inventories of Chile.

	2010 Maule earthquake	2007 Aysén earthquake
Magnitude (M_w)	8.8	6.2
Total affected area (km^2)	12,500	1,350
Total number of landslides	1,226	781
Total volume slide (Mm^3)	10.6	122.3

The difference between total numbers of coseismic landslides during Aysén earthquake obtained by *Sepúlveda et al. (2010)* and *this study* is mainly due to the incorporation of previously unidentified landslides.

Figure 6.2 shows the frequency distribution curves of landslides in Aysén and Maule earthquakes, compared with other important cases of coseismic landslides inventories like the 1994 M_w 6.7 Northridge and the 2011 M_w 9.0 Tohoku earthquakes.

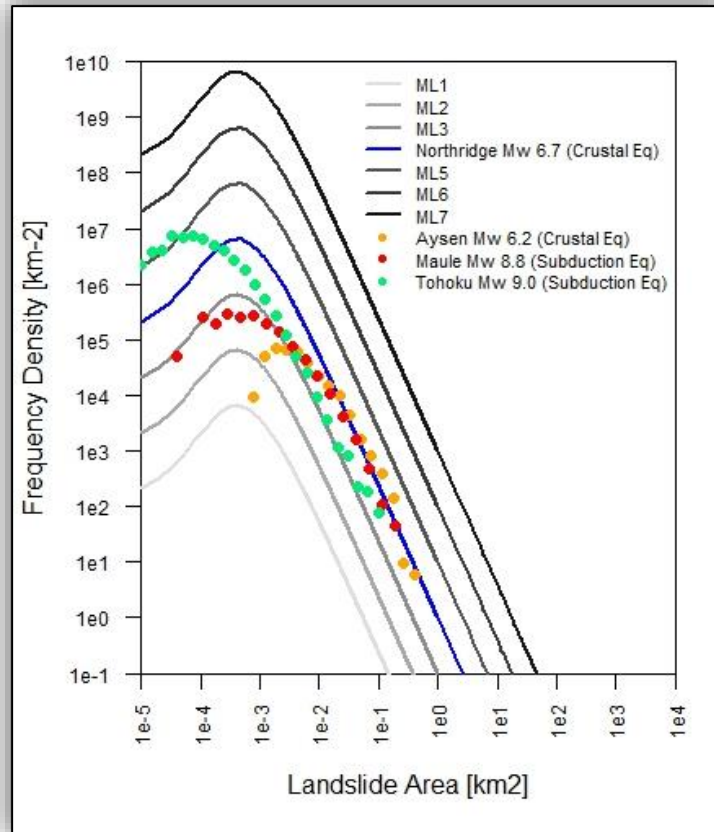


Figure 6.2 Frequency density function of landslides area (km^2), based on Inverse-Gamma distribution function, a theoretical law proposed by *Malamud et al. (2004)*.

Both Chilean inventories curves are similar in form as theoretical law proposed by *Malamud et al. (2004)*. Although they differ in the part before the point of inflection, they have the same decay corresponding to landslides of greater area, even being located above the curve of the Tohoku earthquake, which could suggest that independent of the Chilean earthquake type (megathrust or shallow crustal) the frequency distribution of coseismic landslides is the same.

In the Aysén earthquake, 66% of the landslides start in the upper quarter of the slope, while over 90% start in the upper half, which suggests that larger ground motions due to topographic site effects influenced the triggering of landslides during the earthquake (*Sepúlveda et al., 2010*). Additionally, the location of the landslides is also clearly related to the main fault traces of the seismogenic LOFS (*Sepúlveda et al., 2010*). The number of landslides decreased with distance from the seismic fault. 55% of coseismic landslides triggered by the 2007 Mw 6.2 Aysén earthquake were concentrated within 0-5 km of

seismic faults (Figure 6.4). Even 18% of coseismic landslides were located within the first kilometer of distance to seismic faults (QF, RCF and PCF). A similar distribution of coseismic landslides induced by the 1927 Ms 7.1 earthquake occurred in the study area (Serey, 2011). The highest number of landslides clusters coincided with the Palos Fault (LPF), an N-S striking strike-slip fault traces of the seismogenic LOFS. Thus, distance to the rupture plane of faults is a first-order factor in the distribution of landslides together with topographic amplification site effects.

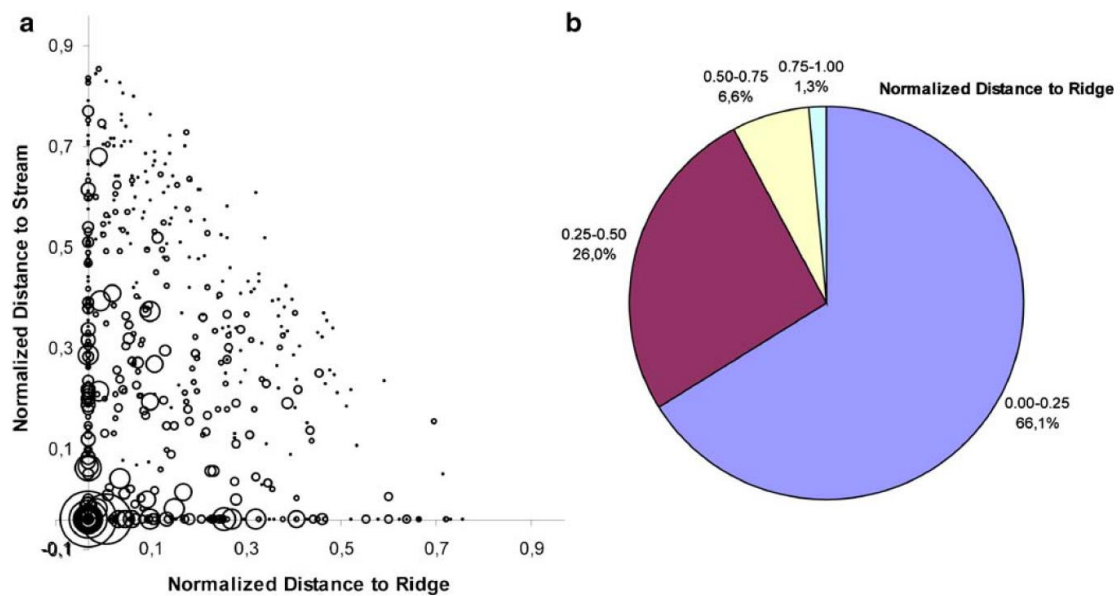


Figure 6.3. Landslide relative position on the slopes. a) Normalized distance of the landslide crowns to ridge tops against normalized distance of landslide toes to nearest streams. b) Distribution in percentage of ranges of normalized distance to ridge crests. Figure extracted from Sepúlveda *et al.*, (2010).

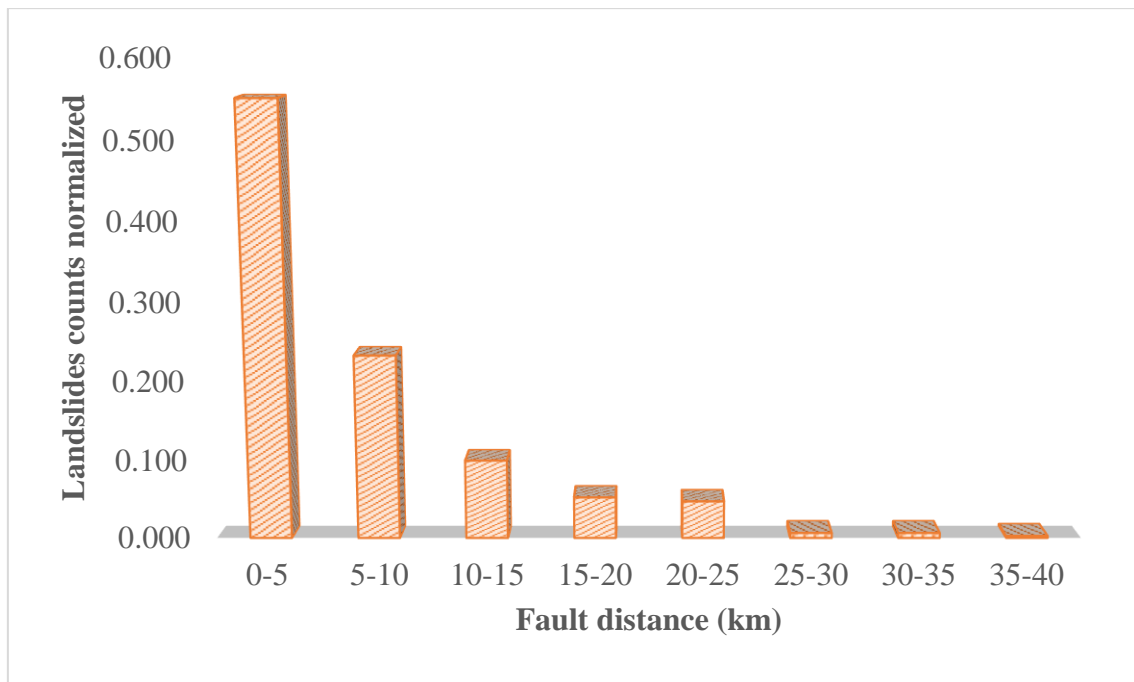


Figure 6.4. Landslides counts normalized vs Distance to the faults.

6.4 DISCUSSIONS

Notorious differences often exist in the total number of coseismic landslides in inventories prepared by different researchers for the same seismic event. Possibly, this could be due to a lack of unified guidelines for the preparation of comprehensive coseismic landslides inventories. For instance, the inventory of landslides triggered by the M_w 6.2 Aysén Fjord earthquake. *Sepúlveda et al., (2010)* mapped and classified from field observations and remote sensing analysis 538 landslides. While that *Xu (2015)* delineated at least 1000 landslides triggered by the Aysén earthquake, and *Gorum et al. (2014)* obtained c.a. 550 coseismic landslides induced by the Aysén event, both studies used remote sensing images methods only. And in this study we re-mapped 781 landslides during a field trip in February 2016, supplemented by interpretation of air photographs at different scales (1:20,000 to 1:70,000) and Landsat satellite images (Landsat 5-7-8; provider, NASA; resolution, 30 m), before and after the earthquake using Google Earth.

The 2007 M_w 6.2 and 1927 M_s 7.1 earthquakes in the study area revealed an unknown situation of seismic and coseismic landslide hazard, from which many researches have emerged. For example, *Villalobos et al., (2020)* paleoseismological analysis reveals at

least seven paleo landslide events buried in the fjord sediments, that were triggered by local paleoearthquakes, which occurred since local ice-sheet retreat, i.e. ca. 12 kyrs.

6.5 CONCLUSIONS

Forecasting the distribution and impact of landslides induced by earthquakes is one of the greatest challenges in the earth sciences. In this chapter, it provides an update comprehensive coseismic landslides inventory of the 2007 M_w 6.2 shallow crustal Aysén earthquake based on *Sepúlveda et al., (2010)*. In total 781 landslides were re-mapped over a total area of c.1,350 km², based on unified coseismic landslides mapping criteria expressed in the third chapter. The total landslide volume is c. 122.3 Mm³. 18% of coseismic landslides were concentrated within 0-1 km of seismic faults, and 55% of landslides within 0-5 km. Hence, distance to the rupture plane of faults is a first-order factor in the distribution of landslides together with topographic amplification site effects.

7 DEVELOPING CONCEPTUAL MODELS FOR THE RECOGNITION OF COSEISMIC LANDSLIDES HAZARD FOR SHALLOW CRUSTAL AND MEGATHRUST EARTHQUAKES IN DIFFERENT MOUNTAIN ENVIRONMENTS– AN EXAMPLE FROM THE CHILEAN ANDES

Published as:

Serey A; Sepúlveda, SA; Murphy, W; Petley DN; De Pascale, G (2020) Developing conceptual models for the recognition of coseismic landslides hazard for shallow crustal and megathrust earthquakes in different mountain environments – an example from the Chilean Andes. Quarterly Journal of Engineering Geology and Hydrogeology, <https://doi.org/10.1144/qjegh2020-023>

ABSTRACT

Landslides represent the most frequent geological hazard in mountainous environments. Most notably, landslides are a major source of fatalities and damage related with strong earthquakes. The main aim of this research is to show through three-dimensional engineer-friendly computer drawings, different mountain environments where coseismic landslides could be generated during shallow crustal and megathrust earthquakes in the Andes of central Chile. From the comparison of local earthquake-induced landslide inventories in Chile, from the M_w 6.2, shallow crustal Aysén earthquake in 2007 (45.3° S) and the M_w 8.8, megathrust Maule earthquake in 2010 (32.5°S - 38.5°S), with others from abroad, as well as analysis of large, prehistoric landslide inventories proposed as likely induced by seismic activity, we have determined topographic, geomorphological, geological and seismic controlling factors in the occurrence of earthquake-triggered landslides. With these results, we have built four representative geomodels of coseismic landslide geomorphological environments in the Andes of central Chile. Each one represents the possible landslide types to be generated by a shallow crustal earthquake versus those likely to be generated by an megathrust earthquake. Additionally, the associated hazards and suggested mitigation measures are expressed in each scenario. These geomodels are a powerful tool for earthquake-induced landslide hazard assessment.

Keywords: coseismic landslides, conceptual hazard models, Chile.

7.1 INTRODUCTION

Landslides represent perhaps the most frequent geological hazard in mountainous environments due to the geological, geomorphological and geotechnical characteristics of steep upland landscapes. In tectonically-active mountain areas, landslides are a major cause of fatalities and economic losses during and after strong earthquakes (*e.g. Sepúlveda et al., 2005; Qi et al., 2010; Dai et al., 2011*).

Coseismic landslide hazard, defined as the relative probability of landslide occurrence at a specific location in a specific event, is a function of intrinsic slope characteristics (slope angle, material strength, lithology, etc.), and earthquake shaking, which acts as a significant trigger mechanism for causing landslides of all types (*Keefner 1984*). In addition to those factors influencing landsliding under ambient conditions, site conditions further influence ground motions through soil and topographic amplification (*Sepúlveda et al. 2005; Meunier et al., 2008; Wang et al., 2018*). Recent studies (*e.g.; Wartman et al., 2013; Marc et al., 2016*) suggest that they are also influenced by the seismogenic zone. *Serey et al. (2019)* observed that shallow crustal and megathrust earthquakes create fundamentally different spatial patterns and densities of landslides.

Selecting seismological inputs for slope stability analysis is challenging given the large number of difficult to quantify variables associated with coseismic landslides, which include seismic wave frequency, wave amplitude and wave interactions. This is especially complex for regional hazard assessments (*Geli et al., 1988; Meunier et al., 2008*). Several statistical methods exist for modelling regional-scale coseismic landslide hazard (*e.g. Jibson et al., 2000; Miles & Keefner, 2000; 2007; 2009; 2009b*), all of them only considering one kind of coseismic trigger, i.e. shallow crustal earthquakes. Thus, a first-order form of hazard identification can prove beneficial prior to considering more complex analytical tools and different kinds of coseismic triggers. One such approach is to visualize all these variables, both conditioning and triggering factors, in the form of graphic 3D ground models, often referred to as geomodels. Such tools are also valuable in explaining complex geotechnical problems to non-specialists such as government and planning agencies.

The concept of a geomodel, and its depiction in simplified block diagrams, aims to allow visualization of the geology in three dimensions and to act as a quick introduction to new or unfamiliar ground conditions or environments (*Jackson, 2016*). *Fookes (1997)* defined conceptual geological models for a number of different environments, which have been linked to hazard assessment and engineering to mitigate geohazards (e.g. *Hearn & Hart, 2011; Hearn et al., 2012; Hearn, 2018*).

Parry et al. (2014) considered that there are two fundamentally different stages for developing engineering geological models: conceptual and observational. The conceptual approach is based on understanding the relationships between engineering geological units, their likely geometry and anticipated distribution. Importantly, these models are largely based on geological concepts such as age, stratigraphy, rock type, unconformity and weathering (the ‘total geological history’ approach by *Fookes et al., 2000*). The main aim of the work presented here has been to develop practitioner-friendly conceptual ground models relating to the performance of slopes subject to strong ground motions during earthquakes in different mountain environments in the Chilean Andes. These were further subdivided into slope performance during (i) megathrust earthquakes and (ii) shallow crustal earthquakes, to indicate expected slope behavior when subjected to earthquakes of different sizes and epicentral distance. The performance of the slopes is derived from the databases outlined in *Serey et al. (2019)*. In addition to the hazards identified, potential mitigation measures are outlined based on the rock slope engineering.

7.2 COSEISMIC LANDSLIDES IN THE MOUNTAIN ENVIRONMENT OF CHILE

The Cordilleran areas in Chile constitute a major part of the landmass and contain nearly all of copper and other precious metals mining that contribute strongly to the Chilean economy. Additionally, mountain infrastructure is a vital lifeline for the flow of materials, access to markets for mountain communities and neighbor countries, and tourism. However, given the mountain conditions it is difficult to provide alternative routes in the event of lifeline disruption.

Seismically-induced landslides are a common phenomenon in the Andes, in central and southern Chile. This is attributed to two factors: firstly, the tectonic evolution of Chile

and secondly, the glaciation of the Andes resulting in variable geological conditions. Chile can be considered the most seismically active country in the world (*Cisternas, 2011; Barrientos, 2018*); ten M8 or larger earthquakes have occurred along the Chilean coast in the past century, with a \geq M8 earthquake occurring approximately every dozen years (*Barrientos, 2018*). The second factor is that the Andes of central and southern Chile were strongly affected by Quaternary glaciations (with many areas still covered in ice), resulting in steep topography, strong erosional features and rock masses weakened by the effects of Late-Quaternary ice action. The pattern of glaciation/deglaciation of the Andes is complex, with changes in moisture in the atmosphere combined with lowering temperatures led to a complex change in seasonal snowline variation during the late Pleistocene.

7.2.1 THE SEISMOTECTONIC SETTING AND SEISMICITY OF CHILE

The Andes of central Chile (32.5° S to 41.5° S) are composed of a number of morphostructural units from west to east: the Coastal Cordillera, the Central Valley, the Principal Cordillera (spanning Chile and Argentina), the Frontal Cordillera, the Argentine Precordillera and the Pampean Ranges (*Jordan et al., 1983*) (Figure 7.1). The Principal Cordillera is a chain of high mountains that in its western part in Chilean territory mostly comprises Oligocene–Miocene continental volcanoclastic rocks, intruded by Miocene–Pliocene granitoids (*Pankhurst & Hervé, 2007; Charrier et al., 2015*). The Cordilleran environment is characterised by being an active, folded orogen with a high topographic relief and steep slopes. Cycles of high activity (driven by periods of relatively rapid uplift) that initiate periods of intense erosion as rivers cut down to lower base levels and produce steep-sided valleys. Many of these valleys have limited stability, with the immature weathered surfaces continually being eroded. Hillslopes are typically mantled with colluvium and/or taluvium that is unstable when undercut.

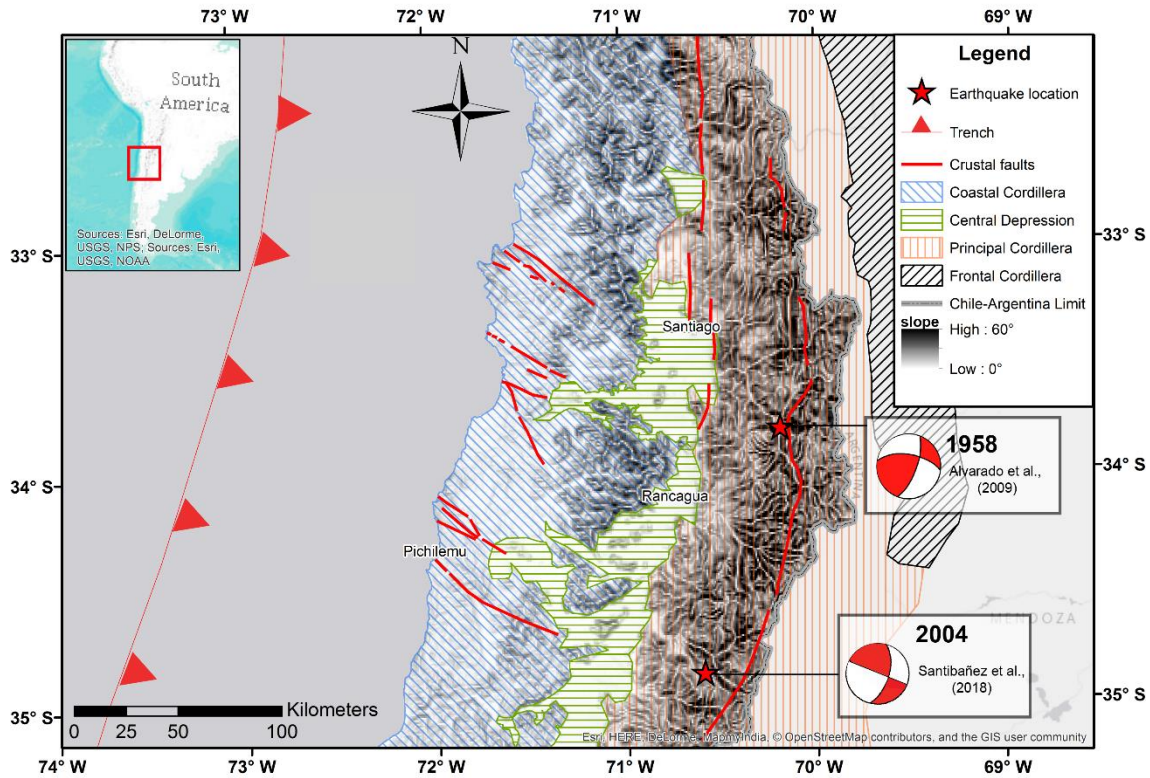


Figure 7.1. Morphostructural and seismotectonic setting of central Chilean Andes. Major crustal fault in the Chilean Andes extracted from *Armijo et al. (2010)* and *Santibañez et al. (2018)*.

Several seismogenic zones are recognized in Chile: large interplate earthquakes (depths 45–55 km); large intermediate-depth earthquakes (60–200 km); shallow crustal seismicity (depths 0–20 km); and outer-rise earthquakes along the subduction margin between the Nazca and South American Plates (*Barrientos, 2018*).

Megathrust seismicity corresponds to large magnitude (above 8) interplate earthquakes in the subduction zone plate contact. Because of their comparatively high frequency of occurrence, these earthquakes are responsible for most of the historic damage. They are located along the coast from Arica (18° S) to the triple junction at Taitao Peninsula (46° S). These events take place as a result of the convergence of the Nazca beneath the South American plate at a rate of about 7.4 cm/yr (*Argus et al., 2010*). Further south, the Antarctic plate subducts beneath the South American plate at a rate of ~8.1 cm/yr (*Lara et al., 2018*). $M \geq 8$ earthquakes are usually accompanied by notable coastal elevation changes and, depending on the amount of seafloor vertical displacement, by catastrophic tsunamis. Their rupture zones extend down to 45–53 km depth (*Tichelaar & Ruff, 1991*) and their lengths can reach well over 1000 km. Return periods for $M \sim 8$ (and above)

events are of the order of 80–130 years for any given region in Chile, and about a dozen years when the country is considered as a whole (*Barrientos, 2018*). The latest examples of these type of earthquakes were the 2010 M 8.8 Maule, the 2014 M 8.2 Iquique, and the 2015 M_w 8.3 Illapel earthquakes (*Barrientos et al., 2004; Candia et al., 2017; Barrientos, 2018*). Megathrust earthquakes seem to have much longer return periods, of the order of a few centuries for any given region (*Cifuentes, 1989; Barrientos & Ward, 1990*). Recent off-fault strong ground motion indicator paleoseismological studies carried out in southern Chile indicate recurrence intervals of ~300 years for these very large earthquakes (*Cisternas et al., 2005; Moernaut et al., 2014*).

The capacity for megathrust earthquakes to induce large numbers of landslides and mobilise large volumes of sediment was highlighted by the 1960 Valdivia (*Duke, 1960*) and the 2010 Maule (*Serey et al., 2019*) earthquakes. During the M 9.5 Valdivia earthquake extensive landsliding occurred (*Wright & Mella, 1963*). Three large landslides (2-30 Mm³ of volume) on poorly consolidated sediments at the San Pedro River attracted particular attention due to the formation of landslide dams and the threat to the city of Valdivia c. 80 km from the slides (*Davis & Karzulovic, 1963*). *Serey et al. (2019)* provide an inventory of landslides induced by the 2010 M_w 8.8 Maule earthquake, one of the few world comprehensive, reliable inventory of coseismic landslides available for megathrust earthquakes. In total, 1,226 landslides were mapped over a total area of c. 120,500 km², dominantly small disrupted slides. However, the estimated total landslide volume is only c. 10.6 M m³. The events are unevenly distributed in the study area, the majority of landslides located in the Principal Andean Cordillera and a very constrained region near the coast on the Arauco Peninsula, forming landslide clusters (*Serey et al., 2019*). Additionally, *Candia et al. (2017)* demonstrated that there were more coseismic landslides that impacted critical infrastructure in areas with the largest fault slip at the plate boundary during the 2015 M_w 8.3 Illapel earthquake (31.6°S).

Shallow crustal seismicity is important in seismic and coseismic hazard assessments because the strong ground motions (measured in % of gravity as peak ground accelerations, or PGA) that reach the surface due to limited distance for the seismic waves to attenuate. Shallow crustal seismicity (0–20 km) that occurs throughout Chile such as the Cordilleran region of south–central Chile (e.g. Liquiñe-Ofqui fault zone) is a consequence of the oblique convergence of the Nazca Plate. Magnitudes up to 7.1 have

been reported for earthquakes in this region (44,5°S y 73°W, 21 November 1927) (*Greve, 1964*). The Andean Principal Cordillera in the central part of Chile is also an important area with important crustal seismicity because of the risk to high population density and critical infrastructure. *Godoy et al. (1999)* and *Barrientos et al. (2004)* carried out structural and seismicity studies to understand this region, in which the largest recorded earthquake (less than 10 km depth) took place on 4 September 1958 (M 6.3, *Alvarado et al., 2009*), causing extensive rockfalls and a few large landslides (*Sepúlveda et al., 2008*). Shallow crustal seismicity with a relative large magnitude (> 5.5) was recently observed beneath the Andes main Cordillera at latitudes 19.6° S (Aroma; July 2001), 35.8° S (Melado River; August 2004), 38° S (Barco Lagoon; December 2006), and 45° S (Aysén Fjord; April 2007). All these events show significant strike-slip component of displacement (*Barrientos, 2018*).

In Southern Chile, The Aysén Fjord earthquake (21 April 2007, M_w 6.2) triggered over 500 landslides of different types (*Sepúlveda et al., 2010*) of which the largest was the Punta Cola rock avalanche with a volume of c. 22 Mm^3 (*Oppikofer et al., 2012*). The triggering of landslides around and into the fjord resulted in a displacement wave that killed eleven people (*Sepúlveda & Serey, 2009; Naranjo et al., 2009*).

7.3 GEOMODEL CONSTRUCTION

7.3.1 DATA USED IN CONSTRUCTION OF THE GEOMODELS

Data used to develop the geomodels presented here can be divided into two broad types: landslide inventory data and limited field observation of critical lithological units. Only two comprehensive inventories of earthquake-triggered landslides exist in Chile, the shallow crustal M_w 6.2, Aysén earthquake in 2007 (45.27°S 72.66°W) (*Sepúlveda et al., 2010*) and the M_w 8.8, megathrust Maule earthquake in 2010 between 32.5° S and 38.5° S° (*Serey et al., 2019*). These inventories are representative of the landslide triggering characteristics of these two Chilean groups of seismic events. These databases were supplemented with observations from databases beyond Chile (*e.g. Malamud et al., 2004; Marc et al., 2016*) in addition to more detailed field investigations of large, historic landslides in Chile (*e.g. Sepúlveda et al., 2008*) and landslide inventories from the geologic record considered likely to have been induced by seismic activity (*Antinao &*

Gosse, 2009; Moreiras & Sepúlveda, 2015). These databases contain data on topographic, geomorphological, geological and seismic controlling factors on the occurrence of earthquake-triggered landslides, which informed model construction.

7.3.2 DISTRIBUTION AND CHARACTERISTIC OF COSEISMIC LANDSLIDES FOR GEOMODELS IN THE CHILEAN ANDES

It is well-established that landslides are not evenly distributed in the affected areas. Landslides tend to form clusters that may be related to geological conditions or ground motion parameters (*e.g. Sepúlveda et al., 2010; Serey et al., 2019*) or to the influence of strong ground motions coincident with fault slip distributions (*Candia et al., 2017*). Furthermore, most occur in the Cordilleran environment where high relief and steeper slopes prevail. Examples of the landslides under investigation can be seen in Figure 7.2. From the analysis of databases, the following general comments can be made:

1. The most common type of landslide observed in the inventories are “disrupted” slides, consistent with observations from other earthquakes (*e.g. Keefer, 1984; Rodriguez et al., 1999; Wartman et al., 2013*).
2. Shallow disrupted slides like debris avalanches, debris slides, rock falls and rock slides, account for approximately 86% and 98% of landslides triggered by the Maule 2010 and Aysén 2007 earthquakes respectively (*Sepúlveda et al., 2010; Serey et al., 2019*) (See figure 7.2).
3. Relatively few slumps, deep block slides, or slow earth flows were observed from Chilean inventories. For example, less than 1% of total slides were classified as coherent slides for the Maule earthquake (*Serey et al., 2019*), and near 1% for the Aysén event (*Sepúlveda et al., 2010*).
4. The number and distribution of coseismic landslides differs significantly between megathrust and shallow crustal earthquakes. The total number of landslides triggered for the megathrust earthquakes is substantially lower, typically by one to two orders of magnitude, than it would be expected for shallow crustal earthquakes, of a similar or even

lower magnitude (*Serey et al., 2019*). This is due to strong ground motion attenuation from megathrust events that reduce the peak ground accelerations.

5. There is a difference in the size of landslides between the two different sources of seismicity. The landslides triggered by the megathrust Maule Earthquake are generally in the range of $10^2 - 10^3 \text{ m}^2$. Approximately 60% of coseismic landslides caused by the Maule Earthquake were in the range of 100 m^2 to $5,000 \text{ m}^2$. This can be contrasted with the fact that just under 50% of landslides induced during the crustal Aysén earthquake that were in the range of $5,000 \text{ m}^2$ to $50,000 \text{ m}^2$. This is likely to be a function of the amount of energy arriving at any given slope due to the attenuation from deeper sources mentioned above.

6. For megathrust earthquakes, such as those in 1960, there seems to be limited occurrence of large volume rock avalanches or rock slides. Although this type of earthquake is relatively frequent in Chile, no large volume rock avalanches have been observed to be triggered by them during the last century. However, as Chile has a high concentration of large volume rock avalanche deposits in the Andes (*Antinao & Gosse, 2009*), it is likely that these are associated with proximal shallow crustal earthquakes. Given the large distance between interplate seismicity and the Andes Principal Cordillera (c. 100-150 km in central Chile) these seem a more likely cause than large farfield events, like the catastrophic avalanche in 1970 triggered by an M_w 7.9 offshore earthquake, originated from Nevados Huascarán, the highest peak in the Peruvian Andes (*Plafker & Ericksen, 1978; Evans et al., 2009*).

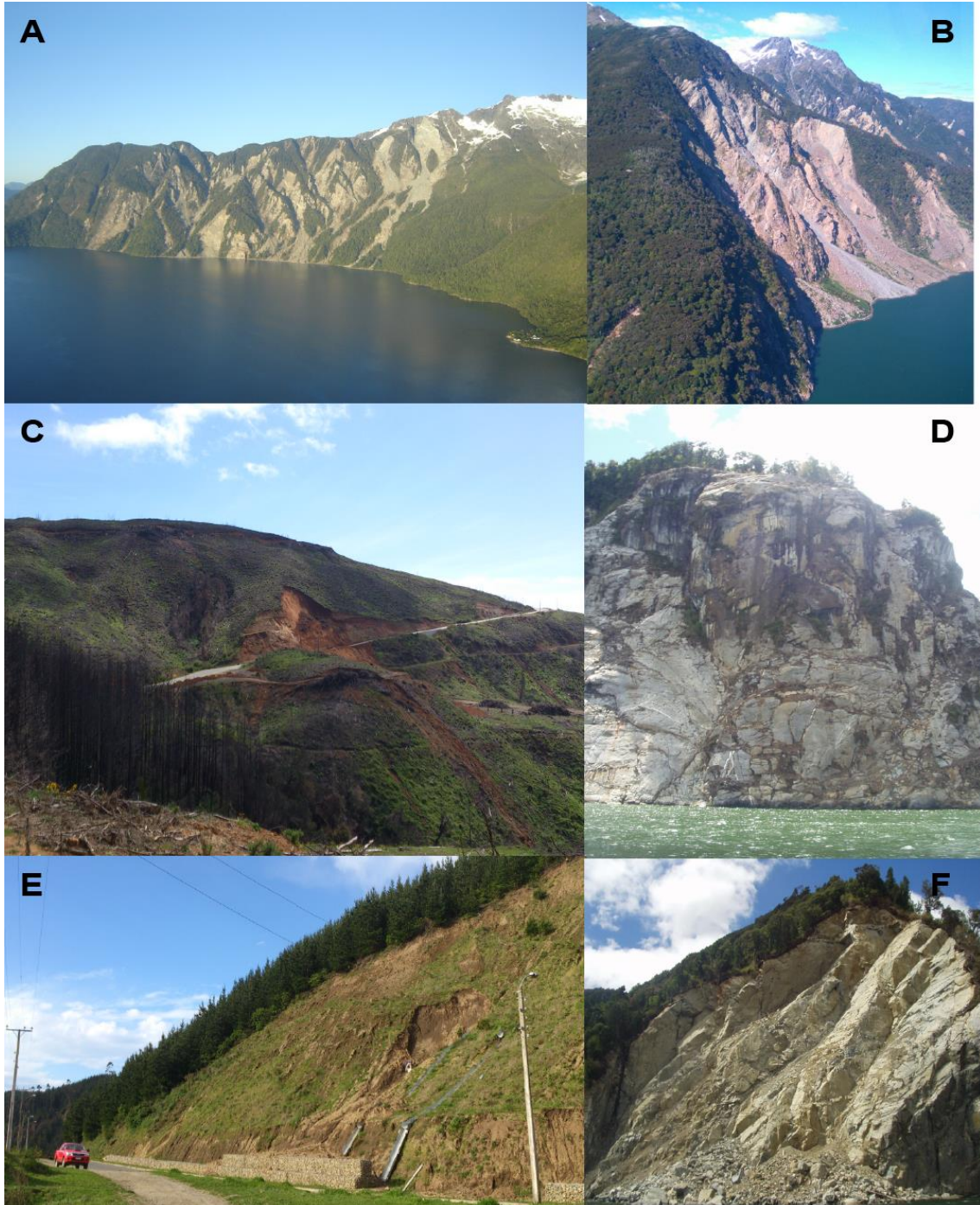


Figure 7.2. Examples of landslides triggered by earthquakes in Chile. A: Overview of debris avalanches (2007 Aysén earthquake); B: Rock slides triggered by the 2007 Earthquake in Aysén Fjord (all in granitic rock masses of the Patagonian Batholith; cliff height c.1000 m);C and E: Debris slides (2010 Maule earthquake); D: Rock falls (2007 Aysén earthquake; cliff height c.400 m) F: Rock block slides (2007 Aysén earthquake; cliff height c.400 m).

7.3.3 FACTORS THAT INFLUENCE THE DYNAMIC RESPONSE OF HILLSLOPES UNDERGOING SEISMIC SHAKING

The factors that influence the dynamic response of hillslopes undergoing seismic shaking (e.g. *Jibson, 2011; Newmark, 1965*) can be broadly grouped into those that influence the intensity of event-specific seismic ground motions, those that influence the strength of hillslope materials and those that influence the static shear stresses. Empirical studies have revealed a number of proxy variables that can be used to represent these factors at the regional scale (*Parker et al., 2015*).

Lithology is an important factor in the generation of coseismic landslides, being relevant mainly during megathrust events. For example, *Wartman et al. (2013)* determined that majority of landslides triggered by M_w 9.0 2011 Tohoku megathrust earthquake occurred in the youngest (Neogene) geological units of the region (Quaternary sediments and Neogene sedimentary rocks). The *Serey et al. (2019)* database indicates that for the 2010 Maule earthquake, relief exerted a dominant control on coseismic landsliding with the lithology the second most relevant conditioning factor, with more landslides in younger rocks (Quaternary deposits and Paleogene-Neogene volcanic and volcano-sedimentary rocks). This is in effect an indication on the degree of cementation and thus strength. On the other hand, in most of shallow crustal events, lithology seem not to be a primary factor to consider in the generation of landslides. For example, according by *Wang (2015)* there is no obvious correlation between landslide concentration and rock age (young or old lithology) for the 2013 Lushan and the 2008 Wenchuan earthquakes. Indeed, differences in the distributions of landslides across different lithologies arise because young or old strata are coincidentally clustered around the rupture zone of the seismogenic fault, and these rock masses are extremely fractured and underwent strong shaking.

Other factors that may have influence on the distribution of landslides are related with seismic effects on shaking in the near field, such as the hanging wall and directivity effects during strong shallow crustal earthquakes. Directivity effects are related with the rupture direction of the fault, tending to generate larger ground motions toward this direction (*Somerville et al., 1997; Somerville, 2003*). The hanging-wall effect relates with larger ground motions on the block above an inclined fault (the hanging-wall block) and is common on earthquakes along thrust faults (e.g. *Abrahamson & Somerville, 1996*;

Zhao et al., 2019). The literature indicates that the landslides triggered by earthquake tending to cluster along the causative fault (*Keefe, 2000; 2002; Khazai and Sitar, 2004; Huang & Li, 2009*). For thrust faults landslide density is highest on the hanging wall (*Meunier et al., 2007*).

Ground motion was found to be the most significant factor in triggering the shallow landslides in the 1999 M_w 7.6 Chi-Chi earthquake. Overall, 74% of all slope failures occurred in regions with vertical ground motions greater than 0.2 g and 81% of all slope failures occurred in the region with mean horizontal peak ground accelerations (PGA) greater than 0.15 g (*Khazai & Sitar, 2004*). On the other hand, *Wartman et al. (2013)* compared the landslide database with ground-motion recordings of the 2011 Tohoku earthquake (M_w 9.0, megathrust event), but found no correlation between landslide intensity and ground shaking within the area affected. Similarly, in the 2010 M_w 8.8 Maule earthquake, very few landslides occurred in the area of higher intensity (VIII) and most of them were in the area of lower intensities (<V). Therefore, there was no strong correlation between landslide density and earthquake intensity (*Serey et al., 2017*) or with PGA or distance from the fault plane. There was a much stronger correlation between landslide concentration and the ratio between horizontal and vertical peak accelerations (*Serey et al., 2019*).

Densmore & Hovius (2000) recognized that earthquake-triggered landslides in rock slopes have a relatively uniform distribution on steep slopes, but in presence of topographic amplification the triggering of landslides at or near the crests is increased. Recent studies have indicated that the ground accelerations at the mountain top can be three to six times than at its foot (*Wang et al., 2012; Wang et al., 2018*), causing higher susceptibility to landsliding in the upper parts of the slopes. In the Aysén event, about two thirds of the landslides start in the upper quarter of the slope, while over 90% start in the upper half, which suggests that larger ground motions due to topographic site effects influenced the triggering of landslides during the earthquake (*Sepúlveda et al., 2010*). On the other hand, landslides induced by the Maule earthquake are not clustered close to the ridge tops, suggesting no predominant topographic site effect in their generation, although it may have played a role locally (*Serey et al., 2019*).

The above is summarized in Table 7.1, which shows the differences between, conditioning factors and characteristics of the coseismic landslides applied to the mountain environment of Chile for both kinds of triggers (shallow crustal and megathrust earthquakes), based on analysis of comprehensive inventories of coseismic landslides in Chile and abroad (*Meunier et al., 2007; Sepúlveda & Serey 2009; Sepúlveda et al., 2010; Gorum et al., 2011; Wartman et al., 2013; Wang et al., 2015; Zhao et al., 2019; Serey et al., 2019; this work*).

Table 7.1. Summary of most common correlations of coseismic landslides in the Chilean Andes contrasting the megathrust earthquakes with shallow crustal earthquakes (*This study; Serey, et al., 2019; Sepúlveda et al., 2010*).

Conditioning Factors/ Characteristic of coseismic landslides	Coseismic landslides triggering by	
	megathrust earthquake	Shallow crustal earthquake (M>4)
Relief	Relief exerts a strongly dominant control on landsliding both in terms of preconditioning (higher, steeper slopes) and local topographic amplification of shaking.	
Bedrock lithology	Relevant conditioning factor, with more landslides in younger (normally weaker) volcanic and volcano-sedimentary rocks.	There is no obvious correlation between landslide concentration and rock age (young or old lithology), even on very resistant rocks such as granitoids.
Proximity of the fault	There is a poor correlation between landsliding and fault rupture distance (subduction zone).	The rupture plane of fault is a first-order factor in the distribution of landslides. Hanging wall and directivity effects.
Seismological parameters	Poor correlation between estimated PGA and landslide occurrence. Better correlation between landslide concentration and the ratio between horizontal and vertical peak accelerations.	Ground motion parameters would be the most significant factors, including horizontal and vertical accelerations, ground velocity, frequency content and epicentral distance.
Topographic Amplification	Moderate or local influence. Landslides generally not clustered close to the ridge tops.	Strong influence. The crowns of the landslides are generally in the uppermost part of the slopes.
Spatial distribution	Landslides are not evenly distributed in the affected area, tending to the formation of clusters of landslides.	
	-	Landslides tend to be limited to the epicentral area.

Type of coseismic landslide	Disrupted slides. Most of them, rock falls and debris slides.	Disrupted slides. Most of them, debris avalanches, rock falls, debris slides and rock slides/avalanches.
N° landslides	The total number of landslides triggered for the megathrust earthquakes is substantially lower, typically by one to two orders of magnitude, than it would be expected for shallow crustal earthquakes of a similar or even lower magnitude.	

7.4 CONCEPTUAL HAZARD MODELS

Using the data mentioned above, four conceptual hazard ground models were developed to guide stakeholders in the hazards faced to critical infrastructure in mountain regions. Representative geomodels describing the hazards for the Andes of central Chile were developed, these are: Glacial Cordilleran, Fluvial Cordilleran, Plutonic Cordilleran and Mountain Front environments. The latter model is the most likely to have significant urban development because of the concentration of infrastructure. The data showing slope performance for the two different earthquake types, based on Table 7.1 and specific geomorphological characteristics, have then been added to the models to use in a semi-predictive capacity.

7.4.1 GLACIAL CORDILLERAN ENVIRONMENT

In central Chile, the glaciated mountain terrain is dominated by andesitic bedrock with local volcanoclastic sediments. Glacial landscapes are essentially high-latitude and/or high-altitude environments. Geomorphology in these areas is characterized by high relief and steep slopes. Furthermore, it is characterized by the presence of glacial deposits (e.g. till and glacial-fluvial deposits) and modified by periglacial processes. Rock slopes tend to be over-steepened. Rock masses quality are often fair to good, locally very good, may be highly fractured in the vicinity of lineaments or faults. Hydrothermal alteration, however, can be extreme locally and reduces the rock mass quality. Most of coseismic landslides are disrupted, principally rock falls, debris avalanches, debris slides, and rock slides. In these environments, large rock avalanches/slides could dam river valley. Landslides may occur on persistent discontinuities or glacial deposits.

Figure 7.3 and Figure 7.4 show conceptual geomodels of coseismic landslides induced by shallow crustal and megathrust earthquakes respectively in a glacial cordilleran environment of central Chilean Andes. Table 7.2 outlines geomorphological characteristics of terrain and possible coseismic landslides that could be triggered in a glacial cordilleran environment for each scenario.

Table 7.2. Terrain characteristics and coseismic landslide hazards for the Glacial Cordilleran environment.

Terrain facet	Terrain element	Site characteristics	Main coseismic landslide type (after Hungr et al., 2014)		Secondary hazards	Engineering intervention / risk reduction strategies
			Shallow crustal earthquake	megathrust earthquake		
Glacial andesitic slopes	Ridges	Ridges characterised by thin soil deposits with bedrock at or close to the surface; rock mass may be frost shattered and highly fractured, or hydrothermally altered. Likely to be a poor to fair quality rock mass at shallow depths but good to very good deeper. This is likely to mitigate against deep seated landslides.	Rock falls; debris falls; rock block topples; debris	Rock falls; debris falls; rock topples; debris topples;	Creation of sediment supply for debris flow activation.	None, at best reactive. In ridges close to infrastructure it may be necessary to remove loose material on a periodic basis.
	Interfluvial slopes	Slopes formed with engineering soils of variable thickness along the slope profile. Dominantly glacial materials, although may have been reworked. Glacial deposits may be mantled by colluvium/talus. Rock mass could present surface-parallel fracture systems in rock (sheet joints), oversteepened slopes and U-shaped valley.	Rock slides, debris slides; debris avalanches. Ancient rock slides can be reactivated.	Debris slides; debris avalanches.	Rock slides may create landslide dams in tributary valleys.	Local stakeholders should carry out inspections after an earthquake. It may prove impossible to access blockages and these will need a monitoring plan.
	Stream channels	Dominated by intercalations of coarse fluvial materials, glacial debris and slope wash deposits. In high slopes (>2000 m) these may contain rock glaciers.	Possible debris flows due to debris avalanche failures into stream channels.	---	Debris flow initiation in tributary valleys creating landslide dams in main valleys.	Monitoring. Infrastructure owners/ stakeholders should consider inspections after strong earthquakes to monitor sediment build-up.
	Cross element	Mixture of the terrain elements (see relevant site characteristics above).	Large rockslides with an origin on upper reaches of glaciated cordillera which spans multiple terrain units.	---	Large slide mass creates temporary dam. Breaching is a major hazard leading to downstream flooding.	Reactive – stakeholders should develop a mitigation plan that includes large landslides resulting in loss of access and long-term planning.
Cordillera river systems	Rock River channel	The river channel slopes are formed in bedrock which has been excavated by valley glaciers; rock mass may be locally frost shattered and hydrothermally altered.	Debris slides, rock falls.	Rock falls.	High turbidity in the river. Large slide mass creates temporary dam. Breaching is a major hazard leading to downstream flooding. Potential breaching of landslide dams creating downstream flooding and problems of suspended sediment in water supply and damage to hydroelectric infrastructure.	Downstream towns and villages should provide evacuation routes and indicate refuge zones in the event of a valley blocking landslide. HEP owners may need to monitor sediment flux post earthquake to reduce risk of damage to turbines.
	Glacial debris river channel	River channel slopes are formed in ice-contact debris and alluvial deposits which are locally oversteepened. These may be mantled by alluvial fans. Glacial soils may be reworked and stratified.	Debris slides, debris falls. There is potential for local liquefaction in alluvial soils.	Debris falls.		

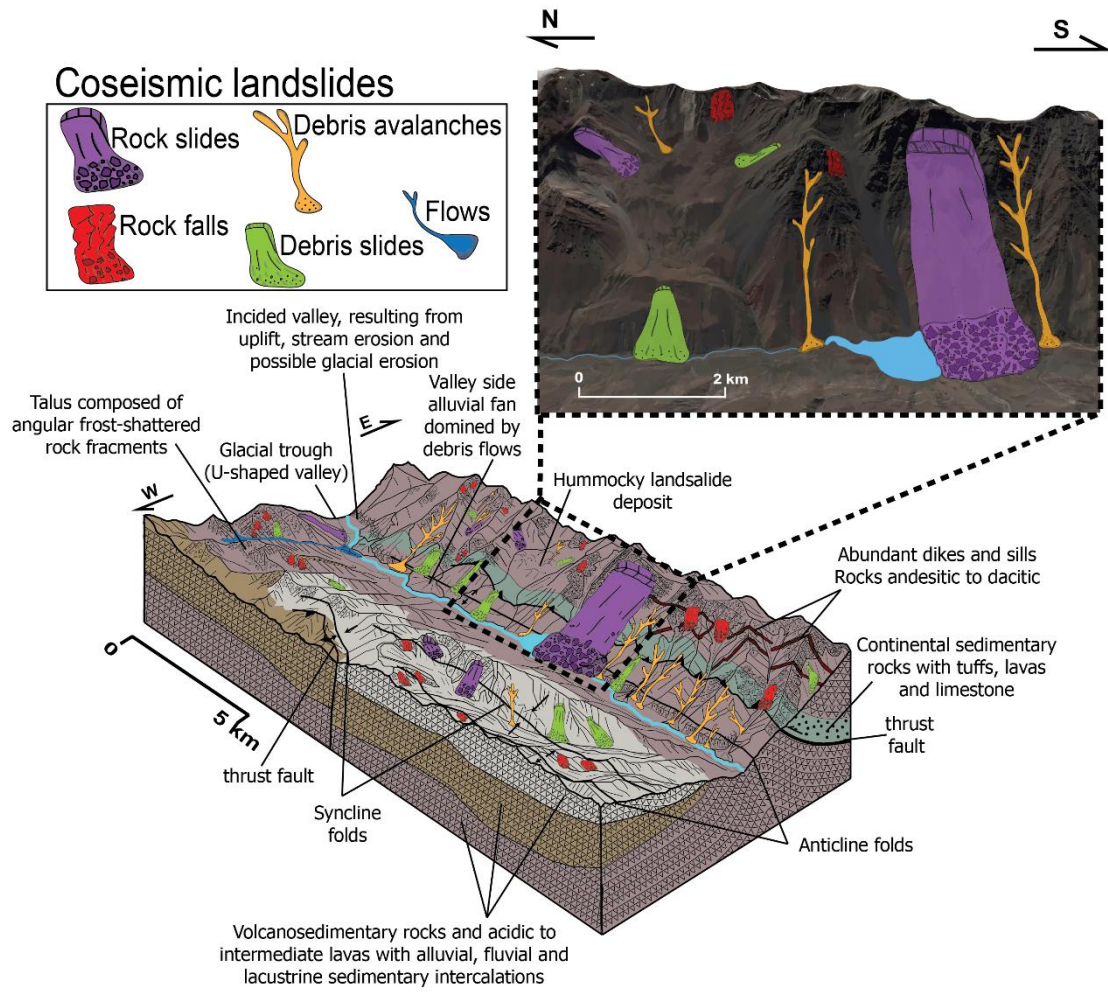


Figure 7.3. Glacial cordilleran environment. Conceptual geomodels of coseismic landslides induced by shallow crustal earthquake.

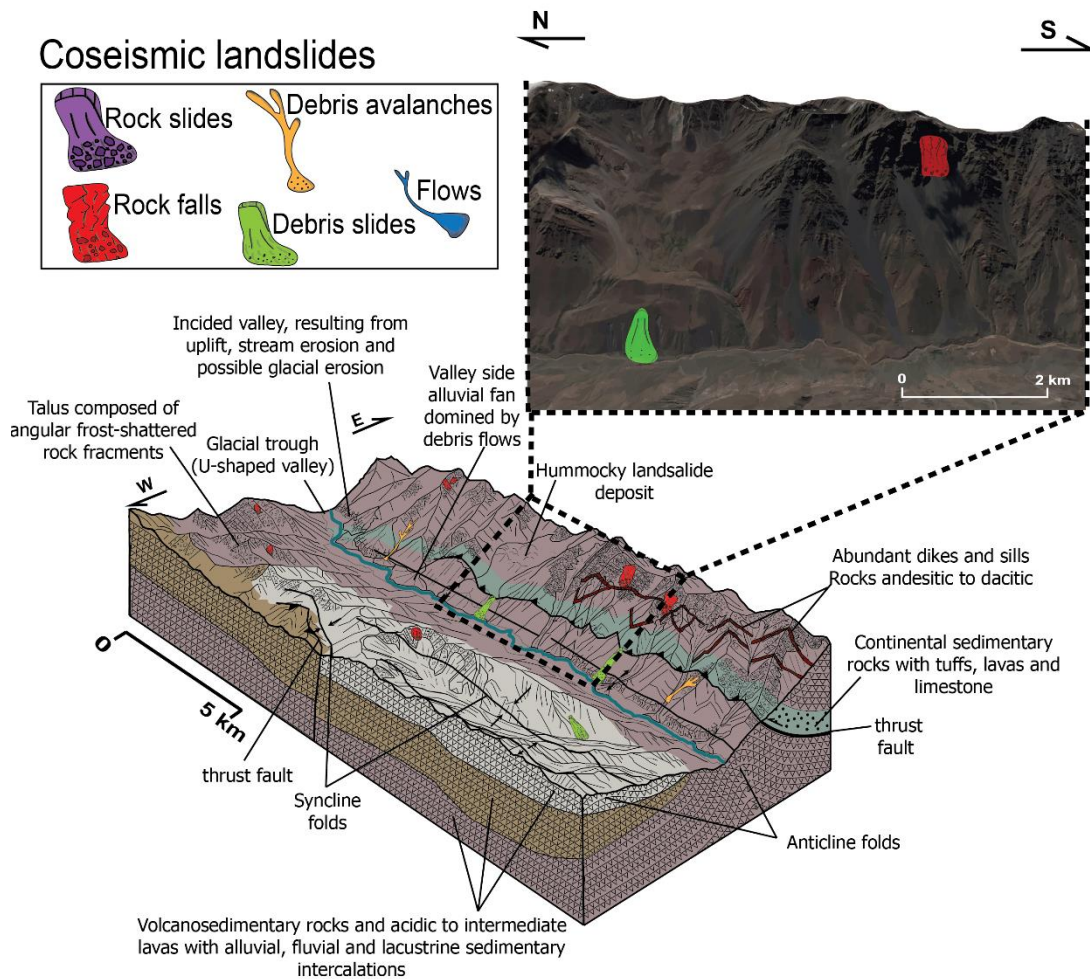


Figure 7.4. Glacial cordilleran environment. Conceptual geomodels of coseismic landslides induced by megathrust earthquake.

7.4.2 FLUVIAL CORDILLERAN ENVIRONMENT

Fluvial mountain terrain dominated by andesitic bedrock with local volcanoclastic sediments. Geomorphology is characterized by a strong relief, medium ranges of altitudes and medium to high gradients forming fluvial troughs (V-shaped valleys). Rock masses quality are often fair to good, locally very good, may be highly fractured near lineaments or faults. Hydrothermal alteration, however, can be extreme in places and reduce the geotechnical quality of intact rock. In these environments, large rock falls, rock avalanches/slides could dam the river valley. In this landscape, large prehistoric landslides are common, in which source areas of future rock slides may be generated by future shallow crustal events.

Figure 7.5 and Figure 7.6 show conceptual geomodels of coseismic landslides induced by shallow crustal and megathrust earthquakes respectively in a fluvial cordilleran environment of central Chilean Andes. Table 7.3 expresses geomorphological characteristics of terrain and possible coseismic landslides that could be triggered in a fluvial cordilleran environment for each scenario.

Table 7.3. Terrain characteristics and coseismic landslide hazards for the Fluvial Cordilleran environment.

Terrain facet	Terrain element	Site characteristics	Main coseismic landslide type (after Hungr et al., 2014)		Secondary hazards	Engineering intervention / risk reduction strategies
			Shallow crustal earthquake	Megathrust earthquake		
Fluvial andesitic slopes	Ridges	Ridges characterised by thin residual soil deposits with bedrock at or close to the surface; rock mass may be highly fractured by thermal oscillation, may be hydrothermally altered. Likely to be a fair to poor quality rock mass.	Rock falls; rock block slides; debris falls; topples.	Rock falls.	Creation of sediment supply for debris flow activation.	Consider installation of ring netting to control sediment supply to rivers. An inspection and maintenance plan will be required to avoid these becoming a hazard in their own right.
	Interfluvial slopes	Rock mass composed of volcanosedimentary bedrock often fair to good quality, may be highly fractured in the vicinity of lineaments or faults. Steep slopes and V shaped valley. They may have the scar of ancient events of mass removals. Slopes formed with engineering soils of variable thickness along the long profile. Dominantly alluvial materials and colluvium.	Rock slides; rock avalanches; debris slides; debris avalanches; Rock falls. Ancient rock slides can be reactivated.	Debris slides; debris avalanches.	Rock slides may create landslide dams in tributary or principal valleys.	Local stakeholders should carry out inspections after an earthquake. It may prove impossible to access blockages and these will need a monitoring and long-term planning is needed.
	Stream channels	Dominated by intercalations of coarse fluvial materials, alluvial deposits and colluvium.	Possible debris flows due to debris avalanche, rock falls or rock slides failures into stream channels.	---	High turbidity events in the channels.	Monitoring. Infrastructure owners/ stakeholders should consider inspections after strong earthquakes to monitor sediment build-up.
	Cross element	Mixture of the terrain elements (see relevant site characteristics above).	Large rockslides or rock avalanches with an origin on upper reaches of Cordillera which spans multiple terrain units.	---	Large slide mass creates temporary dam. Breaching is a major hazard leading to downstream flooding.	Inspections required after shaking. Local action plan for community evacuation should be considered. In the event of large landslide dams local communities may need to refer the matter to Central Government via Ministry of Public Works. Urgent action needed and long-term planning.
Cordillera river systems	Rock River channel	The river channel slopes are formed in bedrock which has been excavated by river or ancient glaciers, may be hydrothermally altered.	Debris slides, rock falls.	Rock falls; debris slides.	Extreme high turbidity events in the river. Large slide mass creates temporary dam. Breaching is a major hazard leading to downstream flooding.	
	Fluvio-alluvial debris river channel	River channel slopes are formed in debris and alluvial deposits which can be locally over-steepened. These may be mantled by colluvium materials.	Debris slides. There is potential for local liquefaction in granular materials likes sandy or silty soils.	Debris slides.		

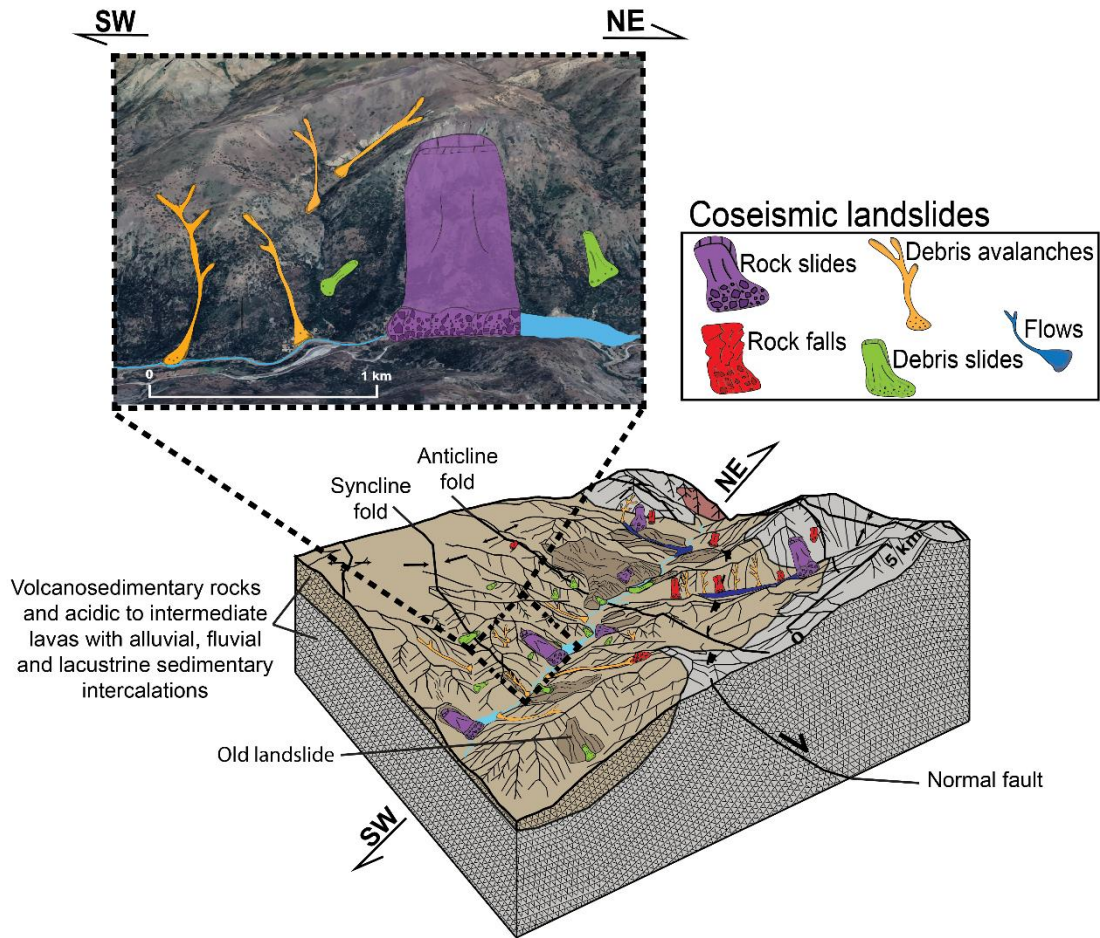


Figure 7.5. Fluvial cordilleran environment. Conceptual geomodels of coseismic landslides induced by shallow crustal earthquake.

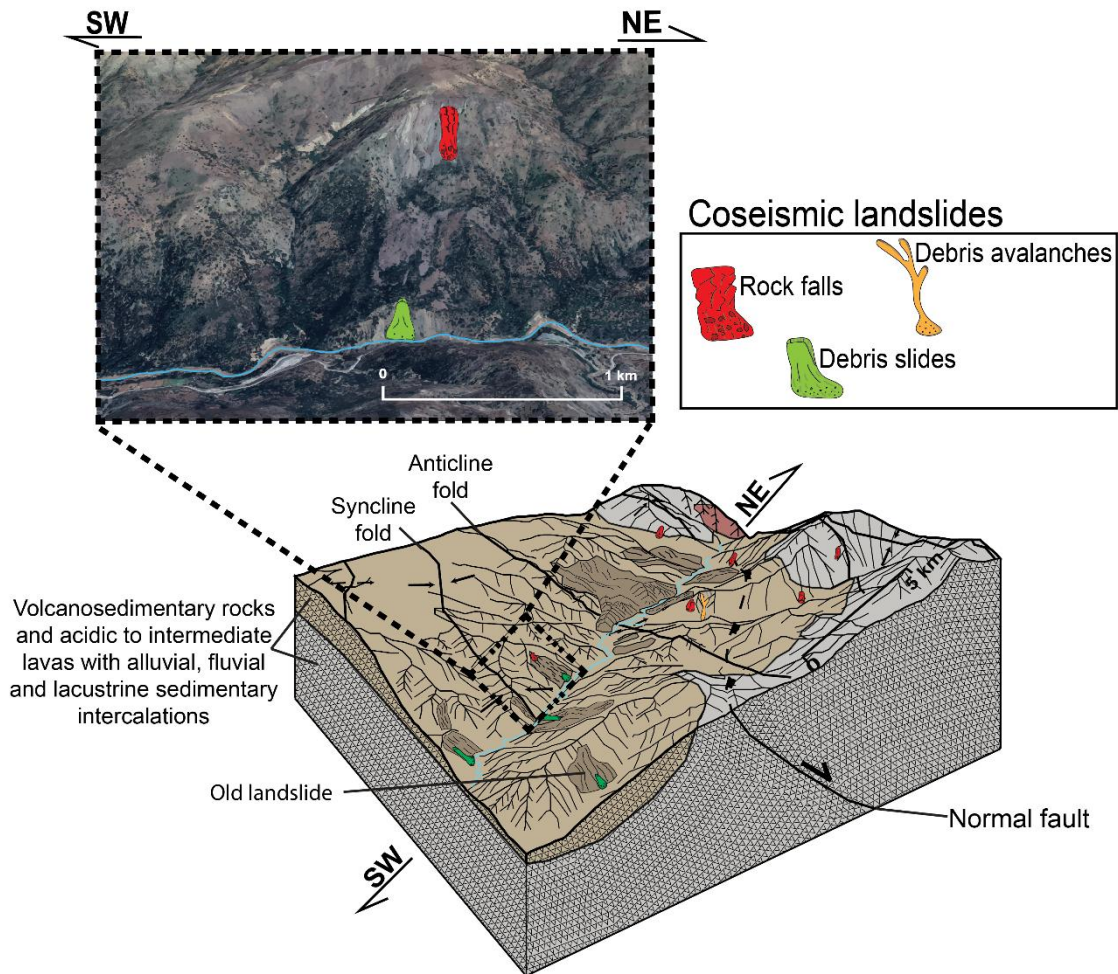


Figure 7.6. Fluvial cordilleran environment. Conceptual geomodels of coseismic landslides induced by megathrust earthquake.

7.4.3 PLUTONIC CORDILLERAN ENVIRONMENT

Plutonic mountain terrain dominated by intrusive igneous bedrock with local volcanoclastic sediments. This environment is characterized by a strong relief, steep slopes (medium to high ranges) and high altitudes. In general terms, plutonic rocks develop competent rock massif and tight valleys. Rock masses quality are often good to very good, may be highly fractured in the vicinity of lineaments or faults. In these environment are very common large pre-historic landslides, in which new rock slides can be generated by a future shallow crustal earthquake. In addition, large rock falls, rock avalanches/slides could dam a river valley.

Figure 7.7 and Figure 7.8 show conceptual geomodels of coseismic landslides induced by shallow crustal and megathrust earthquakes respectively in a plutonic cordilleran

environment of central Chilean Andes. Table 7.4 outlines geomorphological characteristics of terrain and possible coseismic landslides that could be triggered in a plutonic cordilleran environment for each scenario.

Table 7.4. Terrain characteristics and coseismic landslide hazards for the Plutonic Cordilleran environment.

Terrain facet	Terrain element	Site characteristics	Main coseismic landslide type (after Hungr et al., 2014).		Secondary hazards	Engineering interventions/ risk reduction strategies
			Shallow crustal earthquake	Megathrust earthquake		
Plutonic slopes	Ridges	Ridges characterised by thin residual soil deposits with bedrock at or close to the surface; rock mass may be highly fractured by thermal oscillation, may be hydrothermally altered. Variable rock mass geotechnical quality.	Rock falls; rock block slides.	Rock falls.	Creation of sediment supply for debris flow activation.	None. Reactive at best. Inspection of sediment build-up after earthquakes with higher priority after a local shallow crustal event and long-term planning is needed.
	Interfluvial slopes	Rock mass compound of plutonic bedrock often good to very good geotechnical quality, steep slopes and cliffs. It may be highly fractured, present stress-relief fractures parallel to a cliff face, or hydrothermally altered, in the vicinity of lineaments or faults. Slopes formed with engineering soils of variable thickness along the long profile. Dominantly fluvio-alluvial materials and colluvium deposits.	Rock slides; rock avalanches; debris slides; debris avalanches; Rock falls.	Debris slides; debris avalanches.	Rock slides may create landslide dams in tributary or principal valleys.	Local stakeholders should carry out inspections after an earthquake. It may prove impossible to access blockages and these will need a monitoring plan.
	Stream channels	Glacial valley: Dominated by intercalations of coarse fluvial materials, glacial debris and slope wash deposits.	Possible debris flows due to debris avalanche, rock falls or rock slides failures into stream channels.	---	High turbidity events in the channels. Debris flow initiation in tributary valleys creating landslide dams in main valleys.	Inspections required after shaking. Local action plan for community evacuation should be considered. In the event of large landslide dams local communities may need to refer the matter to Central Government via Ministry of Public Works. Urgent action needed and long-term planning.
		Fluvial valley: Dominated by intercalations of coarse fluvial materials, alluvial deposits and colluvium.				
Cross element	Mixture of the terrain elements (see relevant site characteristics above).	Large rockslides or rock avalanches with an origin on upper reaches of cordillera which spans multiple terrain units.	---	Large slide mass creates temporary dam. Breaching is a major hazard leading to downstream flooding.		
Cordillera river systems	Rock River channel	The river channel slopes are formed in bedrock which has been excavated by river or valley glaciers.	Debris slides, rock falls.	Rock falls; Debris slides.	Extreme high turbidity events in the river. Large slide mass creates temporary dam. Breaching is a major hazard leading to downstream flooding. Potential breaching of landslide dams creating downstream flooding.	
	Debris river channel	River channel slopes are formed in debris and alluvial deposits which can be locally over-steepened. These may be mantled by colluvium materials.	Debris slides. There is potential for local liquefaction in granular materials like sandy or silty soils.	Debris slides.		

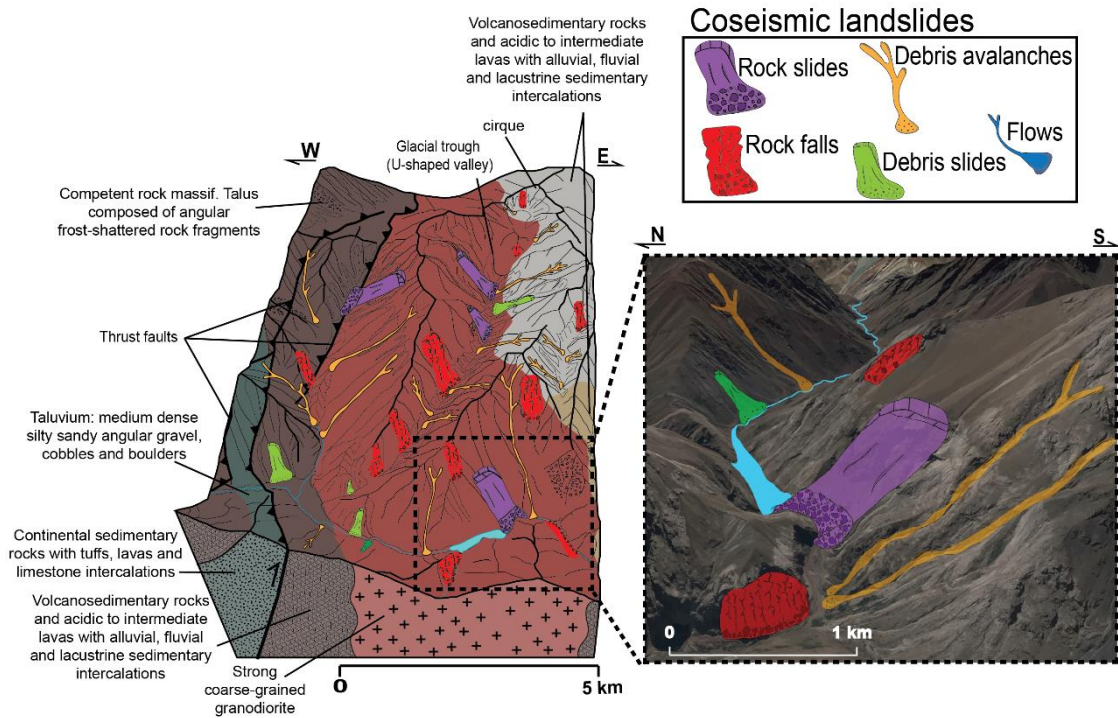


Figure 7.7. Plutonic cordilleran environment. Conceptual geomodels of coseismic landslides induced by shallow crustal earthquake.

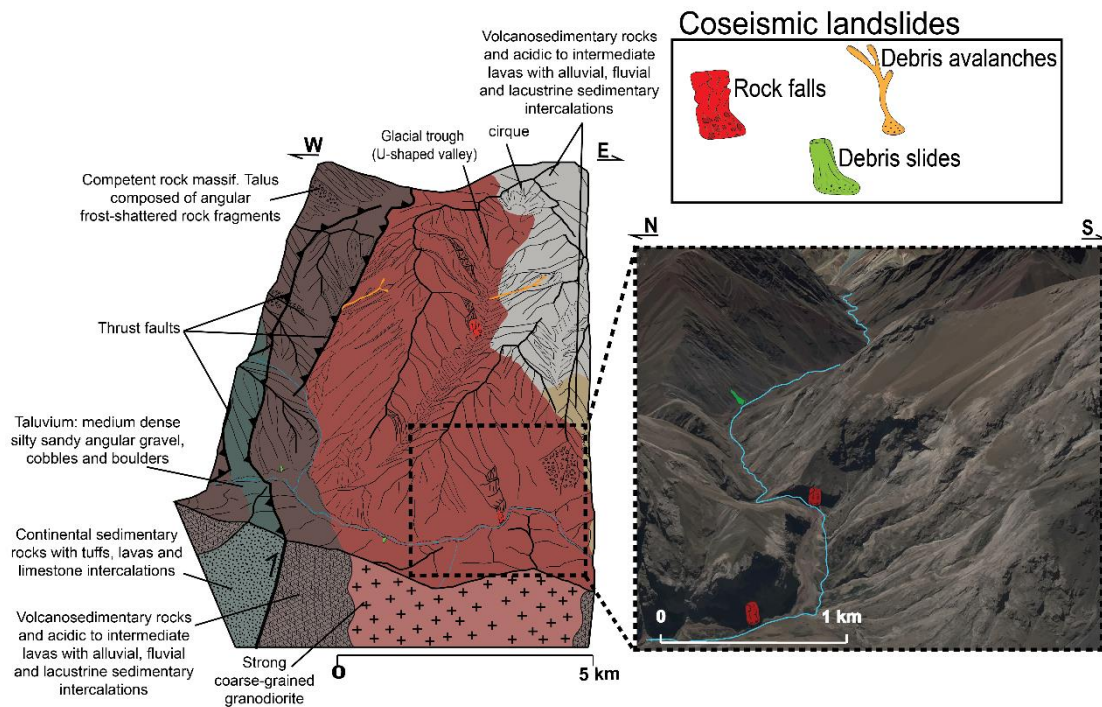


Figure 7.8. Plutonic cordilleran environment. Conceptual geomodels of coseismic landslides induced by megathrust earthquake.

7.4.4 MOUNTAIN FRONT ENVIRONMENT

Mountain front terrain, usually bordering urban areas in central Chile, is dominated by andesitic bedrock with local volcanoclastic sediments and generally forms the at the convergence of high mountains and adjacent basins (e.g. the Santiago basin). Rock masses quality are often fair to good, locally very good, may be highly fractured in the vicinity of lineaments or faults. Hydrothermal alteration, however, can be extreme in places and reduce the geotechnical quality of intact rock. In these environments, geomorphology is characterized by a strong relief, medium ranges of altitudes and medium to high gradients. This environment presents important ravine channels, basins characterized by narrow, steep-sided valleys, in which removed materials flow directly into urban areas located in the central depression. Therefore, large rock avalanches/slides generated by a future crustal earthquake and consequently debris flows due to debris avalanche, rock falls or rock slides failures into channels could result in fatalities and infrastructure damage.

Figure 7.9 and Figure 7.10 show conceptual geomodels of coseismic landslides induced by shallow crustal and megathrust earthquakes respectively in a mountain front environment of central Chilean Andes. Table 7.5 outlines geomorphological characteristics of terrain and possible coseismic landslides that could be triggered in a mountain front environment for each scenario.

Table 7.5. Terrain characteristics and coseismic landslide hazards for the Mountain front environment

Terrain facet	Terrain element	Site characteristics		Main coseismic landslide type (after Hungr et al., 2014)		Secondary hazards	Engineering interventions / risk reduction strategies	
				Shallow crustal earthquake	Megathrust earthquake			
Fluvial andesitic slopes	Ridges	Ridges characterised by thin residual soil deposits with bedrock at or close to the surface; rock mass may be highly fractured by thermal oscillation. Likely to locally be a poor to fair quality rock mass.		Rock falls; rock block slides; debris falls; toppling.	Rock falls.	Creation of sediment supply for debris flow activation.	Reactive. Monitoring needed after earthquake. This should be a higher priority after local shallow crustal earthquakes and long-term planning is needed.	
	Interfluvial slopes	Rock mass composed by volcanosedimentary bedrock, often fair to good, steep slopes. They may have the scar of ancient events of mass removals. Slopes formed with engineering soils of variable thickness along the long profile. Dominantly fluvio-alluvial materials and colluvium.		Rock slides; rock avalanches; debris slides; debris avalanches; Rock falls.	Debris slides; debris avalanches.	Rock slides may create landslide dams.	Monitoring. Slopes adjacent to important infrastructure / property may require intervention for public safety. Draped netting systems should be considered as a means of mitigating small scale failures.	
	Channels	Stream	Dominated by intercalations of coarse fluvial materials, alluvial deposits and colluvium.		Debris flows due to debris avalanche, rock falls or rock slides failures into stream channels.	---	High turbidity events in the channels.	Close to large urban areas check dams or netting should be considered. These should be inspected after shaking to ensure capacity is not being exceeded.
		Ravine	Narrow, steep-sided valley. Dominated by intercalations of coarse alluvial deposits and colluvium.		Debris flows due to debris avalanche, rock falls or rock slides failures into stream channels. Debris avalanches due to rock falls, debris slides or rock slides failures into channels. Rock avalanches or large rockslides with origin on upper reaches of ravine channels.	---		Inspections required after shaking. Local action plan for community evacuation should be considered. In the event of large landslide dams local communities may need to refer the matter to Central Government via Ministry of Public Works. Urgent action needed and long-term planning.
	Cross element	Mixture of the terrain elements (see relevant site characteristics above).		Large rockslides or rock avalanches with an origin on upper reaches of cordillera which spans multiple terrain units.	---	Large slide mass creates temporary dam. Breaching is a major hazard leading to downstream flooding.		

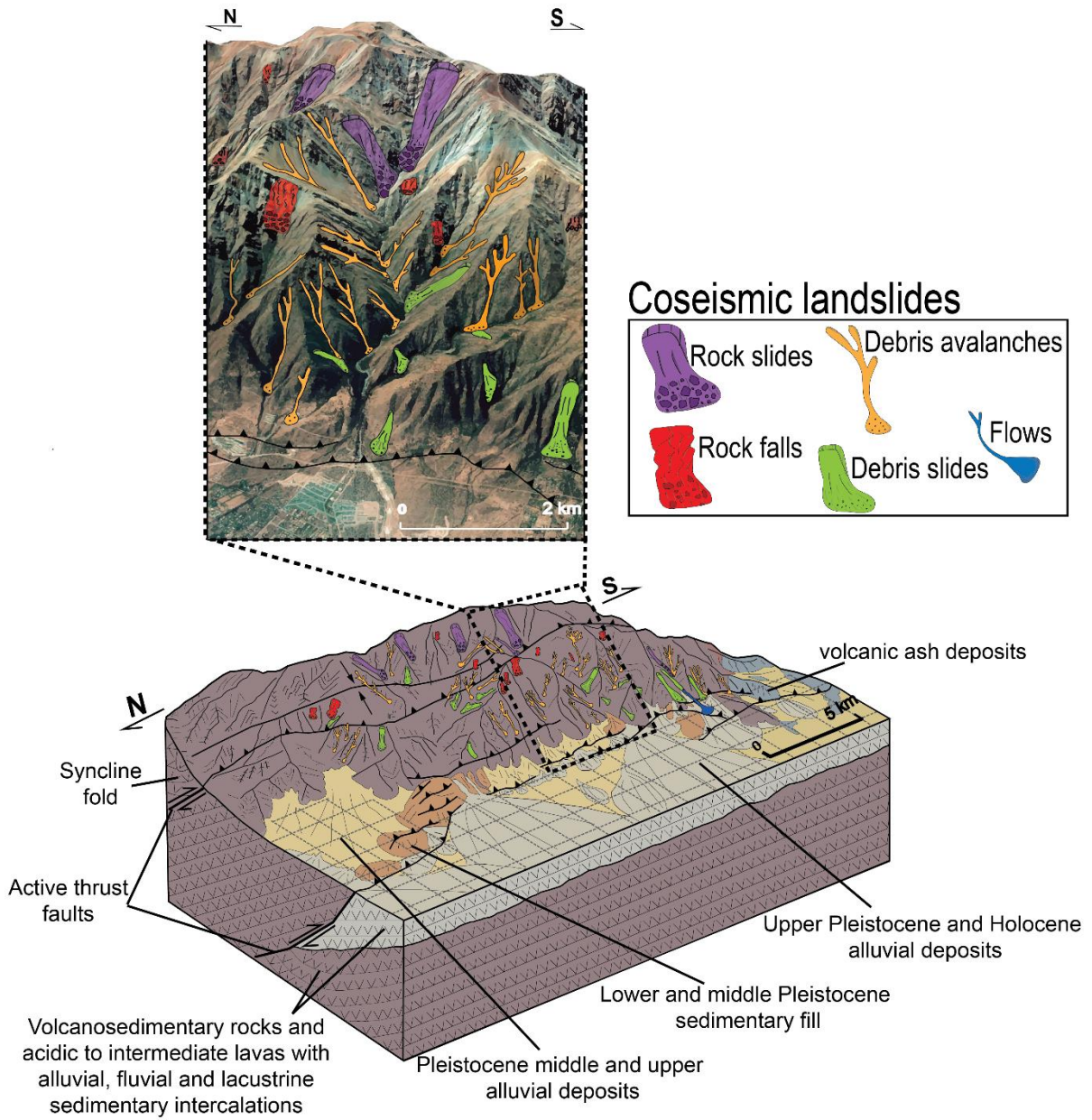


Figure 7.9. Mountain front bordering urban area environment. Conceptual geomodels of coseismic landslide induced by shallow crustal earthquake.

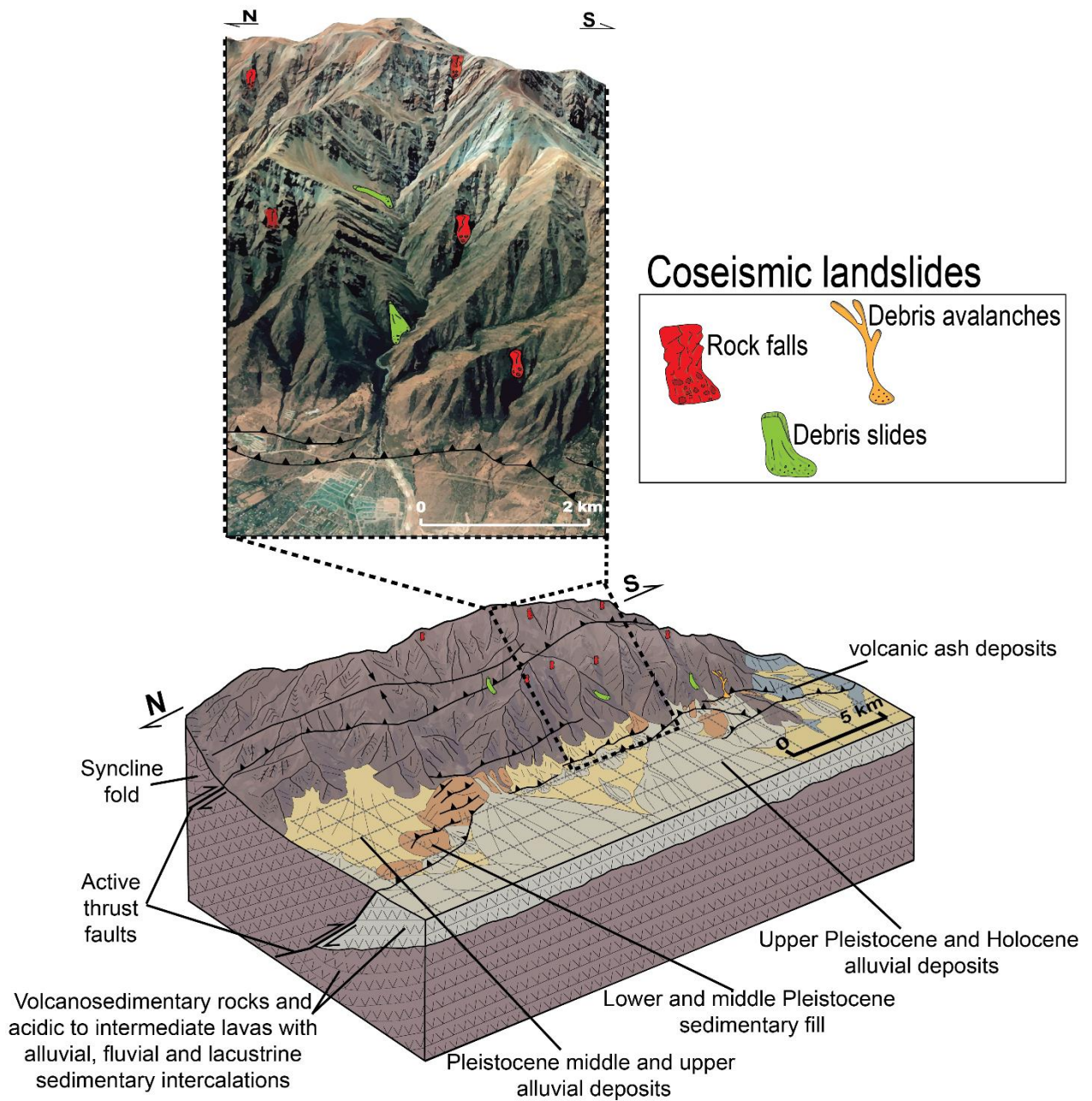


Figure 7.10. Mountain front bordering urban area environment. Conceptual geomodels of coseismic landslides induced by megathrust earthquake.

7.5 DISCUSSION

Landslides are an important coseismic geohazard associated with earthquakes in mountain environments and present a serious threat to communities found in these regions (*Keefer, 1984*). Indeed, in high mountain chains, 20-25% of earthquake-induced fatalities result from the effects of landslides (*Petley et al., 2006*). By visualizing differences between conditioning factors and characteristics of coseismic landslides, using geomodels, between different triggers can be a key factor in the assessment of effective mitigation measures. From the geomodels construction, it is possible to view potential risks, consequences and possible mitigation measures for each coseismic landslides (Table 7.6).

Table 7.6. Potential risks and suggested mitigation measures for coseismic landslides to be generated in the mountain environment of Chile.

Coseismic landslides	Potential Consequences	Risk Level (*)	Mitigation
Rock avalanche	Valley blockage, destruction of lifeline infrastructure, impact on mountain community.	Low due to infrequency of these events. Risk is likely to be higher as a result of a shallow crustal earthquake.	Evacuation plan for valley blockage.
Rock slides	Damage to local lifelines and road blockages. Difficulty in access for emergency services in the event of a local event. Economic losses due to closure of mine roads. Risk to individual road users.	Moderate to High in the event of shallow crustal seismicity, lower in the event of megathrust earthquakes due to large epicentral distances.	For important routes engineering intervention may be needed. Netting systems, localized rock bolting and retaining structures considered for critical routes. For higher hazard zones long-term planning as a tool for risk reduction is needed.
Rock falls	Injury and loss of life to users. Potential lifeline damage to single and multiple block rock falls.	Moderate (subduction zone event) to high (shallow crustal) event.	Critical infrastructure for mineral transport, important access roads (e.g. access to hospitals etc) should be protected. For higher hazard zones “no stopping” zones should be considered and long-term planning is needed for considered other risk reduction options.
Debris avalanches	Valley blockage, destruction of lifeline infrastructure, impact on mountain community.	Low	Slope regrading could be considered in specific areas. More detailed hazard analysis considered.
Debris slides	Damage to local lifelines and road blockages. Difficulty in access for emergency services in the event of a local event. Economic losses due to closure of mine roads. Risk to individual road users.	Low for megathrust earthquakes but moderate for shallow crustal events.	Slope regrading could be considered in specific areas. More detailed hazard analysis considered and long-term planning.

Flows	Likely only to cause localized damage due to liquefaction related movement during shaking but debris flow activation could cause damage to infrastructure / HEP schemes during storm or snow melt after earthquake	Low during shaking but hazard becomes elevated during winter or spring.	Monitoring and inspection. Consider check system for critical infrastructure.
Lateral spreads	Localised sliding only as the presence of liquefiable materials is going to be limited.	Low.	Monitoring and reactive maintenance.

Secondary hazards can be generated from large landslides, such as rock avalanches and rock slides, blocking narrow, steep-sided valleys and forming landslide dams (*Schuster, 1986*), or landslide-induced tsunamis. In some cases, landslides may pose a threat to the population and infrastructure because they dam a watercourse. Landslide dams tend to be a feature of seismically active steep-relief mountain areas undergoing uplift and erosion or deeply dissected thick sequences of weakly consolidated sediments such as lacustrine clays. Landslide dams give rise to two important flood hazards. Upstream or back-water flooding occurs as a result of impounding of water behind the dam leading to the relatively slow inundation of an area to form a temporary dam. Downstream flooding can occur in response to failure of a landslide dam. The most frequent failure modes are overtopping because of the lack of a natural spillway or breaching due to erosion. Failure of the poorly consolidated landslide debris generally occurs within a year of dam formation. The effect of the resultant floods can be devastating, partly because of their magnitude and partly because of their unexpected occurrence (*Lee & Jones, 2004*). For example, in the 2005 M_w 7.6 Kashmir earthquake at least two river blockages occurred. The largest of the two, at Hattian Bala east of Muzaffarabad, created a dam over 100 m high (*Dunning et al., 2007*).

In Chile, the most important historical example of landslide dams took place during the giant 1960 Valdivia earthquake (M_w 9.5, megathrust earthquake). Three large landslides dammed the San Pedro River and threatened the Valdivia City. The biggest landslide removed c. 30 Mm^3 of poorly consolidated sediments, the intermediate transported 6 Mm^3 and, finally, the smallest involved the removal of 2 Mm^3 (*Davis & Karzulovic, 1963*). Given its flow, it was expected that in two months the accumulated water would exceed the landslide dam, producing a huge avalanche that would cover all of Valdivia, already devastated by the earthquake and tsunami, and the surrounding areas. To avoid this disaster, engineers and technicians from ENDESA and the MOP (Ministry of Public Works) started the so-called "Operation Riñihue", which consisted of making a channel through

the undisturbed terrain, so that the water flowed as slowly as possible as it finally happened (*Lazo, 2008*). Historical records highlight this same phenomenon in the 1575 earthquake (M 8-8.5 according to *Lomnitz, 2004*), on that occasion San Pedro River was also blocked by a huge landslide in the same area (*Montessus de Ballore, 1912*), not allowing normal water drainage. The dam accumulated water for five months and finally causing a catastrophic flood taking the lives of more than 1,200 indigenous people and destroyed Valdivia city, founded by the Spaniards a couple of decades before (*Davis & Karzulovic, 1961*).

Earthquakes often leave a legacy of pseudo-stable slopes that continue for years or many decades afterward the main event. These landslides represent a direct threat themselves but also block and cut transportation infrastructure. An aspect that is often overlooked is the increased rate of sediment movement caused by the liberation of hillslope debris, an effect that could depend on the type of earthquake. In the M_w 7.6 Chi-Chi earthquake in Taiwan, a shallow crustal event, this induced aggradation of some river beds by as much as 30 m, which proved to be devastating to local communities and to hydroelectric power systems (*Petley, 2009*). On the other hand, *Tolorza et al. (2019)* demonstrated that the 2010 M_w 8.8 Maule earthquake, an megathrust event, had a limited impact on the overall concentration and transport of suspended sediment loads in the Chilean Andes, which perhaps sheds light on the influence of climate on how these systems will behave post-events (e.g. under dry climate conditions). Thus, the seismically induced erosion and the evacuation of detached sediments are not necessarily a function of earthquake magnitude.

Despite the enormous impact potential of giant landslides, especially of those triggered during earthquakes, relatively little effort is spent to predict them. Thus, only very few case histories are known where large sites ($>1 \text{ km}^2$) had been thoroughly investigated to assess their failure potential under dynamic conditions, in full 3D (*Havenith et al., 2017*). The major problem is the availability of cost-effective methods, both to prospect and to model such sites. Although, all of them only considered one possible seismogenic scenario, i.e. crustal shallow earthquakes. Therefore, in this manuscript, a powerful tool for earthquake-induced landslide hazard assessment applicable to urban/territorial planning and disaster prevention strategies is presented. This is a series of practitioner-friendly conceptual ground models relating to the performance of slopes subject to strong ground motions during earthquakes originated from different seismogenic scenarios (megathrust or crustal shallow earthquake) in the most characteristic mountain environments in the Chilean Andes and expresses the following.

- Main types of landslides that could be triggered, their possible spatial distribution and sizes.
- Geomorphological and geotechnical characteristics of terrain units where coseismic landslides could be located.
- Secondary hazards and suggestions of possible engineering interventions.

This methodology visualizes all factors interacting in the generation of coseismic landslides depending on seismogenic zones (megathrust or crustal shallow earthquake), and considering the low cost (in both the elaboration and the required information) it might be applied elsewhere in the country and Latin America. The continuous, poorly regulated growth of the city into the mountain environment typical in Latin America, the increasing tourism industry in mountain areas, large infrastructure projects (water supply, hydroelectricity, gas pipes, etc.) increase exposure to coseismic landslides and their secondary hazards, thus the need for these to be properly addressed in territorial planning policies and disaster prevention strategies.

It is essential to emphasize that this methodology is a conceptual approach and that it needs to be complemented with an observational model to be applied for hazard assessment at local scales, which is based on the observed and measured distribution of engineering geological units and processes. These data are related to actual space or time and are constrained by surface or sub-surface observations.

7.6 CONCLUSIONS

Landslides are a substantial but often neglected aspect of megathrust and shallow crustal earthquakes in upland areas. Furthermore, in addition to killing people outright, they can also have an extremely serious impact in terms of hampering rescue operations and the delivery of assistance, situations that can vary dramatically between different triggers. Whilst earthquake-induced landslides cannot be prevented, adequate consideration of the problem in advance can allow the impact of coseismic landslides to be minimized.

Practitioner-friendly conceptual ground models relating to the performance of slopes subject to strong ground motions during megathrust or shallow crustal earthquakes in different mountain environments in the Andes of central Chile have been developed. Each model expresses important characteristics about coseismic landslide hazard (main types, spatial distribution and sizes), their

potential consequences and suggestions of possible mitigation actions or engineering interventions. Due to the geological and geomorphological context, these geomodels may be replicated or adapted for other countries of Latin America. In addition, considering the low cost, both in the elaboration and the required information, these models are a very powerful tool to visualize all factors interacting in the generation of coseismic landslides.

8 FINAL DISCUSSION AND CONCLUSIONS

8.1 FINAL DISCUSSION

High-magnitude earthquakes are often associated with a chain of cascading hazards including ground shaking, liquefaction, tsunamis, fault rupture, and coseismic landslides. The distribution and intensity of coseismic landslides and its influence on the landscape are largely determined by the seismogenic zone where generated earthquakes. In our country, the main seismically-induced landslides are originated from megathrust earthquakes and strong shallow crustal events.

Most efforts of coseismic landslides researchers had been focused to reliably estimate the likely pattern of landslides in a future strong shallow crustal earthquakes, based on the extensive database of over 40 complete coseismic landslide inventories available of the world (e.g. *Keefer 1984; Rodriguez et al., 1999; Malamud et al., 2004a; Malamud et al., 2004b; Marc et al., 2016; Havenith et al., 2016*). Nevertheless, in comparison with shallow crustal earthquakes the number of comprehensive landslide inventories for megathrust earthquakes is small (e.g. *Wartman et al. 2013*), meaning that there is huge uncertainty in such estimates. Therefore, there is a need to improve these datasets with representative and comprehensive coseismic landslide inventories of these two Chilean groups of seismic events. For this reason, two recent high magnitude earthquakes were considered as case studies: The 2010 M_w 8.8 megathrust earthquake and the 2007 M_w 6.2 Aysén earthquake.

Shallow crustal seismicity vs megathrust earthquakes

It is well-known that shallow crustal earthquakes tend to have higher intensities than megathrust earthquakes for equal magnitudes. Therefore, it is possible that a shallow crustal earthquake with magnitude of 6-6.5 may produce extreme catastrophic effects. For example, the 2011 M_w 6.2 Christchurch earthquake in New Zealand. This event had PGA's (vertical) close to 2.2 g and a Mercalli intensity of 11 out of 12 (*Kaiser et al., 2012; Stirling et al., 2012*). A similar situation probably occurred during the 2007 M_w 6.2 Aysén earthquake, but most of the local seismic network installed during the seismic swarm was damaged or lost due to the tsunamis (*Naranjo et al., 2009*), difficulting to have accurate data of ground motions parameters. On the other hands, in spite of megathrust earthquakes occur with comparatively high frequency, have lower accelerations when

they reach the Earth's surface. For example, during the 2015 M_w 8.3 Illapel earthquake in central Chile, maximum PGA's of 0.83 g were recorded at one station while most stations had recorded PGA's of less than 0.2 g (*Candia et al., 2017*).

The intensities generated by shallow crustal seismicity in Chile attenuate much more quickly with distance than megathrust earthquakes, thus shallow crustal earthquakes that occur in uninhabited zones could be unnoticed. For example, the 1949 M_s 7.8 Punta Arenas earthquakes occurred in a poorly habited region. Effects of the 1949 earthquakes caused dramatic changes in the water level of Lake Fagnano and landslides in the western coast of Tierra del Fuego as well as three deaths in San Nicolás Bay (*Cisternas and Vera, 2008*).

Additionally, Chilean shallow crustal earthquakes generate high seismic intensities that would rise to about 9 (MSK Scale) and peak accelerations close to 1 g in the epicentral zone when the earthquake magnitude is about 7.0, without the presence of particularly unfavorable local conditions that would produce greater damage due to site effects (*Sepúlveda et al., 2008*).

Roughly 95% of the recorded in central Chile (30°-36°S) seismicity can be linked to the subduction of the Nazca Plate under the South American Plate, along the Chilean margin, while the other 5% (shallow crustal seismicity) is located beneath the western flank of the Andean cordillera with depths between 0 and 30 km (*Ammirati et al., 2019*). For example, on the 4th of September 1958, a sequence of three earthquakes of magnitude 6.7–6.9 struck the Andean Main Cordillera at the latitude of Santiago (33°S). The Las Melosas seismic sequence is the strongest instrumentally recorded crustal event to have occurred in central Chile (*Alvarado et al., 2009*). There is one more recent large event, the 2004 M_w 6.4 Curico earthquake (35°S) with depth < 15 km, in the highlands of the Andes Cordillera.

Although the occurrence of shallow crustal seismicity is far less frequent than megathrust earthquakes, near-surface rupturing related to shallow crustal seismicity represents a considerable threat to urban centers located near to the fault source. An important tectonic feature characterizing the west Andean thrust, close the Santiago metropolitan area is the San Ramón fault (*Armijo et al., 2010*). *Vargas et al. (2014)* measured two major seismic events occurred on the San Ramón Fault, respectively ~8 and ~17 ka. The slip associated with these events has been estimated to 4.7-4.9 m corresponding to seismic events of magnitude $7.2 < M_w < 7.4$. Additionally, *Ammirati et al., (2019)*

results show an important seismicity beneath the eastern Principal Cordillera (33°-34°S) located between 5 and 15 km depths and a deeper seismicity (10-20 km) beneath the western Principal Cordillera aligned with the main Andean thrust, parallel to the scarp of the San Ramón fault. Ground motion prediction results of *Ammirati et al. (2019)* show expected PGA stronger than 0.8 g close to the San Ramón Fault scarp and greater than 0.3 g for most of the metropolitan area.

According to *De Pascale (2020)*, active neotectonic work based on field is a young field in Chile and only c.a 5% of faults segments in the national Chilean fault database are considered “active”. Therefore, probably a minor percentage of the potential generation of landslides triggered by the active faults is known. Additionally, Chilean crustal neotectonic research is not presumably considering complex situations yet, like multi-fault. For instance, the recent 2016 M_w 7.8 Kaikoura New Zealand earthquake was an event that involved a number of smaller crustal faults that connected ruptures and linked up to make a larger earthquake (e.g. *Hamling et al., 2017*).

Spatial analysis of coseismic landslides distribution

An initial objective of this study was to identify the main characteristics of coseismic landslides triggered by megathrust and shallow crustal earthquakes in Chile. Accordingly, the only two comprehensive inventories of earthquake-triggered landslides exist in Chile were developed, the shallow crustal M_w 6.2, Aysén earthquake in 2007 (45.27°S 72.66°W), revised from Sepúlveda et al. (2010) and the M_w 8.8, megathrust Maule earthquake in 2010 between 32.5° S and 38.5° S°. Most landslides occur in the Cordilleran environment where high relief and steeper slopes prevail. Furthermore, landslides are not evenly distributed in the affected areas and tend to form clusters. The most common type of landslide observed are “disrupted” slides. Shallow disrupted slides like debris avalanches, debris slides, rock falls and rock slides, account for approximately 86% and 98% of landslides triggered by the Maule 2010 and Aysén 2007 earthquakes respectively. Relatively few slumps, deep block slides, or slow earth flows were observed from Chilean inventories (c.a. 1%), According to *Mahdavifar et al. (2006)*, an equal percentage of coherent landslides were triggered by the 2002 Avaj earthquake.

One of the most important findings to emerge from the analysis is that the number and distribution of coseismic landslides differ significantly between megathrust earthquakes and shallow crustal seismicity. The total number of landslides triggered for the megathrust earthquakes is substantially

lower, typically by one to two orders of magnitude, than it would be expected for shallow crustal earthquakes, of a similar or even lower magnitude. Another important finding was that there is a difference in the size of landslides between the two broad types of Chilean earthquakes-induced landslides. These findings suggest that landslides triggered by megathrust tend to be smaller (c.a. 10^3 - 10^4 m²) than landslides induced by shallow crustal seismicity. Additionally, bigger landslides (> 1 Mm³) are more abundant in shallow crustal coseismic inventories.

Factor that influence the dynamic response of hillslopes undergoing seismic shaking

The present study was designed to compare and differentiate topographic, geomorphological, geological and seismic controlling factors in the occurrence of earthquake-triggered landslides originated by megathrust and shallow crustal earthquakes in Chile and abroad:

- The total number of landslides triggered for the megathrust earthquakes is substantially lower, typically by one to two orders of magnitude, than it would be expected for shallow crustal earthquakes of a similar or even lower magnitude.
- In both of them, the events are unevenly distributed in the study areas, dominantly disrupted slides, tending to the formation of clusters of landslides. Debris avalanches, rock falls, debris slides and rock slides/avalanches are most of coseismic landslides triggered by a shallow crustal earthquake, while that, rock falls and debris slides are commonly related to a megathrust earthquake.
- To both kinds of earthquakes, relief exerts a strongly dominant control on landsliding both in terms of preconditioning (higher, steeper slopes) and local topographic amplification of shaking.
- Bedrock lithology is a relevant conditioning factor in the generation of landslides triggered by megathrust earthquakes, with more landslides in younger (normally weaker) volcanic and volcano-sedimentary rocks. In the other hand, there is no obvious correlation between landslide concentration induced by strong shallow crustal seismicity and rock age (young or old lithology), even on very resistant rocks such as granitoids.
- Distance to the rupture plane of faults is a first-order factor in the distribution of landslides triggered by a strong shallow crustal earthquake together with topographic amplification site effects. The crowns of the landslides are generally in the uppermost part of the slopes. Ground motion parameters would be the most significant factors, including horizontal and

vertical accelerations, ground velocity, frequency content and epicentral distance. On the other hand, the current study found a poor correlation between estimated PGA and landslide occurrence related to a megathrust earthquake. A better correlation was found between landslide concentration and the ratio between horizontal and vertical peak accelerations.

Although overall correlations related to shallow crustal seismicity were established, there are still many unanswered questions at present about coseismic landslides triggered by different kinds of Chilean shallow crustal earthquakes, like seismicity generated by thrust and normal faults.

The long-term evolution of coseismic landslides

Tolorza et al. (2019) evaluate the catchment-wide erosive response to the 2010 Maule earthquake. We analyze daily suspended sediment samples in 31 river gauges located in areas affected by macro-seismic intensities up to V. The studied catchments differ greatly in terms of topography, vegetation cover and hydroclimatic conditions, which allows us to detect potential controlling factors. Surprisingly, the results record a decrease in sediment fluxes during moderate to high streamflows with respect to the pre-seismic baseline. By means of Random Forest regressions, we quantify the possible environmental and hydro-climatic controls on the observed suspended sediment responses. Our results indicate first-order controls of topography and land cover, which are particularly pronounced under dry climate conditions. Our study demonstrates that the Mw 8.8 megathrust Maule earthquake had a limited impact on the overall concentration and transport of suspended sediment loads in the Chilean Andes. This finding is contrary to previous researches which have suggested that shallow crustal earthquakes impart an impressive force on epicentral landscapes, with immediate catastrophic hillslope response, post-seismic increase in landslide rates (*Marc et al., 2015*) and the catchment-wide erosion (*Hovius et al., 2011; Wang et al., 2015*) may last several years.

Coseismic landslides and conceptual model for the recognition of landslides hazard

With all information developed in this research, we have built four pairs of representative geomodels of coseismic landslide geomorphological environments in the Andes of central Chile: Glacial cordilleran, Fluvial cordilleran, Plutonic cordilleran and Mountain front bordering urban area. Providing expected slope performance during megathrust earthquakes and shallow crustal

earthquakes. Each one express representative characteristics about coseismic landslide hazard (main types, spatial distribution and sizes), their potential consequences and suggestions of possible mitigation actions or engineering interventions. Although this methodology is a very powerful tool to visualize all factors interacting in the generation of coseismic landslides, additionally at low cost, these practitioners –friendly conceptual ground models need necessarily to be complemented with an observational model to be applied for hazard assessment at local scales.

8.2 THESIS CONCLUSION

The main goal of the current research was to identify the main characteristics of landslide occurrence during strong shallow crustal seismicity and megathrust earthquakes. It set out to improve the understanding of their mechanics, spatial distribution and geological controlling factors as well as to obtain qualitative inputs for the development of conceptual models for the recognition of coseismic landslides hazard for shallow crustal and megathrust earthquakes in different mountain environments in the Chilean Andes.

This research provide unified guidelines for preparation of comprehensive coseismic landslides inventories in Chile from remote sensing images. The only two comprehensive inventories of recent strong earthquake-triggered landslides in Chile were developed following these guidelines; the seismic events are the 2010 Mw 8.8 megathrust Maule earthquake and the 2007 Mw 6.2 shallow crustal Aysén earthquake. In total 1,226 landslides (total affected area c.120,500 km²) and 781 landslides (total affected area c. 1,350 km²) were mapped, respectively. The total landslide volume triggered is c. 10.6 Mm³ by the Maule earthquake and c. 122.3 Mm³ by the Aysén earthquake. In both of them, the events are unevenly distributed in the study areas, dominantly disrupted slides.

This study has identified the main factors that influence the dynamic response of hillslopes undergoing seismic shaking during megathrust and strong shallow crustal earthquakes in Chile, based on analysis of the two Chilean comprehensive inventories of coseismic landslides and abroad. Statistical analysis of the Maule earthquake database suggests that relief and lithology are the main geological factors controlling coseismic landslides, while the seismic factor with higher correlation with landslide occurrence is the ratio between peak horizontal and peak vertical ground accelerations. The results and comparison with other seismic events elsewhere suggest that the number of landslides generated by megathrust earthquakes is lower than events triggered by

shallow crustal earthquakes by at least one or two orders of magnitude. On the other hand, Aysén earthquake database suggests that distance to the rupture plane of faults is a first-order factor in the distribution of landslides together with topographic amplification site effects.

One of the most significant results to emerge from this research is the development of practitioner-friendly conceptual ground models relating to the performance of slopes subject to strong ground motions during megathrust or shallow crustal earthquakes in different mountain environments in the Andes of central Chile. These models have significant implications for the understanding of Chilean coseismic landslides hazard.

This thesis has supplied a deeper insight into Chilean coseismic landslides, describing the differences between conditioning factors and characteristics of landslides triggered by megathrust and strong shallow crustal earthquakes. This is a pioneer study and the first investigation to include the two main types of earthquakes-induced landslides in our country.

The present thesis provides a first baseline about coseismic landslides in Chile. Therefore, the generalization of these research results related to each type of seismicity is subject to certain limitations. The study did not include specific diversity of source mechanisms shallow crustal earthquakes supported by comprehensive inventories, like shallow crustal seismicity generated by thrust and normal faults, which must be subject of further research.

8.3 FUTURE PERSPECTIVE

A natural progression of this research is to develop a methodology for seismically-induced landslide hazard assessment at a regional scale adapted for the Chilean tectonic conditions. Then, it is required to verify the proposed methodology in a cordilleran environment area near to an important urban center like the Andean Range of the Santiago and Rancagua cities, conducting a hazard assessment study at a regional scale.

The study did not include specific diversity of source mechanisms shallow crustal earthquakes supported by comprehensive inventories, like shallow crustal seismicity generated by thrust and normal faults, which must be subject of further research.

Additionally, further work is required to establish the long –term evolution of Chilean coseismic landslides. A relevant topic considering the current climatic change.

BIBLIOGRAPHY

- Abrahamson NA, Somerville PG (1996) Effects of the hanging wall and footwall on ground motions recorded during the Northridge earthquake. *Bulletin of the Seismological Society of America*, 86(1B): S93-S99
- ADB and WB (2005) Preliminary Damage and Needs Assessment. 124. Asian Development Bank and World Bank, Islamabad, Pakistan.
- Alcántara-Ayala I (2002) Geomorphology, natural hazards, vulnerability and prevention of natural disasters in developing countries. *Geomorphology*, 47(2-4):107-124
- Alexander ED (2004) Vulnerability to landslides, *in* Glade T. et al., eds., *Landslide risk assessment*: New York, John Wiley, 175–198
- Allmendinger RW, Jordan TE, Kay SM, Isacks BL (1997) The evolution of the Altiplano-Puna plateau of the Central Andes. *Annual review of earth and planetary sciences* 25(1):139-174
- Alvarado P, Barrientos S, Saez M, Astroza M, Beck S (2009) Source study and tectonic implications of the historic 1958 Las Melosas crustal earthquake, Chile, compared to earthquake damage, *Phys. Earth Planet. In.* 175:26–36
- Ammirati JB, Vargas G, Rebolledo S, Abrahami R, Potin B, Leyton F, Ruiz S (2019) The Crustal Seismicity of the Western Andean Thrust (Central Chile, 33°–34° S): Implications for Regional Tectonics and Seismic Hazard in the Santiago Area. *Bulletin of the Seismological Society of America*, 109(5):1985-1999.
- Angermann D, Klotz J, Reigber C (1999) Space-geodetic estimation of the Nazca-South America Euler vector. *Earth and Planetary Science Letters* 171:329-334
- Antinao JL, Gosse J (2009) Large rockslides in the Southern Central Andes of Chile (32–34.5 S): Tectonic control and significance for Quaternary landscape evolution. *Geomorphology*, 104(3-4):117-133
- Araya C, Cisternas M, Gorioitía N (2013) Deslizamientos generados por el terremoto gigante de Chile de 1960 en el río San Pedro, región de los ríos: Antecedentes históricos y datación geomorfológica de sus precesores. In *En: Anales de la Sociedad Chilena de Ciencias Geográficas. XXXIV Congreso Nacional y XIX Internacional de Geografía*. Universidad del Bío-Bío, Chillán, 24-31
- Aravena N (2017) Análisis 3D del deslizamiento de roca de Punta Cola generado por el terremoto de Aysén del año 2007. Undergraduate dissertation, Dept. of Geology, University of Chile (in Spanish). Available in <http://repositorio.uchile.cl/handle/2250/150620>
- Armijo R, Rauld R, Thiele R, Vargas G, Campos J, Lacassin R, Kausel E (2010) The West Andean thrust, the San Ramon fault, and the seismic hazard for Santiago, Chile. *Tectonics*, 29(2)
- Astroza M, Ruiz S, Astroza R (2012) Damage assessment and seismic intensity analysis of the 2010 (M_w 8.8) Maule earthquake. *Earthquake Spectra* 28(S1):S145-S164
- Baltzer A (1875) *Über bergstürze in den Alpen*. Verlag der Schabelitz'schen buchhandlung, Zurich
- Barnard PL, Owen LA, Sharma MC, Finkel RC (2001) Natural and human-induced landsliding in the Garhwal Himalaya of northern India. *Geomorphology*, 40(1-2):21-35
- Barrientos S (2010) Terremoto ($M= 8.8$) del 27 de febrero de 2010 en Chile. *Revista de la asociación Geológica Argentina* 67(3):412-420

- Barrientos S, National Seismological Center (CSN) Team (2018) The seismic network of Chile. *Seismological Research Letters*, 89(2A):467-474
- Barrientos S, Vera E, Alvarado P, Monfret T (2004) Crustal seismicity in central Chile. *Journal of South American Earth Sciences*, 16(8):759-768
- Barrientos S, Ward S (1990) The 1960 Chile earthquake: Inversion for slip distribution from surface deformation, *Geophys. J. Int.* 103:589–598
- Bartholomew DS (1984) *Geology and geochemistry of the Patagonian Batholith (45-46 S), Chile* (Doctoral dissertation, University of Leicester).
- Bilek SL, Lay T (2018) Subduction zone megathrust earthquakes. *Geosphere*, 14(4):1468-1500
- Bird JF, Bommer JJ (2004) Earthquake losses due to ground failure. *Engineering geology*, 75(2):147-179
- Bird P (2003) An updated digital model of plate boundaries. *Geochem.Geophys.Geosyst.* 4(1):1027
- Bojadjieva J, Sheshov V, Bonnard C (2018) Hazard and risk assessment of earthquake-induced landslides—case study. *Landslides*, 15(1):161-171
- Boroschek R, Contreras V, Kwak DY, Stewart JP (2012) Strong ground motion attributes of the 2010 M_w 8.8 Maule, Chile, earthquake. *Earthquake Spectra* 28(S1):S19-S38
- Brabb, EE, and B L Harrod (eds.) (1989) *Landslides: Extent and economic significance*. Proceedings 28th international geological congress: Symposium on landslides, Washington, DC, 17 July 1989, 385
- Bradley BA (2012) Strong ground motion characteristics observed in the 4 September 2010 Darfield, New Zealand earthquake. *Soil Dynamics and Earthquake Engineering*, 42:32-46
- Brain MJ, Rosser NJ, Norman EC, Petley DN (2014) Are microseismic ground displacements a significant geomorphic agent? *Geomorphology* (207):161-173
- Brennan AJ, Madabhushi SG (2009) Amplification of seismic accelerations at slope crests. *Canadian Geotechnical Journal* 46:585-594
- Bucknam RC, Coe JA, Chavarria MM, Godt JW, Tarr AC, Bradley L-A, Rafferty S, Hancock D, Dart RL, Johnson ML (2001) *Landslides Triggered by Hurricane Mitch in Guatemala – Inventory and Discussion*. US Geological Survey Open File Report 01–443
- Caccavale M, Matano F, Sacchi M (2017) An integrated approach to earthquake-induced landslide hazard zoning based on probabilistic seismic scenario for Phlegrean Islands (Ischia, Procida and Vivara), Italy. *Geomorphology*, 295:235-259
- Campos J, Hatzfeld D, Madariaga R, Lopez G, Kausel E, Zollo A, Barrientos S, Lyon-Caen H (2002) The 1835 seismic gap in South Central Chile, *Phys. Earth Planet. Int.* 132:177–195
- Candia G, de Pascale GP, Montalva G, Ledezma C (2017) Geotechnical aspects of the 2015 M_w 8.3 Illapel megathrust earthquake sequence in Chile. *Earthquake Spectra*, 33(2):709-728
- Cao J, Zhang Z, Wang C, Liu J, Zhang L (2019) Susceptibility assessment of landslides triggered by earthquakes in the Western Sichuan Plateau. *Catena*, 175:63-76
- Cardinali M, Ardizzone F, Galli M, Guzzetti F, Reichenbach P (2000) Landslides triggered by rapid snow melting: the December 1996–January 1997 event in Central Italy. Proceedings 1st Plinius Conference on Mediterranean Storms. Claps P, Siccardi F (eds). Bios: Cosenza; 439–448

- Casagli N, Cigna F, Bianchini S, Hölbling D, Füreder P, Righini G, Del Conte S, Friedl B, Schneiderbauer S, Iasio C, Vlcko J, Greif V, Proske H, Granica K, Falco S, Lozzi S, Mora O, Arnaud A, Novali F, Bianchi M (2016) Landslidemapping and monitoring by using radar and optical remote sensing: examples from the EC-FP7 project SAFER. *Remote Sens. Appl. Soc. Environ.* 4, 92–108
- Cembrano, J, Hervé F (1993) The Liquiñe Ofqui-Fault Zone: a major Cenozoic strike-slip duplex in the Southern Andes. Second ISAG. In *International Symposium Andean geodynamics: extended abstracts*. Paris, ORSTOM, 175-178
- Cembrano J, Hervé F, Lavenu A (1996) The Liquiñe Ofqui Fault Zone: a long-lived intraarc fault system in southern Chile. *Tectonophysics*, 259:55-66
- Cembrano J, Lavenu A, Reynolds P, Arancibia G, López G, Sanhueza A (2002) Late Cenozoic transpressional ductile deformation north of the Nazca–South America–Antarctica triple junction. *Tectonophysics*, 354(3-4):289-314
- Cembrano J, Lara L, Lavenu A, Hervé F (2007) Long-term and short-term kinematic history of the Liquiñe-Ofqui fault zone: a review and implications for geologic hazard assessment. In: *Proceedings Geosur 2007*, Santiago de Chile, 30
- Cifuentes IL (1989) The 1960 Chilean earthquakes, *J. Geophys. Res.* 94:665–680
- Cisternas A (2011) El país más sísmico del mundo. *Revista Anales Séptima Serie*
- Cisternas M, Atwater BF, Torrejón F, Sawai Y, Machuca G, Lagos M, Shishikura M (2005) Predecessors of the giant 1960 Chile earthquake. *Nature*, 437(7057):404
- Cisternas A, Vera E (2008) Sismos históricos y recientes en Magallanes. *Magallania (Punta Arenas)*, 36(1), 43-51.
- Charrier R, Ramos VA, Tapia F, Sagripanti L (2015) Tectono-stratigraphic evolution of the Andean Orogen between 31 and 37°S (Chile and Western Argentina). *Geological Society Special Publications*, London, 13-61
- Chen XL, Zhou Q, Ran H, Dong R (2012) Earthquake-triggered landslides in southwest China. *Natural Hazards and Earth System Sciences*, 12(2):351-363
- Cisternas A (2011) El país más sísmico del mundo: *Revista Anales, Séptima Serie*, 1
- Clapperton C (1994) The quaternary glaciation of Chile: a review. *Revista Chilena de Historia Natural*, 67:369 – 383
- Cluff, LS (1971) Peru earthquake of May 31, 1970; engineering geology observations. *Bulletin of the Seismological Society of America*, 61(3):511-533
- Costa J E, Schuster R L (1988) The formation and failure of natural dams: *Geological Society of America Bulletin*, 100:1054-1068
- Crozier MJ, Glade T (2005) Landslide hazard and risk: issues, concepts and approach. *Landslide hazard and risk*, 1-40
- Cruden DM (1991) A Simple definition of a landslide. *Bulletin of the International Association of Engineering Geology*, 43:27–29
- Cruden DM (2003) The first classification of landslides? *Environ. Eng. Geosci.* 9(3):197–200

- Cruden DM, Varnes DJ (1996) Landslides: investigation and mitigation. Chapter 3-Landslide types and processes. Transportation research board special report, 247
- Dadson SJ, Hovius N, Chen H, Dade WB, Lin JC, Hsu ML, ...& Stark C P (2004) Earthquake-triggered increase in sediment delivery from an active mountain belt. *Geology*, 32(8):733-736
- Dai FC, Lee CF, Deng JH, Tham LG (2005) The 1786 earthquake-triggered landslides dam and subsequent dam-break flood of the Dadu river, southwestern China: *Geomorphology*, 65:205-221
- Dai FC, Xu C, Yao X, Xu L, Tu XB, Gong QM (2011) Spatial distribution of landslides triggered by the 2008 Ms 8.0 Wenchuan earthquake, China. *Journal of Asian Earth Sciences*, 40(4):883-895
- Davis SN, Karzulovic J, (1963) Landslides of Lago Riñihue, Chile. *Geological Society of America Bulletin*. 53(6):1403-1414
- Delouis B, Nocquet JM, Vallée M (2010) Slip distribution of the February 27, 2010 $M_w = 8.8$ Maule earthquake, central Chile, from static and high-rate GPS, InSAR, and Broadband teleseismic data. *Geophysical Research Letters* <https://doi.org/10.1029/2010GL043899>
- Densmore A, Hovius N (2000) Topographic fingerprints of bedrock landslides. *Geology* 28(4):371–374
- Díaz, SR, Cadena E, Adame S, Dávila N, (2019) Landslides in Mexico: their occurrence and social impact since 1935. *Landslides*. <https://doi.org/10.1007/s10346-019-01285-6>
- Dunning SA, Mitchell WA, Rosser NJ, Petley DN (2007) The Hattian Bala rock avalanche and associated landslides triggered by the Kashmir Earthquake of 8 October 2005. *Engineering Geology* 93:130-144
- Duke, CM (1960) The Chilean Earthquakes of May 1960. *Science*, 132(3442):1797-1802
- EPOCH (1993) Temporal occurrence and forecasting of landslides in the European community. EUR 15805 EN, 1, contract no. 900025
- Escobar P (2013) Inventario de remociones en masa desencadenadas por el sismo del 27 de febrero de 2010 en Chile central. Disponible en <http://repositorio.uchile.cl/handle/2250/115454>
- Escudero I (2017) Modelamiento dinámico mediante elementos discretos del deslizamiento de roca de Punta Cola generado por el terremoto del fiordo Aysén del 2007. Undergraduate dissertation, Dept. of Geology, University of Chile (in Spanish). Available in <http://repositorio.uchile.cl/handle/2250/146808>
- Fan X, Scaringi G, Domènech G, Yang F, Guo X, Dai L, He C, Xu Q, Huang R (2019a). Two multi-temporal datasets that track the enhanced landsliding after the 2008 Wenchuan earthquake. *Earth Syst. Sci. Data* 11(1):35–55
- Fan X, Scaringi G, Korup O, West AJ, vanWesten CJ, Tanyas H, Hovius N, Hales TC, Jibson RW, Allstadt KE, Zhang L, Evans SG, Xu C, Li G, Pei X, Xu Q, Huang R (2019b) Earthquake-induced chains of geologic hazards: patterns, mechanisms, and impacts. *Rev. Geophys.* 57(2):421–503
- Fan X, Van Westen CJ, Xu G, Gorum T, Dai F, Wang G, Huang R (2009) Distribution of large landslides and landslide dams triggered by the Wenchuan earthquake, Sichuan, China: *Geophysical Research Abstracts*, 11
- Fookes P (1997) First Glossop Lecture: Geology for engineers: The geological model, prediction and performance. *Quarterly Journal of Engineering Geology* 30:293–424
- Fookes P, Pettifer G, Waltham T (2015) *Geomodels in engineering geology: an introduction*. Whittles Publishing.

- Forsythe R, Prior D (1992) Cenozoic Continental Geology of South America and Its Relations to the Evolution of the Chile Triple Junction. In *Proceedings of the Ocean Drilling Program, Initial Reports*, 141:23-31
- Gallen SF, Clark MK, Godt JW, Roback K, Niemi NA (2017) Application and evaluation of a rapid response earthquake-triggered landslide model to the 25 April 2015 M_w 7.8 Gorkha earthquake, Nepal. *Tectonophysics*, 714:173-187
- Geli L, Bard PY, Jullien B (1988) The effect of topography on earthquake ground motion: a review and new results. *Bulletin of the Seismological Society of America*, 78(1):42-63
- Glade T, Crozier MJ (2005) *The nature of landslide hazard impact*. Landslide hazard and risk. Wiley, Chichester, 43-74.
- Gledhill K, Ristau J, Reyners M, Fry B, Holden C (2011) The darfield (Canterbury, New Zealand) M_w 7.1 earthquake of september 2010: a preliminary seismological report. *Seismological Research Letters*, 82(3): 378-386
- Godoy E, Yanez G, Vera E (1999) Inversion of an Oligocene volcano-tectonic basin and uplifting of its superimposed Miocene magmatic arc in the Chilean Central Andes: First seismic and gravity evidences, *Tectonophysics* 306:217–236
- Gorum T, Fan X, van Westen CJ, Huang RQ, Xu Q, Tang C, Wang G (2011) Distribution pattern of earthquake-induced landslides triggered by the 12 May 2008 Wenchuan Earthquake. *Geomorphology* 133(3-4):152-167
- Guzzetti F, Mondini AC, Cardinali M, Fiorucci F, Santangelo M, Chang KT (2012) Landslide inventory maps: New tools for an old problem. *Earth-Science Reviews*, 112(1-2), 42-66.
- Hamling IJ, Hreinsdóttir, S., Clark, K., Elliott, J., Liang, C., Fielding, E., ... & D’Anastasio, E. (2017) Complex multi-fault rupture during the 2016 M_w 7.8 Kaikoura earthquake, New Zealand. *Science*, 356: 6334
- Harp EL, Jibson RL (1995) Inventory of landslides triggered by the 1994 Northridge, California earthquake. US Geological Survey Open File Report 95–213
- Harp EL, Jibson RL (1996) Landslides triggered by the 1994 Northridge, California earthquake. *Seismological Society of America Bulletin* 86: S319–S332
- Harp EL, Keefer DK, Sato HP, Yagi H (2011) Landslide inventories: the essential part of seismic landslide hazard analyses. *Engineering Geology*, 122(1-2): 9-21
- Hauser A (2002) Rock avalanche and resulting debris flow in Estero Parraguire and Río Colorado, Región Metropolitana, Chile. In: Evans SG, Degraff JV (eds) *Catastrophic landslides: Effects, occurrence, and mechanisms*. *Reviews in Engineering Geology*, 15:135-148
- Havenith HB, Torgoev A, Braun A, Schlögel R, Micu M (2016) A new classification of earthquake-induced landslide event sizes based on seismotectonic, topographic, climatic and geologic factors. *Geoenvironmental Disasters* 3(1):6
- Hearn G (2018) Slope hazards on the Ethiopian road network *Quarterly Journal of Engineering Geology and Hydrogeology*, 21 August 2018, <https://0-doi-org.wam.leeds.ac.uk/10.1144/qjgegh2018-058>
- Hearn G, Hart A (2011) Geomorphological contributions to landslide risk assessment: theory and practice. In: Smith M.J., Paron P., Griffiths J. (eds) *Geomorphological Mapping: Methods and Applications*. Elsevier, Amsterdam, *Developments in Earth Surface Processes*, 15:107–148

- Hearn G, Wise D, Hart A, Morgan C, O'Donnell N (2012) Assessing the potential for future first-time slope failures to impact the oil and gas pipeline corridor through the Makarov Mountains, Sakhalin Island, Russia. *Quarterly Journal of Engineering Geology and Hydrogeology*, 45:79-88
- Hermanns RL, Sepúlveda SA, Lastras G, Amblas D, Canals M, Aspiroz M, Bascañan I, Calafat AM, Duhart P, Frigola J, Iglesias O, Kempf P, Lafuerza S, Longva O, Micallef A, Oppikofer T, Rayo, X, Vargas G, Molina Y (2014) Earthquake-triggered subaerial landslides that caused large scale fjord sediment deformation: combined subaerial and submarine studies of the 2007 Aysén Fjord event, Chile. In *Engineering Geology for Society and Territory – Volume 4 Marine and Coastal Processes*, Chapter: 14, Publisher: Springer, Editors: G. Lollino, A. Manconi, J. Locat, Y. Huang, M. Canals, 67-70
- Hervás J, Barredo JI, Rosin PL, Pasuto A, Mantovani F, Silvano S (2003) Monitoring landslides from optical remotely sensed imagery: the case history of Tessina landslide, Italy. *Geomorphology* 54 (1–2):63–75
- Hervé F (1994) The southern Andes between 39 and 44 S latitude: The geological signature of a transpressive tectonic regime related to a magmatic arc. In *Tectonics of the Southern Central Andes*, 243-248. Springer, Berlin, Heidelberg.
- Hovius N, Meunier P, Lin CW, Chen H, Chen YG, Dadson S, Horng MJ, Lines M (2011) Prolonged seismically induced erosion and the mass balance of a large earthquake. *Earth and Planetary Science Letters*, 304(3-4):347-355
- Howe E (1909) Landslides in the San Juan Mountains, Colorado, Including a Consideration of their Causes and their Classification
- Huang, R, Fan X (2013) The landslide story. *Nature Geoscience*, 6(5):325-326
- Huang RQ, Li AW (2009) Analysis of the geo-hazards triggered by the 12 May 2008 Wenchuan Earthquake, China. *Bulletin of Engineering Geology and the Environment*, 68(3):363-371
- Huang CC, Lee YH, Liu HP, Keefer DK, Jibson RW (2001) Influence of Surface-Normal Ground Acceleration on the Initiation of the Jih-Feng-Erh-Shan Landslide during the 1999 Chi-Chi, Taiwan, Earthquake. *Bulletin of the Seismological Society of America*, 91(5):953–958
- Hung JJ (2000) Chi-Chi earthquake induced landslides in Taiwan. *Earthquake Engineering and Engineering Seismology*, 2(2):25-33
- Hung O (2018) A review of landslide hazard and risk assessment methodology. In *Landslides and engineered slopes. Experience, theory and practice*, CRC Press, 3-27
- Hung O, Evans SG (2004) The occurrence and classification of massive rock slope failure. *Felsbau*, 22(2):16-23
- Hung O, Evans SG, Hutchinson IN (2001) A Review of the Classification of Landslides of the Flow Type. *Environmental & Engineering Geoscience*, 7(3):221-238
- Hung O, Leroueil S, Picarelli L (2014) The Varnes classification of landslide types, an update. *Landslides* 11(2):167-194.
- Hutchinson JN (1968) Mass movement. *Geomorphology. Encyclopedia of Earth Science*. Springer, Berlin, Heidelberg
- Idini, B, Rojas F, Ruiz S, Pastén C (2017) Ground motion prediction equations for the Chilean subduction zone. *Bulletin of Earthquake Engineering*, 15(5):1853-1880
- International Association for Engineering Geology and the Environment (IAEG) Commission, 1990. Suggested nomenclature for landslides. *Bull. Int. Assoc. Eng. Geol.* 41 (1):13–16

- Isacks BL (1988) Uplift of the central Andean plateau and bending of the Bolivian orocline. *Journal of Geophysical Research: Solid Earth* 93(B4):3211-3231
- Jaboyedoff M, Michoud C, Derron MH, Voumard J, Leibundgut G, Sudmeier-Rieux K, ... & Leroi E (2018) Human-induced landslides: Toward the analysis of anthropogenic changes of the slope environment. In *Landslides and Engineered Slopes. Experience, Theory and Practice*,). CRC Press, 217-232
- Jackson, R (2016) *Geomodels in Engineering Geology—An Introduction*. *Environmental & Engineering Geoscience* 22(2):171-172
- Jibson E (1995) Inventory of landslides triggered by the 1994 Northridge, California earthquake. <http://pubs.usgs.gov/of/1995/ofr-95-0213/>
- Jibson RW (2011) Methods for assessing the stability of slopes during earthquakes—A retrospective, *Engineering Geology* 122(1-2):43-50
- Jibson RW, Harp E L, Schulz W, Keefer DF, (2006) Large rock avalanches triggered by the M 7.9 Denali Fault, Alaska, earthquake of 3 November 2002. *Engineering Geology*, 83:144-160
- Jordan TE, Isacks B, Allmendinger R, Brewer J, Ramos V, Ando C (1983) Andean tectonics related to geometry of the subducted Nazca plate. *Geol. Soc. Am. Bull* 94:341-361
- Kaiser A, Holden C, Beavan J, Beetham D, Benites R., Celentano A, Collett D, Cousins J, Cubrinovski M, Dellow G, Denys P, Fielding E, Fry B, Gerstenberger M, Langridge R, Massey C, Motagh M, Pondard N, McVerry G, Ristau J, Stirling M, Thomas J, Uma SR, Zhao J (2012) The M_w 6.2 Christchurch earthquake of February 2011: preliminary report. *New Zealand Journal of Geology and Geophysics* 55(1):67–90
- Kamp U, Owen LA, Benjamin J, Growley BJ, Khattak GA (2010) Back analysis of landslide susceptibility zonation mapping for the 2005 Kashmir earthquake: An assessment of the reliability of susceptibility zoning maps. *Natural Hazards* 54:1–25
- Khajavi N, Quigley M, McColl ST, Rezanejad A (2012) Seismically induced boulder displacement in the Port Hills, New Zealand during the 2010 Darfield (Canterbury) earthquake. *New Zealand Journal of Geology and Geophysics*, 55(3):271-278
- Khattak, G. A., Owen, L. A., Kamp, U., & Harp, E. L. (2010). Evolution of earthquake-triggered landslides in the Kashmir Himalaya, northern Pakistan. *Geomorphology*, 115(1-2), 102-108
- Khazai B, Sitar N (2004) Evaluation of factors controlling earthquake-induced landslides caused by Chi-Chi earthquake and comparison with the Northridge and Loma Prieta events. *Engineering geology* 71(1):79-95
- Keefer, DK (1984) Landslides caused by earthquakes. *Geological Society of America Bulletin* 95:406-421
- Keefer DK (1994). The importance of earthquake-induced landslides to long-term slope erosion and slope-failure hazards in seismically active regions. In *Geomorphology and Natural Hazards*, Elsevier, 265-284
- Keefer DK (2000) Statistical analysis of an earthquake-induced landslide distribution—the 1989 Loma Prieta, California event. *Engineering geology* 58(3):231-249
- Keefer DK (2002) Investigating Landslides Caused By Earthquakes – a Historical Review. *Surveys in geophysics* (1):473–510
- Lacroix P, Zavala B, Berthier E, & Audin L (2013) Supervised method of landslide inventory using panchromatic SPOT5 images and application to the earthquake-triggered landslides of Pisco (Peru, 2007, Mw8. 0). *Remote Sensing* 5(6):2590-2616

- Larsen IJ, Montgomery DR, Korup O (2010) Landslide erosion controlled by hillslope material. *Nat Geosci* 3(4):247–251
- Lastras G, Amblas D, Calafat AM, Canals M, Frigola J, Hermanns RL, ... & Vargas G (2013) Landslides cause tsunami waves: insights from Aysén Fjord, Chile. *Eos, Transactions American Geophysical Union*, 94(34):297-298
- Lastras G, Amblas D, Canals M, Party DS (2016) Fjord-flank collapse and associated deformation in Aysén Fjord, Chile. *Geological Society, London, Memoirs*, 46(1):107-108
- Lavenu A, Cembrano J (1994) Neotectónica de rumbo dextral en la zona de falla Liquiñe–Ofqui: geometría, cinemática y tensor de esfuerzo. In *Congreso Geológico Chileno*, 7:81-85
- Lavenu A, Cembrano J (1999) Compressional- and transpressional-stress pattern for Pliocene and Quaternary brittle deformation in fore arc and intra-arc zones (Andes of Central and Southern Chile). *Journal of Structural Geology* 21:1669–1691
- Lay T, Ammon CJ, Kanamori H, Koper KD, Sufri O, Hutko AR (2010) Teleseismic inversion for rupture process of the 27 February 2010 Chile (Mw 8.8) earthquake. *Geophysical Research Letters* <https://doi.org/10.1029/2010GL043379>
- Lazo R (2008) Estudio de los Daños de los Terremotos del 21 y 22 de Mayo de 1960. Disponible en <http://repositorio.uchile.cl/handle/2250/104856>
- Legrand D, Barrientos S, Bataille K, Cembrano J, Pavez A (2011) The fluid-driven tectonics warm of Aysén Fjord Chile (2007) associated with two earthquakes (Mw=6.1 and Mw=6.2) within the Liquiñe–Ofqui Fault Zone. *Continental Shelf Research* 31:154-161
- Lin CW, Liu SH., Lee SY, Liu CC (2006) Impacts of the Chi-Chi earthquake on subsequent rainfall-induced landslides in Central Taiwan. *Eng. Geol.* 86(2):87–101
- Lomnitz C (1960) A study of the Maipo Valley earthquakes of September 4, 1958, *Proc. of the 2nd World Conf. Earthquake Engineering*, Vol. 1, Tokyo-Kyoto, Japan, 501–520
- Lomnitz C (2004) Major earthquakes of Chile: a historical survey, 1535-1960. *Seismological Research Letters*, 75(3):368-378
- Lorito S, Romano F, Atzori F, Tong X, Avallone A, McCloskey J, Cocco M, Boshi E, Piatanesi A (2011) Limited overlap between the seismic gap and co-seismic slip of the great 2010 Chilean earthquake. *Nature Geoscience Letters* 4(3):173–177
- Lyell, C (1833) *Principles of Geology, Being an Attempt to Explain the Former Changes of the Earth's Surface, by Reference to Causes Now in Operation.* vol. 3 (London)
- Mahdavi MR, Solaymani S, Jafari MK (2006) Landslides triggered by the Avaj, Iran earthquake of June 22, 2002. *Engineering Geology*, 86(2-3):166-182
- Mahmood I, Qureshi SN, Tariq S, Atique L, Iqbal M (2015) Analysis of landslides triggered by October 2005, Kashmir earthquake. *PLoS currents*, 7
- Malamud BD, Turcotte DL, Guzzetti F, Reichenbach P (2004a) Landslide inventories and their statistical properties. *Earth Surface Processes and Landforms* 29(6):687-711
- Malamud BD, Turcotte DL, Guzzetti F, Reichenbach P (2004b) Landslides, earthquakes, and erosion. *Earth and Planetary Science Letters*, 229(1-2):45-59

- Marc O, Hovius N (2015) Amalgamation in landslide maps: effects and automatic detection. *Natural Hazards and Earth System Sciences*, 15(4):723-733
- Marc O, Hovius N, Meunier P, Gorum T, Uchida T (2016) A seismologically consistent expression for the total area and volume of earthquake-triggered landsliding. *J. Geophys. Res. Earth Surf.* 121(4):640-666
- Marc O, Hovius N, Meunier P, Uchida T, Hayashi S (2015) Transient changes of landslide rates after earthquakes. *Geology*, 43(10):883-886
- Mardones M, Rojas J (2012) Procesos de remoción en masa inducidos por el terremoto del 27F de 2010 en Martha TR, Kerle N, Jetten V, van Westen CJ, Kumar KV (2010) Characterising spectral, spatial and morphometric properties of landslides for semi-automatic detection using object-oriented methods. *Geomorphology*, 116(1-2): 24-36
- Marín M, Muñoz A, Naranjo J (2019) Víctimas fatales causadas por remociones en masa en Chile (1928-2017). In XV Congreso Geológico de Chile Actas, Concepción
- Martha TR, Kerle N, vanWesten CJ, Jetten V, Kumar KV (2012) Object-oriented analysis of multi-temporal panchromatic images for creation of historical landslide inventories. *ISPRS journal of photogrammetry and remote sensing* 67: 105e119
- Marui H, Nadim F (2009) Landslides and multi-hazards." *Landslides–Disaster Risk Reduction*. Springer, Berlin, Heidelberg, 435-450
- Massey C, Townsend D, Rathje E, Allstadt KE, Lukovic B, Kaneko Y, Bradley B, Wartman J, Jibson RW, Petley DN, Horspool N, Hamling I, Carey J, Cox S, Davidson J, Dellow S, Godt JW, Holden C, Jones K, Kaiser A, Little M, Lyndsell B, McColl S, Morgenstern R, Rengers FK, Rhoades D, Rosser B, Strong D, Singeisen C, Villeneuve M (2018) Landslides Triggered by the 14 November 2016 Mw 7.8 Kaikōura Earthquake, New ZealandLandslides Triggered by the 14 November 2016 Mw 7.8 Kaikōura Earthquake, New Zealand. *Bulletin of the Seismological Society of America*, 108(3B), 1630-1648.
- McCulloch RD, Bentley MJ, Purves RS et al (2000) Climatic inferences from glacial and palaeoecological evidence at the last glacial termination, southern South America. *J Quat Sci* 15:15
- Meunier P, Hovius N, Haines AJ (2007) Regional patterns of earthquake-triggered landslides and their relation to ground motion. *Geophysical Research Letters*, 34(20)
- Meunier P, Hovius N, Haines AJ (2008) Topographic site effects and the location of earthquake induced landslides. *Earth and Planetary Science Letters* (275):221-232
- Meunier P, Uchida T, Hovius N (2013) Landslide patterns reveal the sources of large earthquakes. *Earth and Planetary Science Letters*, 363:27-33
- Moernaut J, Van Daele M, Heirman K, Fontijn K, Strasser M, Pino M, Urrutia R, De Batist M (2014) Lacustrine turbidites as a tool for quantitative earthquake reconstruction: New evidence for a variable rupture mode in south–central Chile, *Journal of Geophysical Research: Solid Earth*, 119(3):1607-1633
- Mondini AC, Chang KT, Yin HY (2011) Combining multiple change detection indices for mapping landslides triggered by typhoons. *Geomorphology*, 134(3-4):440-451
- Montgomery DR, Dietrich WE (1994) A physically based model for the topographic control on shallow landsliding. *Water Resour Res* 30:1153–1171
- Moosavi V, Talebi A, Shirmohammadi B (2014) Producing a landslide inventory map using pixel-based and object-oriented approaches optimized by Taguchi method. *Geomorphology* 204:646e656

- Moreiras SM, Sepúlveda SA, González P (2012) Nuevos estudios en los grandes movimientos en masa en la alta cordillera de la cuenca del río Maipo, Chile Central. In Congreso Geológico Chileno, 11
- Moreiras SM, Sepúlveda SA (2015) Megalandslides in the Andes of central Chile and Argentina (32°–34° S) and potential hazards. Geological Society, London, Special Publications, 399(1):329-344
- Moreno M, Klotz J, Melnick D, Echtler H, Bataille K (2008) Active faulting and heterogeneous deformation across a megathrust segment boundary from GPS data, south central Chile (36-39 S). *Geochemistry Geophysics Geosystems*, 9 12:Q12024
- Moya S (2016) Comportamiento monótonico y cíclico de suelos y rocas blandas afectadas por remociones en masa cosísmicas. Disponible en <http://repositorio.uchile.cl/handle/2250/143497>
- Moya S, Sepúlveda SA, Serey A, García M (2015) Remociones en masa generadas por el terremoto del Maule del 2010 en la Península de Arauco. In XIV Congreso Geológico de Chile Actas, La Serena
- Murphy B (2015) Coseismic landslides. In *Landslide Hazards, Risks and Disasters*. Academic Press, 91-129
- Naranjo JA, Arenas M, Clavero J, Muñoz O, (2009) Mass movement-induced tsunamis: main effects during the Patagonian Fjordland seismic crisis in Aisén (45°25'S). *Chilean Andean Geology* 36(1):137–146
- Newmark NM (1965) Effects of earthquakes on dams and embankments." *Geotechnique* 15(2):139-160
- Onions CT (1993) *The Oxford English Dictionary*. Oxford University Press, Oxford.
- Oppikofer T, Hermanns R, Redfield TF, Sepúlveda SA, Duhart P, Bascuñán I (2012) Morphologic description of the Punta Cola rock avalanche and associated minor rockslides caused by the 21 April 2007 Aysén earthquake (Patagonia, southern Chile). *Revista Asociación Geológica Argentina* 69(3):339-353
- Owen, LA, Kamp U, Khattak GA, Harp EL, Keefer DK, Bauer MA (2008) Landslides triggered by the October 8, 2005, Kashmir earthquake. *Geomorphology*, 94:1–9
- Pankhurst R, Hervé F (2007) Introduction and overview. The Geological Society of London, 1-4
- Pardo-Casas F, & Molnar P (1987) Relative motion of the Nazca (Farallon) and South American plates since Late Cretaceous time. *Tectonics* 6(3):233-248
- Pareek N, Sharma ML, Arora MK (2010) Impact of seismic factors on landslide susceptibility zonation: a case study in part of Indian Himalayas. *Landslides*, 7(2):191-201
- Parker RN, Densmore AL, Rosser NJ, de Michele M, Li Y, Huang RQ, Whadcoat S, Petley DN (2011) Mass wasting triggered by the 2008 Wenchuan earthquake is greater than orogenic growth: *Nature Geoscience*, 4(7), 449–452
- Parker RN, Hancox GT, Petley DN, Massey CI, Densmore AL, Rosser NJ (2015) Spatial distributions of earthquake-induced landslides and hillslope preconditioning in northwest South Island, New Zealand. *Earth surface dynamics*. 3(4):501-525
- Parry (2016) *Geomodels in Engineering Geology – An Introduction*, P. Fookes, G. Pettifer, T. Waltham, Whittle Publishing (2015), ISBN 978-1-84995-139-5.
- Petley DN (2009) Landslides and multi-hazards. In *Landslides–Disaster Risk Reduction* (pp. 435-450). Springer, Berlin, Heidelberg
- Petley DN (2010) Landslide hazards, in Alcantara-Ayala I, Goudie A., eds., *Geomorphological hazards and disaster prevention*: Cambridge, UK, Cambridge University Press, 63–74

- Petley DN (2012) Global patterns of loss of life from landslides. *Geology*, 40(10):927-930
- Petley DN, Dunning SA, Rosser NJ, Kausar AB (2006) Incipient earthquakes in the Jhelum Valley, Pakistan following the 8th October 2005 earthquake. In: Marui, H. (Ed.) *Disaster mitigation of debris flows, slope failures and landslides*. *Frontiers of Science Series 47*, Universal Academy Press, Tokyo, Japan, 47–56
- Plafker G, Ericksen GE (1978) Nevados Huascaran avalanches, Peru. In *Developments in Geotechnical Engineering*, Elsevier, 14:277-314
- Pourghasemi HR, Mohammady M, Pradhan B (2012) Landslide susceptibility mapping using index of entropy and conditional probability models in GIS: Safarood Basin, Iran. *Catena*, 97, 71-84
- Pradhan B, Lee S (2007) Utilization of optical remote sensing data and GIS tools for regional landslide hazard analysis using an artificial neural network model. *Earth Science Frontiers*, 14(6):143-151
- Pradhan B, Lee S (2010) Landslide susceptibility assessment and factor effect analysis: backpropagation artificial neural networks and their comparison with frequency ratio and bivariate logistic regression modelling. *Environmental Modelling & Software*, 25(6):747-759
- Qi S, Xu Q, Lan H, Zhang B, Liu J (2010) Spatial distribution analysis of landslides triggered by 2008.5.12 Wenchuan Earthquake, *China Engineering Geology*, 116 (1–2):95-108
- Redfield TF, Hermanns RL, Oppikofer T, Duhart P, Mella M, Derch P, Bascuñan I, Fernández J, Arenas M, Sepúlveda S, Rebolledo S, Loew S, Yugsi Molina F, Abächerli A, Henderson I, Jaboyedoff M, Kveldevisk V (2011) Analysis of the 2007 earthquake-induced Punta Cola rockslide and tsunami, Aysén Fjord, Patagonia, Chile (45.3 S, 73.0 W). In *5th International Conference on Earthquake Geotechnical Engineering*, Santiago de Chile, 2011
- Robinson TR, Davies TR, Reznichenko NV, De Pascale GP (2015) The extremely long-runout Komansu rock avalanche in the Trans Alai range, Pamir Mountains, southern Kyrgyzstan. *Landslides*, 12(3):523-535
- Rodriguez CE, Bommer JJ, Chandler RJ (1999) Earthquake induced landslide 1980-1997. *Soil Dyn Earthquake Eng* 18: 225-346
- Ruegg, JC, Rudloff A, Vigny C, Madariaga R, De Chabaliér JB, Campos J, Kausel E, Barrientos S, Dimitrov D (2009) Interseismic strain accumulation measured by GPS in the seismic gap between Constitución and Concepción in Chile. *Physics of the Earth and Planetary Interiors* 175:78-85
- Ruiz S, Madariaga R, Astroza M, Saragoni R, Lancieri M, Vigny C, Campose J (2012) Short-Period Rupture Process of the 2010 Mw 8.8 Maule Earthquake in Chile. *Earthquake Spectra* 28 (S1):S1–S18
- Saba SB, van der Meijde M, van der Werff H (2010) Spatiotemporal landslide detection for the 2005 Kashmir earthquake region. *Geomorphology* 124(1–2):17–25
- Sánchez C, Lee T-S, Young S, Batts D, Benjamin J, Malilay J (2009) Risk factors for mortality during the 2002 landslides in Chuuk, Federated States of Micronesia: *Disasters*, 33(4):705–720
- Santibanez I, Cembrano J, García-Pérez T, Costa C, Yanez G, Marquardt C, Arancibia G, Gonzalez G (2019) Crustal faults in the Chilean Andes: geological constraints and seismic potential. *Andean Geology* 46(1):32-65
- Saputra A, Sartohadi J, Hadmoko DS, Gomez C (2016). *Geospatial Assessment of Coseismic Landslides in Baturagung Area*. *Forum Geografi*, 29(2):99-114
- Saragoni R, y Ruiz S (2012) *Implicancias y nuevos desafíos del diseño sísmico de los acelerógramas del Terremoto del 2010, en Mw=8.8: Terremoto en Chile, 27 de febrero 2010*. Primera edn, Departamento Ingeniería Civil FCFM Universidad de Chile, 127-146

- Sato H, Hasegawa H, Fujiwara S, Tobita M, Koarai M, Une H, Iwahashi J (2007) Interpretation of landslide distribution triggered by the 2005 Northern Pakistan earthquake using SPOT 5 imagery. *Landslides*, 4:113-122
- Shafique M (2020) Spatial and temporal evolution of co-seismic landslides after the 2005 Kashmir earthquake. *Geomorphology*, 107228
- Sharpe CFS (1938) *Landslides and Related Phenomena: A Study of Mass Movement of Soil and Rock*. Columbia University Press, New York
- Sheffels BM (1990) Lower bound on the amount of crustal shortening, in the central Bolivian Andes. *Geology* 18(9):812-815
- Shinoda M, Miyata Y, Kurokawa U, Kondo K (2019) Regional landslide susceptibility following the 2016 Kumamoto earthquake using back-calculated geomaterial strength parameters. *Landslides*, 16(8):1497-1516
- Shrestha S, Kang TS (2019) Assessment of seismically-induced landslide susceptibility after the 2015 Gorkha earthquake, Nepal. *Bulletin of Engineering Geology and the Environment*, 78(3):1829-1842
- Schuster RL, Salcedo DA, Valenzuela L, (2002) Overview of catastrophic landslides of South America in the twentieth century In *Catastrophic landslides: Effects, occurrence, and mechanisms*. *Reviews in Engineering Geology* 15, Geological Society of America, 1-34
- Sepúlveda SA (2004) *The effect of topographic amplification on seismic rock slope instability* (Doctoral dissertation, University of Leeds)
- Sepúlveda SA, Astroza M, Kausel E, Campos J, Casas EA, Rebolledo S, Verdugo R (2008) New findings on the 1958 Las Melosas earthquake sequence, central Chile: implications for seismic hazard related to shallow crustal earthquakes in subduction zones. *Journal of Earthquake Engineering*, 12(3):432-455
- Sepúlveda SA, Murphy W, Petley DN (2005) Topographic controls on coseismic rock slides during the 1999 Chi-Chi Earthquake, Taiwan. *Quarterly Journal of Engineering Geology and Hydrogeology*, 38, 189-196
- Sepúlveda SA, Pastén C, Moya S, García M, Lara M, Montalva G,... & Penna I (2016) Site investigation and modelling of earthquake-induced rock slides in central-southern Chile.
- Sepúlveda SA, Serey A (2009) Tsunamigenic, earthquake-triggered rock slope failures during the 21st of April 2007 Aisén earthquake, Southern Chile (45.5°S). *Andean Geology* 36(1):131-136
- Sepúlveda SA, Serey A, Lara M, Pavez A, Rebolledo S (2010) Landslides induced by the 2007 Aysén Fjord earthquake, Chilean Patagonia. *Landslides* 7(4):483-492
- Serey A (2011) Análisis de las Remociones en Masa Generadas por el Terremoto del Fiordo Aysén de 2007 (45,5°S). Available in <http://repositorio.uchile.cl/handle/2250/102608>
- Serey A, Escobar P, Moya S, Sepúlveda SA, Petley D (2017) Landslide inventory of the 2010 Mw 8.8 Maule earthquake, Central Chile. 16th World Conference on Earthquake 16WCEE 2017, 1873
- Serey A, Piñero-Feliciangeli L, Sepúlveda SA, Poblete F, Petley DN, Murphy W (2019) Landslides induced by the 2010 Chile megathrust earthquake: a comprehensive inventory and correlations with geological and seismic factors. *Landslides*, 16(6):1153-1165
- Serey A, Sepúlveda SA, Murphy W, Petley DN, De Pascale G (2020) Developing conceptual models for the recognition of coseismic landslides hazard for shallow crustal and megathrust earthquakes in different mountain environments – An example from the Chilean Andes <https://doi.org/10.1144/qjegh2020-023>

- SERNAGEOMIN (2003) Mapa Geológico de Chile a escala 1:1.000.000: versión digital. Servicio Nacional de Geología y Minería, Publicación Geológica Digital N°4
- Soeters R, Van Westen CJ (1996) Slope instability recognition, analysis and zonation. In: Turner AK and Schuster RL (eds). Landslides, investigation and mitigation. Transportation Research Board, National Research Council, special report 247, National Academy Press, Washington D.C., U.S.A., 129–177
- Somerville PG, Graves RW (2003) Characterization of earthquake strong ground motion. In *Landslide Tsunamis: Recent Findings and Research Directions*, Birkhäuser Basel, 1811-1828
- Somerville PG, Smith NF, Graves RW, Abrahamson N A (1997) Modification of empirical strong ground motion attenuation relations to include the amplitude and duration effects of rupture directivity. *Seismological Research Letters* 68:199-222
- Song Y, Gong J, Gao S, Wang D, Cui T, Li Y, Wei B (2012) Susceptibility assessment of earthquake-induced landslides using Bayesian network: A case study in Beichuan, China. *Computers & Geosciences*, 42:189-199
- Stahl T, Bilderback EL, Quigley MC, Nobes DC, Massey CI (2014) Coseismic landsliding during the Mw 7.1 Darfield (Canterbury) earthquake: Implications for paleoseismic studies of landslides. *Geomorphology*, 214:114-127
- Stevenson, JR (2017) Economic and social reconnaissance: Kaikōura earthquake 2016, Kaikōura earthquake special issue, *Bull. New Zeal. Soc. Earthq. Eng.* 50:343–351
- Stirling M, McVerry G, Gerstenberger M, Litchfield N, Van Dissen R, Berryman K, ... & Lamarche G (2012) National Seismic Hazard Model for New Zealand: 2010 update. *Bulletin of the Seismological Society of America*. 102(4):1514–1542
- Sudmeier-Rieux K, Qureshi RA, Peduzzi P, Jaboyedoff MJ, Breguet A, Dubois J, Jaubert R, Cheema MA (2007) An interdisciplinary approach to understanding landslides and risk management: a case study from earthquake-affected Kashmir. *Mountain Forum, Mountain GIS e-Conference*, January 14–25
- Tang C, Ma G, Chang M, Li W, Zhang D, Jia T (2015) Landslides triggered by the 20 April 2013 Lushan earthquake, Sichuan Province, China. *Eng Geol* 187:45–55
- Tang C, Van Westen CJ, Tanyas H, Jetten VG (2016) Analysing post-earthquake landslide activity using multi-temporal landslide inventories near the epicentral area of the 2008 Wenchuan earthquake. *Natural Hazards & Earth System Sciences*, 16(12)
- Tang C, Zhu J, Liang J (2009) Emergency assessment of seismic landslide susceptibility: a case study of the 2008 Wenchuan earthquake affected area. *Earthquake Engineering and Engineering Vibration*, 8(2):207-217
- Tanoli JJ, Ningsheng C, Regmi AD, Jun L (2017) Spatial distribution analysis and susceptibility mapping of landslides triggered before and after Mw7. 8 Gorkha earthquake along Upper Bhothe Koshi, Nepal. *Arabian Journal of Geosciences*, 10(13):277
- Tanyas H, Rossi M, Alvioli M, van Westen C J, Marchesini I (2019) A global slope unit-based method for the near real-time prediction of earthquake-induced landslides. *Geomorphology*, 327, 126-146
- Terzaghi K (1950) *Mechanisms of landslides, Application of Geology to Engineering Practice*. Berkey Volume S Geological Soc. of America
- Tichelaar BW, Ruff LJ (1991) Seismic coupling along the Chilean subduction zone, *J. Geophys. Res.* 98:2017–2038.

- Tolorza V, Mohr CH, Carretier S, Serey A, Sepúlveda SA, Tapia J, Pinto L (2019) Suspended sediments in Chilean rivers reveal low postseismic erosion after the Maule earthquake (Mw 8.8) during a severe drought. *Journal of Geophysical Research: Earth Surface*, 124(6):1378-1397
- Tong X, Sandwell D, Luttrell K, Brooks B, Bevis M, Shimada M, Foster J, Smalley R, Parra H, Baez JC, Blanco M, Kendrick E, Genrich J, Caccamise D (2010) The 2010 Maule, Chile earthquake: Downdip rupture limit revealed by space geodesy. *Geophysical Research Letters*, 37 (24): L24311
- United States Geological Survey (USGS) (2008) *The Landslide Handbook - A Guide to Understanding Landslides*. <https://pubs.usgs.gov/circ/1325>.
- Valagussa A, Frattini P, Crosta GB, Valbuzzi E, Gambini S (2017) Regional landslide susceptibility analysis following the 2015 Nepal Earthquake. In *Workshop on World Landslide Forum*, Springer, Cham, 1035-1042
- Van Daele M, Versteeg W, Pino M, Urrutia R, De Batist M (2013) Widespread deformation of basin-plain sediments in Aysén fjord (Chile) due to impact by earthquake-triggered, onshore-generated mass movements. *Marine Geology*, 337:67-79
- Vargas G, Klinger Y, Rockwell TK, Forman SL, Rebolledo S, Baize S, Lacassin R, Armijo R (2014) Probing large intraplate earthquakes at the west flank of the Andes, *Geology* 42(12): 1083-1086
- Vargas G, Rebolledo S, Sepúlveda SA, Lahsen A, Thiele R, Townley B, Padilla C, Rauld R, Herrera M, Lara M (2013) Submarine earthquake rupture, active faulting and volcanism along the major Liquiñe-Ofqui Fault Zone and implications for seismic hazard assessment in the Patagonian Andes. *Andean Geology* 40(1):141-171
- Varnes DJ (1958) Landslide types and processes. In: Eckel, E.B. (Ed.), *Special Report 29: Landslides and Engineering Practice*. Highways Research Board, National Academy of Sciences, Washington DC
- Varnes DJ (1978) Slope movement types and processes. In: Schuster, R.L., Krizek, R.J. (Eds.), *Special Report 176: Landslide: Analysis and Control*. Transportation Research Board, National Academy of Sciences, Washington DC.
- Verdugo R, González J, González V, Torres A (2012) Características y efectos del fenómeno de licuefacción. En *Mw=8.8: Terremoto en Chile, 27 de febrero 2010*. Primera edn., Departamento Ingeniería Civil FCFM Universidad de Chile
- Villalobos A, Vargas G, Maksymowicz A, Lastras G (2015) Evidencias paleosismológicas del origen cortical de la Crisis Sísmica del año 2007 en la región de Aysén. In *Congreso Geológico Chileno N°14*, 306-309
- Villalobos A, Vargas G, Maksymowicz A, Ruiz S, Lastras G, De Pascale GP, Agurto-Detzel H (2020) Active faulting, submarine surface rupture and seismic migration along the Liquiñe-Ofqui fault system, Patagonian Andes. *Journal of Geophysical Research: Solid Earth*, e2020JB019946.
- Vollmer M (2017) Simulación numérica de la avalancha de roca del 21 de abril de 2007 en Punta Cola, Región de Aysén, Chile. Undergraduate dissertation, Dept. of Geology, University of Chile (in Spanish). Available in <http://repositorio.uchile.cl/handle/2250/14705>
- Wang G (2015) Comparison of the landslides triggered by the 2013 Lushan earthquake with those triggered by the strong 2008 Wenchuan earthquake in areas with high seismic intensities. *Bulletin of Engineering Geology and the Environment* 74(1):77-89
- Wang G, Du C, Huang D, Jin F, Koo RC, Kwan JS (2018) Parametric models for 3D topographic amplification of ground motions considering subsurface soils. *Soil Dynamics and Earthquake Engineering*, 115:41-54

- Wang Y, Luo Y, Wang F, Wang D, Ma X, Li S, Deng X (2012) Slope seismic response monitoring on the aftershocks of the Wenchuan earthquake in the Mianzhu section. *Journal of Mountain Science*, 9(4):523-528
- Wartman J, Dunham L, Tiwari B, Pradel D (2013) Landslides in Eastern Honshu induced by the 2011 off the Pacific Coast of Tohoku earthquake. *Bulletin of the Seismological Society of America* 103 (2B):1503–1521
- Wasowski J, Keefer DK, Lee CT (2011) Toward the next generation of research on earthquake-induced landslides: current issues and future challenges. *Engineering Geology*, 122(1-2):1-8
- Wessel P, and Smith WHF (1998) New, improved version of the Generic Mapping Tools released. *Eos, Transactions American Geophysical Union*, 79(47): 579-579
- Wright C, Mella A (1963) Modifications to the soil pattern of South-Central Chile resulting from seismic and associated phenomena during the period May to August 1960. *Bulletin of the Seismological Society of America*, 53(6):1367-1402.
- Xu C (2015) Preparation of earthquake-triggered landslide inventory maps using remote sensing and GIS technologies: Principles and case studies. *Geoscience Frontiers*, 6(6):825-836
- Xu C, Dai FC, Chen J, Tu XB, Xu L, Li WC, Tian W, Cao YB, Yao X (2009b) Identification and analysis of secondary geological hazards triggered by a magnitude 8.0 Wenchuan earthquake. *Journal of Remote Sensing* 13(4):754e762
- Xu C, Dai F, Xu X, Lee YH (2012a). GIS-based support vector machine modeling of earthquake-triggered landslide susceptibility in the Jianjiang River watershed, China. *Geomorphology*, 145:70-80
- Xu C, Dai F, Yao X (2009a) Incidence number and affected area of Wenchuan earthquake-induced landslides. *Science & Technology Review*, 27(11):79e81
- Xu Q, Li WL (2010) Study on the direction effects of landslides triggered by Wenchuan earthquake. *Journal of Sichuan University (Engineering Science Edition)*, 42(1):7-14
- Xu C, Shen L, Wang G (2016) Soft computing in assessment of earthquake-triggered landslide susceptibility. *Environmental Earth Sciences*, 75(9):767
- Xu C, Xu X (2012) Comment on “Spatial distribution analysis of landslides triggered by 2008.5. 12 Wenchuan Earthquake, China” by Shengwen Qi, Qiang Xu, Hengxing Lan, Bing Zhang, Jianyou Liu [*Engineering Geology* 116 (2010) 95–108]. *Engineering Geology*, 133:40-42
- Xu C, Xu X, Dai F, Saraf AK (2012) Comparison of different models for susceptibility mapping of earthquake triggered landslides related with the 2008 Wenchuan earthquake in China. *Computers & Geosciences*, 46:317-329
- Xu C, Xu X, Yu G (2013) Landslides triggered by slipping-fault-generated earthquake on a plateau: an example of the 14 April 2010, Ms 7.1, Yushu, China earthquake. *Landslides*, 10(4):421-431
- Yalcin A, Reis S, Aydinoglu AC, Yomralioglu T (2011) A GIS-based comparative study of frequency ratio, analytical hierarchy process, bivariate statistics and logistics regression methods for landslide susceptibility mapping in Trabzon, NE Turkey. *Catena*, 85(3):274-287
- Yugsi-Molina F, Oppikofer T, Hermanns RL, Redfield T, Bascuñán I, Loew S, Sepúlveda SA (2012) Mechanism and volume estimation of the 2007 Punta Cola rockslide-debris avalanche using terrestrial laser scanning and aerial photogrammetry. In: Eberhardt, E., Froese, C., Turner, A.K., Leroueil, S.(eds.), *Landslides and Engineered Slopes: Protecting Society through Improved Understanding*. Taylor & Francis Group, London, 1:553-559

Zhang S, Zhang LM (2017) Impact of the 2008 Wenchuan earthquake in China on subsequent long-term debris flow activities in the epicentral area. *Geomorphology* 276, 86–103.

Zhang XM, Du GB, Liu J, Yang ZG, Zou LY, Wu XY (2018) An M6.9 earthquake at Mainling, Tibet on Nov.18, 2017. *Earth Planet Phys* 2(1):1–2

Zhao B, Li W, Wang Y, Lu J, Li X (2019) Landslides triggered by the Ms 6.9 Nyingchi earthquake, China (18 November 2017): analysis of the spatial distribution and occurrence factors. *Landslides*, 16(4):765-776

Landslides

DOI 10.1007/s10346-019-01150-6

Received: 13 August 2018

Accepted: 31 January 2019

© Springer-Verlag GmbH Germany
part of Springer Nature 2019

Alejandra Serey · Laura Piñero-Feliciangeli · Sergio A. Sepúlveda · Fernando Poblete · David N. Petley · William Murphy

Landslides induced by the 2010 Chile megathrust earthquake: a comprehensive inventory and correlations with geological and seismic factors

Abstract The 2010 $M_w = 8.8$ Maule earthquake, which occurred in the subduction contact between the Nazca and the South American tectonic plates off the coast of Chile, represents an important opportunity to improve understanding of the distribution and controls for the generation of landslides triggered by large megathrust earthquakes in subduction zones. This paper provides the analysis of the comprehensive landslide inventory for the Maule earthquake between 32.5° S and 38.5° S. In total, 1226 landslides were mapped over a total area of c. 120,500 km², dominantly disrupted slides. The total landslide volume is c. 10.6 Mm³. The events are unevenly distributed in the study area, the majority of landslides located in the Principal Andean Cordillera and a very constrained region near the coast on the Arauco Peninsula, forming landslide clusters. Statistical analysis of our database suggests that relief and lithology are the main geological factors controlling coseismic landslides, whilst the seismic factor with higher correlation with landslide occurrence is the ratio between peak horizontal and peak vertical ground accelerations. The results and comparison with other seismic events elsewhere suggest that the number of landslides generated by megathrust earthquakes is lower than events triggered by shallow crustal earthquakes by at least one or two orders of magnitude, which is very important to consider in future seismic landslide hazard analysis.

Keywords Coseismic landslides · Megathrust earthquake · Chile

Introduction

Landslides represent perhaps the most frequent geological hazard present in mountainous environments, due to the geological, geomorphological and geotechnical characteristics of steep upland landscapes. Most notably, in tectonically active mountain areas, landslides are a major cause of fatalities and economic losses during and after strong earthquakes (e.g. Sepúlveda et al. 2005; Jibson et al. 2006; Sato et al. 2007; Qi et al. 2010; Dai et al. 2011).

A key focus for research on seismically triggered landslides in high-mountain areas had been the development of approaches to create reliable estimates of the likely pattern of landslides in future earthquakes. This has usually undertaken through the development of statistical relations between specific earthquake events of different magnitudes and the number, area or volume of landslides triggered by each event (e.g. Keefer 1984; Rodriguez et al. 1999; Malamud et al. 2004a; Malamud et al. 2004b; Marc et al. 2016; Havenith et al. 2016). Recently Marc et al. (2016) compiled and analysed extensive databases of over 40 earthquakes ranging between $M_w = 5.1$ and $M_w = 8.6$, with a primary focus on shallow crustal earthquakes, allowing the presentation of a seismologically consistent expression for the total area and volume of populations of earthquake-triggered landslides. Similarly, Malamud et al.

(2004a), provided quantitative estimates of the total number of landslides (N_{LT}) expected for an earthquake of a given magnitude; for example this estimates that around 500,000 landslides would be generated for an event on the scale of the 2010 $M_w = 8.8$ Maule earthquake, which occurred in the subduction zone between the Nazca and the South American tectonic plates of the coast of Chile. However, in comparison with shallow crustal earthquakes, the number of complete landslide inventories for subduction zone earthquakes is small, meaning that there is huge uncertainty in such estimates. Prior to the study reported here, only one fully comprehensive, reliable inventory of coseismic landslides, based on field inventories and visual analysis of aerial or satellite images, has been available for subduction zone earthquakes. This is the inventory for the 2011 $M_w = 9.0$ Tohoku earthquake (Wartman et al. 2013). Therefore, there is a need to improve these datasets. The 2010 Maule earthquake, reported here, provides a key opportunity to understand better the distribution and controls for the generation of landslides triggered by large subduction zone earthquakes.

This paper builds on the pilot study of Serey et al. (2017) to provide a comprehensive inventory of landslides induced by the Maule earthquake, and to analyse their correlations with geological (slope, lithology) and seismic factors (rupture distance, PGA, PGV), thereby providing new insight into the factors controlling coseismic landslides in subduction zone earthquakes.

The 2010 $M_w = 8.8$ Maule earthquake

The 2010 $M_w = 8.8$ Maule earthquake, which occurred on 27 February 2010, is the sixth largest event in the United States Geological Survey (USGS) global catalogue and the second largest to have been recorded in Chile, just behind the 1960 Valdivia earthquake. It is the largest earthquake to have been recorded instrumentally in Chile. The rupture zone matches a seismic gap dating to 1835. Prior to the earthquake, several authors (Campos et al. 2002; Moreno et al. 2008; Ruegg et al. 2009) suggested that the area had a high probability of generating an earthquake in the near future, based on GPS data that showed an eastward terrain shift up to 4 cm a^{-1} (Cisternas 2011).

The earthquake rupture was located along the tectonic zone in which the Nazca plate is subducted beneath the South American plate, for which the convergence rate is c. 6.6 cm a^{-1} (Angermann et al. 1999). The hypocentre was located at the geographic coordinates 36.290° S, 73.239° W with a depth of 37 km according to the National Seismological Service of University of Chile (SSN). The rupture zone extended 450 km along the Chilean coast and 150 km from east to west. The speed and time of propagation is of the order of 2.5 to 3.5 km/s and 110 s respectively (Barrientos 2010).

Thirty-two accelerometers recorded the strong motion, with reliable peak values of 0.93 g (horizontal component) at Angol station and 0.70 g (vertical component) at Llolleo station (Boroschek et al. 2012; Fig. 1).

The rupture process of the Maule earthquake was characterised by the behaviour of asperities (Lay et al. 2010; Delouis et al. 2010; Tong et al. 2010; Lorito et al. 2011) (Fig. 1). An asperity with high levels of slip (the main asperity) was located in the northern part of the seismic gap, approximately in the same rupture area as the 1928 $M_w = 7.6$ Talca earthquake (Ruiz et al. 2012).

Geological and geomorphological setting of the coseismic landslides

The Andes represent the geodynamic archetype of a convergent, non-collisional mountain range, generated by subduction of the oceanic lithosphere of the Nazca (Farallon) Plate beneath the continental lithosphere of the South American Plate (Pardo-Casas and Molnar 1987). Consequently, the present-day architecture of the Andes Mountains is largely the result of convergence between the Pacific–Nazca and South American plates. These mountains are a consequence of crustal shortening, principally accommodated by eastward thrusting, which leads to crustal

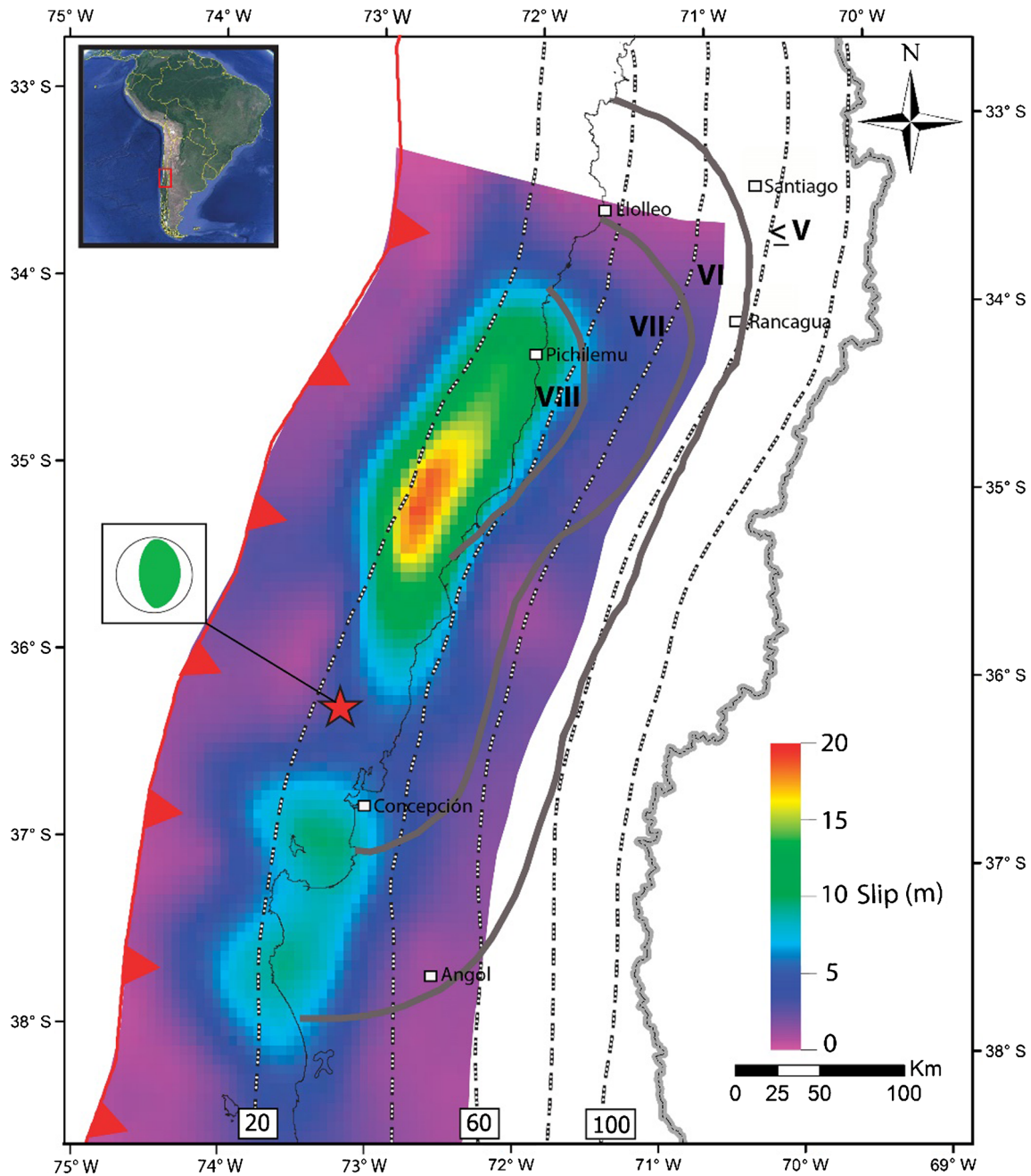


Fig. 1 Rupture zone, slip distribution (extracted from Lorito et al. 2011) and the isoseismal map (grey lines) inside the damage area of 2010 Maule earthquake (based upon data from Astroza et al. 2012). The red line with triangles is the trench between the Nazca and South America Plates (Bird 2003); Slab 1.0 plate interface contours from the USGS (grey dotted lines). The green and white focal mechanism is taken from the United States Geological Survey centroid moment tensor

thickening and surface uplift (Isacks 1988; Sheffels 1990; Allmendinger et al. 1997). Subduction is also evidenced by an almost continuous line of both active and dormant volcanoes, mostly andesitic stratovolcanoes, which run almost the entire length of the country. The Andes of Central Chile (32.5° S to 41.5° S) are composed of a number of morphostructural units from west to east: the Coastal Cordillera, the Central Valley, the Principal Cordillera (spanning Chile and Argentina), the Frontal Cordillera, the Argentine Precordillera and the Pampean Ranges (Jordan et al. 1983). For reference, Fig. 2 shows a simplified geologic map and the distribution of slope angle in the area of the Maule earthquake coseismic landslide inventory (elevation data for the slope angle map is coming from ASTER GDEM, product of METI and NASA, resolution 30 m). The Chilean Coastal Cordillera consists of low and topographically smooth mountains composed predominantly of Late Palaeozoic and Mesozoic igneous rocks, with paired belts of Palaeozoic metamorphic rocks cropping out south of Pichilemu (34° S). The Central Valley is a depression with a Mesozoic to Quaternary sedimentary infill (Charrier et al. 2015; Pankhurst and Hervé 2007); from Santiago to the south, this is the main agricultural zone and contains several major cities, including the capital. The Principal Cordillera is a chain of high mountains with a strong relief and

steep slopes that in its western part in Chilean territory mostly comprises Oligocene–Miocene continental volcanoclastic rocks, intruded by Miocene–Pliocene granitoids (Charrier et al. 2015; Pankhurst and Hervé 2007). The Frontal Cordillera is composed of units formed during the Gondwana orogeny in the Late Palaeozoic to Early Mesozoic. Older Palaeozoic rocks appear in the Pampean range.

The 2010 Mw = 8.8 Maule earthquake ground motion distribution

Interpolated maps of the peak horizontal and vertical acceleration components (PGA_H), (PGA_V) and normalised PGA_H/PGA_V values have been generated (Fig. 3), based on information available from 32 stations from the strong motion network of the National Seismological Centre, Universidad de Chile (see supplementary material (S1) for detailed information). The interpolation methodology used for all maps was based on an adjustable tension continuous curvature surface gridding algorithm, with the tension parameter set to 0.25. The implementation was done using Generic Mapping Tools (GMT).

In previous studies, co-seismic landslide initiation has in general been related to the peak horizontal ground acceleration parameter (PGA_H) (following Terzaghi 1950). For the Maule earthquake, the maximum horizontal acceleration recorded was

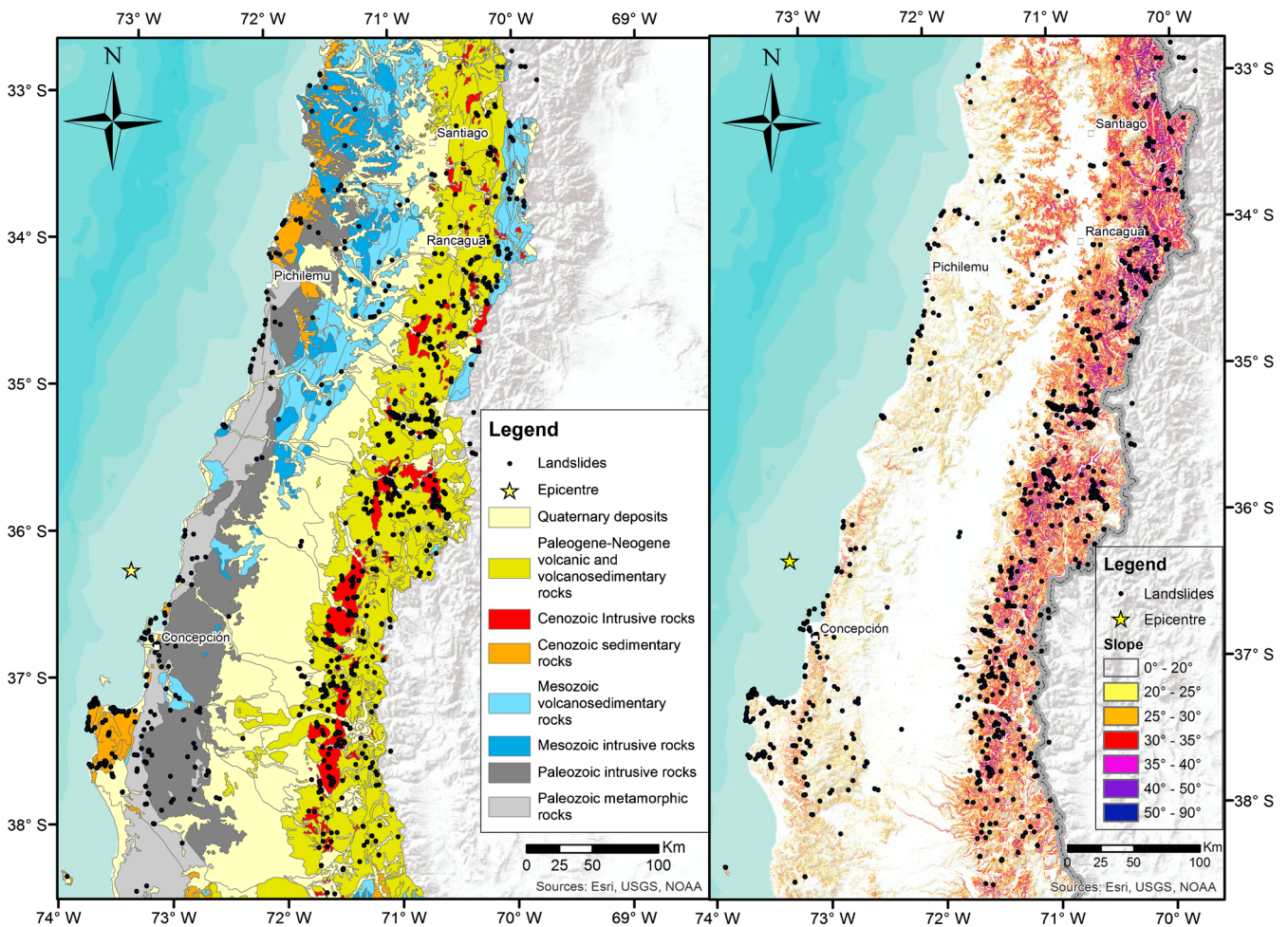


Fig. 2 Simplified geologic map (modified from SERNAGEOMIN 2003) and the distribution of slope angle in the area of 2010 coseismic landslide inventory

1.25 g at Cauquenes station, although the accelerometer saturated because the different components over-crossed (Saragoni and Ruiz 2012). Thus the PGAH value for Cauquenes has not been included in our analysis (Fig. 3a) because it is not considered to be a reliable measurement.

The distribution of PGAH values of the 2010 Mw = 8.8 Maule earthquake show a minimum measured ground shaking value of 0.02 g at Vallenar station (latitude -28.576) north of the study area, and a maximum reliable value at Angol station of 0.97 g. However, Angol may have been severely affected by site effects (Felipe Leyton, personal communication), which directly affects the interpolation result, indicating a zone of intense shaking centered at Angol. In general, the Tohoku 2011 earthquake generated higher values of PGAH (max. = 2.02 g) (Wartman et al. 2013) than the Maule earthquake.

In common with Saragoni and Ruiz (2012), our PGAH map shows attenuation towards the east, with peak PGAH values reducing from c. 1.0 g to c. 0.2 g for distances of 100 km from the rupture plane that defines the main asperity.

The PGAV distribution is shown in Fig. 3b (see supplementary data (S1) for detailed information). The recorded values for this parameter range between 0.008 and 0.700 g. Notably, the spatial distribution of PGAV does not resemble the PGAH map. From Fig. 3b, a peak value of 0.7 g at Lillole in the north of the rupture area, and a more extended area of high values (up to 0.55 g) recorded near the coast at Concepcion close to the southernmost asperity, dominate the pattern. PGAV values are typically c. 0.3 g at a distance of 100–120 km from the asperities.

In Fig. 3c, we show the ratio between PGAH and PGAV. An interesting pattern is observed for this parameter, giving smaller values near the coast, nearer to the asperity, and greater values are observed in further regions, up to 120–140 km from the asperities at the Principal Cordillera.

Landslides induced by the 2010 Maule megathrust earthquake

Landslide inventory and correlations with relief and geology

Serey et al. (2017) presented a pilot inventory of landslides generated by the Maule earthquake from the analysis of satellite images and bibliographic information for a part of the area affected by the earthquake, between 32.5° S and 38.5° S, with the Chile–Argentina border providing the eastern boundary of the mapped area. This paper expands the dataset to the Principal Cordillera (Argentine side) and the Frontal Cordillera, providing for the first time a complete landslide inventory for the Maule earthquake. This represents only the second full inventory of coseismic landslides for a subduction zone earthquake based on field inventories and visual analysis of aerial or satellite images.

For the bibliographic compilation, Serey et al. (2017) collected information about recorded landslide events triggered by the Maule earthquake. They reviewed 107 technical reports of the National Geological and Mining Survey of Chile (SERNAGEOMIN) related to the earthquake, from which the relevant information pertaining to landslides and lateral spreads was extracted. They also reviewed the georeferenced reports of road network interruption problems caused by the earthquake, undertaken by the Ministry of Public Works and

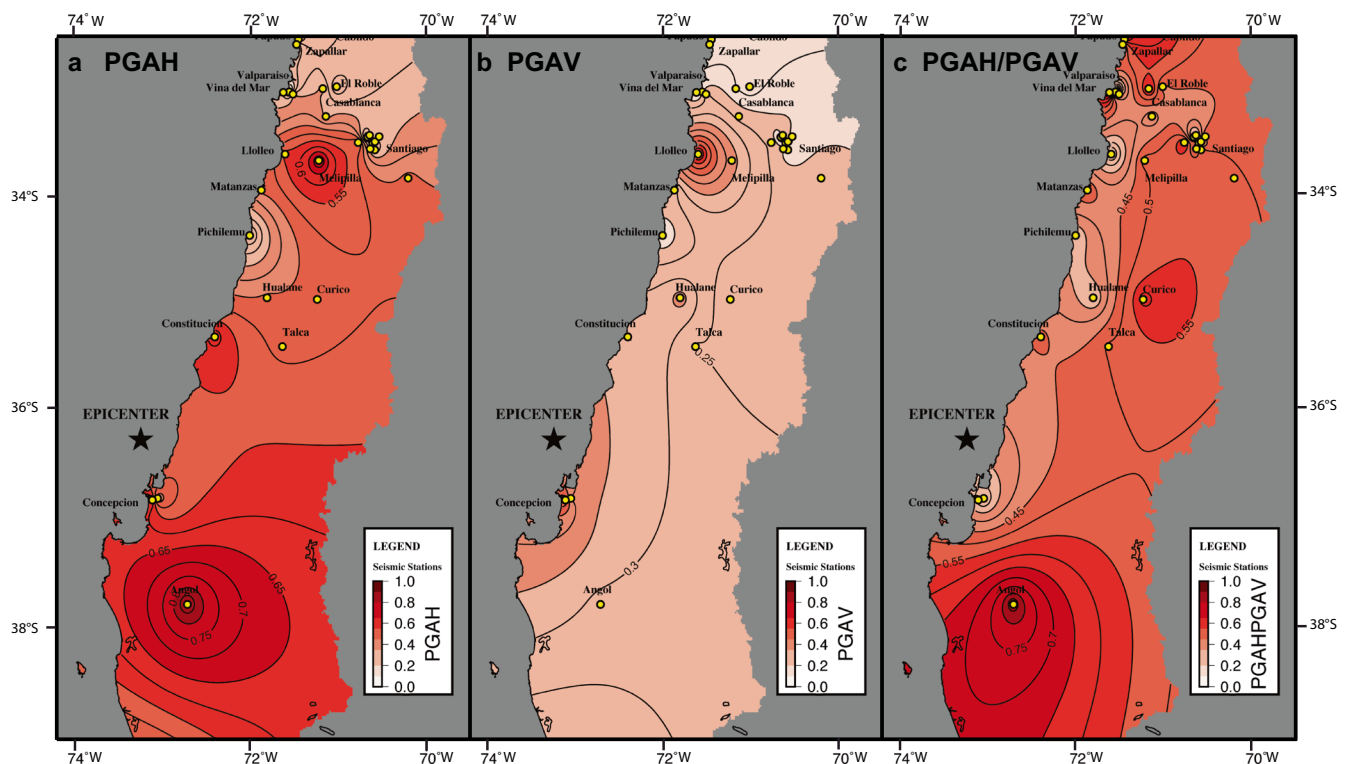


Fig. 3 Interpolated maps of the peak ground accelerations of a PGAH, b PGAV and c PGAH/PGAV ratio obtained from 32 stations from the Accelerograph Chilean Network from Universidad de Chile

incorporated an inventory of lateral spreads provided by *Verdugo et al. (2012)*, and the inventory of landslides in the coastal fringe of the Biobio administrative region provided by *Mardones and Rojas (2012)*.

The landslides were mapped by interpreting Landsat satellite images (Landsat 5-7-8; provider, NASA; resolution, 30 m; mostly temporal span, 2008–2013) before and after the earthquake using Google Earth. A visual inspection of these strips was done at an eye height of ~1–2 km, decreasing the height when an alteration was detected in the vegetation, or when bare spots or typical mass movement morphologies were present (*Soeters and Van Western 1996*). We visually inspected the earliest available images after the earthquake, mapping at 1:2000 and 1:10,000. Once a landslide was identified, the location was compared with the latest available pre-seismic image without cloud or snow cover and the landslide was mapped as polygon. Validation fieldwork was undertaken in the coastal regions, where the higher densities of landslides are located, in order to identify and classify landslides by failure mode. Field inspections allowed the addition of a number of small mass movements that were not identified in the satellite images. The minimum size considered for the mapping was 30 m², although field inspections showed that an indefinite number of small mass movements were not recognised on the satellite images. Thus in keeping with all such studies, our inventory is censored for very small landslides (i.e. those with a surface area of less than 30 m²).

In total, 1226 landslides were mapped (Fig. 4) over a total area of c. 120,500 km². The maximum distance to the epicentre is 487 km. The total landslide volume is c. 10.6 Mm³, estimated using published area–volume relationships proposed by *Larsen et al. (2010)* (Methodology is described in supplementary material S1). The inventory includes 1059 disrupted slides, 110 flows, 49 lateral spreads and eight coherent slides, following the *Keefer (1984)* classification for earthquake-induced landslides. Most of the landslides (over 850, mainly disrupted shallow slides and falls) are located in the farther Andes Principal Cordillera, which has a stronger relief and steeper slopes than the Coastal Cordillera, despite the lower earthquake intensities. A large number of landslides (387) are in the size range of 1000 to 5000 m², whilst just a few (29) have more than 50,000 m². Landslides located in the Central Valley are limited and are mainly lateral spreads caused by liquefaction.

The compiled dataset has been compared with the curves by *Keefer (1984)* and *Rodriguez et al. (1999)* regarding the maximum landslide area and the epicentral distance (*Serey et al. 2017*). It was observed that the geographical distribution is in agreement with the predictions defined for an earthquake of magnitude Mw = 8.8. However, the events are not evenly distributed in the study area, and *Serey et al. (2017)* highlighted the presence of landslide clusters. The most important cluster (127 failures) is located in the Arauco Peninsula, Biobio region, mainly triggered in low strength Neogene, marine sedimentary rocks. These rocks have been tested by *Moya (2016)*, showing differential stress-strain behaviour depending on the testing conditions and an increase in the shear strength under cyclic testing.

Figure 5a shows a 3D histogram of landslide counts normalised by geologic unit area based on the landslide classification, simplified geologic units and landslide types. Landslide occurrence is more frequent in Paleogene–Neogene volcanic and volcano sedimentary rocks, with a total of 42% of landslides. The Quaternary deposits and Cenozoic intrusive rocks represent 20% and 16%,

respectively. In total, these three geologic units cover 79% of the whole inventory. Disrupted landslides were the dominant type of landslides triggered by the 2010 Maule earthquake. Other types of landslides, coherent slides and flows and lateral spreads were minor, representing less than 2% of the total. The percentage of disrupted landslides generated in Paleogene–Neogene volcanic and volcano sedimentary rocks, which was the most dominant from the classified geologic units, covered c. 41%. The other two most important geological units that exhibit landslide occurrence were Quaternary deposits and Cenozoic intrusive rocks, adding up 36% of the total. In other words, the majority of the landslides triggered by the Maule earthquake occurred in the youngest geological units in the area. Furthermore, in one of the landslide clusters of the Maule inventory, in the Arauco Peninsula, landslides were mainly triggered in low strength Neogene, marine sedimentary rocks, suggesting an important lithologic control as a major factor in the generation of landslides (*Moya et al. 2015; Moya 2016*). These results coincide well with those obtained for coseismic landslides triggered by the 2011 Tohoku earthquake (Mw = 9.0, subduction earthquake), where majority of landslides occurred in the youngest (Neogene) geologic units of the region (*Wartman et al. 2013*). Thus, for both comprehensive megathrust coseismic landslide inventories lithology proves to be an extremely important factor.

In total, 55% of landslides occurred on slope angles between 20° and 40° (Fig. 5b), whilst 39% of landslides occurred on slopes of less than 20°. In contrast, less than 6.3% of slope failures occurred for angles greater than 40°. This predominance of coseismic landslides on slopes between 20° and 40° has been observed elsewhere, including the 2005 Mw = 7.6 Kashmir earthquake (*Sato et al. 2007; Kamp et al. 2008; Owen et al. 2008*) and the 2008 Mw = 8.3 Wenchuan earthquake (*Gorum et al. 2011*).

Spatial analysis of coseismic landslide distribution and ground motion

The spatial pattern of landslides was analysed calculating a map of landslide density or landslide concentration (LC). The calculation was done across a moving grid of size 0.5° × 0.5° through the 120,500 km² landslide-affected area. LC was defined as

$$LC = (\text{sum area of all landslides within the grid}) / (\text{total area of the grid}).$$

Python and GMT (Generic Mapping Tool) scripting were used for the implementation of the calculation.

In Fig. 6, the LC results from calculation is shown for: (a) all landslides, (b) coherent slides, (c) disrupted slides and (d) flows and lateral spreads triggered by the 2010 Mw = 8.8 Maule earthquake. The LC map for all landslides (Fig. 6a) shows that the events are very unevenly distributed in the study area, with the majority of landslides are located in the Principal Andean Cordillera (especially in the vicinity of Río Claro, Laguna El Maule, Rancagua) and a limited zone near the coast on the Arauco Peninsula, as noted previously.

Coherent slides provide less than 0.5% of the whole database and are well constrained in the Laguna El Maule cluster (Fig. 6b). The geologic units with maximum coherent landslide occurrence are the Quaternary deposits and Paleogene–Neogene volcanic and volcano-sedimentary rocks.

Disrupted landslides were concentrated in two main areas, corresponding to the Río Claro and Arauco clusters noted above (Fig. 6c). The Río Claro cluster, with an approximate

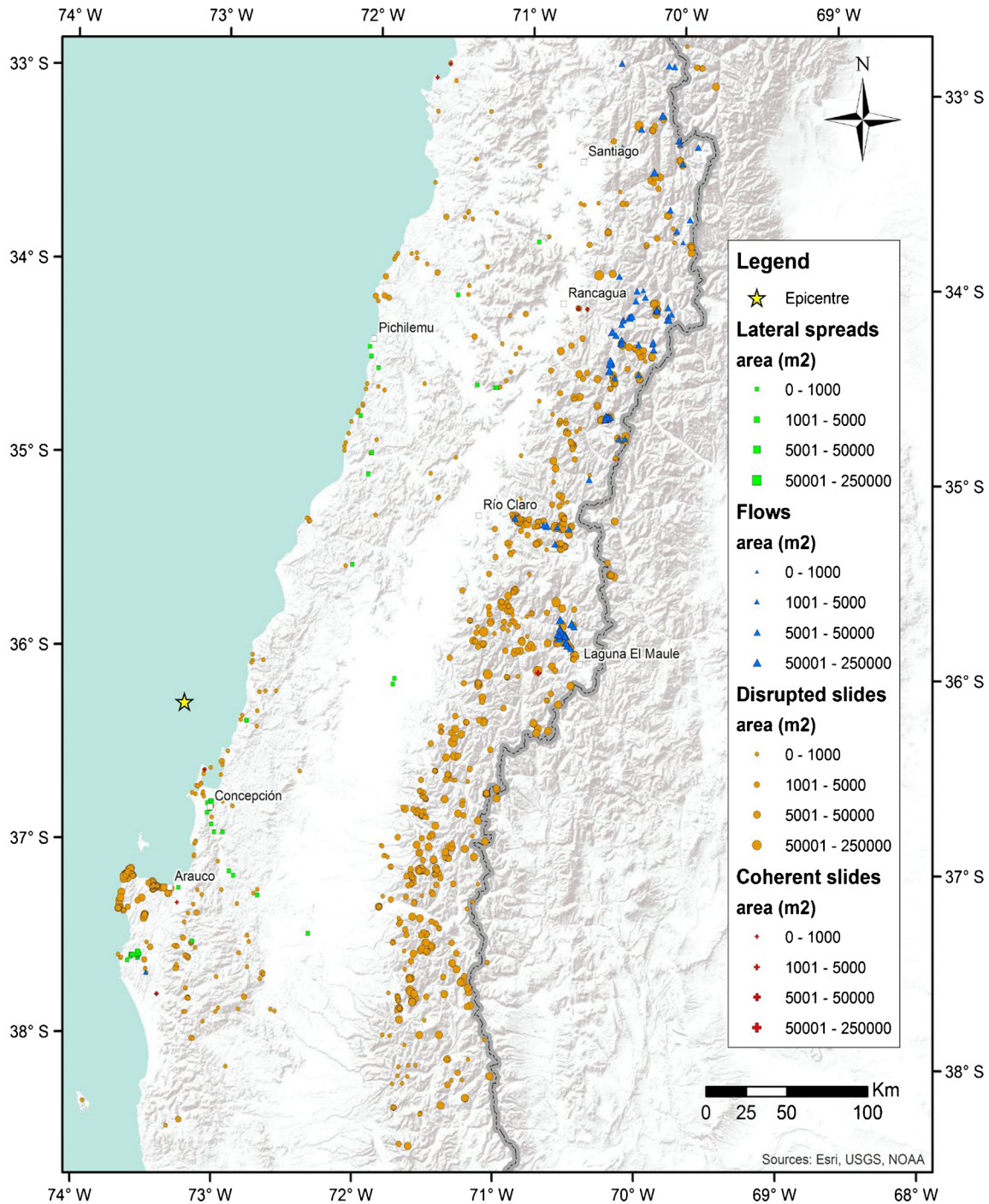


Fig. 4 The comprehensive landslide inventory for the 2010 Maule earthquake

area of 2500 km², lies in an area in which Paleogene–Neogene volcanic and volcanic sedimentary rocks, in which Cenozoic intrusive rocks crop out. The second disrupted slides cluster lies near the coast in the Arauco zone, with an area of c. 500 km², where Cenozoic sedimentary rocks are the main geologic unit cropping out in the area. The areas of high concentration for flows and lateral spreads, which represent less than 2% of the total, correspond to the Laguna El Maule and Rancagua clusters (Fig. 6d).

The spatial distribution of PGAH has two zones of higher shaking, with the largest being located at Angol in the south of our study area and the other in the area of Melipilla in the north, near Santiago. There is no evident correlation between the horizontal peak ground acceleration and the LC distributions for different landslide types (disrupted slide, coherent, flows and lateral spreads). It is noted that the PGAV the values attenuate from west to east from Concepcion (maximum value of 0.55 g) to smaller values in the east of the country. This

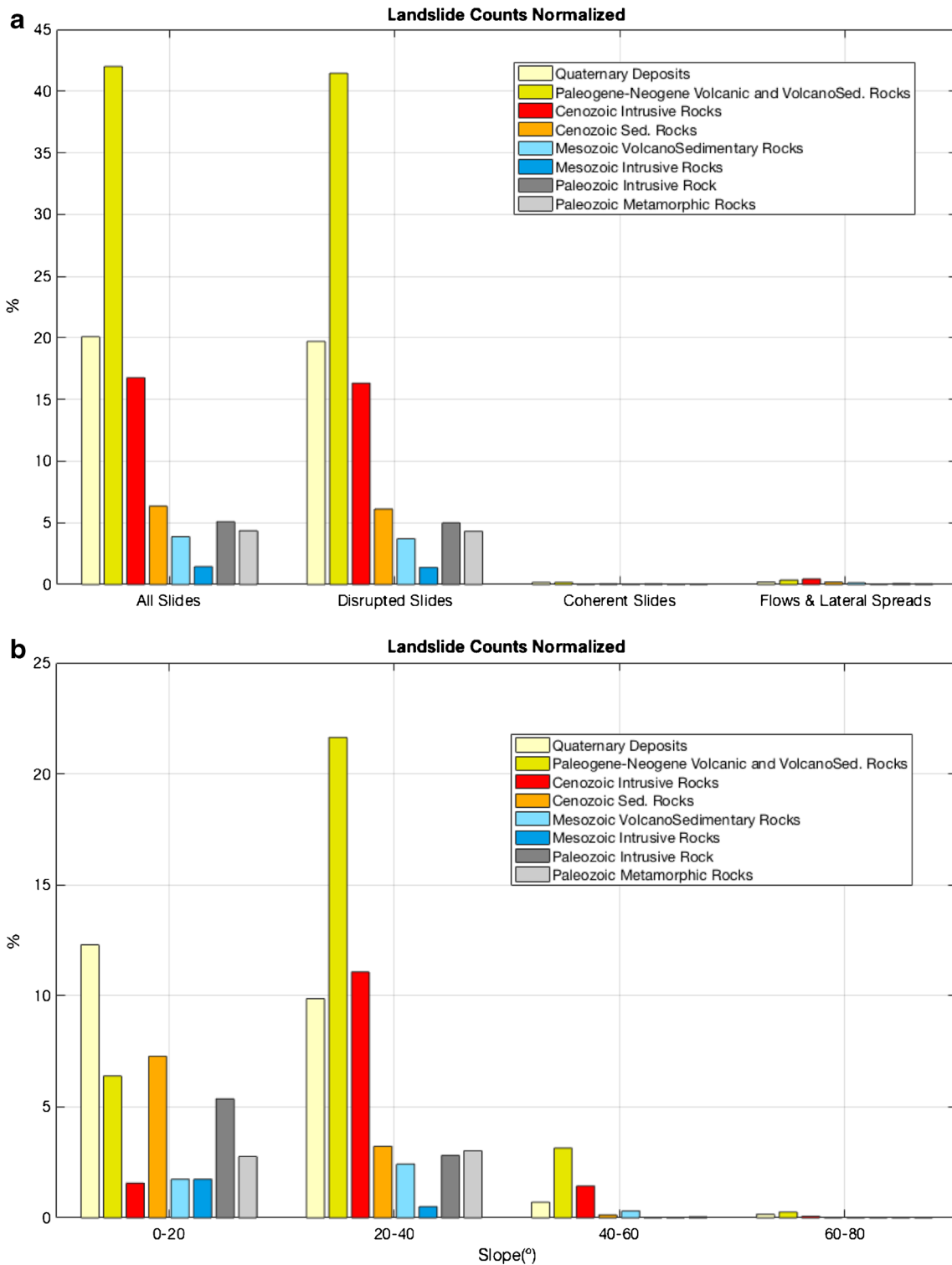


Fig. 5 **a** Histogram of landslide counts normalised by geologic unit based on landslide classification, simplified geologic units and landslide types. **b** Histogram shows landslide counts normalised by geologic units and disaggregated slope intervals of 20°

means that for the locations of high landslide concentration, the values for the vertical acceleration parameter are low, typically less than 0.3 g. In conclusion, our analysis suggest no evident correlation between the LC distribution and the regional PGA

distribution (for PGAH as for PGAV), which mirrors the conclusion of *Wartman et al. (2013)* for the 2011 Mw = 9.0 Tohoku earthquake. However, the correction with the ratio of PGAH to PGAV appears to be stronger. Scatter plots of LC against PGAH/

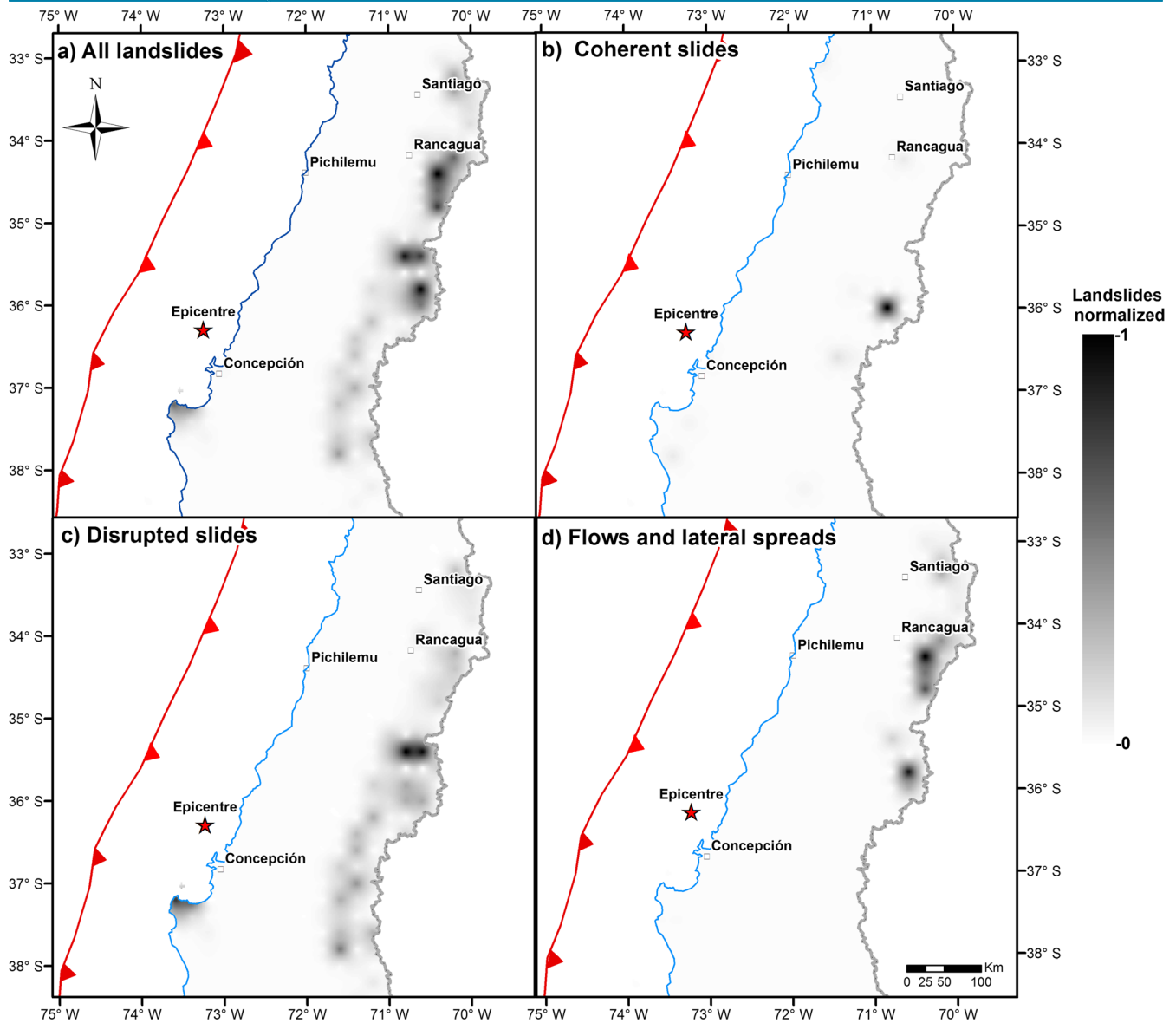


Fig. 6 Landslide concentrations (LC) normalised to the maximum concentration value. Areas in dark colours show landslide clusters described in the text. In blue coastline. The red line with triangles is the trench between the Nazca and South America Plates (Bird 2003). **a** LC of all landslides. **b** LC of coherent slides. **c** LC of disrupted slides. **d** LC of flows and lateral spreads

PGAV suggest that most of landslides are triggered for values that are bounded between PGAH/PGAV values of 0.45 and 0.60 (Fig. 7a). This area coincides exactly with the Principal Cordillera, corresponding to high mountains with a strong relief and steep slopes. The distribution is controlled by disrupted landslides (Fig. 7c). For the coherent slides, the PGAH/PGAV band is very narrow, approximately 0.5 and 0.52 (Fig. 7b). A secondary peak is observed in the range of 0.6 and 0.7. A much broader band for flows and lateral spreads is observed between 0.45 and 0.58 (Fig. 7d).

We also evaluated the potential correlation between LC parameter with distance by calculating the landslide smallest distance (linear distance) to the rupture plane, analogous to the analysis of Keefer (2000) for the 1989 Loma Prieta, California event (plotted in bins on numbers of landslides in Fig. 8 and as a

scattergraph of LC in Fig. 8b). The rupture plane grid points were obtained by joint inversion from Lorito et al. (2011), and the smallest distance was calculated using a Matlab script developed by Escobar (2013).

Overall, a substantial number of landslides occur near the source, at distances from 20 to 40 km. This pattern reduces at 40 to 70 km. At 80 km from the source, landslide occurrence drastically increases and then starts to reduce systematically. A likely interpretation to the result could be related to the fact that rupture plane (zone) is parallel to the mountain ranges. Basins with low relative relief (i.e. low landslide potential) located between the cordilleras typically lie at 40 to 60 km from the rupture plane. Therefore, landslide occurrence is not to be correlated directly to the distance to the rupture plane, but is mainly controlled by the surface relief.

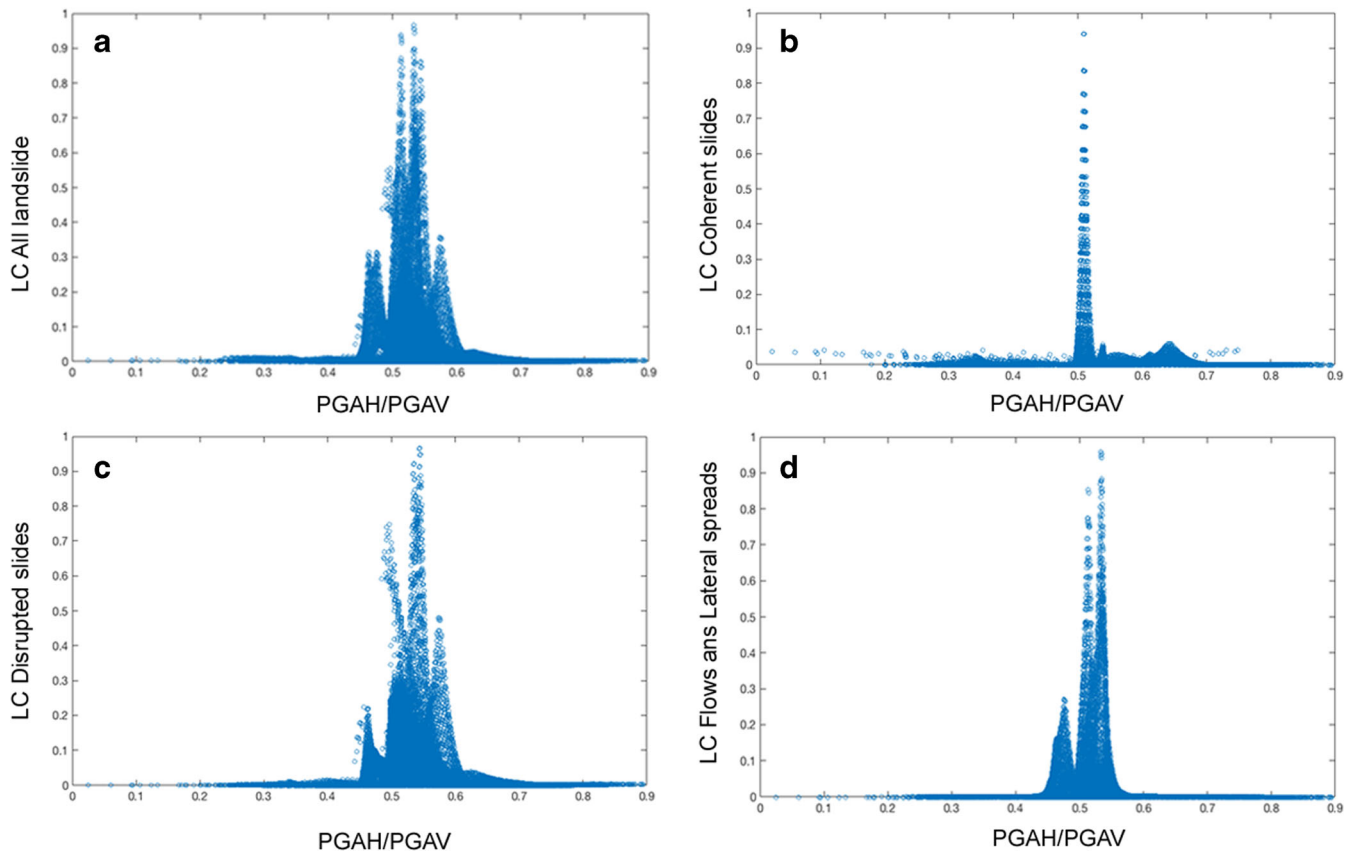


Fig. 7 Scatter plots of landslide concentration (LC), obtained from Fig. 6, vs PGAH/PGAV values obtained from map (Fig. 3). **a** Corresponds to all landslides; **b** disrupted landslide; **c** coherent landslides and **d** flows and lateral spreads

Discussion

In general, there is a strong coincidence between the results of this study and those from a study of the 2010 $M = 9.0$ Tohoku earthquake (Wartman et al. 2013), as follows:

- Given the width of the rupture zone generating this large magnitude earthquake, a substantial majority of landslides occurred in a zone underlain by the causative thrust.
- The spatial distribution of landslides is extremely heterogeneous, with clusters of landslides being observed.
- Disrupted landslides were the dominant type of landslides triggered by the Maule earthquake and associated aftershocks.
- A majority of landslides occurred in the youngest geologic units. The young rock materials are poorly cemented weak rocks and the degree of cementation of these poor quality rock masses is likely to be a controlling factor rather than the age.
- There is no clear correlation between ground motion (PGA) and landslide intensity. It should be recognised that PGA does not represent other potentially important characteristics such as frequency content, duration or the multiple phases of shaking recorded at some locations, whose influence on landslides should be studied in more depth.

Figure 9 shows the relationship between the total number of landslide (N_{LT}) and earthquake moment magnitude (M_w) for shallow crustal and megathrust earthquakes (Table 2 of supplementary data (S1)). It is notable that the total number of

landslides triggered for the megathrust earthquakes is substantially lower, typically by one to two orders of magnitude, than it would be expected for shallow crustal earthquakes. We suggest that there may be a fundamentally different landslide response to megathrust earthquakes in subduction plate contacts compared with shallow crustal events. The former tend to trigger a much smaller number of landslides compared to those generated by shallow crustal earthquakes.

Attenuation models predict PGA values, but not the specific waves that cause them (P, S or surface waves). Earthquakes that generate fault rupture at the surface are likely to produce greater amounts of surface waves, which typically is what causes damage. We can speculate that a megathrust earthquake suffers much higher surface wave attenuation than shallow crustal earthquakes, triggering a smaller amount of landslides.

It is difficult to draw definitive conclusions about this observation, given the limited number of megathrust events. However, we can speculate as to possible reasons for this effect. These might include the following:

1. In the case of the subduction zone earthquakes, the distance from the fault plane to the topography is much larger than is the case for many shallow crustal earthquakes. This may affect the key seismic parameters that control slope stability. Whilst it is conventionally considered that this parameter may be PGAH, this

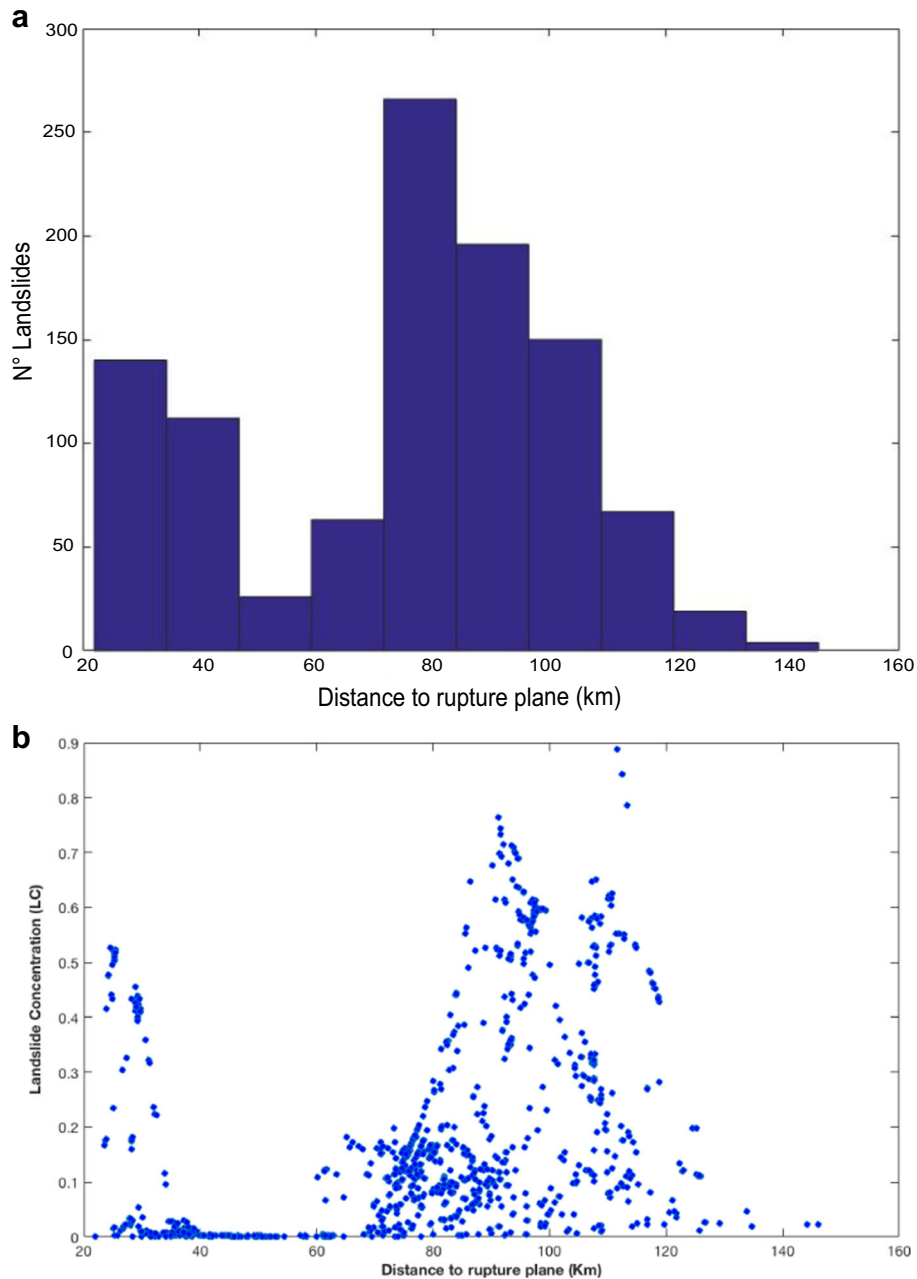


Fig. 8 a N° landslides vs distance to rupture plane. b LC vs distance to rupture plane

study and others fail to find a strong relationship between landslide occurrence and the regional distribution of PGAH. It is not known if this is because modelled values of PGAH are incorrect, or that this parameter is not the key control.

2. The type of faulting mechanism may affect the characteristics of the seismic waves, such as for example the frequency range. Whether faulting produces surface rupture may also change the characteristics of shaking.
3. The availability of topography susceptible to failure varies between the two settings, with shallow crustal earthquakes often being associated with areas of steep terrain and high relative relief close to the fault plane. Whilst megathrust

earthquake may also be associated with areas of steep terrain, these are typically at a much larger distance from the fault plane.

4. The susceptibility of the rocks may vary across the two tectonic settings. Thus, for example the lithologies close to the fault plane for shallow crustal earthquakes may be weaker, with higher densities of persistent discontinuities, allowing more landslides to be generated

In the case of the 2011 Mw = 9.0 Tohoku earthquake, the majority of the disrupted landslides appear to have originated at or near the crest of steep slope, suggesting that the topographic modification of ground

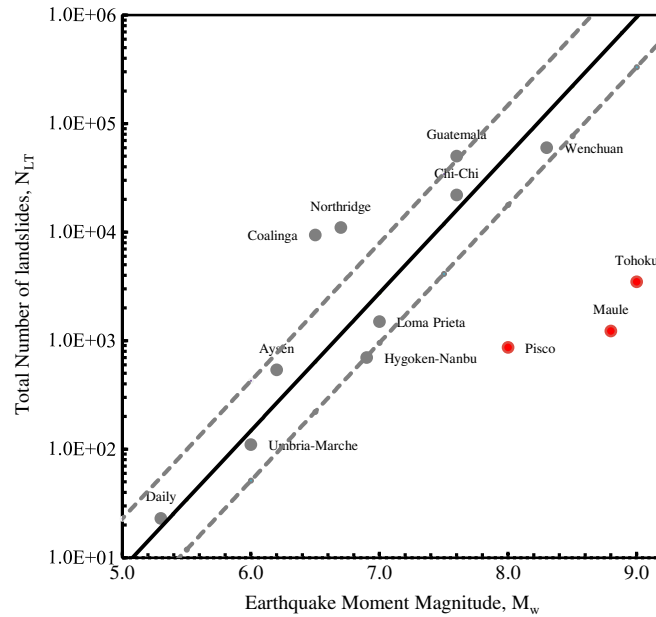


Fig. 9 Dependence of total number of landslide N_{LT} and earthquake moment magnitude M_w to shallow crustal (grey) and megathrust (red) earthquakes. Solid line is the correlation from the relationship proposed by *Malamud et al. (2004b)* with the grey dashed lines providing the corresponding error bounds. Data for the 13 earthquakes are given in Table 2 of supplementary material (S1)

motion played a role in their initiation (*Wartman et al. 2013*). Topographic amplification is a site effect caused by the interaction of the incoming seismic waves with certain geomorphological features, such

as steep slopes in areas of strong topographic relief, which results in larger amplitudes of the ground motion towards the ridge crests (e.g., *Densmore and Hovius 2000; Sepúlveda et al. 2005; Meunier et al. 2008*).

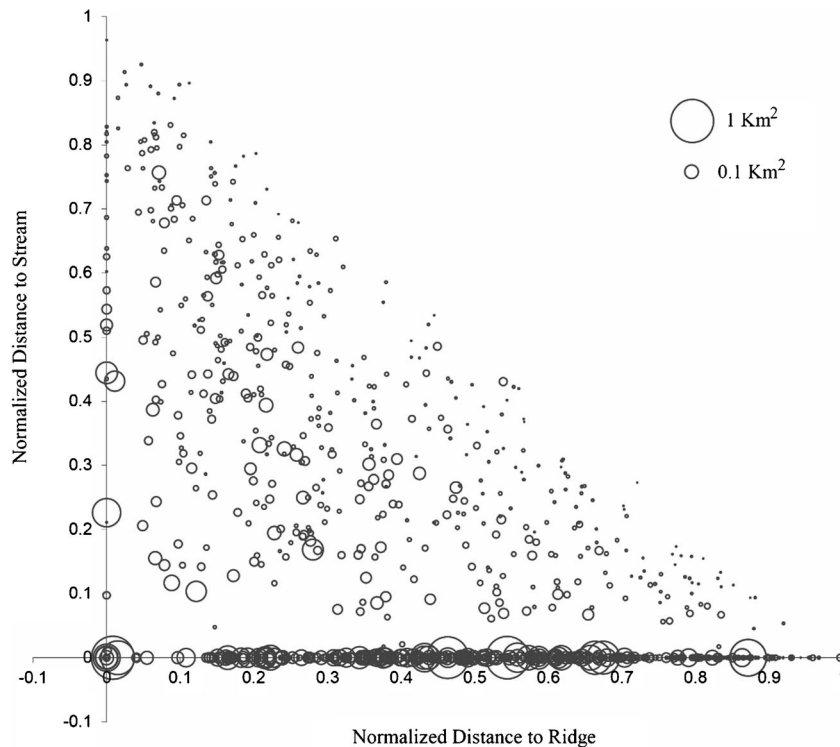


Fig. 10 Landslide relative position on the slopes. Normalised distance of the landslide crowns to ridge tops against normalised distance of landslide toes to nearest streams. The size (surface area) of the landslide is indicated with a circle of variable diameter

Meunier et al. (2008) proposed a graphic method to represent the position of landslides on the slopes, combining the normalised distance of the landslide top to the ridge crest and the normalised distance of the landslide toe to the nearest stream. This method is applied in Fig. 10. A concentration of circles close to the y -axis represents that coseismic landslides are strongly clustered near ridge crests, such as for shallow crustal earthquakes of Northridge (Meunier et al. 2008) and Aysén in southern Chile (Sepúlveda et al. 2010). In the last one, about two-thirds of the landslides start in the upper quarter of the slope, whilst over 90% start in the upper half, which suggests that larger ground motions due to topographic site effects influenced the triggering of landslides during the earthquake (Sepúlveda et al. 2010). Figure 10 shows that landslides induced by the Maule earthquake are not clustered close to the ridge tops, so we could disregard a predominant topographic site effect in their generation, although it may have played a role locally.

It is difficult to establish a direct correlation between observed PGA values and does PGAs obtained from ground motion prediction equations. In this context, GMPE for Chilean subduction zone (Idini et al. 2017) estimate a decrease from c. 0.2 to 0.15 g (in a normalised logarithmic scale) up to a rupture distance c. 200 km. These results correlate well with our PGAV map (Fig. 5b) but not with PGAH values (Fig. 5a) that could be caused by other effects (e.g. site effect, Angol station).

We observe that the key seismic parameter that appears to explain the distribution of landslides best is the ration between PGAH and PGAV. It is not clear as to why this might be the case, but Brain et al. (2014) suggested that wave phasing, and the associated coincidence of horizontal and vertical accelerations, may play a key role in determining slope response. The role of slip surface normal accelerations in the initiation of landslides is seen as significant by Huang et al. (2001) and the complexity generated by rapidly fluctuating normal and shearing stresses during shaking deserves much further investigation.

Conclusions

We have compiled and analysed an inventory of landslides triggered by the 2010 $M = 8.8$ Maule earthquake in the Chilean subduction zone. We find that the number and density of landslides triggered by the earthquake is lower than might have been expected for a seismic event of this scale (by one to two orders of magnitude) than for a shallow crustal earthquake of a similar or even lower magnitude, in common with observations for the 2011 $M_w = 9.0$ Tohoku earthquake in Japan. Landslides occurred primarily on low to moderate angled slopes towards the western side of the main Andean range, accompanied by clusters of landslides in the lower Coastal Range. For the 2010 Maule earthquake, we suggest that relief exerted a strongly dominant control on coseismic landsliding, with lithology the second most relevant conditioning factor, with more landslides in younger rocks. We find a poor correlation between PGA and landslide occurrence, and with distance from the fault plane, but note a much stronger correlation between landslide concentration and the ratio between horizontal and vertical peak accelerations.

These results suggest that the number and distribution of coseismic landslides may differ significantly between megathrust and shallow crustal earthquakes; although further research through the collation of high quality inventories is required as further megathrust earthquakes occur. At present, the paucity of inventories for megathrust earthquakes defies the proposal of a

definitive explanation for this observation. However, it may prove to be important in terms of the relative distribution of hazards associated with earthquakes in areas affected by megathrust earthquakes. Chile has a high concentration of large magnitude rock avalanches in the Andes; these results may suggest that they may be associated with proximal, lower magnitude shallow crustal earthquakes rather than larger but distal megathrust events.

Acknowledgments

We thank valuable comments by D.R. Tippin and two anonymous reviewers that allowed improvement of the manuscript. Mapping work collaboration and support by S. Moya, J. Tondreau, C. Apablaza, M. Froude and M. Brain are greatly acknowledged. Figures 3 and 6 were prepared with the Generic Mapping Tools (Wessel and Smith 1998).

Funding information This work is supported by the RCUK-Conicyt Newton Fund International Cooperation Programme Project NE/N000315/1 “Seismically-induced landslides in Chile: New tools for hazard assessment and disaster prevention” and Fondecyt project 1140317.

References

- Allmendinger RW, Jordan TE, Kay SM, Isacks BL (1997) The evolution of the Altiplano-Puna plateau of the Central Andes. *Annu Rev Earth Planet Sci* 25(1):139–174
- Angermann D, Klotz J, Reigber C (1999) Space-geodetic estimation of the Nazca-South America Euler vector. *Earth Planet Sci Lett* 171:329–334
- Astroza M, Ruiz S, Astroza R (2012) Damage assessment and seismic intensity analysis of the 2010 (M_w 8.8) Maule earthquake. *Earthquake Spectra* 28(S1):S145–S164
- Barrientos SE (2010) Terremoto ($M = 8.8$) del 27 de febrero de 2010 en Chile. *Rev Asoc Geol Argent* 67(3):412–420
- Bird P (2003) An updated digital model of plate boundaries. *Geochem Geophys Geosyst* 4(1):1027
- Boroschek R, Contreras V, Kwak DY, Stewart JP (2012) Strong ground motion attributes of the 2010 M_w 8.8 Maule, Chile, earthquake. *Earthquake Spectra* 28(S1):S19–S38
- Brain MJ, Rosser NJ, Norman EC, Petley DN (2014) Are microseismic ground displacements a significant geomorphic agent? *Geomorphology* 207:161–173
- Campos J, Hatzfeld D, Madariaga R, Lopez G, Kausel E, Zollo A, Barrientos S, Lyon-Caen H (2002) The 1835 seismic gap in South Central Chile. *Phys Earth Planet Inter* 132:177–195
- Charrier R, Ramos VA, Tapia F, Sagripanti L (2015) Tectono-stratigraphic evolution of the Andean Orogen between 31 and 37° S (Chile and Western Argentina). *Geological Society Special Publications*, London, pp 13–61
- Cisternas A (2011) El país más sísmico del mundo. *Revista Anales Séptima Serie*
- Dai FC, Xu C, Yao X, Xu L, Tu XB, Gong QM (2011) Spatial distribution of landslides triggered by the 2008 M_s 8.0 Wenchuan earthquake. *China J Asian Earth Sci* 40(4):883–895
- Delouis B, Nocquet JM, Vallée M (2010) Slip distribution of the February 27, 2010 $M_w = 8.8$ Maule earthquake, central Chile, from static and high-rate GPS, InSAR, and Broadband teleseismic data. *Geophys Res Lett* 37(17):L17305. <https://doi.org/10.1029/2010GL043899>
- Densmore A, Hovius N (2000) Topographic fingerprints of bedrock landslides. *Geology* 28(4):371–374
- Escobar P (2013) Inventario de remociones en masa desencadenadas por el sismo del 27 de febrero de 2010 en Chile central. Universidad de Chile, Departamento de Geología, Memoria de título
- Gorum T, Fan X, van Westen CJ, Huang RQ, Xu Q, Tang C, Wang G (2011) Distribution pattern of earthquake-induced landslides triggered by the 12 May 2008 Wenchuan earthquake. *Geomorphology* 133:152–167. <https://doi.org/10.1016/j.geomorph.2010.12.030>
- Havenith HB, Torgoev A, Braun A, Schlögel R, Micu M (2016) A new classification of earthquake-induced landslide event sizes based on seismotectonic, topographic, climatic and geologic factors. *Geoenvironmental Disasters* 3(1):6
- Huang CC, Lee YH, Liu HP, Keefer DK, Jibson RW (2001) Influence of surface-normal ground acceleration on the initiation of the Jih-Feng-Erh-Shan landslide during the 1999 Chi-Chi, Taiwan, earthquake. *Bull Seismol Soc Am* 91(5):953–958

- Idini B, Rojas F, Ruiz S, Pastén C (2017) Ground motion prediction equations for the Chilean subduction zone. *Bull Earthq Eng* 15(5):1853–1880
- Isacks BL (1988) Uplift of the central Andean plateau and bending of the Bolivian orocline. *J Geophys Res Solid Earth* 93(B4):3211–3231
- Jibson RW, Harp EL, Schulz W, Keefer DF (2006) Large rock avalanches triggered by the M 7.9 Denali fault, Alaska, earthquake of 3 November 2002. *Eng Geol* 83:144–160
- Jordan TE, Isacks B, Allmendinger R, Brewer J, Ramos V, Ando C (1983) Andean tectonics related to geometry of the subducted Nazca plate. *Geol Soc Am Bull* 94:341–361
- Kamp U, Growley BJ, Khattak GA, Owen LA (2008) GIS-based landslide susceptibility mapping for the 2005 Kashmir earthquake region. *Geomorphology* 101(4):631–642
- Keefer DK (1984) Landslides caused by earthquakes. *Geol Soc Am Bull* 95:406–421
- Keefer DK (2000) Statistical analysis of an earthquake-induced landslide distribution—the 1989 Loma Prieta, California event. *Eng Geol* 58(3):231–249
- Larsen IJ, Montgomery DR, Korup O (2010) Landslide erosion controlled by hillslope material. *Nat Geosci* 3(4):247–251
- Lay T, Ammon CJ, Kanamori H, Koper KD, Sufri O, Hutko AR (2010) Teleseismic inversion for rupture process of the 27 February 2010 Chile (Mw 8.8) earthquake. *Geophys Res Lett* 37(13):L13301. <https://doi.org/10.1029/2010GL043379>
- Lorito S, Romano F, Atzori F, Tong X, Avallone A, McCloskey J, Cocco M, Boshi E, Piatanesi A (2011) Limited overlap between the seismic gap and co-seismic slip of the great 2010 Chilean earthquake. *Nature Geoscience Letters* 4(3):173–177
- Malamud BD, Turcotte DL, Guzzetti F, Reichenbach P (2004a) Landslide inventories and their statistical properties. *Earth Surf Process Landf* 29(6):687–711
- Malamud BD, Turcotte DL, Guzzetti F, Reichenbach P (2004b) Landslides, earthquakes, and erosion. *Earth Planet Sci Lett* 229(1–2):45–59
- Marc O, Hovius N, Meunier P, Gorum T, Uchida T (2016) A seismologically consistent expression for the total area and volume of earthquake-triggered landsliding. *J Geophys Res Earth Surf* 121(4):640–663
- Mardones M, Rojas J (2012) Procesos de remoción en masa inducidos por el terremoto del 27F de 2010 en la franja costera de la Región del Biobío, Chile. *Revista de Geografía Norte Grande* 53:57–74
- Meunier P, Hovius N, Haines JA (2008) Topographic site effects and the location of earthquake induced landslides. *Earth Planet Sci Lett* 275:221–232
- Moreno M, Klotz J, Melnick D, Echter H, Bataille K (2008) Active faulting and heterogeneous deformation across a megathrust segment boundary from GPS data, south central Chile (36–39 S). *Geochem Geophys Geosyst* 12:Q12024
- Moya S (2016) Comportamiento monótono y cíclico de suelos y rocas blandas afectadas por remociones en masa cosísmicas. Universidad de Chile, Departamento de Geología
- Moya S, Sepúlveda SA, Serey A, García M (2015) Remociones en masa generadas por el terremoto del Maule del 2010 en la Península de Arauco. In XIV Congreso Geológico de Chile Actas, La Serena
- Owen LA, Kamp U, Khattak GA, Harp EL, Keefer DK, Bauer MA (2008) Landslides triggered by the 8 October 2005 Kashmir earthquake. *Geomorphology* 94(1):1–9
- Pankhurst R, Hervé F (2007) Introduction and overview. *The Geological Society of London*, pp 1–4
- Pardo-Casas F, Molnar P (1987) Relative motion of the Nazca (Farallon) and South American plates since Late Cretaceous time. *Tectonics* 6(3):233–248
- Qi S, Xu Q, Lan H, Zhang B, Liu J (2010) Spatial distribution analysis of landslides triggered by 2008.5.12 Wenchuan earthquake. *China Engineering Geology* 116(1–2):95–108
- Rodriguez CE, Bommer JJ, Chandler RJ (1999) Earthquake-induced landslides: 1980–1997. *Soil Dyn Earthq Eng* 18:325–346
- Ruegg JC, Rudloff A, Vigny C, Madariaga R, De Chaballier JB, Campos J, Kausel E, Barrientos S, Dimitrov D (2009) Interseismic strain accumulation measured by GPS in the seismic gap between Constitución and Concepción in Chile. *Phys Earth Planet Inter* 175:78–85
- Ruiz S, Madariaga R, Astroza M, Saragoni R, Lancieri M, Vigny C, Campose J (2012) Short-period rupture process of the 2010 Mw 8.8 Maule earthquake in Chile. *Earthquake Spectra* 28(S1):S1–S18
- Saragoni R, y Ruiz S (2012) Implicancias y nuevos desafíos del diseño sísmico de los acelerógramas del Terremoto del 2010, en Mw=8.8: Terremoto en Chile, 27 de febrero 2010. Primera edn, Departamento Ingeniería Civil FCFM Universidad de Chile, pp 127–146
- Sato H, Hasegawa H, Fujiwara S, Tobita M, Koarai M, Une H, Iwahashi J (2007) Interpretation of landslide distribution triggered by the 2005 Northern Pakistan earthquake using SPOT 5 imagery. *Landslides* 4:113–122
- Sepúlveda SA, Murphy W, Petley DN (2005) Topographic controls on coseismic rock slides during the 1999 Chi-Chi Earthquake, Taiwan. *Q J Eng Geol Hydrogeol* 38:189–196
- Sepúlveda SA, Serey A, Lara M, Pavez A, Rebolledo S (2010) Landslides induced by the 2007 Aysen Fjord earthquake, Chilean Patagonia. *Landslides* 7(4):483–492
- Serey A, Escobar P, Moya S, Sepúlveda SA, Petley D (2017) Landslide inventory of the 2010 Mw 8.8 Maule earthquake, Central Chile. 16th world conference on earthquake 16WCEE 2017: 1873
- SERNAGEOMIN (2003) Mapa Geológico de Chile a escala 1:1.000.000: versión digital. Servicio Nacional de Geología y Minería, Publicación Geológica Digital N°4
- Sheffels BM (1990) Lower bound on the amount of crustal shortening, in the central Bolivian Andes. *Geology* 18(9):812–815
- Soeters R, Van Western CJ (1996) Slope instability recognition, analysis and zonation. In: Turner AK and Schuster RL (eds). *Landslides, investigation and mitigation*. Transportation Research Board, National Research Council, special report 247, National Academy Press, Washington D.C., U.S.A., 129–177
- Terzaghi K (1950) Mechanisms of landslides, application of geology to engineering practice. *Berkey Volume S Geological Soc. of America*
- Tong X, Sandwell D, Luttrell K, Brooks B, Bevis M, Shimada M, Foster J, Smalley R, Parra H, Baez JC, Blanco M, Kendrick E, Genrich J, Caccamise D (2010) The 2010 Maule, Chile earthquake: Downdip rupture limit revealed by space geodesy. *Geophys Res Lett* 37(24):L24311
- Verdugo R, González J, González V, Torres A (2012) Características y efectos del fenómeno de licuefacción. En Mw=8.8: Terremoto en Chile, 27 de febrero 2010. Primera edn., Departamento Ingeniería Civil FCFM Universidad de Chile
- Wartman J, Dunham L, Tiwari B, Pradel D (2013) Landslides in Eastern Honshu induced by the 2011 off the Pacific Coast of Tohoku earthquake. *Bull Seismol Soc Am* 103(2B):1503–1521
- Wessel P, Smith WHF (1998) New, improved version of the generic mapping tools released. *EOS Trans Am Geophys Union* 79(47):579–579

Electronic supplementary material The online version of this article (<https://doi.org/10.1007/s10346-019-01150-6>) contains supplementary material, which is available to authorized users.

A. Serey (✉) · **S. A. Sepúlveda**

Departamento de Geología,
Universidad de Chile,
Santiago, Chile
Email: alejandra.serey@gmail.com

L. Piñero-Feliciangeli · **S. A. Sepúlveda** · **F. Poblete**

Instituto de Ciencias de la Ingeniería,
Universidad de O'Higgins,
Rancagua, Chile

D. N. Petley

Department of Geography,
University of Sheffield,
Sheffield, England

W. Murphy

School of Earth and Environment,
University of Leeds,
Leeds, England



Developing conceptual models for the recognition of coseismic landslides hazard for shallow crustal and megathrust earthquakes in different mountain environments – an example from the Chilean Andes

Alejandra Serey^{1,2*}, Sergio A. Sepúlveda^{1,2}, William Murphy³, David N. Petley⁴ and Gregory De Pascale¹

¹ Departamento de Geología, Universidad de Chile, Santiago 8370450, Chile

² Instituto de Ciencias de la Ingeniería, Universidad de O'Higgins, Chile

³ School of Earth and Environment, University of Leeds, UK

⁴ Department of Geography, University of Sheffield, UK

AS, 0000-0001-8746-7989; SAS, 0000-0001-6943-362X; WM, 0000-0002-7392-1527; DNP, 0000-0002-3061-6282

* Correspondence: alejandra.serey@gmail.com

Abstract: Landslides represent the most frequent geological hazard in mountainous environments. Most notably, landslides are a major source of fatalities and damage related to strong earthquakes. The main aim of this research is to show through three-dimensional engineer-friendly computer drawings, different mountain environments where coseismic landslides could be generated during shallow crustal and megathrust earthquakes in the Andes of central Chile. We have determined topographic, geomorphological, geological and seismic controlling factors in the occurrence of earthquake-triggered landslides from: (1) a comparison of local earthquake-induced landslide inventories in Chile (the M_w 6.2, shallow crustal Aysén earthquake in 2007 (45.3° S) and the M_w 8.8, megathrust Maule earthquake in 2010 (32.5°S–38.5°S)) with others from abroad; and (2) analysis of large, prehistoric landslide inventories proposed as likely induced by seismic activity. With these results, we have built four representative geomodels of coseismic landslide geomorphological environments in the Andes of central Chile. Each one represents the possible landslide types that could be generated by a shallow crustal earthquake v. those likely to be generated by a megathrust earthquake. Additionally, the associated hazards and suggested mitigation measures are expressed in each scenario. These geomodels are a powerful tool for earthquake-induced landslide hazard assessment.

Thematic collection: This article is part of the Ground models in engineering geology and hydrogeology collection available at: <https://www.lyellcollection.org/cc/Ground-models-in-engineering-geology-and-hydrogeology>

Received 30 January 2020; revised 13 May 2020; accepted 21 May 2020

Landslides represent perhaps the most frequent geological hazard in mountainous environments due to the geological, geomorphological and geotechnical characteristics of steep upland landscapes. In tectonically active mountain areas, landslides are a major cause of fatalities and economic losses during and after strong earthquakes (e.g. Sepúlveda *et al.* 2005; Qi *et al.* 2010; Dai *et al.* 2011).

Coseismic landslide hazard, defined as the relative probability of landslide occurrence at a specific location in a specific event, is a function of intrinsic slope characteristics (slope angle, material strength, lithology, etc.) and earthquake shaking, which acts as a significant trigger mechanism for causing landslides of all types (Keefer 1984). In addition to those factors influencing landsliding under ambient conditions, site conditions further influence ground motions through soil and topographic amplification (Sepúlveda *et al.* 2005; Meunier *et al.* 2008; Wang *et al.* 2018). Recent studies (e.g. Wartman *et al.* 2013; Marc *et al.* 2016) suggest that they are also influenced by the seismogenic zone. Serey *et al.* (2019) observed that shallow crustal and megathrust earthquakes create fundamentally different spatial patterns and densities of landslides.

Selecting seismological inputs for slope stability analysis is challenging given the large number of variables associated with coseismic landslides that are difficult to quantify; these include seismic wave frequency, wave amplitude and wave interactions. This is especially complex for regional hazard assessments (Geli *et al.* 1988; Meunier *et al.* 2008). Several statistical methods exist

for modelling regional-scale coseismic landslide hazard (e.g. Jibson *et al.* 2000; Miles and Keefer 2000, 2007, 2009; Lee *et al.* 2008), all of them considering only one kind of coseismic trigger, i.e. shallow crustal earthquakes. Thus, a first-order form of hazard identification can prove beneficial prior to considering more complex analytical tools and different kinds of coseismic triggers. One such approach is to visualize all these variables, both conditioning and triggering factors, in the form of graphic 3D ground models, often referred to as geomodels. Such tools are also valuable in explaining complex geotechnical problems to non-specialists, such as governments and planning agencies.

The concept of a geomodel, and its depiction in simplified block diagrams, aims to allow visualization of the geology in three dimensions and to act as a quick introduction to new or unfamiliar ground conditions or environments (Jackson 2016). Fookes (1997) defined conceptual geological models for a number of different environments, which have been linked to hazard assessment and engineering to mitigate geohazards (e.g. Hearn and Hart 2011; Hearn *et al.* 2012; Hearn 2018).

Parry *et al.* (2014) considered that there are two fundamentally different stages for developing engineering geological models: conceptual and observational. The conceptual approach is based on understanding the relationships between engineering geological units, their likely geometry and anticipated distribution. Importantly, these models are largely based on geological concepts

such as age, stratigraphy, rock type, unconformity and weathering (the 'total geological history' approach by Fookes *et al.* 2000). The main aim of the work presented here has been to develop practitioner-friendly conceptual ground models relating to the performance of slopes subject to strong ground motions during earthquakes in different mountain environments in the Chilean Andes. These were further subdivided into slope performance during (i) megathrust earthquakes and (ii) shallow crustal earthquakes, to indicate expected slope behaviour when subjected to earthquakes of different sizes and epicentral distance. The performance of the slopes is derived from the databases outlined in Serey *et al.* (2019). In addition to the hazards identified, potential mitigation measures are outlined based on the rock slope engineering.

Coseismic landslides in the mountain environment of Chile

The Cordilleran areas in Chile constitute a major part of the landmass and contain nearly all copper and other precious metal mining that contributes significantly to the Chilean economy. Additionally, mountain infrastructure is a vital lifeline for the flow of materials, access to markets for mountain communities, neighbouring countries, and tourism. However, given the mountain conditions it is difficult to provide alternative routes in the event of lifeline disruption.

Seismically induced landslides are a common phenomenon in the Andes, in central and southern Chile. This is attributed to two factors: first, the tectonic evolution of Chile and, secondly, the glaciation of the Andes resulting in variable geological conditions. Chile can be considered the most seismically active country in the world (Cisternas 2011; Barrientos 2018); ten $M_w \geq 8$ or larger earthquakes have occurred along the Chilean coast in the past

century, with a $M_w \geq 8$ earthquake occurring approximately every dozen years (Barrientos 2018). The second factor is that the Andes of central and southern Chile were strongly affected by Quaternary glaciations (with many areas still covered in ice), resulting in steep topography, strong erosional features and rock masses weakened by the effects of Late Quaternary ice action. The pattern of glaciation/deglaciation of the Andes is complex, changes in moisture in the atmosphere combined with lowering temperatures led to a complex change in seasonal snowline variation during the Late Pleistocene.

The seismotectonic setting and seismicity of Chile

The Andes of central Chile (32.5° S to 41.5° S) are composed of a number of morphostructural units from west to east: the Coastal Cordillera, the Central Valley, the Principal Cordillera (spanning Chile and Argentina), the Frontal Cordillera, the Argentine Precordillera and the Pampean Ranges (Jordan *et al.* 1983) (Fig. 1). The Principal Cordillera is a chain of high mountains that in its western part in Chilean territory mostly comprises Oligocene–Miocene continental volcaniclastic rocks, intruded by Miocene–Pliocene granitoids (Pankhurst and Hervé 2007; Charrier *et al.* 2015). The Cordilleran environment is characterized by being an active, folded orogen with a high topographic relief and steep slopes. Cycles of high activity (driven by periods of relatively rapid uplift) that initiate periods of intense erosion as rivers cut down to lower base levels and produce steep-sided valleys. Many of these valleys have limited stability, with the immature weathered surfaces continually being eroded. Hillslopes are typically mantled with colluvium and/or taluvium that is unstable when undercut.

Several seismogenic zones are recognized in Chile: large interplate earthquakes (depths 45–55 km); large intermediate-depth earthquakes (60–200 km); shallow crustal seismicity (depths

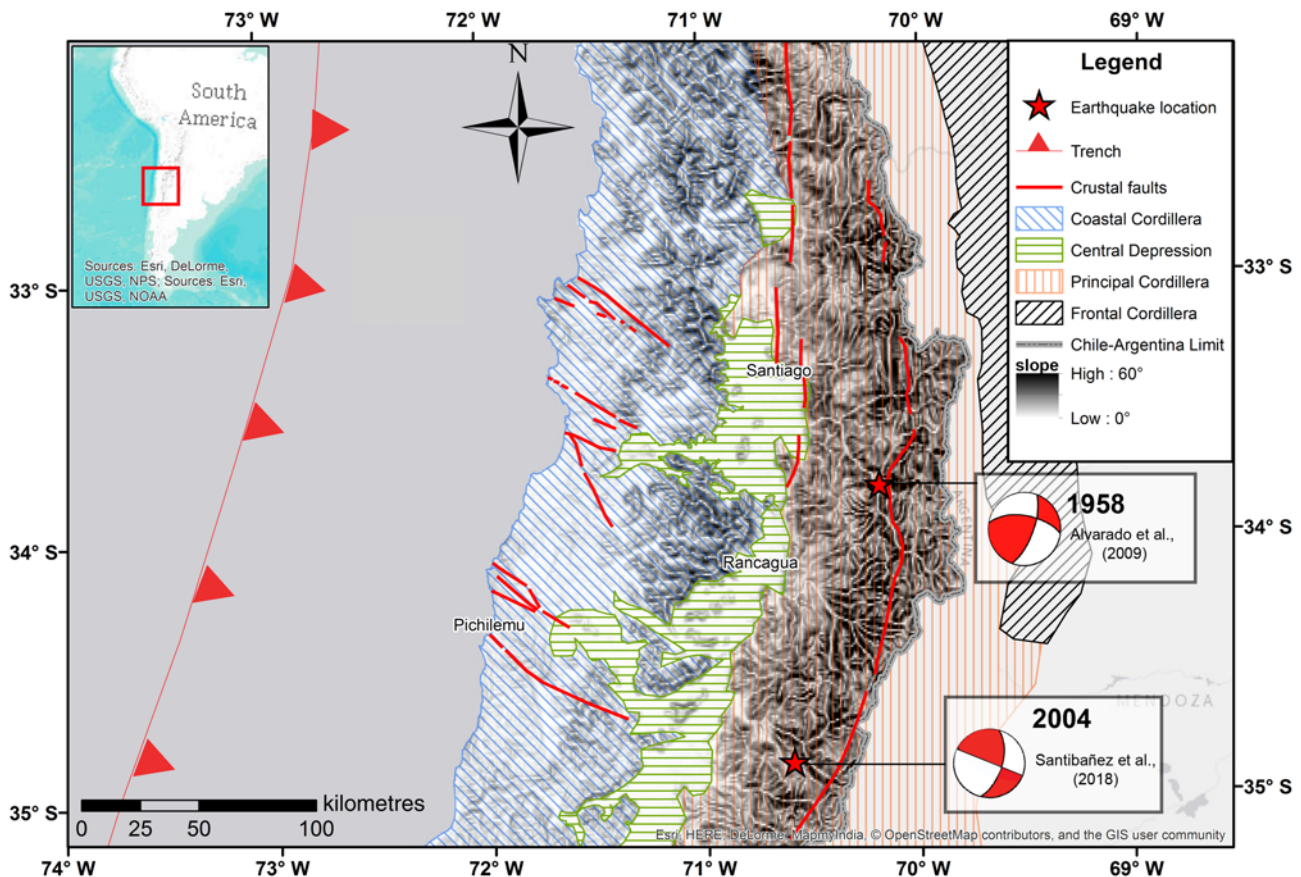


Fig. 1. Morphostructural and seismotectonic setting of central Chilean Andes. Major crustal fault in the Chilean Andes after Armijo *et al.* (2010) and Santibáñez *et al.* (2018).

0–20 km); and outer-rise earthquakes along the subduction margin between the Nazca and South American plates (Barrientos 2018).

Megathrust seismicity corresponds to large magnitude (above 8) interplate earthquakes in the subduction zone plate contact. Because of their comparatively high frequency of occurrence, these earthquakes are responsible for most of the historical damage. They are located along the coast from Arica (18° S) to the triple junction at Taitao Peninsula (46° S). These events take place as a result of the convergence of the Nazca beneath the South American plate at a rate of about 7.4 cm a⁻¹ (Argus *et al.* 2010). Further south, the Antarctic plate subducts beneath the South American plate at a rate of *c.* 8.1 cm a⁻¹ (Lara *et al.* 2018). $M_w \geq 8$ earthquakes are usually accompanied by notable coastal elevation changes and, depending on the amount of seafloor vertical displacement, by catastrophic tsunamis. Their rupture zones extend down to 45–53 km depth (Tichelaar and Ruff 1991) and their lengths can reach well over 1000 km. Return periods for $M \sim 8$ (and above) events are of the order of 80–130 years for any given region in Chile, and about a dozen years when the country is considered as a whole (Barrientos 2018). The latest examples of these type of earthquakes were the 2010 M_w 8.8 Maule, the 2014 M_w 8.2 Iquique and the 2015 M_w 8.4 Illapel earthquakes (Barrientos *et al.* 2004; Candia *et al.* 2017; Barrientos 2018). Megathrust earthquakes seem to have much longer return periods, of the order of a few centuries for any given region (Cifuentes 1989; Barrientos and Ward 1990). Recent off-fault strong ground motion indicator palaeoseismological studies

carried out in southern Chile indicate recurrence intervals of *c.* 300 years for these very large earthquakes (Cisternas *et al.* 2005; Moernaut *et al.* 2014).

The capacity for megathrust earthquakes to induce large numbers of landslides and mobilize large volumes of sediment was highlighted by the 1960 Valdivia (Duke 1960) and the 2010 Maule (Serey *et al.* 2019) earthquakes. During the M_w 9.5 Valdivia earthquake, extensive landsliding occurred (Wright and Mella 1963). Three large landslides ($2\text{--}30 \times 10^3 \text{ m}^3$ of volume) on poorly consolidated sediments at the San Pedro River attracted particular attention due to the formation of landslide dams and the threat to the city of Valdivia *c.* 80 km from the slides (Davis and Karzulovic 1963). Serey *et al.* (2019) provide an inventory of landslides induced by the 2010 M_w 8.8 Maule earthquake, one of the few world comprehensive, reliable inventories of coseismic landslides available for subduction zone earthquakes. In total, 1226 landslides were mapped over a total area of *c.* 120 500 km², dominantly small disrupted slides. However, the estimated total landslide volume is only *c.* $10.6 \times 10^3 \text{ m}^3$. The events are unevenly distributed in the study area, the majority of landslides are located in the Principal Andean Cordillera and a very constrained region near the coast on the Arauco Peninsula, forming landslide clusters (Serey *et al.* 2019). Additionally, Candia *et al.* (2017) demonstrated that there were more coseismic landslides that impacted critical infrastructure in areas with the largest fault slip at the plate boundary during the 2015 M_w 8.4 Illapel earthquake (31.6° S).

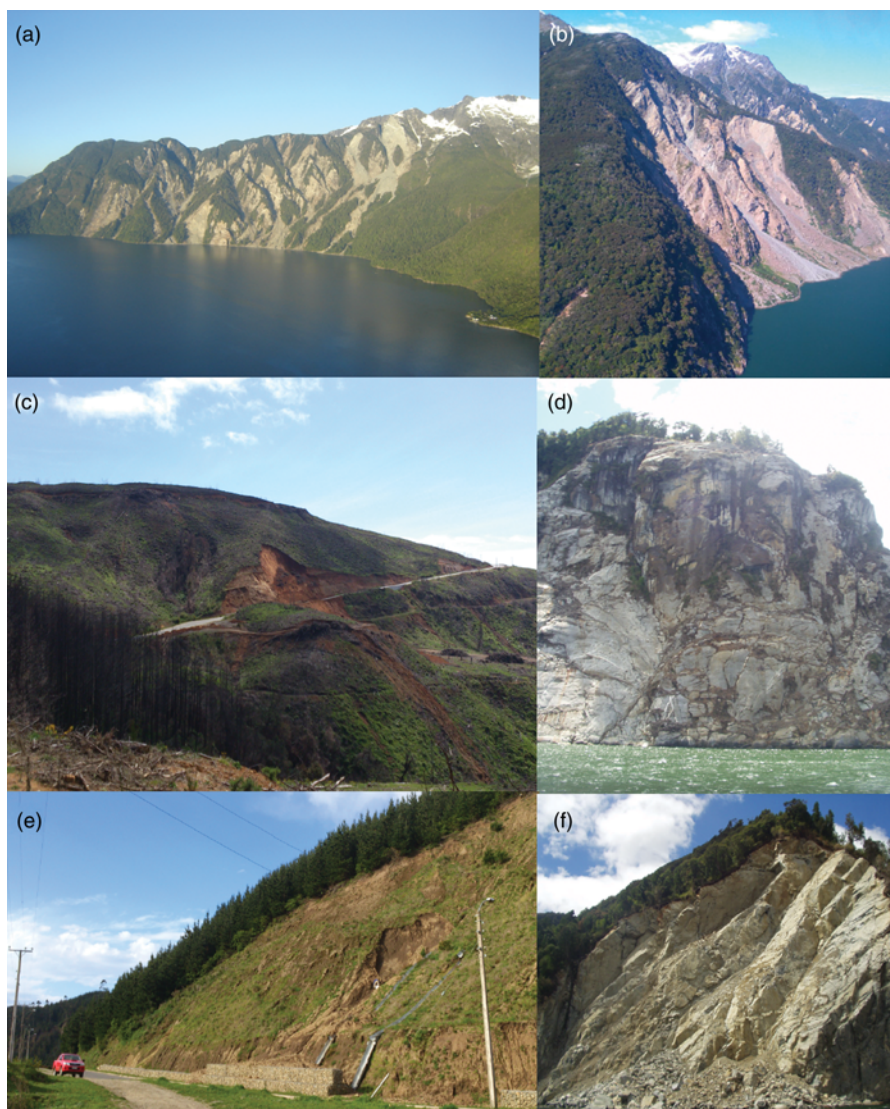


Fig. 2. Examples of landslides triggered by earthquakes in Chile. (a) Overview of debris avalanches (2007 Aysén earthquake); (b) Rock slides triggered by the 2007 earthquake in Aysén Fjord (all in granitic rock masses of the Patagonian Batholith; cliff height *c.* 1000 m); (c, e) debris slides (2010 Maule earthquake); (d) Rock falls (2007 Aysén earthquake; cliff height *c.* 400 m); (f) rock block slides (2007 Aysén earthquake; cliff height *c.* 400 m)

Shallow crustal seismicity is important in seismic and coseismic hazard assessments because of the strong ground motions (measured in % of gravity as peak ground accelerations, or PGA) that reach the surface due to limited distance for the seismic waves to attenuate. Shallow crustal seismicity (0–20 km) that occurs throughout Chile, such as in the Cordilleran region of south-central Chile (e.g. Liquiñe-Ofqui fault zone), is a consequence of the oblique convergence of the Nazca plate. Magnitudes up to 7.1 have been reported for earthquakes in this region (44.5° S 73° W, 21 November 1927) (Greve 1960). The Andean Principal Cordillera in the central part of Chile is also an important area with important crustal seismicity because of the risk to high population density and critical infrastructure. Godoy *et al.* (1999) and Barrientos *et al.* (2004) carried out structural and seismicity studies to understand this region, in which the largest recorded earthquake (less than 10 km depth) took place on 4 September 1958 (M_w 6.3, Alvarado *et al.* 2009), causing extensive rockfalls and a few large landslides (Sepúlveda *et al.* 2008). Shallow crustal seismicity with a relatively large magnitude (>5.5) was recently observed beneath the Andes main Cordillera at latitudes 19.6° S (Aroma; July 2001), 35.8° S (Melado River; August 2004), 38° S (Barco Lagoon; December 2006) and 45° S (Aysén Fjord; April 2007). All these events show a significant strike-slip component of displacement (Barrientos 2018).

In southern Chile, the Aysén Fjord earthquake (21 April 2007, M_w 6.2) triggered over 500 landslides of different types (Sepúlveda *et al.* 2010), of which the largest was the Punta Cola rock avalanche with a volume of $c. 22 \times 10^3 \text{ m}^3$ (Oppikofer *et al.* 2012). The triggering of landslides around and into the fjord resulted in a displacement wave that killed 11 people (Naranjo *et al.* 2009; Sepúlveda and Serey 2009).

Geomodel construction

Data used in construction of the geomodels

Data used to develop the geomodels presented here can be divided into two broad types: landslide inventory data and limited field observation of critical lithological units. Only two comprehensive inventories of earthquake-triggered landslides exist in Chile, the shallow crustal M_w 6.2 Aysén earthquake in 2007 (45.27° S 72.66° W) (Sepúlveda *et al.* 2010; Serey 2020) and the M_w 8.8, megathrust Maule earthquake in 2010 between 32.5° S and 38.5° S (Serey *et al.* 2019). These inventories are representative of the landslide-triggering characteristics of these two Chilean groups of seismic events. These databases were supplemented with observations from databases beyond Chile (e.g. Malamud *et al.* 2004; Marc *et al.* 2016) in addition to more detailed field investigations of large, historical landslides in Chile (e.g. Sepúlveda *et al.* 2008) and inventories of landslides from the geological record that are considered likely to have been induced by seismic activity (Antinao and Gosse 2009; Moreiras and Sepúlveda 2015). These databases contain data on topographic, geomorphological, geological and seismic controlling factors on the occurrence of earthquake-triggered landslides, which informed model construction.

Distribution and characteristic of coseismic landslides for geomodels in the Chilean Andes

It is well established that landslides are not evenly distributed in the affected areas. Landslides tend to form clusters that may be related to geological conditions or ground motion parameters (e.g. Sepúlveda *et al.* 2010; Serey *et al.* 2019) or to the influence of strong ground motions coincident with fault slip distributions (Candia *et al.* 2017). Furthermore, most occur in the Cordilleran environment where high relief and steeper slopes prevail. Examples

of the landslides under investigation can be seen in Figure 2. From the analysis of databases, we can make a number of general comments.

(1) The most common type of landslide observed in the inventories is ‘disrupted’ slides, consistent with observations from other earthquakes (e.g. Keefer 1984; Rodriguez *et al.* 1999; Wartman *et al.* 2013).

(2) Shallow disrupted slides, such as debris avalanches, debris slides, rock falls and rock slides, account for *c.* 86 and 98% of landslides triggered by the Maule 2010 and Aysen 2007 earthquakes respectively (Sepúlveda *et al.* 2010; Serey *et al.* 2019) (see Fig. 2).

Table 1. Summary of most common correlations of coseismic landslides in the Chilean Andes contrasting the megathrust earthquakes with shallow crustal earthquakes

Conditioning factors/ characteristic of coseismic landslides	Coseismic landslides triggering by	
	megathrust earthquake	shallow crustal earthquake ($M > 4$)
Relief	Relief exerts a strongly dominant control on landsliding both in terms of preconditioning (higher, steeper slopes) and local topographic amplification of shaking.	
Bedrock lithology	Relevant conditioning factor, with more landslides in younger (normally weaker) volcanic and volcano-sedimentary rocks.	There is no obvious correlation between landslide concentration and rock age (young or old lithology), even on very resistant rocks such as granitoids.
Proximity of the fault	There is a poor correlation between landsliding and fault rupture distance (subduction zone).	The rupture plane of fault is a first-order factor in the distribution of landslides. Hanging wall and directivity effects.
Seismological parameters	Poor correlation between estimated PGA and landslide occurrence. Better correlation between landslide concentration and the ratio between horizontal and vertical peak accelerations.	Ground motion parameters would be the most significant factors, including horizontal and vertical accelerations, ground velocity, frequency content and epicentral distance.
Topographic amplification	Moderate or local influence. Landslides generally not clustered close to the ridge tops.	Strong influence. The crowns of the landslides are generally in the uppermost part of the slopes.
Spatial distribution	Landslides are not evenly distributed in the affected area, tending to the formation of clusters of landslides.	–
		Landslides tend to be limited to the epicentral area.
Type of coseismic landslide	Disrupted slides. Most of them, rock falls and debris slides.	Disrupted slides. Most of them, debris avalanches, rock falls, debris slides and rock slides/avalanches.
Number of landslides	The total number of landslides triggered for the megathrust earthquakes is substantially lower, typically by one to two orders of magnitude, than would be expected for shallow crustal earthquakes of a similar or even lower magnitude.	

After this study, Sepúlveda *et al.* (2010) and Serey *et al.* (2019).

(3) Relatively few slumps, deep block slides or slow earth flows were observed from Chilean inventories. For example, less than 1% of total slides were classified as coherent slides for the Maule earthquake (Serey *et al.* 2019), and nearly 1% for the Aysen event (Sepúlveda *et al.* 2010).

(4) The number and distribution of coseismic landslides differs significantly between interplate/megathrust and shallow crustal earthquakes. The total number of landslides triggered by the megathrust earthquakes is substantially lower, typically by one to two orders of magnitude, than would be expected for shallow crustal earthquakes, of a similar or even lower magnitude (Serey *et al.* 2019). This is due to strong ground motion attenuation from interplate/megathrust events that reduce the PGA.

(5) There is a difference in the size of landslides between the two different sources of seismicity. The landslides triggered by the megathrust Maule earthquake are generally in the range of 10^2 – 10^3 m². Approximately 60% of coseismic landslides caused by the Maule earthquake were in the range of 100–5000 m². This can be contrasted with the fact that just under 50% of landslides induced during the crustal Aysen earthquake were in the range of 5000–50 000 m². This is likely to be a function of the amount of energy arriving at any given slope due to the attenuation from deeper sources mentioned above.

(6) For megathrust earthquakes, such as those in 1960, there seems to be limited occurrence of large volume rock avalanches or rock slides. Although this type of earthquake is relatively frequent in Chile, no large volume rock avalanches have been observed to be triggered by them during the last century. However, as Chile has a high concentration of large volume rock avalanche deposits in the Andes (Antinao and Gosse 2009), it is likely that these are associated with proximal shallow crustal earthquakes. Given the large distance between interplate seismicity and the Andes Principal Cordillera (c. 100–150 km in central Chile) these seem a more likely cause than large farfield events, like the catastrophic avalanche in 1970 triggered by an M_w 7.9 offshore earthquake, originating from Nevados Huascarán, the highest peak in the Peruvian Andes (Pflafer and Ericksen 1978; Evans *et al.* 2009).

Factors that influence the dynamic response of hillslopes undergoing seismic shaking

The factors that influence the dynamic response of hillslopes undergoing seismic shaking (e.g. Newmark 1965; Jibson 2011) can be broadly grouped into those that influence the intensity of event-specific seismic ground motions, those that influence the strength of hillslope materials and those that influence the static shear stresses.

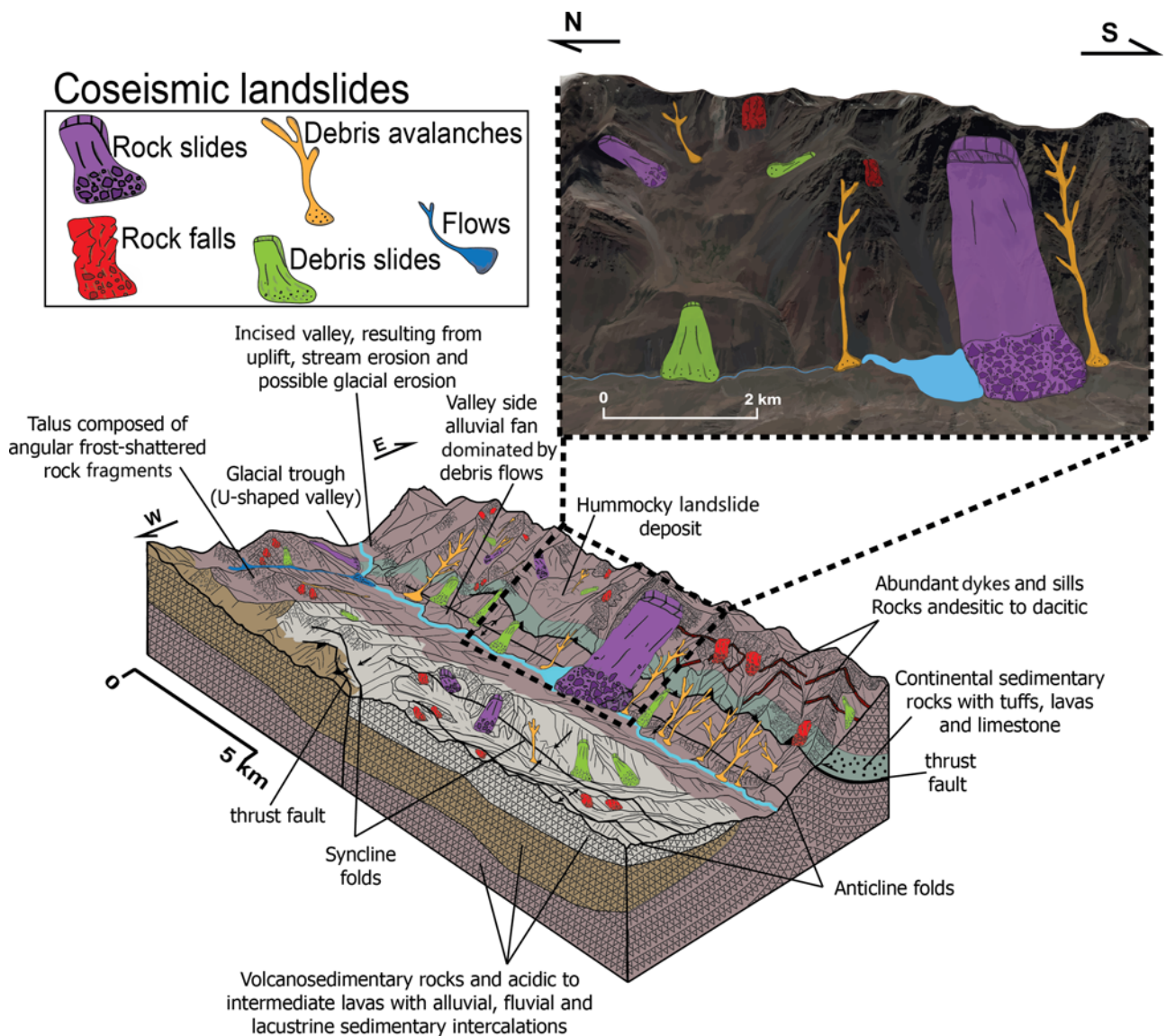


Fig. 3. Glacial Cordilleran environment. Conceptual geomodel of coseismic landslides induced by shallow crustal earthquake.

Empirical studies have revealed a number of proxy variables that can be used to represent these factors at the regional scale (Parker *et al.* 2015).

Lithology is an important factor in the generation of coseismic landslides, being relevant mainly during megathrust events. For example, Wartman *et al.* (2013) determined that the majority of landslides triggered by the M_w 9.0 2011 Tohoku megathrust earthquake occurred in the youngest (Neogene) geological units of the region (Quaternary sediments and Neogene sedimentary rocks). The Serey *et al.* (2019) database indicates that for the 2010 Maule earthquake, relief exerted a dominant control on coseismic landsliding, with the lithology the second most relevant conditioning factor, with more landslides in younger rocks (Quaternary deposits and Paleogene–Neogene volcanic and volcano-sedimentary rocks). This is in effect an indication of the degree of cementation and thus strength. On the other hand, in most shallow crustal events, lithology seems not to be a primary factor to consider in the generation of landslides. For example, according to Wang (2015) there is no obvious correlation between landslide concentration and rock age (young or old lithology) for the 2013 Lushan and the 2008 Wenchuan earthquakes. Indeed, differences in the distributions of landslides across different lithologies arise because young or old strata are coincidentally clustered around the

rupture zone of the seismogenic fault, and these rock masses are extremely fractured and undergo strong shaking.

Other factors that may have influence on the distribution of landslides are related to seismic effects on shaking in the near field, such as the hanging-wall and directivity effects during strong shallow crustal earthquakes. Directivity effects are related to the rupture direction of the fault, tending to generate larger ground motions in this direction (Somerville *et al.* 1997; Somerville and Graves 2003). The hanging-wall effect relates to larger ground motions on the block above an inclined fault (the hanging-wall block) and is common with earthquakes along thrust faults (e.g. Abrahamson and Somerville 1996; Zhao *et al.* 2019). The literature indicates that the landslides triggered by earthquakes tend to cluster along the causative fault (Keefer 2000, 2002; Khazai and Sitar 2004; Huang and Li 2009). For thrust faults, landslide density is highest on the hanging wall (Meunier *et al.* 2007).

Ground motion was found to be the most significant factor in triggering the shallow landslides in the 1999 M_w 7.6 Chi-Chi earthquake. Overall, 74% of all slope failures occurred in regions with vertical ground motions greater than 0.2 g and 81% of all slope failures occurred in the region with mean horizontal PGA greater than 0.15 g (Khazai and Sitar 2004). On the other hand, Wartman *et al.* (2013) compared the landslide database with ground-motion

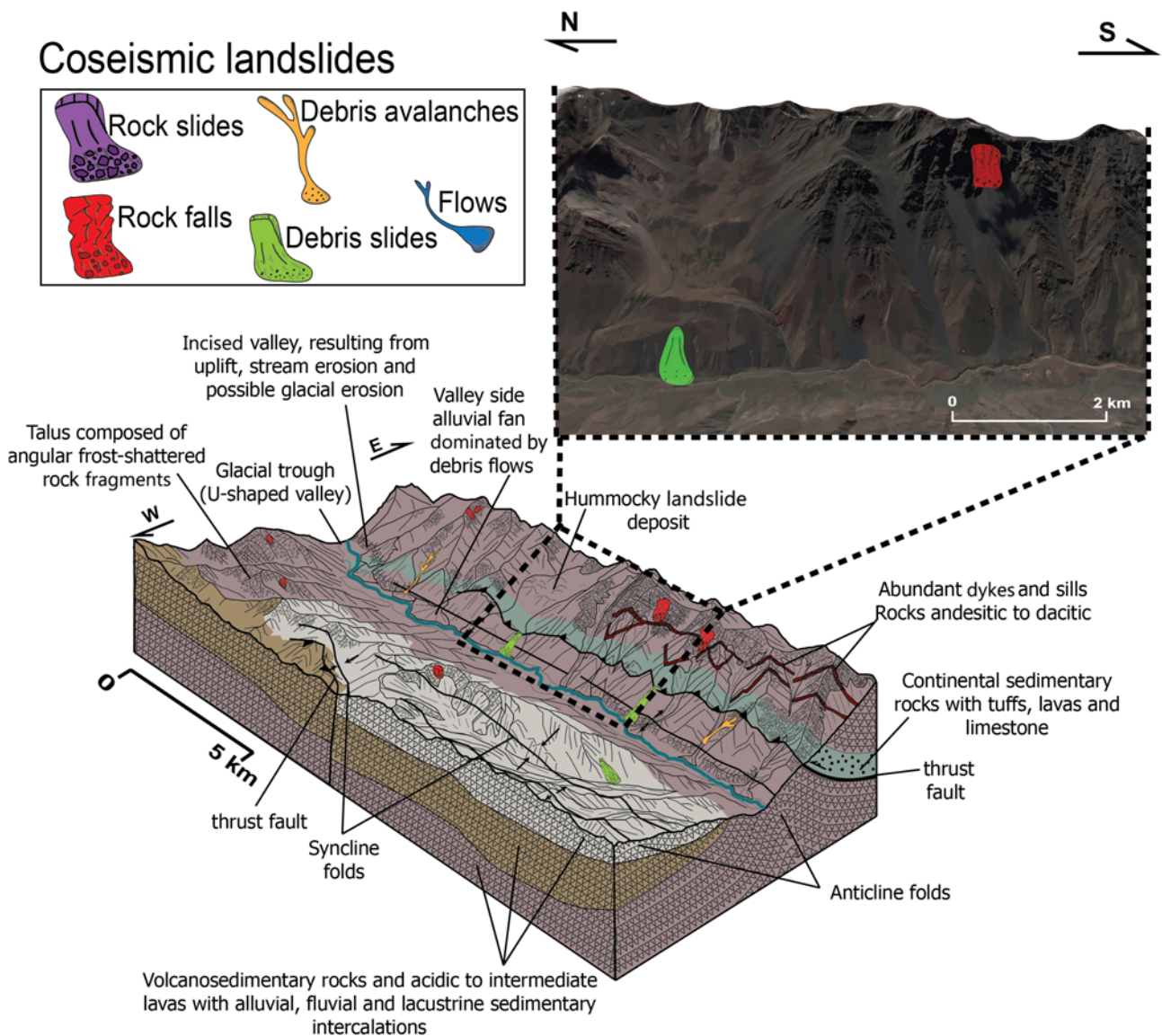


Fig. 4. Glacial Cordilleran environment. Conceptual geomodel of coseismic landslides induced by megathrust earthquake.

Conceptual models of coseismic landslides hazard

Table 2. Terrain characteristics and coseismic landslide hazards for the Glacial Cordilleran environment

Terrain facet	Terrain element	Site characteristics	Main coseismic landslide type (after Hungr <i>et al.</i> 2014)		Secondary hazards	Engineering intervention/ risk-reduction strategies
			shallow crustal earthquake	megathrust earthquake		
Glacial andesitic slopes	Ridges	Ridges characterized by thin soil deposits with bedrock at or close to the surface; rock mass may be frost shattered and highly fractured, or hydrothermally altered. Likely to be a poor to fair quality rock mass at shallow depths but good to very good deeper. This is likely to mitigate against deep-seated landslides.	Rock falls; debris falls; rock block topples; debris topples.	Rock falls; debris falls; rock topples; debris topples.	Creation of sediment supply for debris flow activation.	None, at best reactive. In ridges close to infrastructure it may be necessary to remove loose material on a periodic basis.
	Interfluvial slopes	Slopes formed with engineering soils of variable thickness along the slope profile. Dominantly glacial material, although may have been reworked. Glacial deposits may be mantled by colluvium/ talus. Rock mass could present surface-parallel fracture systems in rock (sheet joints), over-steepened slopes and U-shaped valley.	Rock slides, debris slides; debris avalanches. Ancient rock slides can be reactivated.	Debris slides; debris avalanches.	Rock slides may create landslide dams in tributary valleys.	Local stakeholders should carry out inspections after an earthquake. It may prove impossible to access blockages and these will need a monitoring plan.
	Stream channels	Dominated by intercalations of coarse fluvial material, glacial debris and slope wash deposits. In high slopes (>2000 m) these may contain rock glaciers.	Possible debris flows due to debris avalanche failures into stream channels.	—	Debris flow initiation in tributary valleys creating landslide dams in main valleys.	Monitoring. Infrastructure owners/ stakeholders should consider inspections after strong earthquakes to monitor sediment build-up.
	Cross element	Mixture of the terrain elements (see relevant site characteristics above).	Large rockslides with an origin on upper reaches of glaciated cordillera which spans multiple terrain units.	—	Large slide mass creates temporary dam. Breaching is a major hazard leading to downstream flooding.	Reactive – stakeholders should develop a mitigation plan that includes large landslides resulting in loss of access and long-term planning.
Cordillera river systems	Rock river channel	The river channel slopes are formed in bedrock which has been excavated by valley glaciers; rock mass may be locally frost shattered and hydrothermally altered.	Debris slides, rock falls.	Rock falls.	High turbidity in the river. Large slide mass creates temporary dam. Breaching is a major hazard leading to downstream flooding. Potential breaching of landslide dams creating downstream flooding and problems of suspended sediment in water supply and damage to hydroelectric infrastructure.	Downstream towns and villages should provide evacuation routes and indicate refuge zones in the event of a valley blocking landslide. Hydro Electric Power owners may need to monitor sediment flux post-earthquake to reduce risk of damage to turbines.
	Glacial debris river channel	River channel slopes are formed in ice-contact debris and alluvial deposits which are locally over-steepened. These may be mantled by alluvial fans. Glacial soils may be reworked and stratified.	Debris slides, debris falls. There is potential for local liquefaction in alluvial soils.	Debris falls.		

recordings of the 2011 Tohoku earthquake (M_w 9.0, megathrust event), but found no correlation between landslide intensity and ground shaking within the area affected. Similarly, in the 2010 M_w 8.8 Maule earthquake, very few landslides occurred in the area of higher intensity (VIII) and most of them were in the area of lower intensities (<V). Therefore, there was no strong correlation between landslide density and earthquake intensity (Serey *et al.* 2017), or with PGA and distance from the fault plane. There was a much

stronger correlation between landslide concentration and the ratio between horizontal and vertical peak accelerations (Serey *et al.* 2019).

Densmore and Hovius (2000) recognized that earthquake-triggered landslides in rock slopes have a relatively uniform distribution on steep slopes, but in the presence of topographic amplification the triggering of landslides at or near the crests is increased. Recent studies have indicated that the ground accelerations

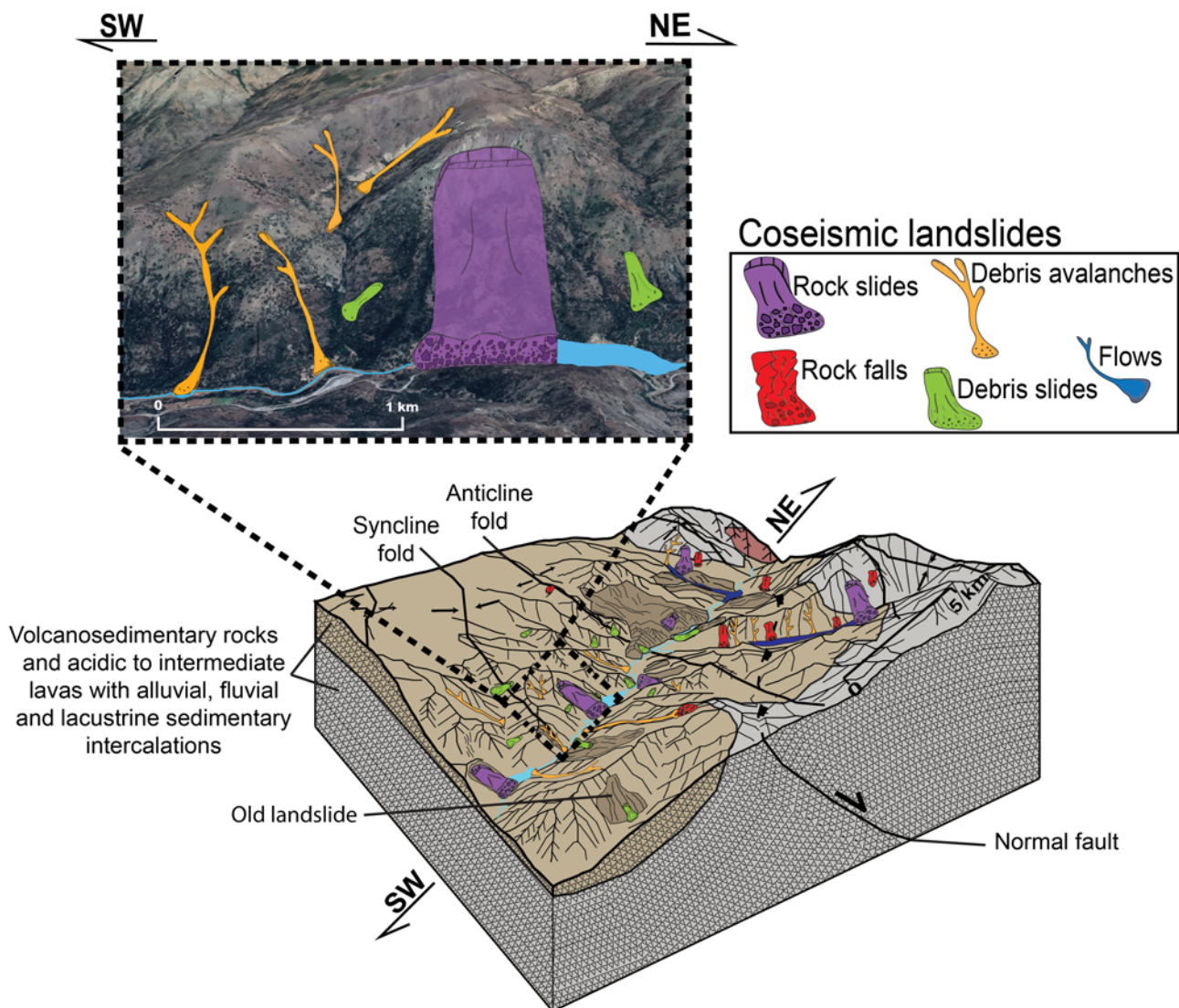


Fig. 5. Fluvial Cordilleran environment. Conceptual geomodel of coseismic landslides induced by shallow crustal earthquake.

at the mountain top can be three to six times that at its foot (Y. Wang *et al.* 2012; G. Wang *et al.* 2018), causing higher susceptibility to landsliding in the upper parts of the slopes. In the Aysen event, about two-thirds of the landslides started in the upper quarter of the slope, while over 90% started in the upper half, which suggests that larger ground motions due to topographic site effects influenced the triggering of landslides during the earthquake (Sepúlveda *et al.* 2010). On the other hand, landslides induced by the Maule earthquake are not clustered close to the ridge tops, suggesting no predominant topographic site effect in their generation, although it may have played a role locally (Serey *et al.* 2019).

The above is summarized in Table 1, which shows the differences between conditioning factors and characteristics of the coseismic landslides applied to the mountain environment of Chile for both kinds of triggers (shallow crustal and interplate/megathrust earthquakes), based on analysis of comprehensive inventories of coseismic landslides in Chile and abroad (Meunier *et al.* 2007; Sepúlveda and Serey 2009; Sepúlveda *et al.* 2010; Gorum *et al.* 2011; Wartman *et al.* 2013; Wang 2015; Serey *et al.* 2017, 2019; Zhao *et al.* 2019; Serey 2020).

Conceptual hazard models

Using the data mentioned above, four conceptual hazard ground models were developed to guide stakeholders in the hazards faced

by critical infrastructure in mountain regions. Representative geomodels describing the hazards for the Andes of central Chile were developed, these are: Glacial Cordilleran, Fluvial Cordilleran, Plutonic Cordilleran and Mountain Front environments. The latter model is the most likely to have significant urban development because of the concentration of infrastructure. The data showing slope performance for the two different earthquake types, based on Table 1 and specific geomorphological characteristics, have then been added to the models to use in a semi-predictive capacity.

Glacial Cordilleran environment

In central Chile, the glaciated mountain terrain is dominated by andesitic bedrock with local volcanoclastic sediments. Glacial landscapes are essentially high-latitude and/or high-altitude environments. Geomorphology in these areas is characterized by high relief and steep slopes. Furthermore, it is characterized by the presence of glacial deposits (e.g. till and glacial-fluvial deposits) and modified by periglacial processes. Rock slopes tend to be oversteepened. Rock mass quality is often fair to good, locally very good, and may be highly fractured in the vicinity of lineaments or faults. Hydrothermal alteration, however, can be extreme locally and reduces the rock mass quality. Most coseismic landslides are disrupted, principally rock falls, debris avalanches, debris slides and rock slides. In these environments, large rock avalanches/slides

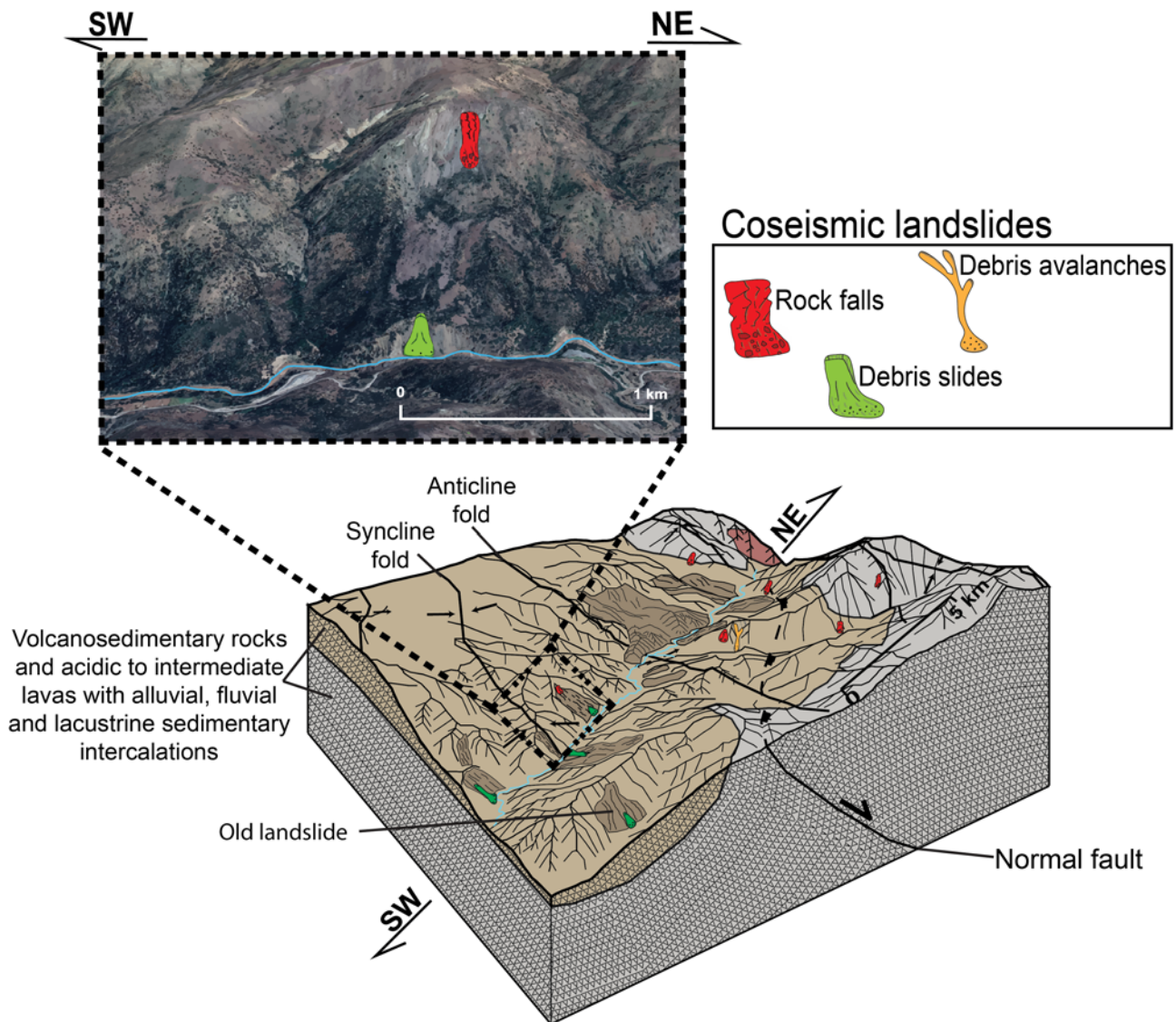


Fig. 6. Fluvial Cordilleran environment. Conceptual geomodel of coseismic landslides induced by megathrust earthquake

could dam a river valley. Landslides may occur on persistent discontinuities or glacial deposits.

Figures 3 and 4 show conceptual geomodels of coseismic landslides induced by shallow crustal and megathrust earthquakes respectively in a Glacial Cordilleran environment of the central Chilean Andes. Table 2 outlines geomorphological characteristics of terrain and possible coseismic landslides that could be triggered in a Glacial Cordilleran environment for each scenario.

Fluvial Cordilleran environment

Fluvial mountain terrain dominated by andesitic bedrock with local volcanoclastic sediments. Geomorphology is characterized by a strong relief, medium ranges of altitudes and medium to high gradients forming fluvial troughs (V-shaped valleys). Rock mass quality is often fair to good, locally very good, and may be highly fractured near lineaments or faults. Hydrothermal alteration, however, can be extreme in places and reduce the geotechnical quality of intact rock. In these environments, large rock falls, rock avalanches/slides could dam a river valley. In this landscape, large prehistoric landslides are common, in which source areas of future rock slides may be generated by future shallow crustal events.

Figures 5 and 6 show conceptual geomodels of coseismic landslides induced by shallow crustal and megathrust earthquakes

respectively in a Fluvial Cordilleran environment of the central Chilean Andes. Table 3 expresses geomorphological characteristics of terrain and possible coseismic landslides that could be triggered in a Fluvial Cordilleran environment for each scenario.

Plutonic Cordilleran environment

Plutonic mountain terrain dominated by intrusive igneous bedrock with local volcanoclastic sediments. This environment is characterized by a strong relief, steep slopes (medium to high ranges) and high altitudes. In general terms, plutonic rocks develop competent rock masses and tight valleys. Rock mass quality is often good to very good, may be highly fractured in the vicinity of lineaments or faults. Large prehistoric landslides are very common in these environments, in which new rock slides can be generated by a future shallow crustal earthquake. In addition, large rock falls, rock avalanches/slides could dam a river valley.

Figures 7 and 8 show conceptual geomodels of coseismic landslides induced by shallow crustal and megathrust earthquakes respectively in a Plutonic Cordilleran environment of the central Chilean Andes. Table 4 outlines geomorphological characteristics of terrain and possible coseismic landslides that could be triggered in a Plutonic Cordilleran environment for each scenario

Table 3. Terrain characteristics and coseismic landslide hazards for the Fluvial Cordilleran environment

Terrain facet	Terrain element	Site characteristics	Main coseismic landslide type (after Hungr <i>et al.</i> 2014)		Secondary hazards	Engineering intervention/risk-reduction strategies
			shallow crustal earthquake	megathrust earthquake		
Fluvial andesitic slopes	Ridges	Ridges characterized by thin residual soil deposits with bedrock at or close to the surface; rock mass may be highly fractured by thermal oscillation, may be hydrothermally altered. Likely to be a fair to poor quality rock mass.	Rock falls; rock block slides; debris falls; topples.	Rock falls.	Creation of sediment supply for debris flow activation.	Consider installation of ring netting to control sediment supply to rivers. An inspection and maintenance plan will be required to avoid these becoming a hazard in their own right.
	Interfluvial slopes	Rock mass composed of volcano-sedimentary bedrock often fair to good quality, may be highly fractured in the vicinity of lineaments or faults. Steep slopes and V-shaped valley. They may have the scar of ancient events of mass removals. Slopes formed with engineering soils of variable thickness along the long profile. Dominantly alluvial material and colluvium.	Rock slides; rock avalanches; debris slides; debris avalanches; Rock falls. Ancient rock slides can be reactivated.	Debris slides; debris avalanches.	Rock slides may create landslide dams in tributary or principal valleys.	Local stakeholders should carry out inspections after an earthquake. It may prove impossible to access blockages and these will need monitoring; long-term planning is needed.
	Stream channels	Dominated by intercalations of coarse fluvial material, alluvial deposits and colluvium.	Possible debris flows due to debris avalanche, rock falls or rock slide failures into stream channels.	—	High turbidity events in the channels.	Monitoring. Infrastructure owners/ stakeholders should consider inspections after strong earthquakes to monitor sediment build-up.
	Cross element	Mixture of the terrain elements (see relevant site characteristics above).	Large rockslides or rock avalanches with an origin on upper reaches of Cordillera which spans multiple terrain units.	—	Large slide mass creates temporary dam. Breaching is a major hazard leading to downstream flooding.	Inspections required after shaking. Local action plan for community evacuation should be considered. In the event of large landslide dams, local communities may need to refer the matter to Central Government via Ministry of Public Works. Urgent action needed and long-term planning.
Cordillera river systems	Rock river channel	The river channel slopes are formed in bedrock which has been excavated by river or ancient glaciers, may be hydrothermally altered.	Debris slides, rock falls.	Rock falls; debris slides.	Extreme high turbidity events in the river. Large slide mass creates temporary dam. Breaching is a major hazard leading to downstream flooding.	
	Fluvio-alluvial debris river channel	River channel slopes are formed in debris and alluvial deposits which can be locally over-steepened. These may be mantled by colluvium material.	Debris slides. There is potential for local liquefaction in granular materials like sandy or silty soils.	Debris slides.		

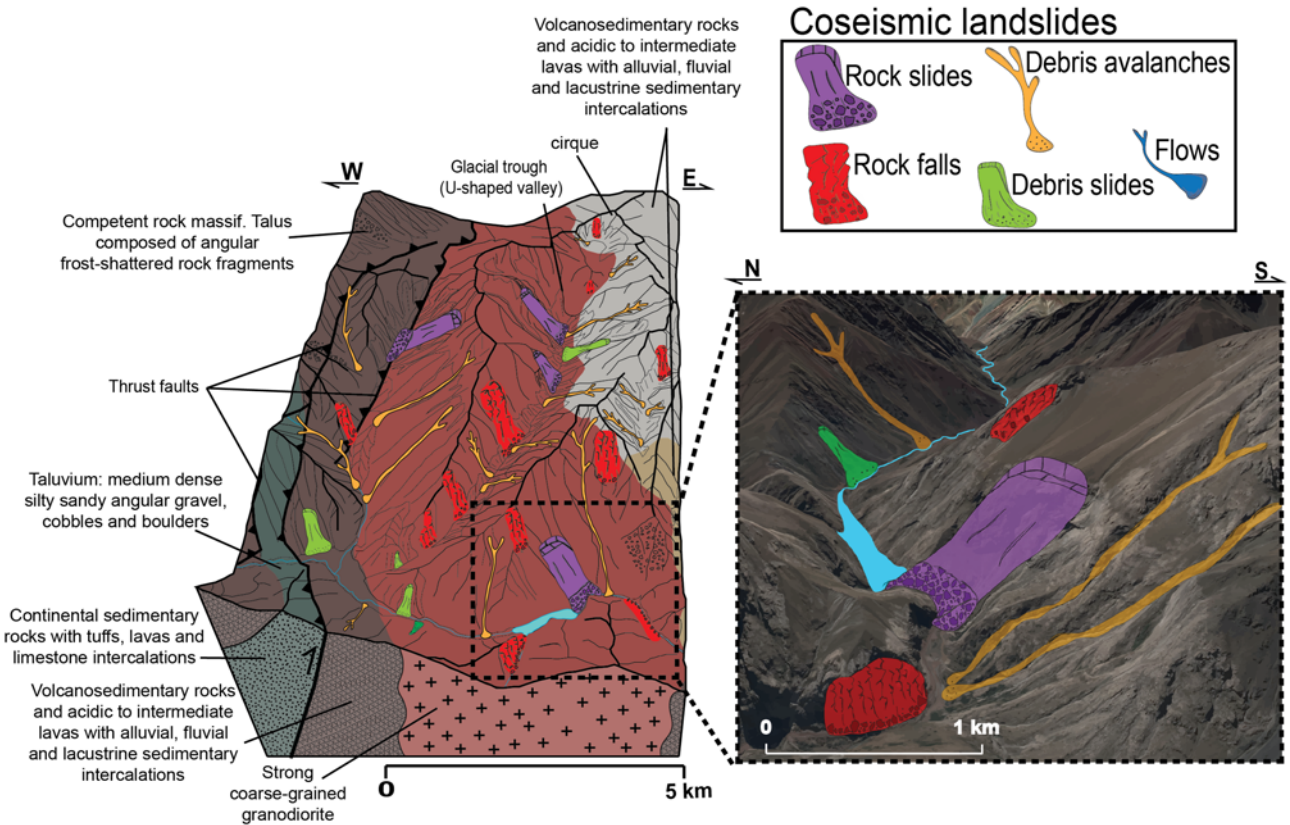


Fig. 7. Plutonic Cordilleran environment. Conceptual geomodel of coseismic landslides induced by shallow crustal earthquake.

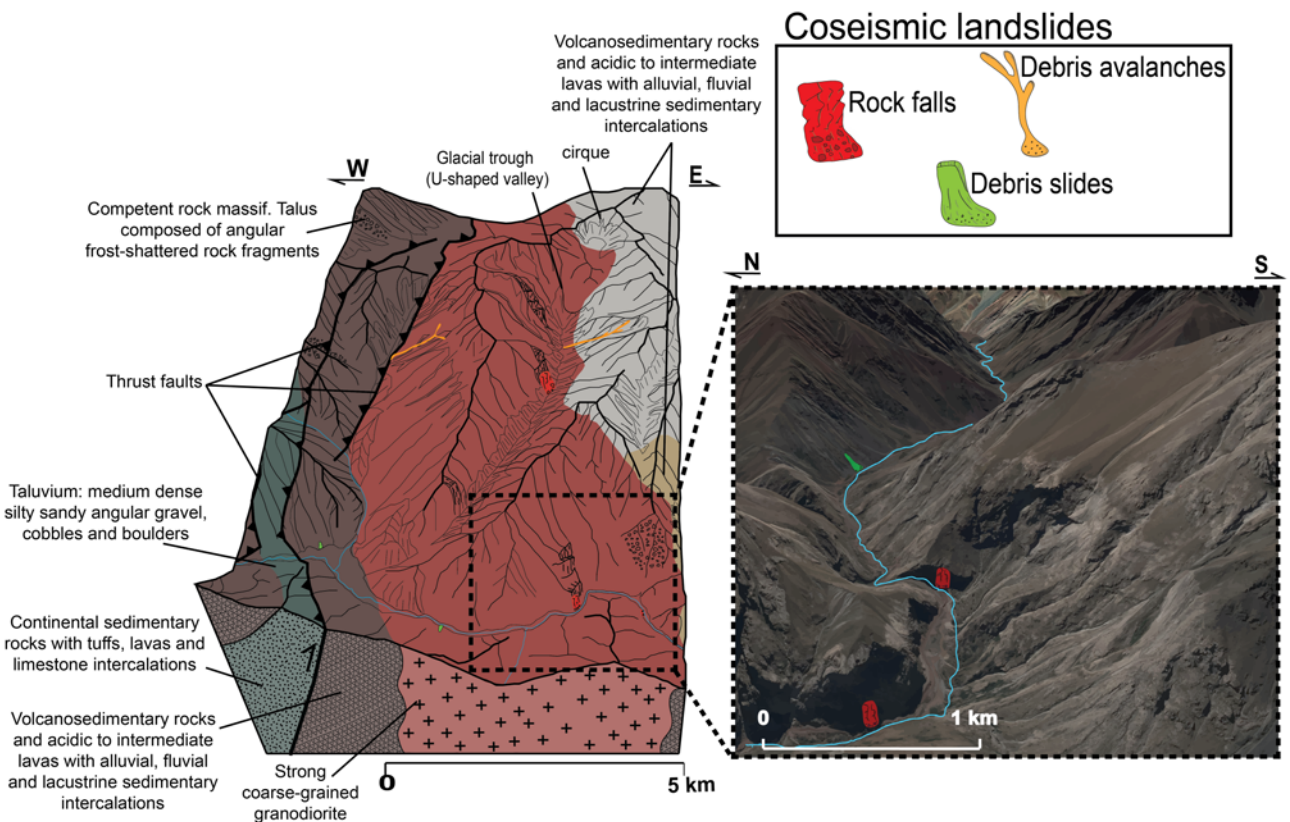


Fig. 8. Plutonic Cordilleran environment. Conceptual geomodel of coseismic landslides induced by megathrust earthquake.

Table 4. Terrain characteristics and coseismic landslide hazards for the Plutonic Cordilleran environment

Terrain facet	Terrain element	Site characteristics	Main coseismic landslide type (after Hungr <i>et al.</i> 2014),			Engineering interventions/risk-reduction strategies
			shallow crustal earthquake	megathrust earthquake	Secondary hazards	
Plutonic slopes	Ridges	Ridges characterized by thin residual soil deposits with bedrock at or close to the surface; rock mass may be highly fractured by thermal oscillation, may be hydrothermally altered. Variable rock mass geotechnical quality.	Rock falls; rock block slides.	Rock falls.	Creation of sediment supply for debris flow activation.	None. Reactive at best. Inspection of sediment build-up after earthquakes with higher priority after a local shallow crustal event and long-term planning is needed.
	Interfluvial slopes	Rock mass compound of plutonic bedrock often good to very good geotechnical quality, steep slopes and cliffs. It may be highly fractured, present stress-relief fractures parallel to a cliff face, or hydrothermally altered, in the vicinity of lineaments or faults. Slopes formed with engineering soils of variable thickness along the long profile. Dominantly fluvio-alluvial material and colluvium deposits.	Rock slides; rock avalanches; debris slides; debris avalanches; rock falls.	Debris slides; debris avalanches.	Rock slides may create landslide dams in tributary or principal valleys.	Local stakeholders should carry out inspections after an earthquake. It may prove impossible to access blockages and these will need a monitoring plan.
	Stream channels	Glacial valley: Dominated by intercalations of coarse fluvial material, glacial debris and slope wash deposits. Fluvial valley: Dominated by intercalations of coarse fluvial material, alluvial deposits and colluvium.	Possible debris flows due to debris avalanche, rock falls or rock slide failures into stream channels.	—	High turbidity events in the channels. Debris flow initiation in tributary valleys creating landslide dams in main valleys.	Inspections required after shaking. Local action plan for community evacuation should be considered. In the event of large landslide dams, local communities may need to refer the matter to Central Government via Ministry of Public Works. Urgent action needed and long-term planning.
	Cross element	Mixture of the terrain elements (see relevant site characteristics above).	Large rockslides or rock avalanches with an origin on upper reaches of Cordillera which spans multiple terrain units.	—	Large slide mass creates temporary dam. Breaching is a major hazard leading to downstream flooding.	
Cordillera river systems	Rock river channel	The river channel slopes are formed in bedrock which has been excavated by river or valley glaciers.	Debris slides, rock falls.	Rock falls; debris slides.	Extreme high turbidity events in the river. Large slide mass creates temporary dam. Breaching is a major hazard leading to downstream flooding. Potential breaching of landslide dams, creating downstream flooding.	
	Debris river channel	River channel slopes are formed in debris and alluvial deposits which can be locally over-steepened. These may be mantled by colluvium material.	Debris slides. There is potential for local liquefaction in granular materials like sandy or silty soils.	Debris slides.		

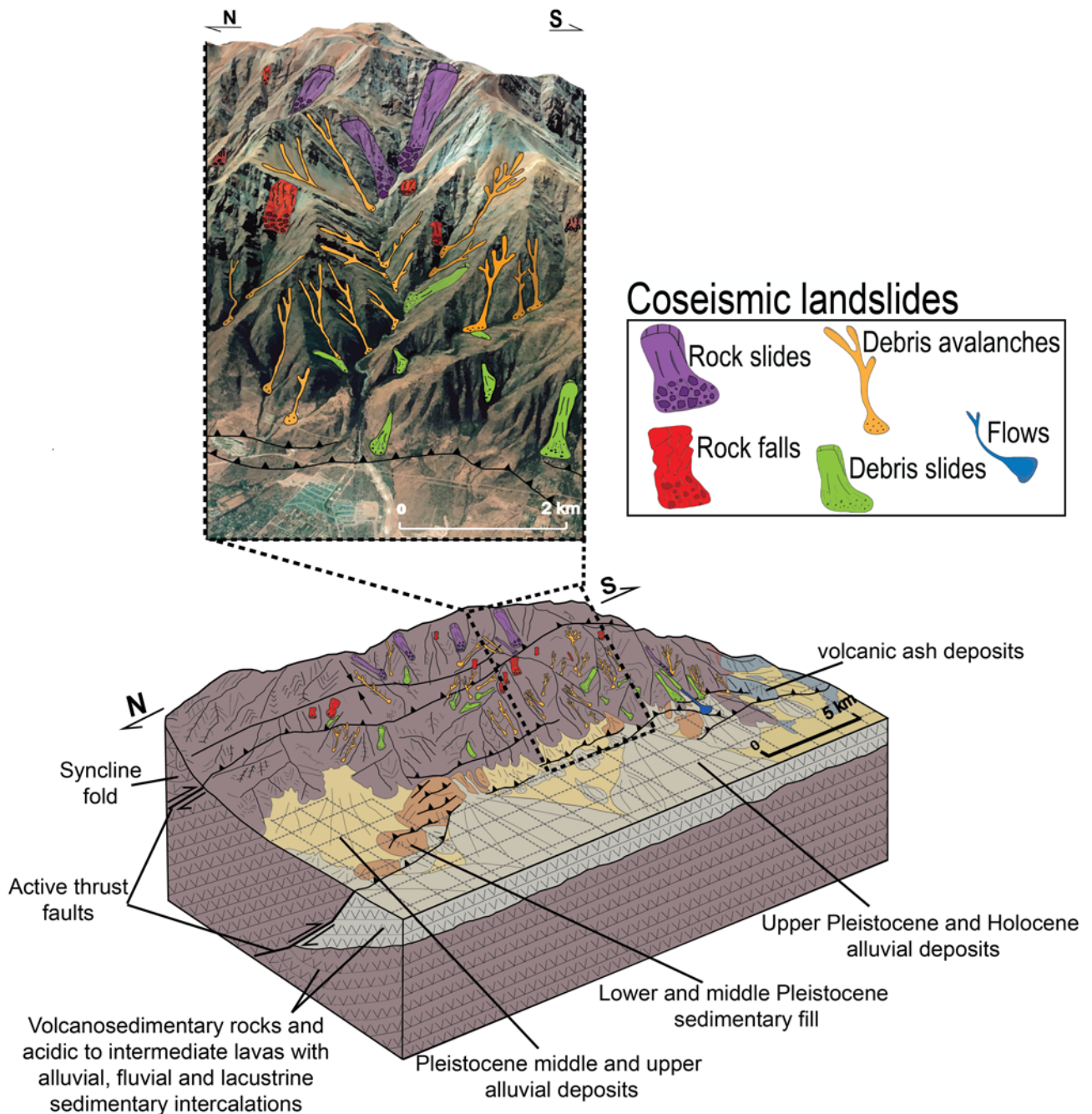


Fig. 9. Mountain Front bordering urban area environment. Conceptual geomodel of coseismic landslide induced by shallow crustal earthquake. The urban area is represented in grey, gridded.

Mountain Front environment

Mountain front terrain, usually bordering urban areas in central Chile, is dominated by andesitic bedrock with local volcanoclastic sediments and generally forms at the convergence of high mountains and adjacent basins (e.g. the Santiago basin). Rock mass quality is often fair to good, locally very good, and may be highly fractured in the vicinity of lineaments or faults. Hydrothermal alteration, however, can be extreme in places and reduce the geotechnical quality of intact rock. In these environments, geomorphology is characterized by a strong relief, medium ranges of altitudes and medium to high gradients. This environment presents important ravine channels, and basins characterized by narrow, steep-sided valleys, in which removed material flows directly into urban areas located in the central depression. Therefore, large rock avalanches/slides generated by a future crustal earthquake

and, consequently, debris flows due to debris avalanche, rock falls or rock slide failures into channels, could result in fatalities and infrastructure damage.

Figures 9 and 10 show conceptual geomodels of coseismic landslides induced by shallow crustal and megathrust earthquakes respectively in a Mountain Front environment of central Chilean Andes. Table 5 outlines geomorphological characteristics of terrain and possible coseismic landslides that could be triggered in a Mountain Front environment for each scenario.

Discussion

Landslides are an important coseismic geohazard associated with earthquakes in mountain environments and present a serious threat to communities found in these regions (Keefer 1984). Indeed, in

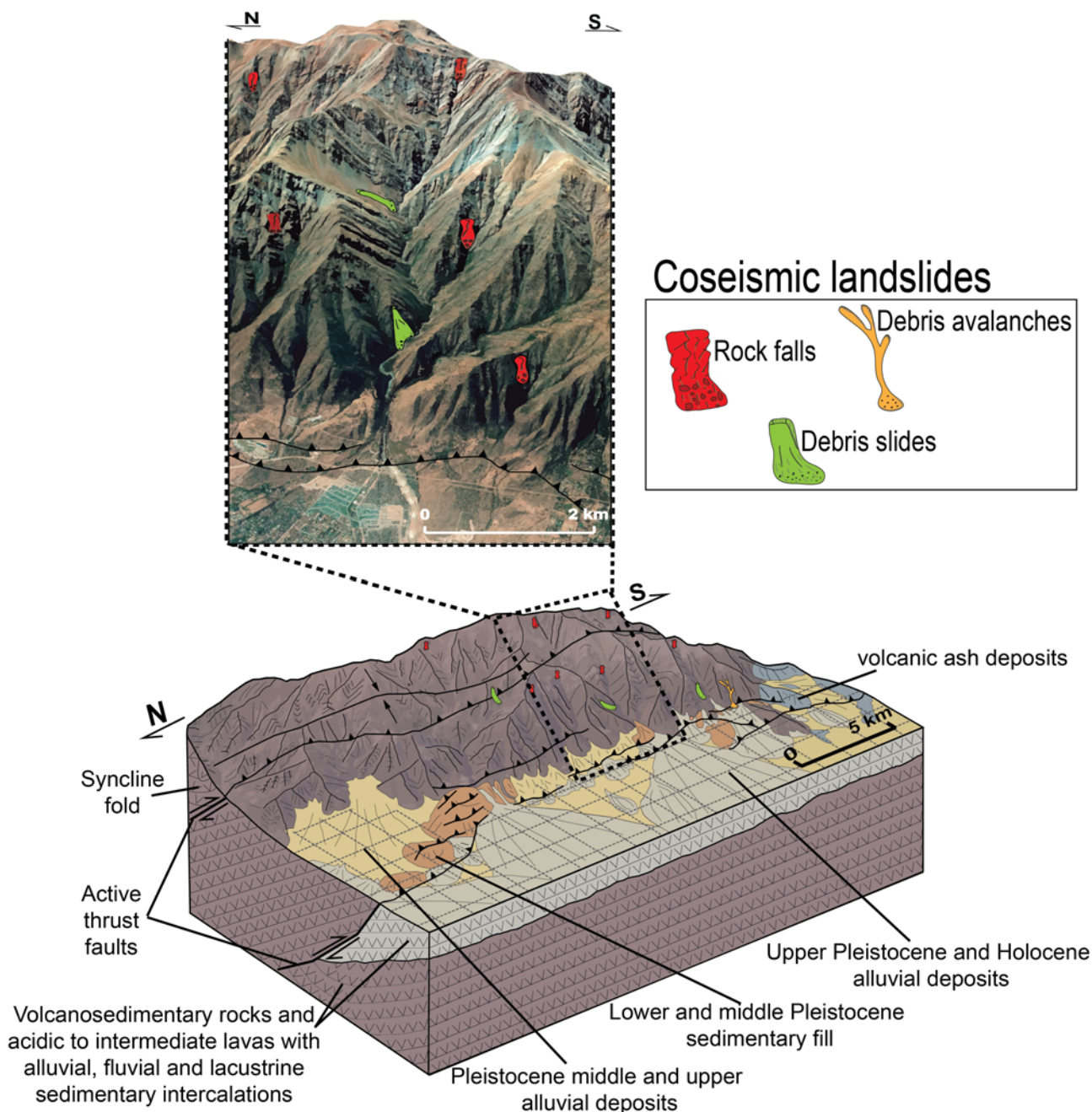


Fig. 10. Mountain Front bordering urban area environment. Conceptual geomodel of coseismic landslides induced by megathrust earthquake. The urban area is represented in grey, gridded.

high mountain chains, 20–25% of earthquake-induced fatalities result from the effects of landslides (Petley *et al.* 2006). By visualizing differences between conditioning factors and characteristics of coseismic landslides, using geomodels, between different triggers can be a key factor in the assessment of effective mitigation measures. From the geomodel construction, it is possible to view potential risks, consequences and possible mitigation measures for each coseismic landslide (Table 6).

Secondary hazards can be generated from large landslides, such as rock avalanches and rock slides, blocking narrow, steep-sided valleys and forming landslide dams (Schuster 1986), or landslide-induced tsunamis. In some cases, landslides may pose a threat to the population and infrastructure because they dam a watercourse. Landslide dams tend to be a feature of seismically active steep-relief mountain areas undergoing uplift and erosion or deeply dissected thick sequences of weakly consolidated sediments such as lacustrine clays. Landslide dams give rise to two important flood hazards.

Upstream or back-water flooding occurs as a result of impounding of water behind the dam leading to the relatively slow inundation of an area to form a temporary dam. Downstream flooding can occur in response to failure of a landslide dam. The most frequent failure modes are overtopping because of the lack of a natural spillway or breaching due to erosion. Failure of the poorly consolidated landslide debris generally occurs within a year of dam formation. The effect of the resultant floods can be devastating, partly because of their magnitude and partly because of their unexpected occurrence (Lee and Jones 2004). For example, in the 2005 M_w 7.6 Kashmir earthquake at least two river blockages occurred. The largest of the two, at Hattian Bala, east of Muzaffarabad, created a dam over 100 m high (Dunning *et al.* 2007).

In Chile, the most important historical example of landslide dams took place during the giant 1960 Valdivia earthquake ($M_w = 9.5$, megathrust earthquake). Three large landslides dammed the San Pedro River and threatened Valdivia city. The biggest landslide

Table 5. *Terrain characteristics and coseismic landslide hazards for the Mountain Front environment*

Terrain facet	Terrain element	Site characteristics	Main coseismic landslide type (after Hungre et al. 2014)				
			shallow crustal earthquake	megathrust earthquake	Secondary hazards	Engineering interventions/risk-reduction strategies	
Fluvial andesitic slopes	Ridges	Ridges characterized by thin residual soil deposits with bedrock at or close to the surface; rock mass may be highly fractured by thermal oscillation. Likely to locally be a poor to fair quality rock mass.	Rock falls; rock block slides; debris falls; toppling.	Rock falls.	Creation of sediment supply for debris flow activation.	Reactive. Monitoring needed after earthquake. This should be a higher priority after local shallow crustal earthquakes and long-term planning is needed.	
	Interfluvial slopes	Rock mass composed of volcano-sedimentary bedrock, often fair to good, steep slopes. They may have the scar of ancient events of mass removals. Slopes formed with engineering soils of variable thickness along the long profile. Dominantly fluvio-alluvial material and colluvium.	Rock slides; rock avalanches; debris slides; debris avalanches; rock falls.	Debris slides; debris avalanches.	Rock slides may create landslide dams.	Monitoring. Slopes adjacent to important infrastructure/property may require intervention for public safety. Draped netting systems should be considered as a means of mitigating small-scale failures.	
	Channels	Stream	Dominated by intercalations of coarse fluvial material, alluvial deposits and colluvium.	Debris flows due to debris avalanche, rock falls or rock slide failures into stream channels.	—	High turbidity events in the channels.	Close to large urban areas checking dams or netting should be considered. These should be inspected after shaking to ensure capacity is not being exceeded.
		Ravine	Narrow, steep-sided valley. Dominated by intercalations of coarse alluvial deposits and colluvium.	Debris flows due to debris avalanche, rock falls or rock slide failures into stream channels. Debris avalanches due to rock falls, debris slides or rock slide failures into channels. Rock avalanches or large rockslides with origin on upper reaches of ravine channels.	—		Inspections required after shaking. Local action plan for community evacuation should be considered. In the event of large landslide dams, local communities may need to refer the matter to Central Government via Ministry of Public Works. Urgent action needed and long-term planning.
Cross element	Mixture of the terrain elements (see relevant site characteristics above).	Large rockslides or rock avalanches with an origin on upper reaches of Cordillera which spans multiple terrain units.	—		Large slide mass creates temporary dam. Breaching is a major hazard leading to downstream flooding.		

Table 6. Potential risks and suggested mitigation measures for coseismic landslides generated in the mountain environment of Chile

Coseismic landslides	Potential consequences	Risk level (*)	Mitigation
Rock avalanche	Valley blockage, destruction of lifeline infrastructure, impact on mountain community.	Low due to infrequency of these events. Risk is likely to be higher as a result of a shallow crustal earthquake.	Evacuation plan for valley blockage.
Rock slides	Damage to local lifelines and road blockages. Difficulty in access for emergency services in the event of a local event. Economic losses due to closure of mine roads. Risk to individual road users.	Moderate to high in the event of shallow crustal seismicity; lower in the event of megathrust earthquakes due to large epicentral distances.	For important routes engineering intervention may be needed. Netting systems, localized rock bolting and retaining structures considered for critical routes. For higher hazard zones long-term planning as a tool for risk reduction is needed.
Rock falls	Injury and loss of life to users. Potential lifeline damage to single and multiple block rock falls.	Moderate (subduction zone event) to high (shallow crustal) event.	Critical infrastructure for mineral transport, important access roads (e.g. access to hospitals etc.) should be protected. For higher hazard zones 'no stopping' zones should be considered, and long-term planning is needed for other considered risk-reduction options.
Debris avalanches	Valley blockage, destruction of lifeline infrastructure, impact on mountain community.	Low	Slope regrading could be considered in specific areas. More detailed hazard analysis considered.
Debris slides	Damage to local lifelines and road blockages. Difficulty in access for emergency services in the event of a local event. Economic losses due to closure of mine roads. Risk to individual road users.	Low for megathrust earthquakes but moderate for shallow crustal events.	Slope regrading could be considered in specific areas. More detailed hazard analysis considered and long-term planning.
Flows	Likely only to cause localized damage due to liquefaction-related movement during shaking but debris flow activation could cause damage to infrastructure/HEP schemes during storm or snow melt after earthquake	Low during shaking but hazard becomes elevated during winter or spring.	Monitoring and inspection. Consider checking system for critical infrastructure.
Lateral spreads	Localized sliding only as the presence of liquefiable materials is going to be limited.	Low.	Monitoring and reactive maintenance.

*Infrastructure vulnerability is assumed in generic actual location.

removed $c. 30 \times 10^3 \text{ m}^3$ of poorly consolidated sediments, the intermediate transported $6 \times 10^3 \text{ m}^3$ and, finally, the smallest involved the removal of $2 \times 10^3 \text{ m}^3$ (Davis and Karzulovic 1963). Given its flow, it was expected that in two months the accumulated water would exceed the landslide dam, producing a huge avalanche that would cover all of Valdivia, already devastated by the earthquake and tsunami, and the surrounding areas. To avoid this disaster, engineers and technicians from ENDESA and MOP (Ministry of Public Works) started the so-called 'Operation Riñihue', which consisted of making a channel through the undisturbed terrain, so that the water flowed as slowly as possible when this finally happened (Lazo 2008). Historical records highlight this same phenomenon in the 1575 earthquake (M_w 8–8.5 according to Lomnitz 2004); on that occasion the San Pedro River was also blocked by a huge landslide in the same area (Montessus de Ballore 1912), not allowing normal water drainage. The dam accumulated water for five months and finally caused a catastrophic flood, taking the lives of more than 1200 indigenous people and destroying Valdivia city, founded by the Spaniards a couple of decades before (Davis and Karzulovic 1963).

Earthquakes often leave a legacy of pseudo-stable slopes that continue for years or many decades after the main event. These landslides represent a direct threat themselves but also block and cut transportation infrastructure. An aspect that is often overlooked is the increased rate of sediment movement caused by the liberation of hillslope debris, an effect that could depend on the type of earthquake. In the M_w 7.6 Chi-Chi earthquake in Taiwan, a shallow crustal event, this induced aggradation of some river beds by as much as 30 m, which proved to be devastating to local communities and to hydroelectric power systems (Marui and Nadim 2009). On the other hand, Tolorza *et al.* (2019) demonstrated that the 2010 M_w 8.8 Maule earthquake, a megathrust event, had a limited impact on the overall concentration and transport of suspended sediment loads in the Chilean Andes, which perhaps sheds light on the influence of climate on how these systems will behave post-events (e.g. under dry climate conditions). Thus, the seismically induced erosion and the evacuation of detached sediments are not necessarily a function of earthquake magnitude.

Despite the enormous impact potential of giant landslides, especially of those triggered during earthquakes, relatively few measures are taken to predict them. Thus, only very few case histories are known where large sites ($>1 \text{ km}^2$) had been thoroughly investigated to assess their failure potential under dynamic conditions, in full 3D (Havenith *et al.* 2017). The major problem is the availability of cost-effective methods, both to prospect and to model such sites – although all of them considered only one possible seismogenic scenario, i.e. crustal shallow earthquakes. Therefore, in this paper, a powerful tool for earthquake-induced landslide hazard assessment applicable to urban/territorial planning and disaster prevention strategies is presented. This is a series of practitioner-friendly conceptual ground models relating to the performance of slopes subject to strong ground motions during earthquakes originating from different seismogenic scenarios (megathrust or crustal shallow earthquake) in the most characteristic mountain environments in the Chilean Andes. These models express the following:

- the main types of landslides that could be triggered, their possible spatial distribution and sizes;
- geomorphological and geotechnical characteristics of terrain units where coseismic landslides could be located;
- secondary hazards and suggestions for possible engineering interventions.

This methodology visualizes all factors interacting in the generation of coseismic landslides depending on seismogenic zones

(megathrust or crustal shallow earthquake). When the low cost (in both the elaboration and the necessary information) is considered, it might be applied elsewhere in the country and Latin America. The continuous, poorly regulated growth of cities into mountain environments typical in Latin America, the increasing tourism industry in mountain areas and large infrastructure projects (water supply, hydroelectricity, gas pipes, etc.) increase the exposure to coseismic landslides and their secondary hazards. There is, thus, a need for these to be properly addressed in territorial planning policies and disaster prevention strategies.

It is essential to emphasize that this methodology is a conceptual approach and must be complemented with an observational model if it is to be applied for hazard assessment at local scales, which is based on the observed and measured distribution of engineering geological units and processes. These data are related to actual space or time and are constrained by surface or subsurface observations.

Concluding remarks

Landslides are a substantial but often neglected aspect of megathrust and shallow crustal earthquakes in upland areas. Furthermore, in addition to the initial loss of life, they can also have an extremely serious impact in terms of hampering rescue operations and the delivery of assistance, situations that can vary dramatically between different triggers. Whilst earthquake-induced landslides cannot be prevented, adequate consideration of the problem in advance can allow the impact of coseismic landslides to be minimized.

Practitioner-friendly conceptual ground models relating to the performance of slopes subject to strong ground motions during megathrust or shallow crustal earthquakes in different mountain environments in the Andes of central Chile have been developed. Each model expresses important characteristics about coseismic landslide hazards (main types, spatial distribution and sizes), their potential consequences and suggestions for possible mitigation actions or engineering interventions. Due to the geological and geomorphological context, these geomodels may be replicated or adapted for other countries in Latin America. In addition, considering the low cost, both in the elaboration and the necessary information, these models are a very powerful tool to visualize all factors interacting in the generation of coseismic landslides.

Scientific editing by Joel Smethurst; Phil Renforth

Acknowledgements We thank Murray Reid and Peter Redshaw for valuable comments that improved the manuscript. A. Velásquez, C. Sánchez and T. Reyes provided assistance with the graphics and support.

Author contributions AS: writing – original draft (lead); SAS: writing – original draft (lead); WM: writing – original draft (lead), writing – review & editing (lead); DNP: writing – review & editing (lead); GDP: writing – review & editing (lead).

Funding This work was funded by the Fondecyt (1140317 and 11160038) and RCUK-Conicyt Newton Fund International Cooperation Programme Project (NE/N000315/1) 'Seismically-induced landslides in Chile: New tools for hazard assessment and disaster prevention'.

Data availability statement All data generated or analysed during this study are included in this published article

References

- Abrahamson, N.A. and Somerville, P.G. 1996. Effects of the hanging wall and footwall on ground motions recorded during the Northridge earthquake. *Bulletin of the Seismological Society of America*, **86**, S93–S99.
- Alvarado, P., Barrientos, S., Saez, M., Astroza, M. and Beck, S. 2009. Source study and tectonic implications of the historic 1958 Las Melosas crustal earthquake, Chile, compared to earthquake damage. *Physics of the Earth and Planetary Interiors*, **175**, 26–36. <https://doi.org/10.1016/j.pepi.2008.03.015>

- Antinao, J.L. and Gosse, J. 2009. Large rockslides in the Southern Central Andes of Chile (32–34.5 S): Tectonic control and significance for Quaternary landscape evolution. *Geomorphology*, **104**, 117–133, <https://doi.org/10.1016/j.geomorph.2008.08.008>
- Argus, D.F., Gordon, R.G. et al. 2010. The angular velocities of the plates and the velocity of Earth's centre from space geodesy. *Geophysical Journal International*, **180**, 913–960, <https://doi.org/10.1111/j.1365-246X.2009.04463.x>
- Armijo, R., Rauld, R., Thiele, R., Vargas, G., Campos, J., Lacassin, R. and Kausel, E. 2010. The West Andean thrust, the San Ramon fault, and the seismic hazard for Santiago, Chile. *Tectonics*, **29**, 1–34, <https://doi.org/10.1029/2008TC002427>
- Barrientos, S. and National Seismological Center (CSN) Team 2018. The seismic network of Chile. *Seismological Research Letters*, **89**, 467–474, <https://doi.org/10.1785/0220160195>
- Barrientos, S.E. and Ward, S.N. 1990. The 1960 Chile earthquake: Inversion for slip distribution from surface deformation. *Geophysical Journal International*, **103**, 589–598, <https://doi.org/10.1111/j.1365-246X.1990.tb05673.x>
- Barrientos, S., Vera, E., Alvarado, P. and Monfret, T. 2004. Crustal seismicity in central Chile. *Journal of South American Earth Sciences*, **16**, 759–768, <https://doi.org/10.1016/j.jsames.2003.12.001>
- Candia, G., De Pascale, G.P., Montalva, G.A. and Ledezma, C. 2017. Geotechnical aspects of the 2015 Mw 8.3 Illapel megathrust earthquake sequence in Chile. *Earthquake Spectra*, **33**, 709–728, <https://doi.org/10.1193/031716EQS043M>
- Charrier, R., Ramos, V.A., Tapia, F. and Sagripanti, L. 2015. Tectono-stratigraphic evolution of the Andean Orogen between 31 and 37°S (Chile and Western Argentina). *Geological Society, London, Special Publications*, **399**, 13–61, <https://doi.org/10.1144/SP399.20>
- Cifuentes, I.L. 1989. The 1960 Chilean earthquakes. *Journal of Geophysical Research*, **94**, 665–680, <https://doi.org/10.1029/JB094iB01p00665>
- Cisternas, A. 2011. El país más sísmico del mundo. Revista Anales Séptima Serie, *Anales de la Universidad de Chile*, **1**, 17–34. <https://doi.org/10.5354/0365-7779.2011.12246>
- Cisternas, M., Atwater, B.F., Torrejón, F., Sawai, Y., Machuca, G., Lagos, M. and Shishikura, M. 2005. Predecessors of the giant 1960 Chile earthquake. *Nature*, **437**, 404, <https://doi.org/10.1038/nature03943>
- Dai, F.C., Xu, C., Yao, X., Xu, L., Tu, X.B. and Gong, Q.M. 2011. Spatial distribution of landslides triggered by the 2008 Ms 8.0 Wenchuan earthquake, China. *Journal of Asian Earth Sciences*, **40**, 883–895, <https://doi.org/10.1016/j.jseaes.2010.04.010>
- Davis, S.N. and Karzulovic, J. 1963. Landslides of Lago Riñihue, Chile. *Geological Society of America Bulletin*, **53**, 1403–1414.
- Densmore, A. and Hovius, N. 2000. Topographic fingerprints of bedrock landslides. *Geology*, **28**, 371–374, [https://doi.org/10.1130/0091-7613\(2000\)28<371:TFOBL>2.0.CO;2](https://doi.org/10.1130/0091-7613(2000)28<371:TFOBL>2.0.CO;2)
- Duke, C.M. 1960. The Chilean Earthquakes of May 1960. *Science*, **132**, 1797–1802, <https://doi.org/10.1126/science.132.3442.1797>
- Dunning, S.A., Mitchell, W.A., Rosser, N.J. and Petley, D.N. 2007. The Hattian Bala rock avalanche and associated landslides triggered by the Kashmir Earthquake of 8 October 2005. *Engineering Geology*, **93**, 130–144, <https://doi.org/10.1016/j.enggeo.2007.07.003>
- Evans, S.G., Bishop, N.F., Smoll, L.F., Murillo, P.V., Delaney, K.B. and Oliver-Smith, A. 2009. A re-examination of the mechanism and human impact of catastrophic mass flows originating on Nevado Huascarán, Cordillera Blanca, Peru in 1962 and 1970. *Engineering Geology*, **108**, 96–118, <https://doi.org/10.1016/j.enggeo.2009.06.020>
- Fookes, P.G. 1997. First Glossop Lecture: Geology for engineers: The geological model, prediction and performance. *Quarterly Journal of Engineering Geology*, **30**, 293–424, <https://doi.org/10.1144/GSL.QJEG.1997.030.P4.02>
- Fookes, P.G., Baynes, F.J. and Hutchinson, J.N. 2000. Total geological history: a model approach to the anticipation, observation and understanding of site conditions. In: *ISRM International Symposium*. International Society for Rock Mechanics and Rock Engineering, **1**, 370–460.
- Geli, L., Bard, P.Y. and Jullien, B. 1988. The effect of topography on earthquake ground motion: a review and new results. *Bulletin of the Seismological Society of America*, **78**, 42–63.
- Godoy, E., Yanez, G. and Vera, E. 1999. Inversion of an Oligocene volcano-tectonic basin and uplifting of its superimposed Miocene magmatic arc in the Chilean Central Andes: First seismic and gravity evidences. *Tectonophysics*, **306**, 217–236, [https://doi.org/10.1016/S0040-1951\(99\)00046-3](https://doi.org/10.1016/S0040-1951(99)00046-3)
- Gorum, T., Fan, X., van Westen, C.J., Huang, R.Q., Xu, Q., Tang, C. and Wang, G. 2011. Distribution pattern of earthquake-induced landslides triggered by the 12 May 2008 Wenchuan Earthquake. *Geomorphology*, **133**, 152–167, <https://doi.org/10.1016/j.geomorph.2010.12.030>
- Greve, F. 1960. Extracto de la historia de la sismología en Chile. *Anales de la Facultad de Ciencias Físicas Y Matemáticas*, **17**, 17.
- Havenith, H.B., Mreyen, A.S., Torgoev, A. and Micu, M. 2017. Numerical models of unstable slopes in seismic areas—based on 3D geomodels. In: *Workshop on World Landslide Forum*. Springer, Cham, 47–57.
- Hearn, G.J. 2018. Slope hazards on the Ethiopian road network Quarterly Journal of Engineering Geology and Hydrogeology, **52**, 295–311, <https://doi.org/10.1144/qjgeh2018-058>
- Hearn, G.J. and Hart, A.B. 2011. Geomorphological contributions to landslide risk assessment: theory and practice. *Developments in Earth Surface Processes*, **15**, 107–148.
- Hearn, G., Wise, D., Hart, A., Morgan, C. and O'Donnell, N. 2012. Assessing the potential for future first-time slope failures to impact the oil and gas pipeline corridor through the Makarov Mountains, Sakhalin Island, Russia. *Quarterly Journal of Engineering Geology and Hydrogeology*, **45**, 79–88, <https://doi.org/10.1144/1470-9236/10-033>
- Huang, R.Q. and Li, W.L. 2009. Analysis of the geo-hazards triggered by the 12 May 2008 Wenchuan Earthquake, China. *Bulletin of Engineering Geology and the Environment*, **68**, 363–371, <https://doi.org/10.1007/s10064-009-0207-0>
- Hungr, O., Leroueil, S. and Picarelli, L. 2014. The Varnes classification of landslide types, an update. *Landslides*, **11**, 167–194.
- Jackson, R. 2016. Geomodels in engineering geology—an introduction. *Environmental & Engineering Geoscience*, **22**, 171–172, <https://doi.org/10.2113/gsegeosci.22.2.171>
- Jibson, R.W. 2011. Methods for assessing the stability of slopes during earthquakes—A retrospective. *Engineering Geology*, **122**, 43–50, <https://doi.org/10.1016/j.enggeo.2010.09.017>
- Jibson, R.W., Harp, E.L. and Michael, J.A. 2000. A method for producing digital probabilistic seismic landslide hazard maps. *Engineering Geology*, **58**, 271–289, [https://doi.org/10.1016/S0013-7952\(00\)00039-9](https://doi.org/10.1016/S0013-7952(00)00039-9)
- Jordan, T.E., Isacks, B., Allmendinger, R., Brewer, J., Ramos, V. and Ando, C. 1983. Andean tectonics related to geometry of the subducted Nazca plate. *Geological Society of America Bulletin*, **94**, 341–361, [https://doi.org/10.1130/0016-7606\(1983\)94<341:ATRTGO>2.0.CO;2](https://doi.org/10.1130/0016-7606(1983)94<341:ATRTGO>2.0.CO;2)
- Keefer, D.K. 1984. Landslides caused by earthquakes. *Geological Society of America Bulletin*, **95**, 406–421, [https://doi.org/10.1130/0016-7606\(1984\)95<406:LCBE>2.0.CO;2](https://doi.org/10.1130/0016-7606(1984)95<406:LCBE>2.0.CO;2)
- Keefer, D.K. 2000. Statistical analysis of an earthquake-induced landslide distribution—the 1989 Loma Prieta, California event. *Engineering Geology*, **58**, 231–249, [https://doi.org/10.1016/S0013-7952\(00\)00037-5](https://doi.org/10.1016/S0013-7952(00)00037-5)
- Keefer, D.K. 2002. Investigating landslides caused by earthquakes – a historical review. *Surveys in Geophysics*, 473–510, <https://doi.org/10.1023/A:1021274710840>
- Khazai, B. and Sitar, N. 2004. Evaluation of factors controlling earthquake-induced landslides caused by Chi-Chi earthquake and comparison with the Northridge and Loma Prieta events. *Engineering Geology*, **71**, 79–95, [https://doi.org/10.1016/S0013-7952\(03\)00127-3](https://doi.org/10.1016/S0013-7952(03)00127-3)
- Lara, L.E., Reyes, J. and Diaz-Naveas, J. 2018. ⁴⁰Ar/³⁹Ar constraints on the age progression along the Juan Fernández Ridge, SE Pacific. *Frontiers in Earth Science*, **6**, 194, <https://doi.org/10.3389/feart.2018.00194>
- Lazo, R. 2008. Estudio de los Daños de los Terremotos del 21 y 22 de Mayo de 1960. <http://repositorio.uchile.cl/handle/2250/104856>
- Lee, C.T., Huang, C.C., Lee, J.F., Pan, K.L., Lin, M.L. and Dong, J.J. 2008. Statistical approach to earthquake-induced landslide susceptibility. *Engineering Geology*, **100**, 43–58, <https://doi.org/10.1016/j.enggeo.2008.03.004>
- Lee, E.M. and Jones, D.K. 2004. *Landslide risk assessment*. Thomas Telford, London, 454.
- Lomnitz, C. 2004. Major earthquakes of Chile: a historical survey, 1535–1960. *Seismological Research Letters*, **75**, 368–378, <https://doi.org/10.1785/gssrl.75.3.368>
- Malamud, B.D., Turcotte, D.L., Guzzetti, F. and Reichenbach, P. 2004. Landslide inventories and their statistical properties. *Earth Surface Processes and Landforms*, **29**, 687–711, <https://doi.org/10.1002/esp.1064>
- Marc, O., Hovius, N., Meunier, P., Gorum, T. and Uchida, T. 2016. A seismologically consistent expression for the total area and volume of earthquake-triggered landsliding. *Journal of Geophysical Research: Earth Surface*, **121**, 640–663, <https://doi.org/10.1002/2015JF003732>
- Marui, H. and Nadim, F. 2009. Landslides and Multi-Hazards. In: Sassa, K. and Canuti, P. (eds) *Landslides - Disaster Risk Reduction*. Springer, Berlin, Heidelberg. https://doi.org/10.1007/978-3-540-69970-5_23
- Meunier, P., Hovius, N. and Haines, A.J. 2007. Regional patterns of earthquake-triggered landslides and their relation to ground motion. *Geophysical Research Letters*, **34**, L20408, <https://doi.org/10.1029/2007GL031337>
- Meunier, P., Hovius, N. and Haines, J.A. 2008. Topographic site effects and the location of earthquake induced landslides. *Earth and Planetary Science Letters*, **275**, 221–232, <https://doi.org/10.1016/j.epsl.2008.07.020>
- Miles, S.B. and Keefer, D.K. 2000. Evaluation of seismic slope-performance models using a regional case study. *Environmental & Engineering Geoscience*, **6**, 25–39, <https://doi.org/10.2113/gsegeosci.6.1.25>
- Miles, S.B. and Keefer, D.K. 2007. *Comprehensive areal model of earthquake-induced landslides: technical specification and user guide*. US Geological Survey, Open-File Report, 2007–1072, 69.
- Miles, S.B. and Keefer, D.K. 2009. Evaluation of CAMEL—comprehensive areal model of earthquake-induced landslides. *Engineering Geology*, **104**, 1–15, <https://doi.org/10.1016/j.enggeo.2008.08.004>
- Moernaut, J., Van Daele, M. et al. 2014. Lacustrine turbidites as a tool for quantitative earthquake reconstruction: New evidence for a variable rupture mode in south–central Chile. *Journal of Geophysical Research: Solid Earth*, **119**, 1607–1633, <https://doi.org/10.1002/2013JB010738>
- Montessus de Ballore, F. 1912. *Historia sísmica de los Andes Meridionales al sur del paralelo XVI*. Imprenta Cervantes, Santiago de Chile.
- Moreiras, S.M. and Sepúlveda, S.A. 2015. Megalandslides in the Andes of central Chile and Argentina (32°–34° S) and potential hazards. *Geological Society, London, Special Publications*, **399**, 329–344, <https://doi.org/10.1144/SP399.18>

Conceptual models of coseismic landslides hazard

- Naranjo, J.A., Arenas, M., Clavero, J. and Muñoz, O. 2009. Mass movement-induced tsunamis: main effects during the Patagonian Fjordland seismic crisis in Aisén (45°25'S), Chile. *Andean Geology*, **36**, 137–146.
- Newmark, N.M. 1965. Effects of earthquakes on dams and embankments. *Geotechnique*, **15**, 139–160, <https://doi.org/10.1680/geot.1965.15.2.139>
- Oppikofer, T., Hermanns, R., Redfield, T.F., Sepúlveda, S.A., Duhart, P. and Bascuñán, I. 2012. Morphologic description of the Punta Cola rock avalanche and associated minor rockslides caused by the 21 April 2007 Aysén earthquake (Patagonia, southern Chile). *Revista Asociación Geológica Argentina*, **69**, 339–353.
- Pankhurst, R. and Hervé, F. 2007. Introduction and overview. In: Moreno, T. and Gibbons, W. (eds) *The Geology of Chile*. Geological Society, London, 1–4, <https://doi.org/10.1144/GOCH.1>
- Parker, R.N., Hancox, G.T., Petley, D.N., Massey, C.I., Densmore, A.L. and Rosser, N.J. 2015. Spatial distributions of earthquake-induced landslides and hillslope preconditioning in northwest South Island, New Zealand. *Earth Surface Dynamics*, **3**, 501–525, <https://doi.org/10.5194/esurf-3-501-2015>
- Parry, B.R., Surovtsev, I.V., Cabeen, M.T., O'Hern, C.S., Dufresne, E.R. and Jacobs-Wagner, C. 2014. The bacterial cytoplasm has glass-like properties and is fluidized by metabolic activity. *Cell*, **156**, 183–194
- Plafker, G. and Ericksen, G.E. 1978. Nevados Huascarán avalanches, Peru. *Developments in Geotechnical Engineering*, **14**, 277–314.
- Petley, D.N., Dunning, S.A., Rosser, N.J. and Kausar, A.B. 2006. Incipient earthquakes in the Jhelum Valley, Pakistan following the 8th October 2005 earthquake. In: Marui, H. (ed.) *Disaster mitigation of debris flows, slope failures and landslides*. Frontiers of Science Series 47, Universal Academy Press, Tokyo, Japan, 47–56
- Qi, S., Xu, Q., Lan, H., Zhang, B. and Liu, J. 2010. Spatial distribution analysis of landslides triggered by 2008.5.12 Wenchuan Earthquake, China. *Engineering Geology*, **116**, 95–108, <https://doi.org/10.1016/j.enggeo.2010.07.011>
- Rodriguez, C.E., Bommer, J.J. and Chandler, R.J. 1999. Earthquake induced landslide 1980–1997. *Soil Dynamics and Earthquake Engineering*, **18**, 225–346, [https://doi.org/10.1016/S0267-7261\(99\)00012-3](https://doi.org/10.1016/S0267-7261(99)00012-3)
- Santibáñez, I., Cembrano, J. et al. 2018. Crustal faults in the Chilean Andes: geological constraints and seismic potential. *Andean Geology*, **46**, 32–65, <https://doi.org/10.5027/andgeoV46n1-3067>
- Schuster, R.L. 1986. *Landslide Dams: Processes, Risk, and Mitigation*. ASCE.
- Sepúlveda, S.A. and Serey, A. 2009. Tsunamiogenic, earthquake-triggered rock slope failures during the 21st of April 2007 Aisén earthquake, Southern Chile (45.5°S). *Andean Geology*, **36**, 131–136, <https://doi.org/10.4067/S0718-71062009000100010>
- Sepúlveda, S.A., Murphy, W. and Petley, D.N. 2005. Topographic controls on coseismic rock slides during the 1999 Chi-Chi Earthquake, Taiwan. *Quarterly Journal of Engineering Geology and Hydrogeology*, **38**, 189–196, <https://doi.org/10.1144/1470-9236/04-062>
- Sepúlveda, S.A., Astroza, M., Kausel, E., Campos, J., Casas, E.A., Rebolledo, S. and Verdugo, R. 2008. New findings on the 1958 Las Melosas earthquake sequence, central Chile: implications for seismic hazard related to shallow crustal earthquakes in subduction zones. *Journal of Earthquake Engineering*, **12**, 432–455
- Sepúlveda, S.A., Serey, A., Lara, M., Pavez, A. and Rebolledo, S. 2010. Landslides induced by the 2007 Aysén Fjord earthquake, Chilean Patagonia. *Landslides*, **7**, 483–492, <https://doi.org/10.1007/s10346-010-0203-2>
- Serey, A. 2020. Coseismic landslides during strong shallow crustal and large interplate earthquakes: Controlling factors and conceptual hazard geomodels, <http://repositorio.uchile.cl/handle/2250/102608>
- Serey, A., Escobar, P., Moya, S., Sepúlveda, S.A. and Petley, D. 2017. Landslide inventory of the 2010 Mw 8.8 Maule earthquake, Central Chile. 16th World Conference on Earthquake, 16WCEE 2017: 1873.
- Serey, A., Piñero-Feliciangeli, L., Sepúlveda, S.A., Poblete, F., Petley, D.N. and Murphy, W. 2019. Landslides induced by the 2010 Chile megathrust earthquake: a comprehensive inventory and correlations with geological and seismic factors. *Landslides*, **16**, 1153–1165, <https://doi.org/10.1007/s10346-019-01150-6>
- Somerville, P.G. and Graves, R.W. 2003. Characterization of earthquake strong ground motion. In: Bardet, J.P., Imamura, F., Synolakis, C.E., Okal, E.A. and Davies, H.L. (eds) *Landslide Tsunamis: Recent Findings and Research Directions*. Birkhäuser, Basel, 1811–1828, https://doi.org/10.1007/978-3-0348-7995-8_2
- Somerville, P.G., Smith, N.F., Graves, R.W. and Abrahamson, N.A. 1997. Modification of empirical strong ground motion attenuation relations to include the amplitude and duration effects of rupture directivity. *Seismological Research Letters*, **68**, 199–222, <https://doi.org/10.1785/gssrl.68.1.199>
- Tichelaar, B.W. and Ruff, L.J. 1991. Seismic coupling along the Chilean subduction zone. *Journal of Geophysical Research*, **98**, 2017–2038, <https://doi.org/10.1029/92JB02045>
- Tolorza, V., Mohr, C.H., Carretier, S., Serey, A., Sepúlveda, S.A., Tapia, J. and Pinto, L. 2019. Suspended sediments in Chilean rivers reveal low postseismic erosion after the Maule earthquake (Mw 8.8) during a severe drought. *Journal of Geophysical Research: Earth Surface*, **124**, 1378–1397.
- Wang, G. 2015. Comparison of the landslides triggered by the 2013 Lushan earthquake with those triggered by the strong 2008 Wenchuan earthquake in areas with high seismic intensities. *Bulletin of Engineering Geology and the Environment*, **74**, 77–89, <https://doi.org/10.1007/s10064-014-0574-z>
- Wang, G., Du, C., Huang, D., Jin, F., Koo, R.C. and Kwan, J.S. 2018. Parametric models for 3D topographic amplification of ground motions considering subsurface soils. *Soil Dynamics and Earthquake Engineering*, **115**, 41–54, <https://doi.org/10.1016/j.soildyn.2018.07.018>
- Wang, Y., Luo, Y., Wang, F., Wang, D., Ma, X., Li, S. and Deng, X. 2012. Slope seismic response monitoring on the aftershocks of the Wenchuan earthquake in the Mianzhu section. *Journal of Mountain Science*, **9**, 523–528, <https://doi.org/10.1007/s11629-012-2179-y>
- Wartman, J., Dunham, L., Tiwari, B. and Pradel, D. 2013. Landslides in Eastern Honshu induced by the 2011 off the Pacific Coast of Tohoku earthquake. *Bulletin of the Seismological Society of America*, **103**, 1503–1521, <https://doi.org/10.1785/0120120128>
- Wright, C. and Mella, A. 1963. Modifications to the soil pattern of South-Central Chile resulting from seismic and associated phenomena during the period May to August 1960. *Bulletin of the Seismological Society of America*, **53**, 1367–1402.
- Zhao, B., Li, W., Wang, Y., Lu, J. and Li, X. 2019. Landslides triggered by the Ms 6.9 Nyingchi earthquake, China (18 November 2017): analysis of the spatial distribution and occurrence factors. *Landslides*, **16**, 765–776, <https://doi.org/10.1007/s10346-019-01146-2>